INVESTIGATING THE ROLE OF AURKAIP1 IN MITOCHONDRIAL GENE EXPRESSION

Kyle Thompson

Wellcome Trust Centre for Mitochondrial Research,
Institute for Ageing and Health
Newcastle University

Thesis submitted to Newcastle University in candidature for the degree of Doctor of Philosophy

May 2014

ABSTRACT

Mitochondria contain their own genome (mtDNA), which encodes 13 polypeptides essential for oxidative phosphorylation. Dysfunctional mitochondria have been associated with disease and the ageing process. Expression of mtDNA requires import of many nuclear-encoded polypeptides that are synthesised in the cytosol and imported into the mitochondrion. As many as 300 nuclear-encoded mitochondrial proteins are estimated to be unidentified or their functions remain unknown. The importance of understanding the nuances of human mitochondrial gene expression machinery has been highlighted by the predisposition of paediatric mitochondrial patients with nuclear gene mutations that manifest as mitochondrial translation defects.

The aim of this research was to further the understanding of mitochondrial gene expression by characterising the protein AURKAIP1, which was identified during a screen of 224 candidate proteins as being likely to have a role in mitochondrial gene expression.

By mitochondrial sub-fractionation techniques I was able to show that AURKAIP1 is a mitochondrial matrix protein. I have shown that AURKAIP1 is involved in mitochondrial gene expression since depletion of AURKAIP1 severely depletes the levels of mitochondrial-encoded proteins ND1, COXI and COXII. In addition, the overexpression of AURKAIP1 in mammalian cell lines causes a dramatic decrease in the *de novo* synthesis of mitochondrial polypeptides, which was studied by labelling nascent peptides with [^{35}S] labelled methionine. The overexpression of AURKAIP1 also reduces the steady state levels of many mitoribosomal proteins, suggesting the reduced level of mitochondrial gene expression is due to a reduction in the number of functional mitoribosomes. I have also demonstrated a novel interaction between AURKAIP1 and the mitochondrial protein, p32, which is essential for mitochondrial translation. A paediatric patient with severe mitochondrial disease was found to have mutations in p32, which highlights the importance of mitochondrial gene expression and the need for further study into the factors involved.

ACKNOWLEDGEMENTS

First, I would like to thank my supervisors Prof. Zofia Chrzanowska-Lightowlers and Prof. Robert Lightowlers for giving me the opportunity to pursue this PhD programme. Their continued support and guidance has been integral to the success of this project and I am very grateful, not only for advice relating to the work presented in this thesis, but for providing a welcoming environment in which it has been a pleasure to work.

I also owe immense gratitude to all of the lab members, past and present, who have helped me over my time spent working on this project. I would like to thank Tran for help with [^{35}S]-labelling, complex activity assays and for providing HEK293 mitoplasts, Francesco for help with [^{35}S]-labelling and Monika for data from patient fibroblasts/muscle (supplemental figures).

I would particularly like to thank Ola, Agata, Francesco, Alina, Paul, Martin and Casey, for their collective patience when teaching me a variety of techniques in the lab at the beginning of my studies and for welcoming me into the lab. Thanks also go to more recent lab members; Abdulraheem, Marysia, Tran, Rawaa, Monika, Anabela, Nicole and Christie for discussions about this work, but more importantly I thank everyone who has been part of our group for their continued friendship and making me enjoy every day (….well, mostly) spent in the lab.

I'd like to thank Dr Jorge Oliveira for collaboration in teaching me imaging techniques and analysis (and for extensive discussions about guitars and Apple products).

Last, but by no means least, I'd like so thank all of my friends and family, particularly my parents and my sister, Reanne, for their constant support not only during the course of this project, but my entire life. Extra special thanks to Jessica Tarn for support throughout this project and for making my life immeasurably better for being a part of it.

I could not have succeeded with this work without any of you!

TABLE OF CONTENTS

LIST OF FIGURES

LIST OF TABLES

LIST OF ABBREVIATIONS

Ψ_m – Mitochondrial membrane potential

aa – Amino acids

aa-tRNA – Aminoacyl-tRNA

Aβ - Amyloid Beta

AD – Alzheimer's disease

ADP – Adenosine diphosphate

AIF – Apoptosis inducing factor

Amp – Ampicillin

APS – Ammonium persulphate

A-site – Aminoacyl-tRNA site

ATP – Adenosine triphosphate

A.U. – Arbitrary units

AURKAIP1 – Aurora-A kinase interacting protein 1

Bcl-2 – B-cell lymphoma 2

bp – Base pair(s)

BSA – Bovine serum albumin

CBB – Coomassie Brilliant Blue

CJ – Cristae Junction

CL – Cardiolipin

CLIP – Crosslinking immunoprecipitation

CMV – Cytomegalovirus

CMT2A – Charcot-Marie-Tooth subtype 2A

CO, COX – Cytochrome *c* oxidase

CoA – Coenzyme A

C_q – Quantification cycle

C-terminal – Carboxyl terminal

Cyt – cytochrome

DAP3 – Death associated protein 3

DEPC – diethyl pyrocarbonate

dH_2O – Distilled water

D-loop – Displacement loop

DMEM – Dulbecco's modified Eagle's medium

DMSO – Dimethyl sulphoxide

DNA – Deoxyribonucleic acid

dNTP – Deoxynucleotide diphosphate

Dox – Doxacycline

Drp1 – Dynamin related protein 1

ds – Double-stranded

DTT – Dithiolthreitol

DUF – Domain of unknown function

E. coli – *Escherichia coli*

EDTA – Ethylene diamine tetra-acetic acid

EF – Elongation factor

EGTA – Ethylene glycol tetra-acetic acid

EM – electron microscopic

EMEM – Earle's Minimal Essential Media

ER – Endoplasmic reticulum

E-site – Exit site

ETC – Electron transport chain

FAD – Flavin-adenine dinucleotide

$FADH_2$ – Reduced flavin-adenine dinucleotide

FCS – foetal calf serum

FCCP – trifluorocarbonylcyanide phenylhydrazone

Fe-S – Iron sulphur

Fis1 – Human fission homologue 1

Fmet – Formyl methionine

FMN – flavin mononucleotide

FRT – Flp-recombination target

GAL – galactose

GDH – Glutamate dehydrogenase

Glu – glucose

GST – Glutathione S-transferase

GTP – Guanine triphosphate

HD – Huntington's disease

HeLa – Cell line derived from Henrietta Lacks cervical cancer cells

HEK293 – Human embryonic kidney 293 FlpIn^{TM}/TRex^{TM} cell line

HPA – Human Protein Atlas

HRP – Horseradish peroxidase

HSP – Heavy strand promoter

H-strand – Heavy strand

IF – Initiation factor

IgG – Immunoglobulin G

IMM – Inner mitochondrial membrane

IMS – Inter-membrane space

IP – Immunoprecipitation

IPTG – Isopropyl β-D-1-thiogalactopyranoside

kDa – kilo Dalton

kbp – kilo base pairs

LB – Luria-Bertani media

LC MS/MS – Liquid chromatography tandem mass spectrometry

LRPPRC – leucine rich pentatricopeptide repeat containing protein

LSP – Light Strand Promoter

L-strand – Light strand promoter

LSU – Large ribosomal subunit (mitochondrial = 39S)

MALDI – Matrix-assisted laser desorption/ionisation

MELAS – Mitochondrial encephalomyopathy, lactic acidosis, and stroke-like episodes

MERRF – Myoclonic Epilepsy with Ragged Red Fibers

Mff – Mitochondrial fission factor

Mfn – Mitofusin

MIA – Mitochondrial Intermembrane Space Import and Assembly

MPP – Mitochondrial processing peptidase

MRP – Mitochondrial ribosomal protein

MOPS – Morpholinopropanesuphonic acid

mRNA – Messenger RNA

mt – Mitochondrial

mtDNA – Mitochondrial DNA

mtPAP – Mitochondrial poly(A) polymerase

mtPTP – Mitochondrial permeability transition pore

mtRF1a – Mitochondrial release factor 1a

mtRRF – Mitochondrial ribosome recycling factor

mtSSB – Mitochondrial single stranded DNA binding protein

MW – Molecular weight

NAD+ – Nicotinamide adenine dinucleotide (oxidised)

NADH – reduced nicotinamide adenine dinucleotide

Na-Pi – Sodium Phosphate buffer (pH 8.1)

NEAA – Non-essential amino acids

nt – Nucleotide(s)

N-terminal – Amino-terminus

OD – Optical density

O_H – Heavy strand origin

O_L – Light strand origin

OMM – Outer membrane

OPA1 – Optic atrophy 1

ORF – Open reading frame

OXPHOS – Oxidative phosphorylation

PAGE – Polyacrylamide gel electrophoresis

PBS – Phosphate buffered Saline

PCR – Polymerase Chain Reaction

PD – Parkinson's disease

Pdf – Peptide deformylase

PE – Phosphatidylethanolamine

P. falciparum – Plasmodium falciparum

PG – Phosphatidylglycerol

PGP – Phosphatidylglycerolphosphate

P_i – Inorganic phosphate

PiGr – PicoGreen

PK – Proteinase K

PMSF – Phenylmethylsulphonyl fluoride

POLγ – DNA polymerase gamma

POLRMT – Mitochondrial RNA Polymerase

P-site – Peptidyl tRNA site

PVDF – Polyvinylidene fluoride

R. americana – Reclinomonas americana

R. prowazekii – Rickettsia prowazekii

RISC – RNA-induced silencing complex

RITOLS – ribonucleotide incorporation throughout the lagging strand

RNA – Ribonucleic acid

rRNA – Ribosomal RNA

ROS – Reactive oxygen species

Q – Ubiquinone

QH_2 – Ubiquinol

qPCR – Quantitative polymerase chain reaction

[^{35}S] – radioactive sulphur-35 isotope

[^{35}S]met – [^{35}S] labelled methionine

SAM – Sorting and Assembly Machinery of the Outer Mitochondrial Membrane

S. cerevisiae – Saccharomyces cerevisiae

SDS – Sodium dodecyl sulphate

SDH-70 – Succinate dehydrogenase (Complex II) 70kDa subunit

SEM – Standard error mean

siRNA – short interfering RNA

SLMO2 – slowmo protein homologue 2 (Drosophila)

SOC – Super-optimal broth with added magnesium and glucose

SSC – Saline sodium citrate buffer

ssDNA – single-stranded DNA

SSPE – Saline sodium phosphate EDTA buffer

SSU – Small ribosomal subunit (mitochondrial = 28S)

TAE – Tris-acetate EDTA buffer

TBS – Tris buffered saline

T-TBS – Tris buffered saline with 0.1% Tween-20

TCA – Trichloroacetic acid

TEMED – N,N,N',N'-tetramethylethylene-diamine

Tet – tetracycline

TFAM – Mitochondrial transcription factor A

TIM – Translocase of the inner membrane

T_m – Melting temperature (salt adjusted)

TMRM – tetramethylrhodamine methyl ester

TOF – Time of flight

TOM – Translocase of the outer membrane

tRNA – transfer RNA

Tris – 2-Amino-2-hydroxymethyl-propane-1,3-diol

Triton X-100 – 4-(1,1,3,3-Tetramethylbutyl)phenyl-polyethylene glycol

Tween 20 – Polyoxyethylene sorbitanmonolaurate

UTR – Untranslated region

UV – ultra violet

V – volt

VDAC – Voltage dependent anion channel

WT – Wild-type

CHAPTER 1: INTRODUCTION

1.1 MITOCHONDRIA: BRIEF INTRODUCTION

Mitochondria are dynamic organelles that are essential to almost all eukaryotic cells, the exceptions being some non-nucleated cells such as mature erythrocytes. A major role of mitochondria is ATP production via oxidative phosphorylation (OXPHOS). Approximately 90% of the energy requirement of the cell is met by hydrolysing the ATP produced by OXPHOS in mitochondria. However, mitochondria also have important roles in iron sulphur cluster formation (Lill, 2009), the citric acid cycle (Rustin et al., 1997), regulation of apoptosis (Chipuk et al., 2006) and calcium homeostasis, in conjunction with the endoplasmic reticulum (ER) (de Brito and Scorrano, 2010). As a result of these various functions, dysfunctional mitochondria can cause a wide variety of diseases ranging from neurodegenerative disorders (Knott and Bossy-Wetzel, 2008), to cancer (Dang, 2012) and other multifactorial diseases such as diabetes (Højlund et al., 2008) among others. Mitochondria are also implicated to play a role in the ageing process (Lesnefsky and Hoppel, 2006). However, the term 'mitochondrial disorder' is often used to refer to defects in the OXPHOS system, which frequently affects multiple tissues and can be lethal early in life (Goldstein et al., 2013). The incidence of mitochondrial disease may be as high as 1 in 5000 (Schaefer et al., 2004), but the clinical manifestations and underlying pathology vary drastically. Mitochondria contain their own genome, which only encodes a small number of components of the OXPHOS system (discussed later). All other mitochondrial proteins, approximately 1500 in number (Lopez et al., 2000; Taylor et al., 2003a; Taylor et al., 2003b), are nuclear-encoded. Therefore, mutations in the mitochondrial genome, in any nuclear gene that encodes a protein required for the expression of mitochondrially encoded proteins or a protein involved in any key mitochondrial function can lead to mitochondrial disease (reviewed in Boesch et al., 2008).

This introductory chapter will focus mainly on current knowledge of the various aspects of mitochondrial gene expression. The structure and functions of mitochondria will also be discussed, but I will start by addressing the origins of the organelle.

1.2 MITOCHONDRIAL EVOLUTION

The serial endosymbiosis theory of mitochondrial evolution was proposed by Margulis (Margulis, 1971) and is now widely accepted (Gray et al., 1999; Kurland and Andersson, 2000). Simply put, this states that an ancestral α-proteobacteria was endocytosed by the common cellular ancestor of eukaryotes and formed a symbiotic relationship. This endosymbiosis event is predicted to have occurred approximately 1.5 billion years ago (Brocks et al., 1999) and since that time, the α-proteobacteria has evolved into the modern mitochondrion. Evidence for this comes from phylogenetic linkage analysis, which suggests a common ancestor for α-proteobacteria and mitochondria, and that mitochondria arose only once in evolution (Gray et al., 1999). Furthermore, the genome of the modern proteobacteria, *Rickettsia prowazekii*, has been shown to be highly similar to the mitochondrial genome (Andersson et al., 1998).

Although phylogenetic evidence strongly suggests an endosymbiotic origin of mitochondria, a single event may be an over-simplification. Indeed, several major components of the mitochondrial transcription and replication machinery, including the DNA and RNA polymerases, are derived from the T-odd lineage of bacteriophage (Shutt and Gray, 2006). The T-odd lineage include T3 and T7 bacteriophages and their close relatives and are known to infect γ-proteobacteria, it has therefore been proposed that some mitochondrial genes were acquired from an ancestral T-odd phage. Whether these genes were acquired by the ancestral α-proteobacteria prior to the endosymbiosis event or in the early evolution of the eukaryotic cell is still a matter of debate (Shutt and Gray, 2006). In the same manner, the timing of the mitochondrial endosymbiosis event in relation to the evolution of the nucleus is also uncertain. Initially it was proposed that the α-proteobacteria was endocytosed by a nucleus-containing amitochondriate eukaryotic cell, whereas more recently it was proposed that mitochondria and the nucleus evolved simultaneously after fusion of an archaebacterium and an α-proteobacterium (reviewed in Gray et al., 1999; Lang et al., 1999), effectively being the origin of eukarya.

Since all nucleated eukaryotic cells (with limited exceptions) contain mitochondria, and the acquisition of mitochondria appears to have been a singular occurrence in evolution, it is reasonable to assume that the endosymbiotic relationship provided an advantage against a strong selection pressure. Initially it was thought that the aerobic respiration of

the α-proteobacteria provided the host with ATP and that the symbiont received organic substrates in return. However, only two parasitic bacteria are known to have an ATP transporter, and in both cases these act as ATP importers (Kurland and Andersson, 2000). On this basis it is difficult to see the immediate benefit of the symbiont to the host if ATP was not made available. One possibility is that the aerobic α-proteobacteria detoxified the cytosol of the host by consuming oxygen (OX-Tox model). The OX-Tox theory is supported by the fact that atmospheric oxygen levels rose dramatically over 200 million years approximately 2 billion years ago (Holland et al., 1994), which would have increased the oxidative stress on anaerobic bacteria. The endosymbiosis event is also predicted to have occurred between 1.5 and 2 billion years ago, which lends credence to the OX-Tox model (Kurland and Andersson, 2000; Gray et al., 1999).

The initial observations in favour of the endosymbiosis hypothesis included the double membrane structure of mitochondria, which could have been formed by endocytosis, and the presence of mitochondrial DNA (mtDNA), which resembled bacterial DNA (Margulis, 1971). Since that time mtDNA has been shown to vary widely in size, genes encoded and form (circular or linear) between species and even more so between more distant taxons. The size of the mitochondrial genome ranges from <6kpb in *Plasmodium falciparum* (Gray et al., 1999) to approximately 16kbp in mammals (Bibb et al., 1981; Anderson et al., 1981), approximately 100kbp in fungi (*Trametes cingulata*) (Haridas and Gantt, 2010) and over 500kbp in the case of several plants (Kitazaki and Kubo, 2010), reaching 2400kbp in muskmelon (Ward et al., 1981). Further, the number of mitochondrially encoded proteins range from 3 (*P. falciparum*) to 67 (*Reclinomonas americana*) in known species, and the mtDNA encoding of tRNAs and 5S rRNA is also not universal (Gray et al., 1999).

Generally, mitochondrial genomes are smaller than the genome of the closest modern relative, the α-proteobacteria *R. prowazekii* (1,111,523bp), which in turn is predicted to be smaller than the ancestral α-proteobacteria (Gray et al., 1999). Most metazoan mitochondrial genomes are very compact, with few non-coding regions. This is in contrast to many plant mitochondria, including angiosperms, which have larger mitochondrial genomes with many non-coding, repeated regions (Kitazaki and Kubo, 2010). However, even in the case of angiosperms, there are far fewer protein coding genes in the mitochondrial genome compared to free living bacteria (Gray et al., 1999;

Kitazaki and Kubo, 2010). This is thought to be a consequence of loss of redundant genes or relocation of genes to the nuclear genome of the host from the original α-proteobacteria. This reduction in genome size has occurred to varying degrees in different species (reviewed in Adams and Palmer, 2003).

Due to this variety in the mitochondrial genome and the fact that all of my research has focused on human mitochondria, for clarity, this report will only refer to features of human mitochondria from this point onwards, unless otherwise specified.

1.3 MITOCHONDRIAL STRUCTURE

Mitochondria have two membranes and have at least four distinct compartments; the outer mitochondrial membrane (OMM), inner mitochondrial membrane (IMM), inter-membrane space (IMS) and the matrix (Figure 1.1).

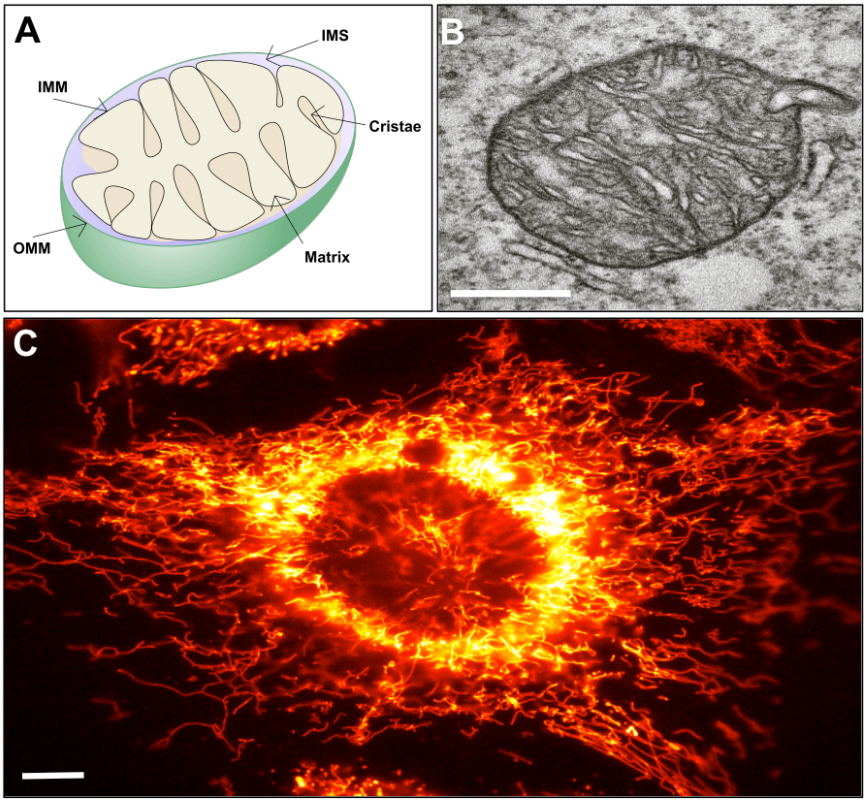

Figure 1.1: Mitochondrial Structure. (A) Diagram depicting the intra-organellar compartments of the mitochondrion: the outer mitochondrial membrane (OMM, green), the inter-membrane space (IMS, purple), the inner mitochondrial membrane (IMM, black line) and mitochondrial matrix (beige). The IMM folds, forming structures called cristae. The cristae (or intracristal space) can be considered as a fifth compartment as the protein composition can differ between the IMS and intracristal space. **(B)** Image of a single mitochondrion captured using electron microscopy. Scale bar = 500nm (image courtesy of Rawaa AliZahid). **(C)** An image illustrating the mitochondrial network of a U2OS cell. Mitochondria were stained with 5nm TMRM and visualised by fluorescent microscopy Scale bar = 10μm (own image).

The OMM is permeable to small molecules and ions of up to approximately 5000Da (Benz, 1994; Mannella, 1992), allowing them to pass into the IMS. This permeability is mediated primarily by the presence of porins (also known as voltage dependent anion channels, VDAC), which are transmembrane, 19 stranded β-barrel structured pores that mediate trafficking of ions and interact with members of the Bcl-2 family to prevent the release of apoptogenic proteins into the cytosol (Hiller et al., 2008).

The IMM is more selective and is not as permeable as the OMM, a feature that is essential for maintaining the mitochondrial membrane potential (Ψ_m). The maintenance of Ψ_m is vital to allow the proton gradient to drive ATP synthesis by the OXPHOS system, which consists of five multi-protein complexes situated in the IMM. The difference in permeability between the IMM and the OMM is due to the different protein content, but also to the phospholipid content of each membrane. The IMM has a much higher proportion of cardiolipin. Indeed, it is debated whether the OMM has any cardiolipin at all (de Kroon et al., 1997; Gerbert et al., 2009) and recent data suggests translocation of cardiolipin to the OMM acts as a signal of mitochondrial damage and targets defective mitochondria for elimination by mitophagy (Chu et al., 2013). Cardiolipin is a predominantly IMM specific phospholipid and is implicated in a wide range of functions (reviewed in Osman et al., 2010).

The permeability of each mitochondrial membrane is not an entirely fixed value. For example, the pore size of porin (VDAC1) is variable depending on the voltage across the OMM and can exist in open or closed forms (Mannella, 1992; Benz, 1994). Additionally, porin overexpression can increase the permeability of the IMM (Tomasello et al., 2009). This results in reduced Ψ_m, swelling of the matrix via osmosis and rupture of the OMM, permitting the release of cytochrome *c* into the cytosol, which is a major mechanism for inducing apoptosis.

The IMM forms folds called cristae to allow a larger surface area for reactions to take place. It is only more recently that the cristae (or intracristal space) have been seen as a separate compartment from the IMS. The relative protein composition can differ between the cristae and the IMS due to the presence of cristae junctions (CJs) (Jourdain and Martinou, 2009). CJs effectively form a collar-like structure at the base of the cristae, which limits the passage of proteins between the cristae and the IMS. OPA1 (optic atrophy 1), mitofilin and the recently characterised ChChd3 (coiled-coil-helix-

coiled-coil-helix domain containing 3) have been shown to be present at CJs and regulate their opening (Darshi et al., 2011). Cytochrome *c* content differs between the IMS and the cristae. There is a minor pool of cytochrome *c* in the IMS, but the major pool is located in the cristae. Increased permeability of the OMM will allow cytochrome *c* release, but as long as the CJs remain closed then only the minor pool can enter the cytosol. In this case, the concentration of cytochrome *c* in the cytosol is too low to activate the apoptotic cascade (Jourdain and Martinou, 2009). This is one line of evidence for viewing the IMS and cristae as separate compartments.

The mitochondrial matrix is enclosed by the IMM and is the site for most of the reactions that take place in mitochondria including, but not limited to, the citric acid cycle, β-oxidation of fatty acids and iron-sulphur cluster formation. The matrix also houses the mtDNA and all of the replication, transcription and translation machinery. Due to the lack of permeability of the IMM, all required proteins and small molecules are imported through an array of membrane proteins. The import of mitochondrial proteins is primarily carried out by the TOM and TIM complexes (translocase of the outer membrane and translocase of the inner membrane respectively), but there are several other mechanisms of import, which I will discuss later.

In addition to transport proteins and OXPHOS subunits the mitochondrial membranes also contain the fission and fusion machinery, which will now be discussed further.

1.4 MITOCHONDRIAL DYNAMICS

Mitochondria are not individual static organelles as depicted in many textbooks; they form dynamic networks that undergo fission and fusion. The classical cross sectional images (as in Figure 1.1A and B) show mitochondria as individual oval shaped organelles simply because they were first identified by electron microscopy on cross sections of cells. Although electron microscopy images are useful for visualising the intra-organellar sub-compartments of mitochondria, they are not representative of mitochondria throughout the cell. Fission and fusion events form fluid, tubular networks of mitochondria throughout healthy cells (Huang et al., 2011) as shown in Figures 1.1C and 1.2. Evidence indicates that mitochondria are also dynamic in that they can move around the cell in response to energy requirements (Nekrasova et al., 2011). The cytoskeleton is important for this mitochondrial motility. Vimentin intermediate fibres

and microtubules have both been shown to associate with mitochondria (Liu et al., 2009; Tang et al., 2008) and depletion of vimentin results in mitochondrial fragmentation (Tang et al., 2008).

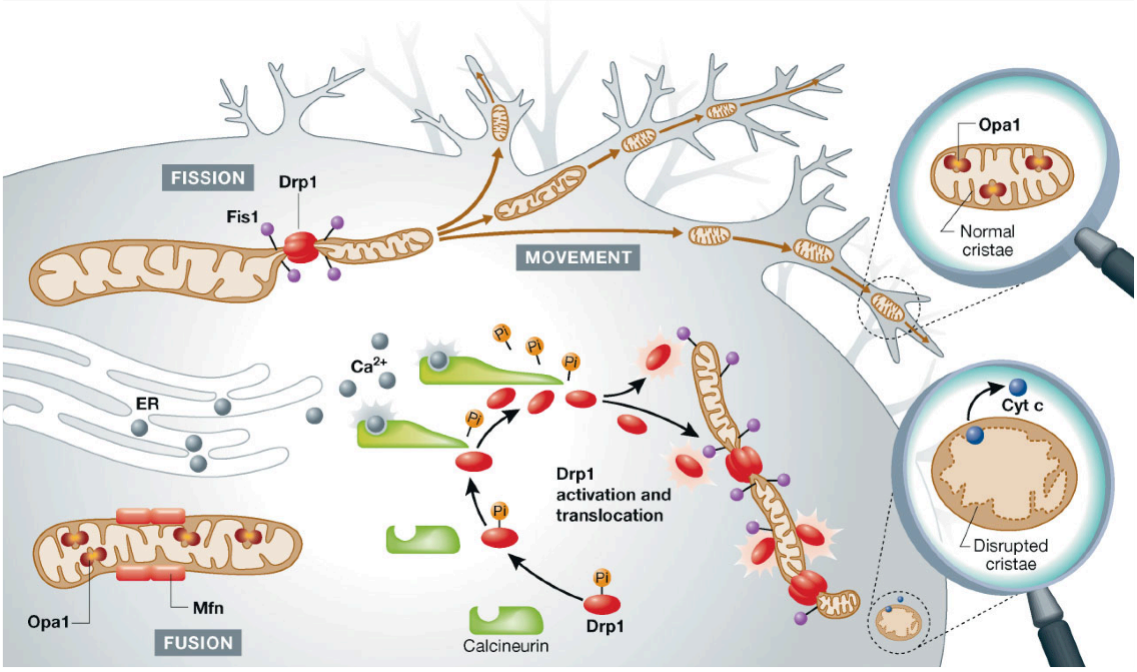

Figure 1.2: Mitochondrial Dynamics. Diagram depicting the dynamic nature of mitochondria in neurons. Drp1 and Fis1 are involved in mitochondrial fission. OPA1 and mitofusins (Mfn) are important for mitochondrial fusion. OPA1 is also involved in cristae formation. Activation of calcineurin by Ca^{2+} promotes dephosphorylation of Drp1 causing translocation to the mitochondria, where it promotes fission and cristae disruption, which can lead to cytochrome *c* release and activate apoptosis. (Image adopted from Oliveira and Lightowlers, 2010).

Two proteins playing crucial roles in mitochondrial fusion are mitofusin 1 and mitofusin 2 (Mfn1 and Mfn2). These are characterised as large GTPases that are present in the OMM and act in concert with OPA1. The latter has at least eight splice variants resulting in various protein isoforms that can be either long (l-OPA1) or short (s-OPA1) (Delettre et al., 2001). OPA1 is found in the IMS but due to the additional hydrophobic domain, l-OPA1 isoforms can also integrate into the IMM (Ishihara et al., 2006). It has been shown that l-OPA1 and s-OPA1 functionally complement each other and have minimal fusion activity alone (Song et al., 2007). Due to the location in the IMM and IMS, OPA1 co-ordinates IMM fusion, whereas the mitofusins are responsible for the fusion of the OMM. Recently it has been shown that mitochondria undergo both transient and complete fusion (Liu et al., 2009). Transient fusion only allows exchange of soluble proteins between two mitochondria in close proximity, whereas complete fusion allows the combining of membrane proteins and mixing of mtDNA populations

(Liu et al., 2009). This allows exchange of proteins and mtDNA between mitochondria when coupled with subsequent fission events. The cytoskeleton partly determines which form of fusion occurs, as two motile mitochondria on separate microtubules can undergo transient fusion, but only those on the same microtubule can undergo complete fusion (Liu et al., 2009). The same machinery governs both transient and complete fusion, but transient fusion can take place when OPA1 levels are either too high or too low to permit complete fusion (Liu et al., 2009).

Dynamin related protein 1 (Drp1) is also a large GTPase located in the OMM, which contrastingly plays an important role in mitochondrial fission. Mitochondrial fission factor (Mff) also regulates fission, and was originally thought to work independently of the other known fission proteins (Gandre-Babbe and van der Bliek, 2008) in the IMM. However recent evidence suggests that Mff is essential for Drp1 recruitment (Otera et al., 2010) and is tail anchored in the OMM (Huang et al., 2011). MTP18 (mitochondrial protein 18kDa) also promotes mitochondrial fragmentation in the OMM, and is also required for fission homologue 1 (Fis1) mediated fission (Tondera et al., 2005).

Mitochondrial dynamics are essential to healthy cell function. This is highlighted by their association with the intrinsic apoptosis system (reviewed in Landes and Martinou, 2011) and the fact that mutations in genes that are known to be involved in fission or fusion can cause disease (reviewed in Knott and Bossy-Wetzel, 2008). For example OPA1 mutations lead to a form of dominant optic atrophy (Alexander et al., 2000) and Mfn2 mutations are the primary cause of Charcot-Marie-Tooth subtype 2A (CMT2A), which is a peripheral neuropathy (Züchner et al., 2004). These examples clearly show that dysfunctional mitochondrial dynamics can lead to disease.

Mitochondrial dysfunction is also commonly seen in the early stages of many neurodegenerative disorders including Alzheimer's disease (AD), Parkinson's disease (PD), Huntington's disease (HD), stroke and epilepsy (Knott and Bossy-Wetzel, 2008). Both amyloid beta (Aβ) (which accumulates in AD) and rotenone (which causes PD-like symptoms in mice) have been shown to induce mitochondrial fragmentation, which indicates that the mitochondrial fragmentation could be a secondary effect rather than being causative of these diseases. However, the link between neurodegenerative disorders and dysfunctional mitochondrial dynamics remains interesting, particularly in the case of AD. A recent study showed that the expression of mitochondrial fusion

proteins (OPA1, Mfn1 and Mfn2) is reduced, whilst expression of fission proteins (Drp1 and Fis1) is increased in AD patients (Manczak et al., 2011). Furthermore, this study demonstrated co-localisation of Aβ with Drp1, thus suggesting a strong link between dysfunctional mitochondrial dynamics and AD (Manczak et al., 2011).

1.5 MITOCHONDRIAL FUNCTIONS

The origins and structure of mitochondria have been discussed. I will now outline a number of the functional roles of the organelle including, the regulation of apoptosis, the citric acid cycle and iron-sulphur cluster (Fe-S) cluster formation. A key role of mitochondria is the production of ATP via the OXPHOS system, as this provides approximately 90% of the usable energy to cells (Harris and Das, 1991).

1.5.1 OXIDATIVE PHOSPHORYLATION

The OXPHOS system consists of 5 multi-subunit complexes embedded in the IMM, namely NADH:ubiquinone oxidoreductase (Complex I), succinate:ubiquinone oxidoreductase (Complex II), ubiquinol:cytochrome *c* oxidoreductase (Complex III), cytochrome *c* oxidase (Complex IV) and F_OF_1 ATP synthase (Complex V).

Put simply, Complexes I and II transfer electrons from reduced cofactors (NADH and $FADH_2$ respectively) to ubiquinone (Q), causing its reduction to ubiquinol (QH_2), which is delivered to Complex III. Complex III then oxidises QH_2 to Q and reduces cytochrome *c*, effectively passing electrons from one to the other. Complex IV oxidises cytochrome *c* and reduces ½ O_2 to H_2O. Transfer of electrons by complex I, III and IV cause protons to by pumped into the IMS from the matrix, and together, Complexes I-IV constitute the electron transport chain (ETC). The proton gradient generated by the ETC provides an electrochemical force and it is this proton motive force (driven by chemiosmosis) that is utilised by Complex V to produce ATP (Mitchell, 1961).

The basic components of the OXPHOS system are illustrated in Figure 1.3; however, the organisation of the complexes and the movement of electrons and protons through the ETC is far more complicated than depicted by this figure. The organisation of the respiratory complexes within the IMM has long been debated, particularly whether the complexes are tightly associated with each other (forming supercomplexes), or whether

the respective complexes are independent units linked only by the fluid movement of coenzyme Q and cytochrome *c* (reviewed in Acin-Perez and Enriquez, 2014).

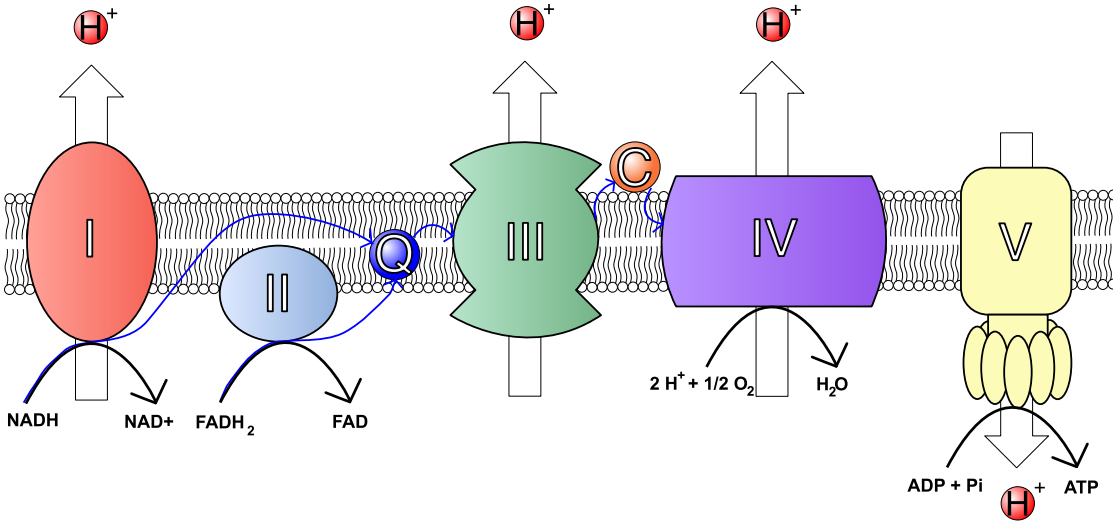

Figure 1.3: The OXPHOS System. Illustration of the major components of the OXPHOS system in the IMM: Complex I (red), Complex II, (light blue), Complex III (green), Complex IV (purple) and Complex V (yellow). The co-factors coenzyme Q (labelled 'Q', dark blue) and cytochrome *c* (labelled 'C', orange) as well as the protons (labelled H^+, dark red) are depicted as spheres. The flow of electrons is shown as blue arrows and the direction of the translocation of protons shown by white arrows. Chemical reactions are shown below the respective complexes in the mitochondrial matrix. Abbreviations: NAD=nicotinamide-adenine dinucleotide, FAD=flavin-adenine dinucleotide, ADP=adenosine diphosphate, ATP=adenosine triphosphate, Pi (inorganic phosphate).

Mammalian Complex I is an approximately 980kDa multi-protein complex that was found to consist of 45 subunits, as analysed by tandem mass spectrometry (Carroll et al., 2006; Hirst et al., 2003). Seven of these subunits are encoded by mtDNA (Chomyn et al., 1985; Chomyn, 2001). NADH is bound and oxidised to form NAD^+ plus 2 free electrons by Complex I via non-covalently bound flavin mononucleotide (FMN) (Sazanov, 2006; Vogel et al., 2007; Hirst, 2005). These electrons are passed through a cascade of up to 9 Fe-S clusters before reducing Q to QH_2 (Sazanov, 2006; Papa et al., 2012; Vogel et al., 2007). Complex I uses the redox energy to pump protons from the matrix into the IMS at a stoichiometry of 4 protons per NADH oxidised (Galkin et al., 2006).

Complex II (also known as succinate dehydrogenase (SDH)) is the only respiratory complex that comprises solely nuclear-encoded components. The four subunits of Complex II are SDHA, SDHB, SDHC and SDHD. The catalytic core of Complex II is made up of SDHA and SDHB, which are hydrophilic and extend into the mitochondrial matrix (Rutter et al., 2010). The complex is anchored into the inner membrane by

SDHC and SDHD. SDHA oxidises succinate to fumarate and transfers the electrons to the covalently bound flavin adenine dinucleotide (FAD), thus reducing FAD to form $FADH_2$. Complex II then re-oxidises $FADH_2$ and passes electrons through 3 Fe-S clusters in SDHB, before the SHDC/SDHD subunits transfer electrons to Q, thus reducing Q to QH_2 (Rutter et al., 2010). Unlike Complex I, Complex II mediated reduction of Q is not coupled to proton transfer across the IMM (Rutter et al., 2010).

Complex III is approximately 480kDa in size and consists of 11 different subunits, only one of which, cytochrome *b*, is mtDNA-encoded (Saraste, 1999). Complex III dimerises and has a catalytic core comprising cytochrome *b*, cytochrome *c* and the Rieske Fe-S cluster protein (Mulkidjanian, 2010). The net transfer of electrons through Complex III is from QH_2 (forming Q) to the electron carrier, cytochrome *c*, thus reducing it via a process called the Q cycle (Mitchell, 1975; Cramer et al., 2011). The transport of each electron through Complex III is coupled to the translocation of 2 protons across the IMM (Mulkidjanian, 2010).

The terminal oxidase of the ETC is Complex IV, which oxidises the reduced cytochrome *c* from the Q cycle in Complex III (Capaldi, 1990). The electrons are passed through heme *a* and copper centres before reducing oxygen to water in a process that pumps 4 protons from the matrix to the IMS for each O_2 reduced (Papa et al., 2012). Mammalian Complex IV was thought to have 13 different protein subunits based on SDS-PAGE separation (Kadenbach et al., 1983) and crystal structure data (Tsukihara et al., 1996). However, recent data suggests that NDUFA4 is a structural subunit of Complex IV rather than Complex I, as previously thought (Balsa et al., 2012). Therefore, current knowledge indicates that there are 14 subunits of Complex IV and 44 subunits of Complex I (Balsa et al., 2012). Complex IV forms a dimer where two monomers are connected by a cardiolipin molecule, and is considered the active form of the enzyme (Tsukihara et al., 1996; Fontanesi et al., 2006). Only 3 subunits of Complex IV are encoded by mtDNA, namely COXI, COXII and COXIII (Capaldi, 1990; Papa et al., 2012).

Complex V, the ATP synthase, consists of two main subunits, F_O and F_1, each of which comprise multiple proteins (reviewed in Yoshida et al., 2001). The electrochemical gradient across the IMM, produced by the proton pumping action of Complex I, II and IV, drives protons through the F_O subunit of Complex V causing it to rotate (Noji et al.,

1997). The F_1 subunit rotates in the opposite direction and this intricate rotary mechanism ultimately allows production of ATP from ADP and P_i (reviewed in Kinosita, 2012).

1.5.2 Citric Acid Cycle

The citric acid cycle is another important mitochondrial function. The ETC is coupled to the citric acid cycle. The initial sources of electrons at the start of the ETC are in the form of reduced cofactors (NADH and $FADH_2$, Figure 1.3). These co-factors are partly provided by the actions of the citric acid cycle.

Pyruvate, derived from sugars in the cytosol via glycolysis, is imported into the mitochondrial matrix. Here, it is subjected to oxidative decarboxylation by the pyruvate dehydrogenase complex to form acetyl-CoA (acetyl coenzyme A). This provides the starting point for the citric acid cycle, which produces three NADH molecules and one $FADH_2$ molecule per each complete oxidation of acetyl-CoA (reviewed in Ochoa, 2006).

1.5.3 Iron-Sulphur Cluster Formation

The mitochondrion is also responsible for the production of Fe-S clusters. This is a vital function as these clusters are present in numerous metalloproteins that are used in many fundamental pathways. Examples include: subunits of Complex I, II and III of the ETC, aconitase that is essential to the citric acid cycle, DNA polymerases and ferredoxins (Reviewed in Rawat and Stemmler, 2011; Lill, 2009). One of the most biologically advantageous features of Fe-S clusters is their ability to accept or donate electrons (Sheftel et al., 2010). It has been suggested that Fe-S cluster formation is the principle function of the mitochondrion based on the evolutionary conservation of the process. Fe-S cluster synthesis is retained even in the most rudimentary mitochondria-like organelles, such as *Giardia* mitosomes and *Trichomonas* hydrogenosomes, whereas OXPHOS is not, suggesting that Fe-S cluster formation is the most vital function of mitochondria (reviewed in Embley and Martin, 2006; Lill and Mühlenhoff, 2005).

1.5.4 APOPTOSIS

Apoptosis can be induced by a variety of factors including oxidative stress from ROS, decrease in Ψ_m, growth factor withdrawal or DNA damage (Landes and Martinou, 2011). There are two major apoptotic pathways, of which mitochondria are involved in the intrinsic pathway that involves Bax and Bak, two pro-apoptotic members of the B-cell lymphoma 2 (Bcl2) family (Jourdain and Martinou, 2009). When activated, the mitochondrial permeability transition pore (mtPTP) can open, causing a collapse of Ψ_m and swelling of the matrix (Kinnally et al., 2011). This ruptures of the OMM, releasing IMS proteins into the cytosol. The IMS protein cytochrome *c* activates the caspase cascade to degrade proteins, whilst the IMS proteins endonuclease G and apoptosis inducing factor (AIF) are thought to be translocated to the nucleus where they condense and degrade chromatin DNA (Li et al., 2001; Lindenboim et al., 2011). There are other mitochondrial apoptotic factors such as Smac/Diablo (second mitochondrial activator of caspases/direct IAP binding protein with low pI) and HtrA2/Omi (reviewed in Vaux, 2011). OPA1 can also affect the apoptotic process through its regulation of CJ opening. As mentioned earlier, the major pool of cytochrome *c* is sequestered in the cristae, but the minor pool is present in the IMS. During apoptosis the OMM is broken down releasing the minor pool of cytochrome *c*, which is not always sufficient to activate the caspase cascade. Over expression of OPA1 is protective against apoptosis because it keeps the CJs tightly closed, thus preventing the release of the major pool of cytochrome *c* into the cytosol after OMM rupture (Frezza et al., 2006). In contrast, siRNA depletion of OPA1 causes leaky CJs, resulting in higher levels of cytochrome *c* release and increases the likelihood of activating the caspase cascade and inducing apoptosis (Olichon et al., 2003).

From the topics discussed above, it is clear that mitochondria have a role in many vital processes within the cell and that a comprehensive review of all of these processes is beyond the scope of this introduction. My studies were concerned with mitochondrial gene expression, so that is what I will now discuss, starting on the topic of the mitochondrial genome itself.

1.6 MITOCHONDRIAL DNA

In humans, mtDNA (Figure 1.4) is a double-stranded circular genome of 16,569bp that is supercoiled and encodes only 13 polypeptides, 22 tRNAs and 2 ribosomal RNAs (rRNAs) (Anderson et al., 1981; Ojala et al., 1981; Falkenberg et al., 2007). The two strands of mtDNA are designated heavy (H-strand) and light (L-strand) because of the H-strands higher intrinsic buoyant density in alkaline caesium chloride gradients owing to its greater guanine nucleotide content. The H-strand is also the location of the majority of mitochondrial genes, with only *MT-ND6* and 8 of the tRNA genes encoded on the L-strand (Anderson et al., 1981).

As mentioned previously (section 1.2) the mitochondrial genome has greatly reduced in size and number of genes compared to the ancestral α-proteobacteria, though mtDNA of different species varies wildly (Gray et al., 1999). In humans, the only proteins encoded by mtDNA are 13 hydrophobic components of the OXPHOS system. All other genes that were present in the ancestral α-proteobacteria, allowing life as an independent organism, have either been lost or translocated to the nuclear genome. During the estimated 1500 million years of mitochondrial evolution (Sicheritz-Ponten 1998), human mtDNA has become incredibly compact with very few non-coding regions, no introns and only a few base pairs separating many of the genes. Indeed, there are two cases of overlapping genes, namely *MT-ND4/MT-ND4L* and *MT-ATP6/MT-ATP8*. The only non-coding region of significant size (approximately 1100bp) contains the displacement loop (D-loop), which houses regulatory sequences for controlling both replication and transcription (described later) and has a triple-stranded structure.

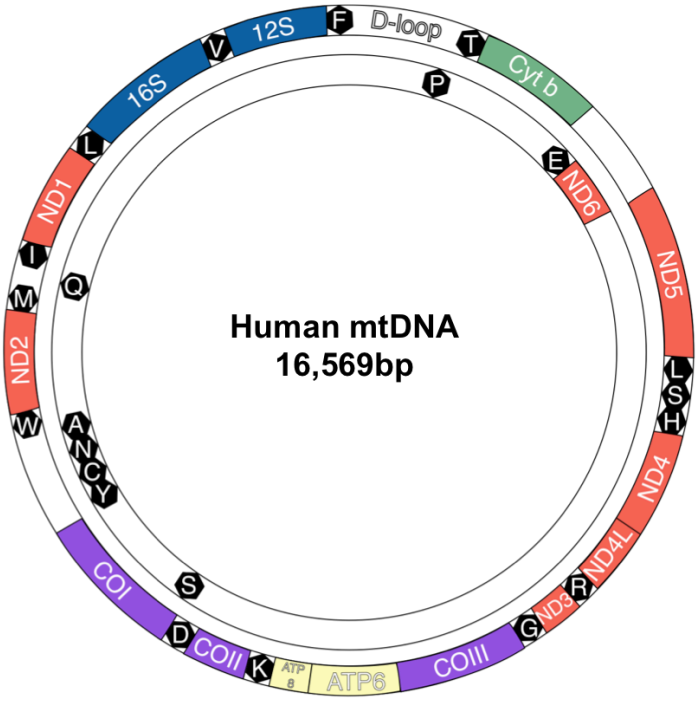

Figure 1.4: The Human Mitochondrial Genome. Genes are labelled and are colour coded to identify genes encoding subunits of Complex I (red), Complex III (green), Complex IV (purple) and Complex V (yellow). The rRNA genes are shown in blue and the tRNA genes are depicted as black hexagons with their respective single letter code. The origins of replication (O_H and O_L) and transcriptional promoters (HSP and LSP) are labelled with arrows depicting their position and direction.

There are many copies of mtDNA in each cell. However the copy number varies dramatically between cell types. For example, HeLa cells have been described as having approximately 8000 copies of mtDNA per cell (Bogenhagen and Clayton, 1974) compared to cultured mouse cell lines that have approximately 1300 (Nass, 1969; Bogenhagen and Clayton, 1974), though the average mtDNA copy number varies between tissues (Veltri et al., 1990). In humans, mature oocytes contain over 150,000 copies of mtDNA (Wai et al., 2010), but the copy number is very variable, with reports of over 1,500,000 copies in a single oocyte (Greggains et al., 2014). Fibroblasts on the other hand, average approximately 1600 copies of mtDNA per cell, which is over 2 orders of magnitude fewer than the average for oocytes (Greggains et al., 2014).

The mechanism of inheritance of mtDNA differs from nuclear DNA in that it is generally solely maternally inherited, though a very rare instance of paternal inheritance has been documented (Schwartz and Vissing, 2002). Cells can be homoplasmic, where all mtDNA molecules are identical. However, mutations in mtDNA can cause heteroplasmy, where two variant populations of mtDNA exist within one cell. A number of mutations are pathogenic and can lead to mitochondrial dysfunction, causing disease (Holt et al., 1989; Wallace, 1989; Saneto and Sedensky, 2013). The

heteroplasmic level of the pathogenic mutated mtDNA can vary i) between mitochondria, as mtDNA is exchanged during fusion and fission; or ii) between cells as, during mitosis, mitochondria are randomly segregated into the daughter cells. The higher severity of clinical presentation correlates with higher ratios of mutant to wild-type mtDNA (Chinnery et al., 1997), thus the presence of a mutation alone is not enough to predict a clinically pathological condition as low levels of mutated mtDNA may not cause disease. The particular mutation has a bearing on the severity of disease for example large deletions or mutations in tRNA genes will affect mitochondrial gene expression more than a single point mutation in one of the protein encoding genes. The levels of mutant heteroplasmy must generally reach a high percentage to manifest clinically. This is termed the threshold effect. The threshold effect of most mtDNA mutations is approximately 70-90% (Rossignol et al., 2003), though can vary between tissues (Rossignol et al., 1999). However, a functionally dominant mutation in the $tRNA^{Trp}$ gene has been described that manifested clinically at <25% mutant heteroplasmy (Sacconi et al., 2008).

The mtDNA is housed in the mitochondrial matrix, but it is not naked, it is protected by DNA-binding proteins that package the mtDNA into structures called nucleoids. The composition of mitochondrial nucleoids is a hotly contested topic, with the distinction between a nucleoid-associated protein and a *bona fide* nucleoid component being difficult to demonstrate (Bogenhagen, 2012; Bogenhagen et al., 2014). It is clear however that the major, if not only, essential component of the nucleoid is TFAM (mitochondrial transcription factor A) (Kukat and Larsson, 2013), which can bind and bend mtDNA without sequence specificity (Fisher et al., 1992). Nucleoids are not static packages of DNA, they are dynamic and allow access to the DNA replication and transcription machinery (Spelbrink, 2010). Therefore, studies that have isolated mammalian mtDNA and identified associated proteins as components of nucleoids may only be seeing peripheral proteins that themselves are not integral to nucleoid formation (see Bogenhagen, 2012 for a review).

1.7 MITOCHONDRIAL GENE EXPRESSION

Mitochondrial gene expression involves many processes that include, but are not limited to the replication and maintenance of mtDNA, the transcription and subsequent processing, maturation and degradation of mitochondrial mRNA, mitochondrial protein synthesis, assembly of the mtDNA-encoded proteins into their respective respiratory complexes and even protein import of all of the nuclear-encoded mitochondrial proteins involved in these processes. Each of these can exert control over mitochondrial gene expression and I will therefore briefly outline these processes below.

1.7.1 MITOCHONDRIAL DNA REPLICATION

The process of mtDNA replication is still a matter of debate. The original model of strand-displacement (Robberson and Clayton, 1972; Berk and Clayton, 1974; Clayton, 1982) is still favoured, however it is possible that replication occurs in more than one distinct way. More recently proposed models of mtDNA replication are the strand-coupled bidirectional model (Bowmaker et al., 2003) and the RITOLS (ribonucleotide incorporation throughout the lagging strand) model (also referred to as the bootlace model) (Holt and Reyes, 2012; Reyes et al., 2013).

The major replication machinery is common to all models and includes the mitochondrial DNA polymerase γ (POLγ), the mitochondrial helicase TWINKLE and the mitochondrial single-strand binding protein (mtSSB). The mitochondrial RNA polymerase (POLRMT) is also required to synthesise the RNA primers to initiate DNA synthesis (Xu, 1996; Wanrooij et al., 2008). POLγ functions as a heterotrimer that consists of the POLγA catalytic subunit and two POLγB accessory subunits. TWINKLE is a 5' to 3' DNA helicase and is found as a stable hexamer or heptamer (Ziebarth et al., 2010; Makowska-Grzyska et al., 2010). The role of mtSSB is to bind, protect and stabilise ssDNA during the course of mtDNA replication and enhances the helicase activity of TWINKLE (Korhonen et al., 2003).

DNA replication using only mitochondrial components has been successfully reconstituted *in vitro*. This work showed that 2kb of ssDNA could be produced using only POLγ and TWINKLE proteins in addition to the basic substrates (Korhonen et al., 2004). The synthesis of over 16kb was possible with the addition of mtSSB (Korhonen et al., 2004), which covers the length of the mitochondrial genome, showing that these

three proteins are the minimum required for full mtDNA replication. However, as mentioned, POLRMT would also be required *in vivo* to produce the required primers (Wanrooij and Falkenberg, 2010).

The strand-displacement (or strand-asynchronous) model states that replication is initiated at O_H and elongation proceeds uni-directionally. After 700bp, POLγ often stalls at the cis-acting TAS site forming a D-loop where the DNA becomes triplex (Falkenberg et al., 2007). The function of the triplex D-loop is still unknown (Wanrooij and Falkenberg, 2010; Nicholls and Minczuk, 2014). If the polymerase continues beyond the TAS site, it proceeds about two thirds of the way around the mtDNA molecule until it reaches the region termed O_L where the lagging strand forms a stem loop structure that prevents mtSSB binding (Shadel and Clayton 1997). This stem loop structure allows initiation of L-strand replication in the opposite direction (Wanrooij and Falkenberg, 2010). Both strands are then fully synthesised before each of their respective 5' and 3' ends are ligated to form closed circles (Falkenberg et al., 2007).

One of the alternative hypotheses is that the mitochondria replicate their DNA symmetrically in a more conventional system, where the leading and lagging strand are synthesised simultaneously from bi-directional origins of replication within the noncoding region (strand-coupled model) (Holt et al., 2000). There is evidence for both models and it is possible that both mechanisms occur under different physiological conditions (Holt et al., 2000). More recent data, however, further reinforces the strength of the strand-displacement model as mutations in O_L were selected against in an mtDNA mutator mouse model compared to mutations in tRNA genes, *COXI* (cytochrome *c* oxidase gene I) and non-coding regions (Wanrooij et al., 2012). The mutator mouse is a knock-in mouse that expresses a catalytic subunit of POLγ that has deficient proof-reading ability, causing mtDNA mutations and deletions to occur with 3-5 fold higher frequency than wild-type mice (Trifunovic et al., 2004). If the strand-coupled model was the principle mechanism of mtDNA replication then O_L would not be important and it would be expected that mutations in the O_L would be tolerated in these mice. Therefore, the fact that O_L mutations are not tolerated strongly suggests that O_L is critically needed for mtDNA replication as would be hypothesised by the strand-displacement model.

A third proposed model is the RITOLS or bootlace model, which proposes that mtSSB is a minimal influence in replication and that much if not all of the single-stranded lagging strand is bound instead by RNA (reviewed in Holt and Reyes, 2012).

Although the exact mechanism of lagging strand mtDNA replication is still debated, it is clear that leading strand synthesis is initiated at O_H. The RNA primer for the initiation of mtDNA replication at O_H is produced via transcription initiated at the light strand promoter (LSP), which is also situated in the D-loop region (Falkenberg et al., 2007; Clayton, 1982). This involvement of the mitochondrial transcription machinery in mtDNA replication highlights that different aspects of mitochondrial gene expression, as displayed in this report, are not necessarily separate entities.

1.7.2 MITOCHONDRIAL TRANSCRIPTION

The single subunit RNA polymerase, POLRMT, is responsible for mitochondrial transcription. However, POLRMT cannot initiate transcription from mitochondrial promoters alone, transcription factors TFAM and either TFB1M or TFB2M (mitochondrial transcription factor B 1 and 2 respectively) are required for mitochondrial transcription *in vitro* (Falkenberg et al., 2002). This study also showed that TFB2M is an order of magnitude more active than TFB1M at activating transcription (Falkenberg et al., 2002). Therefore the contribution of TFB1M to transcription initiation *in vivo* becomes questionable. Indeed, *in vivo* experiments in mice (Metodiev et al., 2009) and drosophila (Matsushima et al., 2005) suggest TFB1M does not play a role in mitochondrial transcription, unlike TFB2M (Matsushima et al., 2004). More recent *in vitro* experiments failed to observe any transcription activation activity of TFB1M (Litonin et al., 2010). Loss of TFB1M has been shown to affect mitochondrial translation (Matsushima et al., 2005; Metodiev et al., 2009). Both TFB1M and TFB2M have been identified as similar to RNA methyltransferases (Seidel-Rogol et al., 2003) and subsequent indirect evidence suggest that they function as such, although TFB1M is believed to be far more active than TFB2M (Seidel-Rogol et al., 2003; Cotney and Shadel, 2006). Furthermore, TFB1M was recently implicated in the methylation of two highly conserved adenines towards the 3' end of the 12S rRNA (Metodiev et al., 2009). Methylation of these adenine residues was found to be important for the stability of mitochondrial ribosomes (mitoribosomes), and therefore translation (Metodiev et al., 2009). Current evidence therefore suggests that TFB1M is

not acting as a transcription factor in mitochondria and that POLRMT, TFAM and TFB2M comprise the essential machinery of mitochondrial transcription initiation (Figure 1.5).

Transcription is initiated independently at the respective LSP and heavy strand promoter (HSP) (Figure 1.5). There are two HSP initiation sites, HSP1 and the somewhat controversial HSP2 situated less than 100 bases apart in the D-loop (Micol et al., 1997). Transcription initiated at HSP1 starts 5' to the phenylalanine mt-tRNA gene and terminates at the 3' end of the 16S rRNA gene and has been suggested to only transcribe 2 tRNAs and the 2 rRNAs. Transcription initiated at HSP2 on the other hand is postulated to produce a long polycistronic transcript that begins at the 5' end of the 12S rRNA gene and includes all of the rRNA, tRNA and mRNA encoded by the H-strand. Similarly transcription from the LSP produces a polycistronic transcript corresponding to the genes on the L-strand. The LSP is also situated in the D-loop, but transcribes in the opposite direction to the HSP. In HeLa cells, the transcription of the rRNA genes was found to be 50 to 100 times more common than transcription of the mRNAs (Gelfand and Attardi, 1981), indicating the HSP1 promoter is more active than HSP2. Recently the activity of the HSP2 promoter has been questioned since, *in vitro*, no HSP2 specific transcripts were observed, nor could POLRMT transcribe from pre-melted promoter templates of HSP2 despite being able to transcribe from HSP1 or LSP (Litonin et al., 2010). However, recent work has now demonstrated transcription form HSP2 *in vitro* using recombinant POLRMT and TFB2M, but found that it is strongly inhibited by addition of TFAM (Lodeiro et al., 2012). The discovery of a potential transcriptional activator and repressor role of TFAM when using different promoters, further complicates the current understanding of mitochondrial transcription and highlights the difficulty in elucidating the *in vivo* situation.

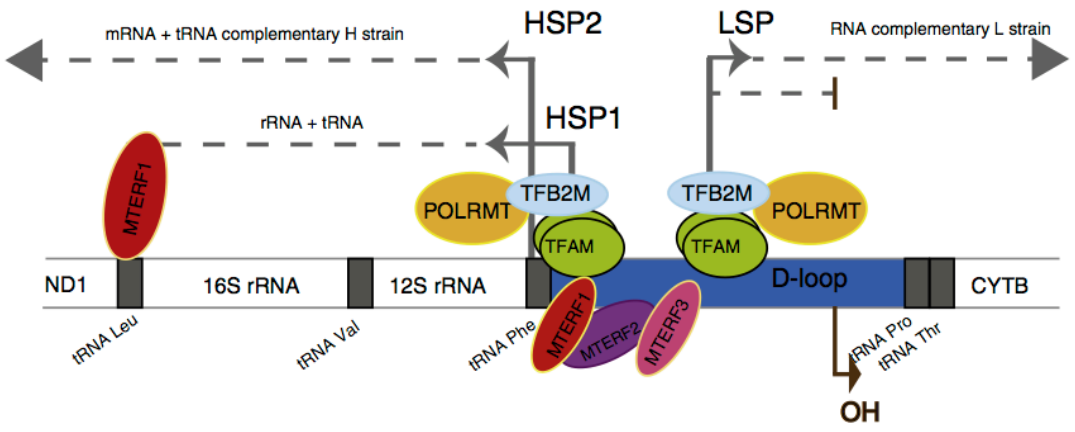

Figure 1.5: The Mitochondrial Transcription Machinery. Transcription initiation requires the recruitment of TFAM TFB2M and POLRMT. MTERF 1-3 also bind the promoter region and modulate transcription. Initiation at HSP1 results in transcription of $tRNA^{Phe}$, $tRNA^{Val}$ and the two rRNAs 12S and 16S, before terminating at the $tRNA^{Leu}$ gene bound to MTERF1. Initiation form HSP2 however continues to transcribe the full length of the H-strand. Similarly initiation at LSP transcribes the full-length mtDNA, but in the opposite direction. Additionally transcription from LSP can be terminated shortly after initiation and the short RNA is used as a primer for H-strand DNA replication from OH (origin of H-strand replication). Image adopted from Peralta et al., 2012.

The specific method of transcription initiation in mitochondria is uncertain, but evidence suggests that TFAM binds to the promoter region, upstream of the initiation site and bends the DNA to a greater degree than non promoter DNA (Malarkey et al., 2012) and that this is required for initiation. This is the case for HSP1 and LSP, but TFAM is inhibitory to transcription from HSP2 (Lodeiro et al., 2012), thus complicating the mechanism of initiation. Recent structural and biochemical observations suggest that, of the components of transcription initiation, only TFAM and POLRMT can interact, albeit weakly, in the absence of DNA (Yakubovskaya et al., 2014). The same study shows that the addition of promoter DNA allows formation of a dense initiation complex, in which TFAM, POLRMT and TFB2M come into close proximity and may interact via protein-protein interactions, although the DNA is the clear anchoring point (Yakubovskaya et al., 2014). After initiation, POLRMT proceeds to transcribe almost the entire mtDNA molecule, forming large polycistronic mRNAs from HSP2 and LSP Transcription must be terminated, but the mechanism is poorly understood and only the HSP1 initiated transcript has a proven termination site located at the first $tRNA^{Leu}$ gene (between the 16s rRNA gene and *MT-ND1*) (Figure 1.5).

Since the transcription of mitochondrial genes generates polycistronic units, the unit will require post-transcriptional processing before its constituents can be translated into protein. The tRNA punctuation model suggests that the polycistronic transcript is

processed following folding and cleavage of the tRNAs that are encoded between the mRNAs (Ojala et al., 1981). Since full-length polycistronic RNAs are not usually observed *in vivo* it is likely that this processing takes place during or shortly after transcription. Most mRNAs have at least one tRNA between them. The tRNA portions of the polycistronic RNA form a secondary structure that allows 5' cleavage by the endoribonuclease mitochondrial RNase P (Ojala et al 1981, Holtzmann et al 2008) and 3' cleavage by ELAC2, which functions as the mitochondrial RNase Z (Brzezniak et al., 2011; Rossmanith, 2011; Vogel et al., 2005). This model will account for most of the separating of the tRNAs and mRNAs, but cannot be the sole system as there is not a tRNA gene between every protein encoding gene, for example *MT-ATP6* and *MT-CO3* (Anderson et al., 1981, reviewed in Temperley et al., 2010a).

Generally, mitochondrial mRNA transcripts differ from nuclear transcripts in that they have no introns, have very short (<3 nucleotides) or absent 5' untranslated regions (UTRs) and no 5' 7-methylguanylate cap. Furthermore, the majority do not have 3' UTRs. In fact, in the case of 7 open reading frames the 'stop' codon is incomplete and therefore 3' polyadenylation is required to complete the termination codons. All mitochondrial mRNAs and tRNAs undergo maturation. Polyadenylation of mRNAs is performed by the mitochondrial poly(A) polymerase (mtPAP) (Gallerani et al., 1976; Tomecki et al., 2004), resulting in frayed polyadenylation of approximately 50 nucleotides. The tRNAs are matured by a post-transcriptional addition of a CCA motif by the ATP(CTP):tRNA nucleotidyltransferase (Nagaike et al., 2001).

1.7.3 MITOCHONDRIAL TRANSLATION

Translation is the process of protein synthesis through conversion of the mRNA code into polypeptides. As is the case in eubacteria and the cytosol, protein synthesis begins with methionine encoded by AUG, however, human mitochondria can also recognise AUA and AUU as initiating methionines (Rustin et al., 1997; Anderson et al., 1981). This is an example of one of the differences between the 'universal' and the mitochondrial code used for protein synthesis; in the cytosol AUA and AUU would encode isoleucine. Additionally, several other codons differ from their 'universal' code. The conventional 'stop' codon UGA is re-coded to be recognised as tryptophan and the two 'universal' arginine codons AGG and AGA were assumed to act as 'stop' codons (Anderson et al., 1981). Recent data, however, has indicated that they are not 'stop'

codons, but simply unassigned codons that promote a -1nt frameshift that results in a standard UAG termination codon becoming positioned in the A site (Temperley, et al., 2010b).

In mitochondria, protein synthesis takes place on mitoribosomes. Mitoribosomes are more closely related to eubacterial ribosomes than eukaryotic cytosolic ribosomes (Desmond et al., 2011), but the evolution of mitoribosomes has been dynamic and the composition has changed drastically from its α-proteobacterial origin. Approximately 50% of MRPs have eubacterial orthologs and are evolving at 10 times the rate of the cytosolic ribosome proteins (O'Brien, 2002). Most ribosomes have a composition of approximately 70% RNA and 30% protein by mass. This is completely reversed in mammalian mitoribosomes to approximately 30% RNA and 70% protein (Koc and Haque, 2010). Mitoribosomes have a greater mass than their eubacterial counterparts but are far less dense, due to numerous parts of the rRNAs not being replaced by protein. A number of mitoribosomal proteins (MRPs) have functionally replaced some rRNAs that have been lost relative to their prokaryotic origin.

The increase in protein content, more porous and less dense nature of mitoribosomes causes a change in sedimentation with respect to other ribosomes. Thus, the mammalian mitoribosome is a 55S particle compared to the 80S or 70S particles of eukaryotic cytosolic or bacterial ribosomes respectively. The 55S mitoribosomes consist of a 28S small subunit (SSU) and a 39S large subunit (LSU). As with most ribosomes, there is an A-site (aminoacyl-tRNA site) and a P-site (peptidyl-tRNA site) (Schmeing and Ramakrishnan, 2009). Eubacterial and cytosolic eukaryotic ribosomes also have an E-site (exit site), but mounting evidence suggests this is either weak or absent from mitoribosomes (Sharma et al., 2003) or at least considerably altered, probably to aid in the insertion of the nascent peptides into the IMM (Greber et al., 2014). Indeed, in mitochondria, translation is sensitive to IMM integrity and it has been demonstrated that that approximately 50% of mitoribosomes are tightly associated with the IMM (Liu and Spremulli, 2000). Recent data suggests that MRPL45 may act as an anchor to align the nascent polypeptide exit tunnel with the membrane insertion machinery (Greber et al., 2014). Mature MRPL32 is also tightly associated with the IMM and the maturation of MRPL32 by the *m*-AAA protease is required for mitochondrial protein synthesis (Nolden et al., 2005).

There are only 22 mitochondrial tRNAs encoded by mtDNA (Anderson et al., 1981) and there is no import of nuclear-encoded tRNAs (Kolesnikova, 2004). Thus, there are fewer tRNA species in mitochondria than the 31 predicted by Crick to be necessary for translation. This is possible because mitochondria use slight variations to the rules of translation, due to the loss of discrimination with the wobble base (Barrell et al., 1980). Modifications to the base in the wobble position are required for certain tRNAs, for example $tRNA^{Lys}$ has a modified uridine (5-taurinomethyl-2-thiouridine) at the wobble position of its anticodon (Umeda et al., 2005). The 2-thio modification is carried out by MTU1 (mitochondrial tRNA-specific 2-thiouridylase 1) in yeast and is essential for mitochondrial protein synthesis (Umeda et al., 2005). In addition to $tRNA^{Lys}$, 5-taurinomethyluridine is also present in $tRNA^{Leu}$, $tRNA^{Glu}$ and $tRNA^{Gln}$ and is important for mitochondrial protein synthesis (Schaffer et al., 2014). Indeed, mutations that interfere with the formation of 5-taurinomethyluridine can lead to mitochondrial disease (MELAS and MERRF) (Schaffer et al., 2014). Another difference between the tRNA content in mitochondria compared to the cytosol is that there is only one $tRNA^{Met}$ for both initiation and elongation in animal mitochondria, whereas there are two distinct $tRNA^{Met}$s in the cytosol (Mikelsaar, 1983). Formylation of the methionine tRNA ($tRNA^{fMet}$) is still required for initiation of translation in mitochondria, as in numerous other systems (Bianchetti et al., 1971). Mitochondrial $tRNA^{fMet}$ binds initiation factor 2 (IF2) to initiate translation (Spencer and Spremulli, 2004). The unformylated $tRNA^{Met}$ is used in translation elongation. Mitochondrial methionyl-tRNA formyltransferase (mtFMT) is responsible for the formylation of $tRNA^{Met}$ to $tRNA^{fMet}$ (Takeuchi et al., 2001).

Translation has four distinct stages: initiation, elongation, termination and ribosome recycling (Figure 1.6). Most mitochondrial translation factors have been named to correspond to their eubacterial homologues, but despite the eubacterial origins of mitochondria and their presence in the eukaryotic cytosol, there are differences between these translation systems, some of which are outlined below.

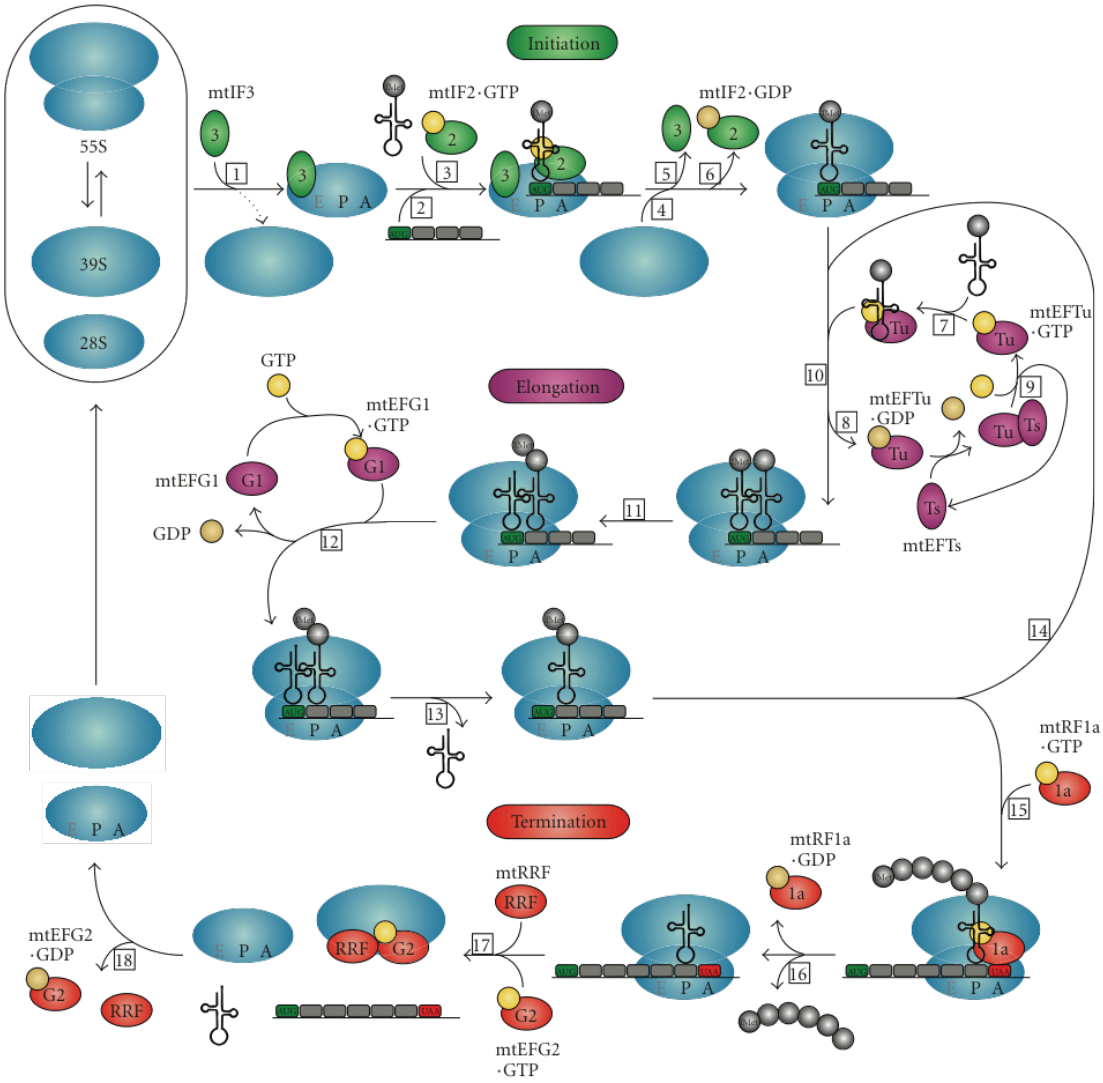

Figure 1.6. Mitochondrial Translation. Diagram of the stages of mitochondrial translation including initiation (green), elongation (purple) and termination (red). The factors involved in each stage are depicted (more detailed information in text) including the stages that require GTP (yellow) hydrolysis to GDP (beige). Image adopted from Smits et al., 2010.

Initiation: In prokaryotes, initiation requires IF1, IF2 and IF3. Of these, IF1 and IF2 are considered universal and essential, as IF3 is not found in the eukaryotic cytosol (Marintchev and Wagner, 2004). Mitochondrial translation differs because only IF2 and IF3 homologues have been found, but mtIF2 was shown to functionally replace both bacterial IF1 and IF2 (Gaur et al., 2008). This appears to be due to the insertion of a conserved 37aa sequence in mtIF2 (Ma et al., 1995), which allows binding to the mitoribosome, therefore assuming the role of IF1 (Gaur et al., 2008). In mitochondria, the initiation of translation is partially mediated by mtIF3, which binds to the 28S SSU, preventing and/or disrupting formation of the 55S (Koc and Spremulli, 2002; Christian

and Spremulli, 2009). This allows the subsequent binding of mtIF2, $tRNA^{fMet}$ and the mRNA. Since the mitochondrial mRNAs essentially have no 5'UTR (up to 3 nucleotides) it is assumed that translation begins at the start codon at the 5' terminus. Supporting this is data where mRNAs with longer 5' UTRs were not translated as efficiently and the formation of the initiation complex was favoured at a terminal AUG rather than an internal AUG (Christian and Spremulli, 2010). A stable initiation complex is only generated when GTP-bound mtIF2 binds $tRNA^{fMet}$, the SSU and mRNA start codon. Without the start codon and/or $tRNA^{fMet}$ the mRNA continues to pass through the SSU and eventually dissociates (Christian and Spremulli, 2010). If $tRNA^{fMet}$ binds the 5' AUG start codon, the LSU is recruited, forming the monosome. The GTP bound to mtIF2 is hydrolysed to GDP and the initiation factors are released. The 55S initiation complex can then proceed to the elongation phase.

Elongation: All three prokaryotic elongation factors namely EFTu, EFTs and EFG have homologues in mitochondria (Xin et al., 1995; Lang et al., 1999; Hammarsund et al., 2001). However, there are two mtEFGs (mtEFG1 and mtEFG2) (Hammarsund et al., 2001). Only mtEFG1 is functional in elongation and is needed for translocation of the mRNA through the ribosome (Bhargava et al., 2004), while mtEFG2 seems to be primarily involved in ribosome recycling (Tsuboi et al., 2009). The elongation process begins with GTP-bound mtEFTu, which is active and can bind an aminoacylated tRNA and allow it to enter the A-site of the mitoribosome. If the anticodon of the tRNA correctly matches the codon on the mRNA, then GTP is hydrolysed and mtEFTu-GDP is released. A peptide bond is formed between the aminoacylated tRNA in the A site and the amino acid at the end of the nascent polypeptide chain in the P-site. This is catalysed by the peptidyl-transferase centre of the LSU and results in the deacylation of the tRNA in the P-site. The new peptidyl tRNA (with the peptide one amino acid longer) in the A-site is then translocated to the P-site, which is driven by GTP hydrolysis from mtEFG1-GTP to mtEFG1-GDP, and results in the displacement of the deacylated tRNA from the P-site. Finally mtEFTs acts as a guanine exchange factor that facilitates the activation of mtEFTu-GDP to mtEFTu-GTP to allow another cycle of elongation to occur. The process described above is based on current knowledge of mitochondrial translation elongation (as reviewed in Christian and Spremulli, 2012).

Termination and ribosome recycling: termination occurs when a 'stop' codon enters the A-site and elongation cannot proceed. Only two triplets are used as stop codons in human mitochondria, UAA and UAG, and there is only one release factor (mtRF1a) that recognises both of these stop codons (Soleimanpour-Lichaei et al., 2007). The recognition of the stop codon by mtRF1a catalyses the cleavage of the ester bond between the terminal amino acid of the nascent polypeptide and the tRNA in the P site in a process that requires GTP hydrolysis (Smits et al., 2010; Christian and Spremulli, 2012). After release of the completed polypeptide, mitochondrial ribosome recycling factor (mtRRF) (Rorbach et al., 2008) and mtEFG2 (also known as mtRRF2) (Tsuboi et al., 2009) bind the A-site and cause the release of the mRNA and deacylated tRNA as well as dissociation of the SSU and LSU (Christian and Spremulli, 2012). This then allows another round of translation to initiate, with the binding of mtIF3 preventing reassembly of the monosome until the initiation complex is reformed (Christian and Spremulli, 2009).

There are still aspects of mitochondrial translation that remain enigmatic. For example, very little is known about the regulation of translation in human mitochondria. In yeast there are translational activators for each mRNA that usually bind the 5' UTR of the transcripts (Herrmann et al., 2013). However, human mitochondria do not have 5' UTRs and only one translational activator, TACO1, has been described, which activates synthesis of COXI (Weraarpachai et al., 2009). It is possible that there could be a family of translation activators yet to be identified that may further elucidate the control of mitochondrial protein synthesis.

1.8 MITOCHONDRIAL PROTEIN IMPORT

Approximately 1500 proteins are estimated to be necessary to generate functional mitochondria. Nuclear-encoded proteins account for 99% of these mitochondrial proteins and are synthesised in the cytosol before being imported into the mitochondria by a variety of mechanisms (reviewed in Endo et al., 2011). Therefore, mitochondrial import is vitally important for all of the mitochondrial processes. There is complex machinery in the mitochondria dedicated to protein sorting and import. Important components of this machinery are the translocases of the outer membrane (TOM) and inner membrane (TIM). Almost all imported proteins are translocated through the outer membrane by the TOM complex, which is made up of various TOM proteins (including

Tom20, 70, 71, 5, 6, 7, 22, 40) (reviewed in Chacinska et al., 2009). The essential pore forming member of the TOM complex is Tom40 (Ahting et al., 2001).

Most imported proteins have an N-terminal mitochondrial targeting sequence, particularly those that are sub-localised to the matrix or IMM. Such targeting sequences generally do not share sequence homology, but form positively charged amphipathic α-helices (Roise and Schatz, 1988). After import through the TOM complex the TIM23 complex sorts and allows import of the N-terminally targeted matrix proteins (Endo et al., 2011). This type of targeting sequence is usually cleaved off after import by the mitochondrial processing peptidase (MPP) in the matrix (Ou et al., 1989; Taylor et al., 2001). In contrast, the N-terminal mitochondrial targeting sequence of MRPL32 is cleaved by the *m*-AAA protease after translocation across the membrane rather than being cleaved during import by the MPP (Bonn et al., 2011). This highlights one exception to the classical import pathway.

There are other import pathways in mitochondria, and many IMM proteins, soluble IMS proteins and OMM proteins do not have N-terminal cleavable pre-sequences, but contain targeting sequences more centrally within the protein (see Chacinska et al., 2009 for a review). The main pathways in addition to the TOM and TIM complexes are the SAM (Sorting and Assembly Machinery of the Outer Mitochondrial Membrane) complex that allows integration of β-barrel containing OMM proteins and the MIA (Mitochondrial Intermembrane Space Import and Assembly) pathway that allows import of IMS proteins that have cysteine-containing signals (Chacinska et al., 2009).

1.9 MITOCHONDRIAL DISEASE

As previously mentioned, mitochondrial disease can be caused by mutations in the mitochondrial genome (reviewed in Taylor and Turnbull, 2005, Pinto and Moraes, 2014). Mutations in the protein encoding mitochondrial genes typically manifest as isolated complex deficiencies. However, mitochondrial diseases are a heterogeneous group of disorders and there are many instances of multiple respiratory complex deficiencies (Kemp et al., 2011). These combined complex deficiencies can be due to mtDNA mutations, for example tRNA mutations leading to generalised mitochondrial translation defects (Pinto and Moraes, 2014), or can be due to mutations in nuclear genes encoding any factors involved in mitochondrial gene expression (reviewed in

Smits et al., 2010). There are many examples of mutations in nuclear genes products leading to mitochondrial disease, including factors involved in mitochondrial translation such as the elongation factors, mtEFTs (Smeitink et al., 2006), mtEFTu and mtEFG1 (Vallente et al., 2007) or mitoribosomal proteins, MRPS16 (Miller et al., 2004) and MRPS22 (Saada et al., 2007) among others.

Due to the heterogeneity of mitochondrial disorders, the molecular aetiology remains unknown in many patients with mitochondrial disease. Recent developments in next generation sequencing, including exome sequencing have allowed identification of mutations in some of these patients (Calvo et al., 2012). In some cases exome sequencing of patients with mitochondrial disease has allowed identification of novel gene products important for mitochondrial function. For example several patients with isolated Complex III deficiency have been shown to have causative mutations in TTC19 (Ghezzi et al., 2011, Morino et al., 2014). Identification of TTC19 mutations in patients with mitochondrial disease allowed for characterisation of the protein as a Complex III assembly factor (Ghezzi et al., 2011). In this way, patients with mitochondrial disease can provide further information as to the factors and mechanisms involved in mitochondrial gene expression. For instance, mutations in mtFMT were found in two patients with Leigh syndrome, which showed that formylation of $tRNA^{Met}$ was important for mitochondrial translation in humans (Tucker et al., 2011), despite mtFMT not being essential for translation in yeast mitochondria (Hughes et al., 2000).

There remain many patients without a genetic diagnosis of mitochondrial disease and by elucidating novel factors involved in mitochondrial gene expression we may be able to further elucidate the processes at work, perhaps leading to potential treatments.

1.9 IDENTIFICATION OF NUCLEAR-ENCODED MITOCHONDRIAL PROTEINS

It is thought that around 15% of the predicted 1500 nuclear-encoded mitochondrial proteins are yet to be identified (Calvo, 2010). Several methods are used to identify such proteins, including algorithms to predict the likelihood of classic N-terminal mitochondrial targeting sequences, such as TargetP (Emanuelsson et al., 2007; 2000), MitoProt II (Claros and Vincens, 1996) or Predator (Small et al., 2004). However, as discussed earlier, there are several mechanisms by which mitochondria import proteins,

hence finding N-terminal pre-sequences will not uncover all of the mitochondria-destined proteins. Another method used is mass spectrometry, which has also identified mitochondrial proteins, where purified mitochondrial proteins were separated using 2D gels and then peptide mass fingerprinting was used to identify particular proteins (Rabilloud et al., 1998; Scheffler et al., 2001). This approach requires very sophisticated machinery and still has a tendency to include contaminant proteins that are not necessarily mitochondrial (Calvo, 2010). There are other methods of identifying mitochondrial proteins, but the most reliable and accurate is to use a combined approach that takes data from all of these sources and scores them to allow predictions of how likely certain proteins are to be mitochondrial.

MitoCarta is a database that uses an integrated approach (Pagliarini et al., 2008) (www.broadinstitute.org/pubs/MitoCarta/human.mitocarta.html). To generate the MitoCarta inventory, mass spectrometry was performed on mitochondria isolated from 14 different mouse tissues and mitochondrial localisation was assessed on a large scale by GFP-tagging and fluorescent microscopy (Pagliarini et al., 2008). The results from these experiments were integrated with bioinformatics approaches including; i) Target P predictions (Emanuelsson et al., 2007), ii) BlastP searches to identify mammalian homologues of known yeast mitochondrial proteins, iii) BlastP searches to identify homologues of *R. prowazekii* proteins, iv) identification of proteins with mitochondrial-specific Pfam domain and v) evidence from literature. Maestro scores are also included on the MitoCarta inventory. Maestro uses a similar Bayesian integrated approach to predict mitochondrial localisation (Calvo et al., 2006). These approaches were compiled into a list of 1098 mouse genes, which are likely to encode mitochondrial proteins (Pagliarini et al., 2008). A human MitoCarta inventory was then produced by identifying human HomoloGene homologues to the mouse MitoCarta collection (Pagliarini et al., 2008).

The data from the human MitoCarta database was used by my host laboratory to identify a list of 224 proteins that are both likely to be mitochondrial and potentially had a role in mitochondrial gene expression, but were largely of undefined function (compiled by Prof R. N. Lightowlers). A screen of these candidate proteins was performed using three different siRNAs targeted to each gene. Depletion (via siRNA) of the transcripts encoding each candidate protein was performed in both HeLa cells and Rho^0 cells. Rho^0 cells lack mtDNA (King and Attardi, 1989) and can therefore grow in

the absence of factors uniquely involved in maintaining or transcribing mtDNA, translating the resultant mRNA or proteins modifying rRNA/tRNAs. If depletion of a particular protein, with at least two of the three siRNAs, caused significant growth or morphology changes in HeLa cells, but not in Rho^0 cells, then that protein was classified as one of those most likely to be both mitochondrial and involved in mitochondrial gene expression (initial siRNA screen performed by Dr J. Rorbach). Thirty-three candidate proteins fulfilled these criteria and were selected for further study (Figure 1.7A).

One optimal siRNA sequence was chosen for each of the 33 genes on the basis of a significant growth defect in Hela cells with no or little growth defect in Rho^0 cells. To give an indication at what stage a defect in mitochondrial gene expression maybe occurring, the levels of mtDNA (as described in 2.3.11) were assessed by qPCR (Figure 1.7). Transcription of mtDNA was estimated by measuring *MT-CO1* mRNA levels using qPCR (Figure 1.7). To investigate translation, [^{35}S]-labelled methionine ([^{35}S]met) was used. Cells were pulse labelled for 1 hour with [^{35}S]met in the presence of emetine, which inhibits cytosolic translation. As translation occurs the [^{35}S]met was incorporated into newly synthesised proteins. Following a three-hour chase with unlabelled methionine, proteinaceous material was precipitated with trichloroacetic acid (TCA) and incorporated radioactivity was measured by scintillation counting as a crude indictor of mitochondrial translation (Figure 1.7). Lower levels of [^{35}S]met incorporation in siRNA treated samples may indicate a role in translation or post transcriptional processing for that candidate protein. O_2 consumption of the cells was measured using Seahorse XF analyser, in order to assess the function of the OXPHOS system (Figure 1.7).

These preliminary data were generated by Dr P. M. Smith and indicated that AURKAIP1 depleted cells show increased mtDNA copy number, but reduced mRNA levels, [^{35}S]met incorporation and O_2 consumption. SLMO2 depleted cells show normal levels of mtDNA and mRNA, but reduced [^{35}S]met incorporation and O_2 consumption. Of the 33 candidate proteins studied further, siRNA-mediated depletion of AURKAIP1 and SLMO2 (also known as c20orf45), caused particularly severe phenotypes in HeLa cells (Figure 1.7B), without any effects on Rho^0 cells, For these reasons, my thesis aimed to focus on these two proteins, each of which will be discussed briefly below.

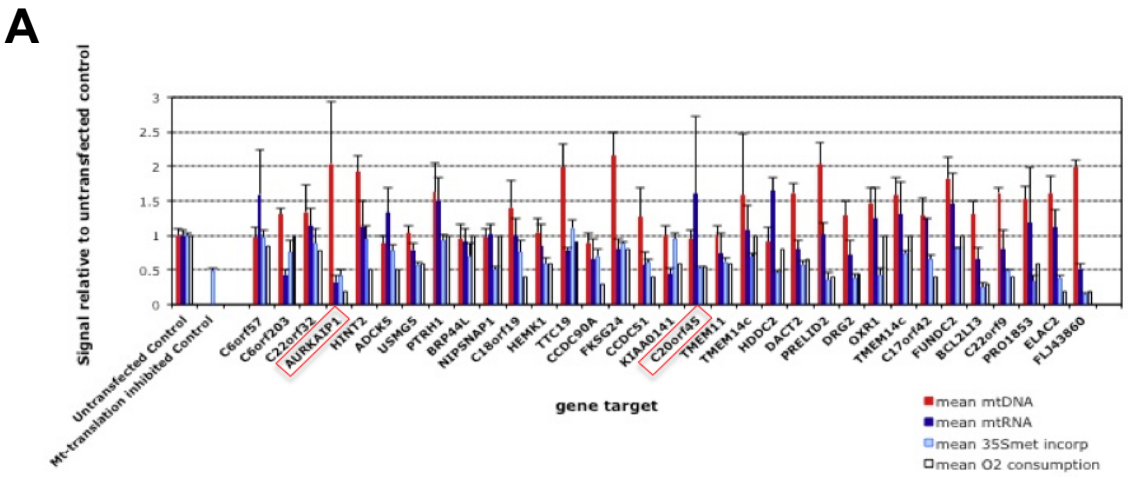

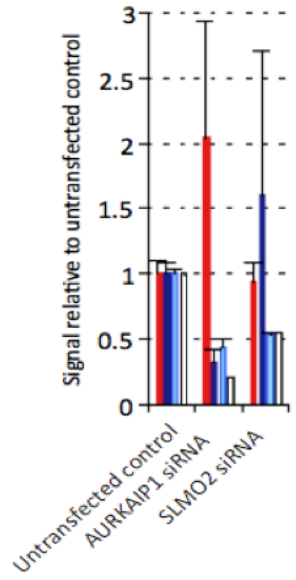

Figure 1.7: Effect on Mitochondrial Metabolism Following Depletion of 33 Mitochondrial Candidate Proteins. A) siRNA depletion of each candidate protein was performed in HeLa cells, after which, mtDNA copy number (red), mRNA levels (dark blue), [S^{35}]met incorporation (light blue) and O_2 consumption (white) were measured. The proteins to be studied in this project, AURKAIP1 and SLMO2 (c20orf45), are highlighted in red boxes. **B)** Enlarged depliction of AURKAIP1 and SLMO2, for ease of viewing.

1.10 SLMO2

SLMO2 is a homologue of the SLMO protein in *Drosophila* (Dee and Moffat, 2005) and is a PRELI domain containing protein. Although the PRELI domain itself is of unknown function, it is highly conserved across species, including a family of yeast proteins called Ups (Sesaki, 2006). Ups proteins have been shown to be important in maintaining the phospholipid content of mitochondria with Ups1 being significant in maintaining normal cardiolipin (CL) levels (Potting et al., 2010).

Involvement in Regulation of Cardiolipin?

CL is an essential phospholipid that is mainly located in the inner membrane of mitochondria (Chang et al., 1998a). CL is thought to be important in diverse functions such as protein import (Gerbert et al., 2009), mitophagy (Chu et al., 2013) and cytochrome *c* oxidase function (Hoffmann et al., 1994; Tsukihara et al., 1996; Fontanesi et al., 2006). CL is synthesised from phosphatidic acid via CDP-diacylglycerol, PGP (phosphatidylglycerolphosphate) and PG (phosphatidylglycerol). There are many enzymes involved in the synthesis of CL, of which most yeast and bacterial homologs are known (Chang et al., 1998b; Osman et al., 2010; 2011).

In yeast, the PRELI domain-containing Ups proteins seem to regulate the phospholipid content of the mitochondria. Cells lacking Ups1 (*Δups1*) have much less CL whereas *Δups2* cells have more CL but less phosphatidylethanolamine (PE) (Osman et al., 2009; Tamura et al., 2009). Recently, Mdm35 has been shown to aid in the import of Ups proteins and binds them stably in the IMS (Tamura et al., 2010; Potting et al., 2010).

Evidence for Mitochondrial Localisation

SLMO2 is one of at least 4 PRELI domain-containing proteins encoded by the human genome (Herrmann, 2010). PRELI domain-containing proteins in yeast are known to be mitochondrial proteins; therefore it is likely that SLMO2 is also mitochondrial. Furthermore, SLMO2 is included in the human MitoCarta database based on the yeast homologues and microscopy of GFP-tagged protein (Pagliarini et al., 2008). Data from the siRNA screen showed SLMO2 depleted cells still have normal levels of mtDNA and mRNA, but less [^{35}S]met incorporation indicating a possible defect in protein synthesis. These data suggest a role for SLMO2 in mitochondrial gene expression (Figure 1.7).

During the course of my studies, it became apparent that SLMO2 was a protein being investigated by another group. This, coupled with problems in generating soluble protein expression, and expression cell lines led me to focus my thesis primarily on AURKAIP1.

1.11 AURKAIP1

AURKAIP1 (Aurora Kinase A Interacting Protein) has previously been described as a nuclear protein involved in targeting Aurora-A kinase for degradation via a proteasome dependent - ubiquitin independent pathway (Lim et al., 2007). However, there is a report to the contrary that suggests AURKAIP1 actually promotes stability of Aurora-A kinase (Katayama et al., 2007). These data also suggest nuclear localisation of AURKAIP1, but these observations were derived from a FLAG-tagged construct of AURKAIP1 where the FLAG-tag was added at the N-terminus (Lim et al., 2007). As mentioned previously, many mitochondrial proteins have cleavable N-terminal pre-sequences that direct subcellular localisation. By altering the N-terminus of the protein it is likely that AURKAIP1 had been aberrantly targeted and mitochondrial localisation has been disrupted.

Bioinformatics approaches, including Target P, have identified AURKAIP1 as being likely to contain an N-terminal mitochondrial targeting sequence (Emanuelsson et al., 2007). AURKAIP1 is also one of the 1013 proteins in the human MitoCarta database, which lists proteins with strong evidence of mitochondrial localisation based on various analytical criteria including analysis of pre-sequence, and subcellular localisation by GFP-tagging and fluorescence microscopy (Pagliarini et al., 2008). Furthermore, preliminary data generated in my host laboratory prior to my investigations, inferred that AURKAIP1 depletion had no effect on mtDNA copy number, but led to a decrease in mRNA (qPCR on *MT-CO1*), *de novo* mitochondrial protein synthesis and O_2 consumption. These data are suggestive of a protein involved in mitochondrial gene expression.

1.12 AIMS

As illustrated throughout this introductory chapter, there are many facets of mitochondrial gene expression that remain to be elucidated. The siRNA screen performed in my host laboratory was used to identify proteins that were likely to be involved in mitochondrial gene expression, with a view to furthering our understanding of gene expression in human mitochondria. As discussed earlier, AURKAIP1 was a strong candidate for further study based on preliminary data and my thesis will focus on the characterisation of AURKAIP1 and its potential role in mitochondrial gene expression.

More specifically, the aims of these studies were as follows:

- To express and purify recombinant AURKAIP1 to use as an antigen for antibody production

- To produce stable human cell lines capable of expressing C-terminal FLAG-tagged AURKAIP1

- To use these tools to determine whether AURKAIP1 is mitochondrial, and if so, the sub-mitochondrial localisation

- To characterise the phenotype of AURKAIP1 depletion, with a view to identifying any critical role of AURKAIP1 in mitochondrial gene expression

- To identify binding partners of AURKAIP1 via immunoprecipitation to elucidate potential functions of AURKAIP1.

CHAPTER 2: GENERAL MATERIALS AND METHODS

2.1 CELL CULTURE

2.1.1 MAMMALIAN CELL LINES

Flp-In™ TREx™ 293 Cell Line: Human Embryonic Kidney (HEK) cell line commercially available from Life Technologies. This cell line constitutively expresses the Tet repressor and has an integrated Flp Recombinase target (FRT) site to allow specific Flp Recombinase mediated integration of a gene of interest into the host genome (Further details on the Flp-In™ TREx™ sytem are discussed in Section 3.1 and the method of generating stable overexpressing cell lines outlined in Section 4.2.1). For the rest of the text these cells will be referred to simply as HEK293 cells as no other HEK293 cell line variant was used in experiments detailed in this report.

Flp-In™ TREx™ U2OS Cell Line: A Flp-In™ TREx™ cell line derived in the same way as the HEK293 cells. However the host cells were of U2OS origin, which is an osteosarcoma cell line. This cell line was kindly donated by Dr Nick Watkins. These cells will be referred to simply as U2OS cells throughout the remaining text.

HeLa Cell Line: Cell line derived from Henrietta Lacks cervical cancer cells.

143B Cell Line: A human osteosarcoma cell line.

143B.206 Rho^0 Cell Line: 143B cells were depleted of mtDNA via ethidium bromide treatment. This line was produced as described in (King and Attardi, 1989) and will be referred in the text as Rho^0 cells.

2.1.2 GENERAL CELL CULTURE AND MAINTENANCE

All cell culture work was carried out in a class II Microflow cabinet with reagents from Sigma Aldrich unless otherwise indicated. Cells were monitored daily using the Axiovert25 microscope (Zeiss).

All cells were propagated at 37°C and in a humidified 5% CO_2 atmosphere. Cells were cultured in monolayers in vented tissue culture flasks (TPP or Corning) or 6-well plates

(Cellstar, Greiner Bio One or TPP). HeLa cells were cultured in Eagle's Minimal Essential Media with Earle's salts containing 2mM L-glutamine (EMEM, M4655) supplemented with 10% foetal calf serum (FCS, F7524) and 1x non-essential amino acids (NEAA, M7145). All other cell types were cultured in Dulbecco's modified Eagle's medium containing 1mM pyruvate, 2mM L-glutamine and 4500mg/L glucose (DMEM, D6540) and was supplemented with 10% FCS, 1x NEAA and 50μg/ml uridine. Blasticidin^{S} (Melford Laboratories, B1105) was routinely added to all Flp-In^{TM}TREx^{TM} cell lines every third feed at a final concentration of 10μg/ml. Media was changed approximately every 3 days or as required. Generally 1-2ml media was used per well for culture in 6 well plates, 5ml for culture in 25cm^2 flasks, 15ml for culture in 75cm^2 flasks and 50-75ml for culture in 300cm^2 flasks.

When cells reached high levels of confluency (80-100%), they were passaged by harvesting in PBS/1mM EDTA (for HEK293, HeLa and Rho^0 cells) or 1x trypsin/ EDTA (PBS used to dilute 10x stock, T4174) for 143B and U2OS cells, adding an equal volume of media and pelleting in a universal at 230*g* for 4 minutes. The cell pellet was resuspended in fresh media and a portion of cells was seeded into new flask(s). The degree of splitting and the flask type used depended on the intended application and the type of cells.

2.1.3 CELL COUNTS

Cells were harvested as above, the cell pellet was resuspended in 1ml fresh media and 10μl was added to each chamber of a Neubauer improved haemocytometer. The cells in the 4 large squares of each chamber were counted and an average was calculated. The average number of cells per square was multiplied by 10^4 to obtain the cell count per ml. If there were too many cells to count accurately a 1 in 10 dilution was made and the average count multiplied by 10^5 to obtain the cell count per ml.

2.1.4 FREEZING AND STORAGE

For long-term storage, cells were harvested and the cell pellet resuspended in 0.5ml FCS with 10% DMSO and transferred to cryostorage vials. The cryostorage vials were then placed in the Nalgene® Mr. Frosty container stored at -80°C. This allowed a cooling rate of 1° per minute and after at least 24 hours, the vials were transferred into a liquid nitrogen storage tank for long-term storage.

To thaw cells, they were placed briefly at 37˚C and pre-warmed medium was slowly added to a final volume of 10ml. Cells were then pelleted as above, resuspended in medium and transferred to a culture flask of the same size as the cells were grown in before they were frozen.

2.1.5 MYCOPLASMA TESTING

Approximately every 3 months or as required, a 1ml aliquot of media from flasks with cells growing for at least 24 hours was taken to test for the presence of mycoplasma. The aliquot of conditioned media was subjected to centrifugation at 230*g* for 4 minutes to pellet any cells that may be present. The supernatant was then transferred to a microcentrifuge tube and stored at 4°C until mycoplasma testing was performed.

The MycoAlert^{TM} mycoplasma testing kit from (Lonza, LT07-118) was used to carry out the analysis as per manufacturer's guidelines. If mycoplasma was detected cells were discarded and replaced with cells from an earlier passage that had tested negative for mycoplasma before being stored in liquid nitrogen (2.1.4).

2.1.6 TRANSFECTING CELLS WITH SIRNA

Depletions were usually performed by 'reverse' transfection of cells with siRNA in 6 well plates, which I will describe now. For each depletion, a transfection mix of 250µl Optimem+GlutaMAX® (Gibco, 51985-026), 2µl lipofectamine RNAiMAX (Invitrogen, 13778150) and the appropriate volume of siRNA (see Table 2.1 for final concentrations of each siRNA used) were mixed gently in a microcentrifuge tube and incubated at room temperature for 15 minutes. During the incubation, cells that had been grown in a 75cm^2 flask were harvested and counted to allow a concentration of 60,000 cells per ml of media to be produced. Each transfection mix was gently mixed and transferred to a 9.6cm^2 well before adding 1ml of the cell mix to each well. The plates were then gently rocked to mix and incubated for 3 days.

After 3 days the cells were either harvested or re-transfected. Re-transfection was carried out by standard (or 'forward') transfection of cells whilst bound to plates. The same volumes were used to make up the transfection mix as above, but during the incubation, the old media was removed from the wells and the cells were washed once

with PBS before adding the transfection mix and 1ml of media to the cells in an adherent state, and incubating for a further 3 days.

When larger amounts of material were required, then $25cm^2$ or $75cm^2$ flasks were used to perform the siRNA depletions. The procedure was the same but the volumes were adapted. For $25cm^2$ knockdowns 1ml of Optimem and 10µl of lipofectamine was used in the transfection mix with the appropriate amount of siRNA. For knockdowns in $75cm^2$ flasks, 1.5ml Optimem and 12µl lipofectamine were used. A total of 300,000 cells were seeded for depletion in $25cm^2$ flasks (in 4ml media) and 1,000,000 cells seeded for depletions in $75cm^2$ flasks (in 7.5ml media).

Table 2.1: Details of siRNA Duplexes Used for Transfection of Cell Lines

Name	Sequences (5' - 3')	Final Concentration
AURKAIP1 siRNA1	5'-GUA CUU GUG GUG GUU CAU C dTdT 5'-GAU GAA CCA CCA CAA GUA C dTdT	33nM/ml
AURKAIP1 siRNA2	5'-CUU CAC CAG CUU CCG GUA C dTdT 5'-GUA CCG GAA GCU GCU GAA G dTdT	33nM/ml
AURKAIP1 siRNA3	5'-CUU CCG GUA CUU GUG GUG G dTdT 5'-CCA CCA CAA GUA CCG GAA G dTdT	33nM/ml
p32 siRNA2	5'-AAG GAA AUC CAU UAG GUG G dTdT 5'-CCA CCU AAU GGA UUU CCU U dTdT	50nM/ml
Non-targeting	siRNA non-targeting negative control duplex OR-0030-NEG05	Same as for the targeted siRNA used

All siRNAs were synthesised by Eurogentech and stored as 20µM or 100µM stocks in RNase-free water at -20°C.

NCBI Reference Sequences: AURKAIP1 = NM_001127229.1, p32 = NM_001212.3

2.2 BACTERIAL MANIPULATIONS

2.2.1 BACTERIAL CULTURE AND STORAGE

All bacteria were grown in LB media (Luria-Bertani: 5g NaCl, 5g bacto-tryptone, 2.5g yeast extract made up to 500ml with dH_2O and autoclaved) either in liquid broth or on 2% agar containing plates with appropriate antibiotics. Ampicillin (100μg/ml final concentration, Formedium, AMP25) and/or chloramphenicol (50μg/ml final concentration, Melford, C0113) were added to LB media or agar plates and bacteria were incubated overnight at 37˚C (with aeration for bacteria grown in suspension). For long-term storage, bacteria were frozen in LB media containing 18% glycerol at -80˚C.

2.2.2 BACTERIAL TRANSFORMATION

Aliquots of Bioline α-select chemically competent cells (40μl per transformation, BIO-85025) were thawed on ice. Up to 4μl DNA was added and incubated on ice for 30 minutes before being heat shocked at 42˚C for 45 seconds. Cells were again placed on ice for 2 minutes before adding 900μl pre-warmed SOC media (2% bacto-tryptone, 0.5% yeast extract, 0.05% NaCl, 2.5mM KCl, 10mM $MgCl_2$ and 20mM Glucose) and incubated at 37˚C, with agitation for one hour. Cells were then pelleted and resuspended in 50μl fresh SOC media, plated out on LB agar with appropriate antibiotics and incubated, inverted overnight at 37˚C.

For antibody production using recombinant protein as the antigen, relevant open reading frames were cloned into pGEX-6P-1. The validated construct as used to transform α-select cells for amplification of the desired plasmid, was subsequently used to transfect Rosetta™ DE3 cells (Novagen) or Tuner™ cells using the same protocol as for α-select cells (see Table 2.2 for details on bacterial strains). These bacterial cell lines allow overexpression of recombinant protein in bacteria.

Table 2.2: Bacterial Strains

Strain	Genotype	Application	Antibiotic Resistance
α-select Bronze Efficiency (Bioline)	F^- *deo*R *end*A1 *rec*A1 *rel*A1 *gyr*A96 *hsd*R17(r_k^-, m_m^+) *sup*E44 *thi*-1 *pho*A Δ(*lac*ZYA-*arg*F)U169 Φ80*lac*ZΔM15 λ^-	Transfection with plasmids	none
Rosetta™ (DE3) (Novagen)	F^- *ompT hsdS*$_B$(r_B^- m_B^-) *gal dcm* (DE3) pRARE (Cam^R)	Expression of recombinant eukaryotic proteins with rare *E.coli* codons	Chloramphenicol
Tuner™ (Novagen)	F^- *ompT hsdS*$_B$ (r_B^- m_B^-) *gal dcm lacY1*	As for Rosetta, but allows titratable IPTG induction	none

2.2.3 Expression of Recombinant Protein from Bacteria

The final protocol for the expression and purification of recombinant mature AURKAIP1 is presented here, but many iterations of the protocol were tested to allow maximum expression of soluble protein, described in detail in 3.2.2.

Tuner cells transformed with pGEX-6P-1/mature AURKAIP1 were grown in 5ml LB+amp (LB supplemented with 100μg/ml ampicillin) at 37°C with aeration overnight. Two 5ml cultures were used to inoculate 500ml LB+amp and incubated at 37°C with aeration for several hours. Every 20-30 minutes 1ml aliquots were taken from the large cultures and the optical density at a wavelength of 600nm (OD_{600}) measured. When an OD_{600} of 0.2 was achieved, the cultures were induced by adding 250μM IPTG (Isopropyl β-D-1-thiogalactopyranoside) and incubated at 37°C for 4 hours with aeration. Cells were pelleted by centrifugation at 5000rpm (Sorvall GSA centrifuge, rotor code 10) for 15 minutes at 4°C before being incubated at -80°C for at least 2 hours to aid in cell breakage. The cell pellet was then thawed and resuspended by vortexing in 10ml PBS supplemented with 1x EDTA-free protease inhibitor cocktail (Pierce, 88666), 1mM PMSF and 250U Benzonase (Novagen, 70746-3) and incubated on ice for 20

minutes. The suspension was sonicated on ice 15 times for 10 seconds with an 18-micron amplitude with 10 second intervals. The suspension was then centrifuged at 30,000*g* for 30 minutes at 4°C to pellet the insoluble fraction and unbroken cells. The supernatant was saved and passed through a 45μm filter before proceeding to the purification step (3.2.2).

2.3 DNA MANIPULATION

2.3.1 ISOLATION OF PLASMID DNA

To amplify plasmid copy number, bacterial cultures (5ml LB + appropriate antibiotics) were inoculated with single colonies and incubated overnight as described above. Cells were pelleted in a microcentrifuge tube and the plasmid DNA was isolated using the GeneJET® plasmid miniprep kit (Thermo, K0503) according to manufacturer's instructions. The isolated DNA was then eluted in 50µl dH_2O and the DNA quality assessed by gel electrophoresis (2.3.8) and concentration measured using the Nano-drop (2.3.4).

2.3.2 POLYMERASE CHAIN REACTION (PCR)

PCR was used to amplify the defined DNA regions required for cloning. Primers were designed to initiate amplification of the open reading frame of AURKAIP1 (Further details and Primer sequences given in 3.2.1 and Table 3.1). Thin walled 0.5ml microcentrifuge tubes and a final volume of 50µl were used in all cases.

Generic Proof Reading Polymerase Reaction Mix:

- 1µM Forward Primer
- 1µM Reverse Primer
- 0.08mM dNTPs
- 1.5mM $MgSO_4$
- 1x Buffer for KOD Hot Start Polymerase
- 20-100ng DNA Template
- 1 U KOD Hot Start DNA polymerase

Generic PCR Cycling Conditions:

Initial Denaturation	95˚C	4 minutes	
Denaturation	95˚C	1 minute	30 Cycles
Annealing	50˚C	1 minute	
Extension	72˚C	4 minutes	
Final Extension	72˚C	7 minutes	
Hold	4°C	Indefinitely	

The annealing temperature of the primers was measured by entering the sequence into OligoCalc (Kibbe, 2007) and using the salt corrected values. The initial annealing temperature used for PCR was approximately 5˚C below the lowest annealing temperature of the two primers used in a particular reaction.

PCR products then underwent agarose gel electrophoresis and were visualised using a UV transilluminator. The PCR product was then cut out of the gel using a scalpel and cleaned up using the QIAquick® Gel Extraction Kit (QIAGEN, 28706) according to manufacturer's guidelines.

2.3.3 Phenol/Chloroform Extraction and Ethanol Precipitation of DNA

Typically for plasmid DNA or PCR products, DNA was diluted in 50µl dH_2O and an equal volume (in this case 50µl) of phenol (Sigma, P-4557) was added. The samples were then vortexed for 30 seconds and centrifuged for 1 minute at 14,000*g*. The upper aqueous phase was carefully removed and placed into a fresh microcentrifuge tube before adding half of the original volume (i.e. 25µl) of phenol and half of the original volume (i.e. 25µl) of chloroform. The samples were again vortexed and centrifuged as described, before removing the top aqueous layer into a new tube. The same process was then repeated after adding an equal volume (50µl) of chloroform.

A tenth of the volume (5µl) of 3M sodium acetate was added to the final aqueous layer before two times the volume (110µl) of 100% ethanol was added. The samples were then incubated at -80°C for at least 1 hour before pelleting the DNA by centrifugation at 20,000*g* for 30 minutes at 4°C and resuspending the pellet in 10µl of sterile dH_2O.

If retaining the maximum amount of DNA was of great importance, the samples were initially diluted in a greater volume and volumes of phenol and chloroform were amended accordingly so that the relative proportion of aqueous phase, and thus, DNA retained was maximised.

2.3.4 Measurement of Nucleic Acid Concentration

All single stranded, double-stranded DNA or RNA concentrations were obtained with the Nano-drop (Spectrophotometer ND-1000) with absorption at 260nm with 1 A260

unit (1cm light path) equivalent to 50μg/ml (double-stranded DNA), 40μg/ml (double-stranded RNA) or 33mg/ml (oligodeoxynucleotide).

2.3.5 RESTRICTION ENDONUCLEASE DIGESTS OF DNA

Different restriction enzymes were used to cut the PCR products and vectors at the relevant restriction sites that had been engineered into the respective primers (Table 3.1). For particular constructs double digests were used, requiring a combination of *Eco*R1 (Roche), *Xho*1 (Roche), *Hin*dIII (Promega) and *Bam*H1 (New England Biolabs) to facilitate insertion of the fragment into the vector in a single orientation. Restriction buffer 2 (New England Biolabs) was used for all digests.

Generic 20μl total volume double restriction digest reaction:

- 2μl 10x NEB restriction buffer 2 pH 7.9
  (1x contains: 50mM NaCl, 10mM Tris/HCl, 10mM $MgCl_2$, 1mM DTT)
- 0.8μl enzyme 1
- 0.8μl enzyme 2
- 16.4μl cleaned up insert, or 0.5-1μg vector (plus dH_2O to make up final volume)

Reactions were typically incubated at 37°C for 3 hours.

2.3.6 DEPHOSPHORYLATION

The 5' dephosphorylation of vectors was performed immediately after restriction digests by adding 2μl 1M Tris pH 9.4, 2μl 10% SDS and 0.5μl alkaline phosphatase to the 20μl digest reaction. The dephosphorylation reaction was then incubated at 37°C for 30 minutes.

2.3.7 LIGATION

Ligation of digested PCR products into digested and de-phosphorylated vectors was catalysed by T4 DNA ligase (Roche). Reactions were typically prepared in a 10μl final volume with 1x T4 DNA ligase buffer (Roche), 1mM ATP and T4 ligase with an insert:vector molar ratio of 3:1 and 50ng of vector. Ligation reactions were incubated overnight at 16˚C.

2.3.8 AGAROSE GEL ELECTROPHORESIS

For analysis of linearised vectors, 0.8% agarose gels were used, whereas 1% agarose gels were used for analysis of PCR products. Agarose (NBS Biologicals, NBS-AG500) was dissolved in 1x TAE buffer (diluted from 50x stock prepared with 12.1g Trizma base, 5ml 0.5M EDTA and 2.86ml glacial acetic acid made up to 50ml with dH_2O. Final concentration of 1x TAE: 40mM Tris acetate, 1mM EDTA pH 8.0) by heating in a microwave. As the dissolved agarose cooled, 0.2µg/ml final concentration of ethidium bromide was added and mixed. The still molten agarose was poured into a gel cast and after setting was placed in an electrophoresis chamber and immersed in 1x TAE buffer. Samples in 1x DNA loading buffer (3% glycerol and approximately 0.025% each of bromophenol blue and xylene cyanol) and the 1kb ladder as a molecular weight marker were loaded and electrophoresed at 70V.

2.3.9 DNA SEQUENCING

Plasmids that were identified as having successfully ligated inserts were cycle sequenced in the PCR machine, using the BigDye® termination system (Applied Biosystems).

Cycle sequencing reaction (15µl total):

- 450ng plasmid DNA (in 9µl dH_2O)
- 3µl 5x sequencing buffer
- 1µl 5µM primer (CMV forward for pcDNA™5 sequencing)
- 2µl BigDye Terminator v3.1 ready reaction mix

Cycle sequencing conditions:

Initial Denaturation	95˚C	5 minutes	
Denaturation	95˚C	30 seconds	30 Cycles
Annealing	50˚C	10 seconds	
Extension	72˚C	4 minutes	
Hold	4°C	Indefinitely	

The cycle-sequenced samples were then stored at -20°C. The samples were kindly analysed by Charlotte Alston.

2.3.10 DNA EXTRACTION FROM HUMAN CELL LINES

Cultured human cells were harvested as described in 2.1.2. Cell pellets were resuspended in 400µl TE buffer (10mM Tris pH 8, 1mM EDTA). Final concentrations of 1% SDS (Sigma, L-4390) and 2mg/ml proteinase K (Roche, 25530-049) were then added, followed by an overnight incubation at 37°C. The samples were visually inspected and if the samples were not clear, they were mixed and further incubated at 37°C until clear. Phenol/chloroform extractions were then performed as described in 2.3.3. The volumes of phenol and chloroform used matched the sample volume. The centrifugation steps were extended to two minutes and the step where both phenol and chloroform were added was performed twice before extracting with chloroform alone. Ethanol precipitation was performed as described in 2.3.3.

2.3.11 QUANTITATIVE POLYMERASE CHAIN REACTION (qPCR)

DNA was isolated from cells as described above (2.3.10) and the DNA concentration was measured using the Nano-drop (2.3.4). For each sample, 50ng of DNA was used as a template in the reaction and each reaction was performed in triplicate. Forward and reverse primers for *MT-ND4* (target gene) and *18S* (reference gene) are detailed in Table 2.3.

Each reaction was prepared in a final volume of 20µl and comprised:

- 1µl of 10mM forward primer
- 1µl of 10mM reverse primer
- 10µl FastStart Essential DNA Green Master Mix (Roche, 06402712001)
- 2µl of 5ng/µl DNA template (10ng total)
- 6µl sterile dH_2O

Negative controls lacked the addition of the DNA template and were therefore supplied with an extra 2µl of dH_2O. Each reaction was prepared in polypropylene qPCR microtube strips, which were pulsed down prior to loading into the Lightcycler® Nano instrument (Roche) for performance of the qPCR.

Initial Denaturation	95˚C	10 minutes	
Denaturation	95˚C	10 seconds	45 Cycles
Annealing	59˚C	10 seconds	
Extension	72˚C	15 seconds	
Final Extension	72˚C	5 minutes	
Melting Curve	60°C-95°C	0.1°C per second	

The C_q (quantification cycle) values for each sample were determined by the Lightcycler® Nano software. The analysis was performed using the normalised expression ratio ($2^{-\Delta\Delta Cq}$) method (Livak and Schmittgen, 2001). This method is effective when both the target and reference genes have an approximately 100% amplification efficiency and are within 5% of each other. The target and reference genes were validated in satisfying these criteria in my host laboratory.

$$\Delta C_{q\,(Test)} = \Delta C_{q\,(Target,\,Test)} - \Delta C_{q\,(Reference,\,Test)}$$

$$\Delta C_{q\,(Calibrator)} = \Delta C_{q\,(Target,\,Calibrator)} - \Delta C_{q\,(Reference,\,Calibrator)}$$

$$\Delta\Delta C_q = \Delta C_{q\,(Test)} - \Delta C_{q\,(Calibrator)}$$

Where: Target = *MT-ND4*,
Reference = *18S*,
Test = either AURKAIP1 depletion or AURKAIP1 overexpression
Calibrator = either non-targeting siRNA treated or uninduced cells

Table 2.3: Primers for qPCR.

Primer Name	**Sequence (5' – 3')**	**T_m**
MT-ND4 Forward	5'-CCA TTC TCC TCC TAT CCC TCA AC	59°C
MT-ND4 Reverse	5'-CAC AAT CTG ATG TTT TGG TTA AAC TAT ATT T	59°C
18S Forward	5'-GTA ACC CGT TGA ACC CCA TT	59°C
18S Reverse	5'-CCA TCC AAT CGG TAG TAG CG	59°C

NCBI Reference Sequences: *MT-ND1* = YP_003024026.1, *18S* = NR_003286.2

2.4 RNA MANIPULATION

All solutions for use in work with RNA were prepared using autoclaved water that had been previously treated with 0.1% DEPC (DEPC water).

2.4.1 RNA EXTRACTION FROM HUMAN CELL LINES

Harvested cells were pelleted and resuspended in 0.5ml Trizol reagent (Invitrogen) and left to incubate at room temperature for 5 minutes. Then, 0.1ml of chloroform was added to each sample followed by 15 second of vigorous shaking. After a 3-minute incubation at room temperature, the samples were subjected to centrifugation at 12,000*g* for 15 minutes at 4°C. The supernatant was carefully removed and transferred to a fresh microcentrifuge tube, before 250μl isopropanol was added. The samples were gently mixed and incubated at room temperature for 10 minutes. The samples were then centrifuged at 12,000*g* for 10 minutes at 4°C and the RNA pellet was briefly dried before being resuspended in an appropriate volume of DEPC water. Samples were stored at -80°C. For large cell pellets, the volumes of all reagents used were doubled.

2.4.2 REVERSE TRANSCRIPTION

The Superscript II Reverse Transcription kit (Invitrogen) was used to generate single stranded cDNA for use as a template in PCR reactions. An aliquot of 1μl of oligo dT primer (100mM stock) was added to 5-10ng of isolated RNA and was made up to 12μl total volume with DEPC treated water. The mix was incubated at 70°C for 10 minutes and then placed on ice whilst 1x First-Strand Reaction Buffer, dNTPs (0.5mM final concentration) and DTT (10mM final concentration) were added. The reaction was then incubated at 42°C for 5 minutes before adding 200U of Superscript II Reverse Transcriptase and continuing the incubation at 42°C for 50 minutes. Inactivation of the Superscript II Reverse Transcriptase was then achieved by heating to 70°C for 15 minutes. The cDNA was then stored at -80°C.

2.4.3 DENATURING AGAROSE GEL ELECTROPHORESIS

Denaturing agarose gel electrophoresis was used to separate RNA samples for subsequent northern blotting. Isolated RNA was subject to phenol/chloroform extraction to improve purity before measuring the concentration using the Nano-drop. A total of

5μg of isolated RNA was prepared in an 8μl total volume of DEPC water. Samples were then made up to a final volume of 20μl by the addition to final concentrations of 1x MOPS (40mM MOPS acid, 10mM NaOAc and 1mM EDTA pH 7.2), 35% formamide and 5.5% formaldehyde. Samples were then heated at 55°C for 15 minutes before adding 0.1μg/μl ethidium bromide and 1x loading dye.

Samples were then loaded and electrophoresed through the denaturing gel (1% agarose, 1x MOPS and 0.9% formaldehyde) in 1x MOPS buffer at 55V for 2 hours. The electrophoresis gel tank and all casting apparatus had been soaked with 3% H_2O_2 for 10 minutes at room temperature, rinsed in DEPC H_2O and subsequently air dried prior to gel preparation.

The electrophoresed RNA was visualised on a UV transilluminator to assess the migration, quality and loading before proceeding with northern blotting.

2.4.4 NORTHERN BLOTTING AND PROBE GENERATION

RNA samples were electrophoresed as described above before being transferred to a Genescreen Plus membrane (Perkin Elmer). Transfer was carried out by capillary transfer in 10x SSPE (3.6M NaCl, 200mM phosphate buffer pH 7 and 20mM EDTA) overnight at room temperature. The membrane was then washed with 2x SSPE and visualised under UV light alongside the gel to confirm transfer efficiency, and rRNA migration. The membrane was then baked at 80°C for 2 hours in a vacuum drier. The membrane was blocked for 2 hours at 42°C in 10ml pre-hybridisation solution (50% formamide, 5x SSPE, 1% SDS and 5x Denhardt's solution) before adding any probes.

Various ^{32}P-labelled DNA probes were produced to target specific desired RNA sequences. DNA templates used for these probes were produced by PCR. These DNA templates (100ng) were denatured in 9μl DEPC water at 95°C for 4 minutes before cooling and adding 1x random hexamer mix, 5U Klenow fragment (DNA polymerase I, Promega) and 2μl ^{32}P α-dCTP (Perkin Elmer NEG513H) in a 15μl reaction. The reaction mix was then incubated for 1 hour at 37°C and then passed through Illustra G-25 columns (GE Healthcare) according to manufacturer's guidelines to remove free nucleotides. The activity of the final probes was then estimated using a Cerenkov counter and a volume equivalent to approximately 500,000cps was added to the pre-hybridisation solution after the aforementioned membrane-blocking step. The

membrane was then hybridised with probe by incubation in this solution overnight at 42°C with rotation.

After hybridisation, the membrane was washed twice in 2x SSPE for 15 minutes at room temperature before a third wash in pre-warmed 2x SSPE/2% SDS and incubated at 65°C for 15 minutes.

The membrane was then wrapped in saran wrap and exposed to a PhosphoImage screen in a cassette before visualising the signal using the Typhoon FLA 9500 and ImageQuant software (GE Healthcare).

For subsequent hybridisation of probes to other targets, the membrane was washed twice in 2x SSPE and once with 2x SSPE/2%SDS at 65°C as described above before adding the next probe. If two different probes targeted RNAs with similar molecular weights then it was necessary to strip the membrane of the first signal before re-probing with the second probe. Membrane stripping was performed by washing the membrane twice in boiling 0.1x SSC (1x SSC: 150mM NaCl, 15mM sodium citrate) and once with SSC/0.1% SDS for 15 minutes. Any radioactive signal present on the membrane was assessed using a Geiger counter to ensure the removal of the previous signal before hybridising with another probe as described above.

2.5 PROTEIN MANIPULATION

2.5.1 PREPARATION OF HUMAN CELL LYSATE

Pellets of harvested cells were resuspended in approximately 50µl of lysate buffer per 10mg of wet cell pellet.

Lysate buffer was prepared with 50mM Tris/HCl pH 7.4, 130mM NaCl, 2mM $MgCl_2$, 1mM PMSF, 1% Nonidet P-40, one EDTA-free protease inhibitor tablet (Pierce) and was made up in a 10ml final volume before being aliquoted and stored at -20°C.

Samples were vortexed for 30 seconds and centrifuged at 1000*g* for 2 minutes to remove nuclei and unbroken cells. The supernatant was then transferred to a fresh microcentrifuge tube, snap frozen in liquid nitrogen and stored at -80°C.

Samples with small cell pellets were resuspended in 15-30µl of lysate buffer and vortexed, but were not subjected to centrifugation in order to prevent loss of material. Instead, 25U Benzonase was added to remove nucleic acids. If any sample for a particular experiment needed to be prepared in this way, then all of the samples were treated in the same manner (samples prepared in this manner will be designated whole cell lysate, whereas samples with nuclei removed by centrifugation will be designated cell lysate). Estimation of protein concentration (2.5.3) was always performed prior to the addition of Benzonase.

2.5.2 MITOCHONDRIAL PREPARATION

Mitochondria were isolated from cells grown in 300cm^2 flasks. These were harvested at approximately 80% confluency and the resulting pellet was resuspended in 2ml ice-cold homogenisation buffer (0.6M mannitol, 10mM Tris pH 7.4 and 1mM EGTA) supplemented with 0.1% BSA and 1mM PMSF. The following steps were carried out at 4°C. The cell suspension was transferred to a glass:Teflon Dounce homogeniser and subjected to 15 passes before being centrifuged at 400*g* for 10 minutes. The supernatant was retained in pre-chilled tubes, and the pellet was resuspended in a further 2ml of supplemented homogenisation buffer and the homogenisation and centrifugation process repeated. The supernatant was again retained and all supernatant tubes were centrifuged at 400*g* for 5 minutes. The supernatants were transferred to new microcentrifuge tubes and the mitochondria were pelleted at 11,000*g* for 10 minutes.

The pellet was washed twice in homogenisation buffer lacking BSA and finally resuspended in 70-150µl homogenisation buffer.

To remove cytosolic contamination 1mg of isolated mitochondria were treated with 1µg proteinase K on ice for 30 minutes. Digestion was then inhibited by addition of 1mM PMSF.

2.5.3 Estimation of Protein Concentration by Bradford Assay

Measurement of protein concentration was performed using the Bradford assay. Samples were added to a final volume of 800µl of dH_2O (usually 1-2µl of cell lysate or mitochondrial preparation) before adding 200µl of Bradford reagent (BioRad) to either the lysate, or BSA standard curve samples. The samples were mixed well, then incubated for 5 minutes at room temperature before 200µl aliquots of each sample to a 96 well plate. The absorbance at 595nm of samples was measured on an ELx800 microplate reader (BioTek). The optical density was used in conjunction with the BSA standard curve to calculate the average protein concentration in the test samples.

2.5.4 SDS-PAGE

This method allows separation of denatured proteins according to their molecular weight. Casting and running of gels was performed using either the Hoefer Mighty Small™ or Bio-Rad Mini-Protean® Tetra Cell system. Gels were cast with resolving phases of 12% or 14% polyacrylamide depending on the molecular weight of the proteins of interest (see Table 2.4 below). Addition of water above the resolving matrix allowed a smooth meniscus to form. This was removed after polymerisation was complete and a 3.75% stacking gel was added on top. Samples for SDS-PAGE analysis were incubated with sample dissociation buffer (final concentrations: 6.25mM Tris/HCl pH 6.8, 2% SDS, 10% glycerol, approximately 0.01% bromophenol blue and 100mM DTT) and incubated for 3 minutes at 95°C or 15 minutes at 37°C before loading. SDS-PAGE was performed in 1x running buffer (192mM glycine, 25mM Tris and 0.1% SDS) at 70V through the stacking gel and 150V though the resolving gel when using the Hoefer system, or a stable 200V when using the Bio-Rad system.

Table 2.4: Reagents and Volumes for SDS-PAGE.

	12% resolving gel	14% resolving gel	3.75% stacking gel
30% acryl/bisacrylamide (29:1)	2ml	2.333ml	0.625ml
3.75M Tris/HCl pH 8.5	0.5ml	0.5ml	--
0.5M Tris/HCl pH 6.8	--	--	1.25ml
dH_2O	2.395ml	2.062ml	3.02ml
10% SDS	50µl	50µl	50µl
TEMED	5µl	5µl	5µl
10% APS	50µl	50µl	50µl
Final Volume	5ml	5ml	5ml

2.5.5 COOMASSIE STAINING

General Coomassie Brilliant Blue (CBB) staining was used for visualising proteins after SDS-PAGE. Typically gels were incubated in CBB stain (45% methanol, 10% acetic acid and 0.2% Coomassie Blue R250) for 8 minutes at room temperature with agitation, before placing in de-staining solution (45% methanol and 10% acetic acid) for 10 minutes. The de-staining solution was then replaced with fresh de-staining solution and incubated at room temperature for a further 10 minutes or until the background of the gel was clear.

If greater sensitivity was required (as low as 5ng can be detected), InstantBlue (Expedeon, ISB1L) stain was used. Gels were washed briefly with water before staining with Instant Blue for at least 1 hour.

If mass spectrometry was to be performed on an excised band then the gel was washed 3 times for 5 minutes with dH_2O and stained for at least 1 hour with SimplyBlue^{TM} SafeStain (Life Technologies, LC6060).

Images of Coomassie-stained gels that had been prepared by any of the methods outlined above were acquired using either an Epsom EU-35 scanner or the Bio-Rad ChemiDoc^{TM} MP system.

2.5.6 WESTERN BLOTTING AND IMMUNODETECTION

To immunodetect proteins separated by SDS-PAGE, they were transferred from the polyacrylamide gel to a PVDF membrane (Immobilon-P, Millipore). The gel was equilibrated in transfer buffer (192mM glycine, 25mM Tris, 0.02% SDS and 15% methanol). The PVDF membrane was activated in 100% methanol for 15 seconds before washing in distilled water and then transfer buffer. The gel and membrane were placed between double thickness 3MM Whatman filter paper and sponges in a cassette, which was placed in the transfer tank (TE22, Hoefer or Mini Trans-Blot^{TM} module, Bio-Rad). The transfer of proteins from the gel to the membrane was performed at 100V for 2 hours at 4°C with the Hoefer system, or 100V for 1 hour at 4°C with the Bio-Rad system. The PVDF membrane was blocked for 1 hour at room temperature in 5% milk/T-TBS (Tris buffered saline with Tween-20: 50mM Tris, 150mM NaCl, 0.05% Tween-20), before incubation with primary antibodies. Primary antibodies were generally diluted (as indicated by manufacturer) in 5% milk/T-TBS (see Table 2.5 for specific antibody dilutions) and incubated with the membrane overnight at 4°C, with agitation. The membrane was then washed three times for 10 minutes in T-TBS before being incubated with the appropriate HRP-coupled secondary antibody (Dako Cytomation, Table 2.6) for 1 hour at room temperature. After a further 5 washes, each of 10 minutes in T-TBS, detection was carried out using either ECL+, ECL Prime (both GE Healthcare) or the Immun-Star^{TM} WesternC^{TM} kit (Bio-Rad) according to manufacturer's instructions. Fluorescent signals produced by ECL+ were visualised on the STORM PhosphorImager (Molecular Dynamics) and analysed using ImageQuant software (Molecular Dynamics). Chemiluminescent signals were visualised using the ChemiDoc^{TM} MP system (Bio-Rad).

Table 2.5: Primary Antibodies Used for Immunoblotting.

Antibodies	Type	Dilution	Company
α-AIF	Rabbit Polyclonal	1:1000	NEB (4642S)
α-AURKAIP1	Rabbit Polyclonal	1:1000	Produced as detailed in Chapter 3 (Eurogentech)

α-AURKAIP1 (Sigma)	Rabbit Polyclonal	1:1000	Sigma Aldrich (Prestige/Atlas) HPA031821
α-β actin	Mouse Monoclonal	1:10000	Sigma Aldrich (A1978)
α-COXI	Mouse Monoclonal	1:1000	Abcam (Mitosciences MS404) ab14705
α-COXII	Mouse Monoclonal	1:1000	Abcam (Mitosciences MS405) ab110258
α-DAP3	Mouse Monoclonal	1:1000	Abcam (ab11928)
α-FLAG	Mouse Monoclonal	1:2000	Sigma Aldrich (F1804)
α-GDH	Rabbit Polyclonal	1:1000	Custom antibody (Eurogentech)
α-MRPL3	Goat Polyclonal	1:1000	Abcam (ab39268)
α-MRPL11	Rabbit Monoclonal	1:1000	NEB (2066S) (XP, D68F2)
α-MRPL12	Rabbit Polyclonal	1:1000	Custom antibody (Eurogentech)
α-MRPS18B	Rabbit Polyclonal	1:1000	ProteinTech (16139-1-AP)
α-MRPS22	Rabbit Polyclonal	1:1000	ProteinTech (10984-1-AP)
α-mtPAP (mouse)	Mouse Monoclonal	Co-IP only	GeneTex (GTX70156)
α-mtPAP (rabbit)	Rabbit Polyclonal	1:1000	Abcam (Epitomics S3295) ab137643

α-ND1	Rabbit Polyclonal	1:1000	Gift from A. Lombes
α-NDUFA9	Mouse Monoclonal	1:1000	Abcam (Mitosciences MS111) ab14713
α-p32 (rabbit) (GC1qR)	Rabbit Monoclonal	1:1000	Abcam (ab131284)
α-p32 (mouse) (GC1qR)	Mouse Monoclonal	1:1000	Abcam (ab24733)
α-Porin (VDAC1)	Mouse Monoclonal	1:10000	Abcam (Mitosciences MSA03) ab14734
α-Tom20	Rabbit Polyclonal	1:1000	Santa Cruz Biotechnology (Sc-17764)
α-SDH-70	Mouse Monoclonal	1:5000	Abcam (Mitoscience MS204) ab14715

Table 2.6: HRP-Conjugated Secondary Antibodies Used for Immunodetection.

Antibody	**Type**	**Dilution**	**Company**
α-Mouse secondary	Rabbit Polyclonal	1:2000	Dako Cytomation P0260
α-Rabbit secondary	Swine Polyclonal	1:3000	Dako Cytomation P0339
α-Goat secondary	Rabbit Polyclonal	1:2000	Dako Cytomation P0449

CHAPTER 3:

GENERATION OF ANALYTICAL TOOLS FOR CHARACTERISATION OF AURKAIP1

3.1 INTRODUCTION

In order to study the role of AURKAIP1 in human mitochondrial gene expression, several tools were required. The generation of the majority of the required tools will be described in this chapter.

Due to a lack of available commercial antibodies, custom antibodies that would recognise endogenous AURKAIP1 were required. In order to produce these, recombinant protein corresponding to the predicted mature form of AURKAIP1 needed to be expressed in bacteria and then purified, to be used as an antigen.

To achieve this goal, it was necessary to design primers to allow amplification of the designated sequence of the open reading frame that would correspond with the mature form of AURKAIP1. *AURKAIP1* has three validated transcript variants that have different 5' UTRs produced by alternate splicing. However, there is only one common open reading frame (consensus CDS: CCDS25.1), therefore all nucleotide numbers relating to the *AURKAIP1* gene from now on will be given with reference to the start of the open reading frame.

AURKAIP1 was predicted to have an N-terminal mitochondrial targeting sequence by the Target P 1.1 server (Emanuelsson et al., 2007; 2000). The reliability class (RC) value given for the prediction of an N-terminal mitochondrial targeting sequence for AURKAIP1 was 2 out of a classification scale of 5, with 1 being the strongest prediction. Therefore, this was a strong predictor, so the program was also used to predict if there was a cleavage site of the potential mitochondrial targeting sequence (Nielsen et al., 1997) or whether this was left as part of the imported protein. The predicted cleaved pre-sequence length (TPlen) was given as 76 amino acids, which suggests that the mature AURKAIP1 protein would consist of amino acids 77-199. However, the MitoProt II server (Claros and Vincens, 1996) predicts the cleavage site to be at position 55, removing 54 amino acids upon import. Despite predicting a different

cleavage site, the MitoProt II analysis is nevertheless strongly indicative of mitochondrial localisation for AURKAIP1 (probability 0.9771) (Claros and Vincens, 1996). In addition, other localisation predictors (that do not allow cleavage site prediction) also suggest mitochondrial localisation e.g. Predotar (probability 0.78) (Small et al., 2004), pTARGET (probability 0.751) (Guda, 2006) and MultiLoc2 (probability 0.96 low res, 0.98 high res) (Blum et al., 2009). The latter is particularly interesting as MultiLoc2 also gives a probability for nuclear localisation of 0.01 using either resolution and is claimed to outperform other prediction programs (Blum et al., 2009). Together, the results from several localisation prediction programs strongly predict AURKAIP1 to be a mitochondrial, rather than nuclear protein.

The presence of an N-terminal mitochondrial targeting sequence could be problematic for expressing the recombinant protein in bacteria because prokaryotes do not possess mitochondria, and therefore could not process the full length AURKAIP1 protein to the mature form by cleaving the mitochondrial targeting sequence. Thus, expressing full-length recombinant AURKAIP1 protein would be inappropriate as the additional mitochondrial targeting sequence could cause misfolding relative to mature AURKAIP1. Additionally, the use of full length AURKAIP1 as an antigen for antibody production could potentially raise antibodies to antigens that would not be present in the mature protein in human cells. To minimise this possibility, it was important to design primers that would only amplify the section of the *AURKAIP1* gene that would correspond to the mature protein.

The prediction of the TargetP program suggests that mature AURKAIP1 would be missing a 76 amino acid N-terminal mitochondrial targeting sequence (Emanuelsson et al., 2007; Nielsen et al., 1997). This prediction suggested that the ideal primers would allow for amplification of nucleotides 229-600 of the *AURKAIP1* open reading frame, which correspond to amino acids 77-199 of the protein. However, the size of the cleaved N-terminal targeting sequence predicted by the MitoProt II program was 54 amino acids (Claros and Vincens, 1996). These predictions were therefore used as a starting point to aid primer design, but other considerations also had to be taken into account. For example, designing primers to amplify the DNA from position 229 (corresponding to Target P prediction) would have been problematic since the nucleotide sequence immediately downstream is very G-C rich (78% for an 18 nucleotide primer) and would therefore produce a primer with a very high melting

temperature. G-C rich regions have been shown to be difficult to amplify and generally primers with 40-60% G-C content are widely used (Mitsuhashi, 1996). Therefore, the sequence of the *AURKAIP1* open reading frame that corresponded to the region between the two predicted cleavage sites was studied to find a sequence that was suitably balanced between G-C and A-T content as to allow for the design of primers more likely to produce successful amplification. The final primers were designed to allow amplification of nucleotides 199-600 of the AURKAIP1 open reading frame, which corresponds to amino acids 67-199 of the protein.

The mature version of AURKAIP1 needed to be expressed in bacteria and purified in order to be used as an antigen for antibody production and subsequently for affinity purification. The speedy 28-day protocol of antibody production offered by Eurogentech was selected for this purpose, as it uses a novel adjuvant that allows for faster antibody production. This protocol claimed to produce antibodies with comparable titres and affinities to the 87-day procedures using Freund's adjuvant. The selected protocol was used in rabbits to produce polyclonal antibodies to the mature AURKAIP1 protein. Using the mature protein as an antigen would produce antibodies that would be more likely to recognise the endogenous protein than an antibody raised against a single small peptide due to the number of potential epitopes being much greater. This should also increase the likelihood that the polyclonal antibody would be appropriate for immunoprecipitation in addition to western blotting.

Since overexpression of the mature protein in bacteria and subsequent purification of the mature protein was necessary for antibody production, an appropriate system needed to be selected to achieve this. The Glutathione S-Transferase (GST) Gene Fusion system (Amersham) is a versatile system for the expression and purification of protein produced in *E. coli*. There are several pGEX vectors all of which allow IPTG inducible expression of fusion proteins with a GST moiety at the N-terminus, and the protein of interest at the C-terminus. This N-terminal tag was an important factor for several reasons. First, the addition of the GST tag improves protein solubility, and soluble protein was required for both antibody production and subsequent affinity purification. Second, GST fusion proteins can be purified via affinity chromatography using immobilised glutathione, which is a gentle purification method that maximises the preservation of protein antigenicity. Finally, the GST coding sequence is situated upstream of the multiple cloning site of the pGEX vectors, which means that the

inserted gene must be in-frame, but does not require a start codon. As mentioned previously, primers were designed to allow expression of mature AURKAIP1, so they did not include the start codon.

Of the available pGEX vectors, pGEX-6P-1 was selected for the additional benefits of the PreScission Protease site inserted between the GST coding region and the multiple cloning site. The PreScission protease site allows the most efficient method for purification as the site specific cleavage causes immobilisation of the protease on the column, thus the protease and GST tag are removed in the same step. The protease allows for elution at 4°C as it is highly active at low temperatures. This aids in protecting the integrity of the target protein.

The selection of pGEX-6P-1 as a vector influenced the design of primers as it was vitally important to ensure that the amplified product would be in-frame once cloned into the vector. Primers were designed to allow incorporation of a *Bam*HI restriction site upstream of the designated mature AURKAIP1 sequence and a *Xho*I restriction site downstream. The addition of these restriction sites would allow the mature AURKAIP1 gene to be cloned into the multiple cloning site of pGEX-6P-1, which could then be used to subsequently transform a variety of *E. coli* strains.

AURKAIP1 has previously been described as a nuclear protein in experiments using cell lines that overexpressed N-terminal FLAG-tagged AURKAIP1 (FLAG-AURKAIP1) (Lim et al., 2007; Kiat, 2002). As AURKAIP1 is predicted to have a mitochondrial targeting sequence, it is probable that the N-terminal FLAG tag interfered causing mislocalisation of AURKAIP1 to the nucleus. A C-terminal FLAG tag would not interfere with the mitochondrial targeting sequence and therefore a cell line capable of expressing AURKAIP1 with a C terminal FLAG tag (AURKAIP1-FLAG) could be used to confirm whether or not there is mitochondrial localisation of AURKAIP1.

To this end, primers were designed to allow amplification of the full length *AURKAIP1* open reading frame with the addition of a FLAG coding sequence at the 3' end. The inducible expression vector pcDNA^{TM}5/FRT/TO was selected to clone the *AURKAIP1-FLAG* insert into. The advantage of using pcDNA^{TM}5/FRT/TO is that upon transfection of a Flp-In^{TM}TRex^{TM} mammalian host cell line in tandem with the pOG44 Flp recombinase expression plasmid, the gene of interest is stably integrated into a defined site in the host genome. This integration is Flp recombinase dependent hence the

requirement for transient expression from the pOG44 vector. This system prevents the gene of interest being inserted randomly into the host genome. Random insertion can be problematic if for example the integration disrupts another open reading frame, inactivates an enhancer region, or activates an oncogene. If such integration were to occur, any phenotype seen in the host cell line post transfection could be wrongly attributed to the expression of the gene of interest. Thus the use of pcDNA^{TM}5/FRT/TO with a Flp-In^{TM}TRex^{TM} host cell line negated this potential problem. Further, the pcDNA^{TM}5/FRT/TO vector has a hybrid human cytomegalovirus (CMV)/TetO_2 promoter, which allows tetracycline regulated expression of the protein of interest.

Unlike the pGEX-6P-1 vector, pcDNA^{TM}5/FRT/TO does not encode a protein tag to produce a fusion protein. Therefore the sequence encoding the C-Terminal FLAG tag was incorporated into the sequence of the reverse primer. Since this is a mammalian expression system, mitochondrial targeting and import would occur and so it was important to clone the full length *AURKAIP1* open reading frame. Therefore the forward primer was designed to include the start codon of *AURKAIP1* with an upstream *Hind*III restriction site. The reverse primer was designed to be complimentary to the 3' end of the open reading frame immediately upstream of the stop codon. The stop codon sequence was removed to allow read-through of the inserted FLAG sequence. A stop codon was incorporated downstream of the FLAG sequence followed by a *Xho*I site. These restriction sites were chosen because *Hin*dIII and *Xho*I are present in the appropriate positions in the multiple cloning site of pcDNA^{TM}5/FRT/TO, facilitating insertion of the AURKAIP1-FLAG insert in the correct orientation.

Generation of a stable inducible AURKAIP-FLAG expressing cell line would also allow the flexibility of using anti-FLAG antibodies for western blot detection or immunoprecipitation. Further, overexpression of AURKAIP1 would facilitate validation of any antibodies against endogenous anti-AURKAIP1.

The generation of the tools described above is detailed in the next section. However, since this chapter is solely concerned with generation and development of tools/methods the results and the iterative modifications to improve the data will be presented together under a single heading of 'Method Development'.

3.2 METHOD DEVELOPMENT

3.2.1 PRODUCING AURKAIP1 GENE CONSTRUCTS

3.2.1.1 PRIMERS AND PCR CONDITIONS FOR PRODUCTION OF INSERTS

Primer pairs were designed to allow amplification of the open reading frame of AURKAIP1 with a C-terminal FLAG tag (henceforth designated AURKAIP1-FLAG insert) or to allow amplification of the open reading frame of AURKAIP1 with a 5' deletion of 198 nucleotides (henceforth designated truncated AURKAIP1 insert).

Table 3.1: Primers Used for the Generation of AURKAIP1 Constructs.

Primer Name	Sequence (5' -> 3')	Restriction Site	T_m
AURKAIP1 For (pcDNA™5)	5'-TACTAT**AAGCTT**CCACAGACCATGCTCCTG	*Hin*dIII	58.4°C
AURKAIP1 Rev-FLAG (pcDNA™5)	5'-ATACTA**CTCGAG**CTACTTATCGTCGTCATCCTTGTAATCTGCCCGCAGGTAGATCTTGG	*Xho*I	58.4°C
AURKAIP1 For (pGEX6P1)	5'-TACTAT**GGATCC**AGGAAGATGTCCGTCAGC	*Bam*HI	56.3°C
AURKAIP1 Rev (pGEX6P1)	5'-ATACTA**CTCGAG**CGGATCACAGCAGCAACG	*Xho*I	58.4°C

Table shows sequences of primers used for generation of pcDNA™5/FRT/TO/AURKAIP1-FLAG and pGEX-6P-1/AURKAIP1 constructs. **Key:** bold = restriction site, green = start codon, red = stop codon, yellow = FLAG tag coding sequence and underline = initial annealing portion of primer. T_M is the melting temperature of the underlined sequence. Melting temperatures were calculated using the OligoCalc online oligonucleotide properties calculator (Kibbe 2007). NCBI Reference Sequence: AURKAIP1 = NM_001127229.1.

PCR was performed as described in 2.3.2. Initial attempts used cDNA from HEK293 cells as a template, which was generated by reverse transcription (2.4.2) of RNA using oligo dT primers. All initial PCR reactions were performed using an annealing temperature of 52°C. An aliquot of 4µl of the final PCR reactions were then subjected to electrophoresis through a 1% agarose gel containing 0.2µg/ml ethidium bromide and visualised under UV light to assess the amount and purity of the products. These

conditions were unsuccessful in producing a product for AURKAIP1, although a product was produced using primers specific to a fragment of the SLMO2 gene, which had been used as a positive PCR control (Figure 3.1). The SLMO2 primers also acted as a positive control to confirm that the reverse transcription had produced amplifiable cDNA.

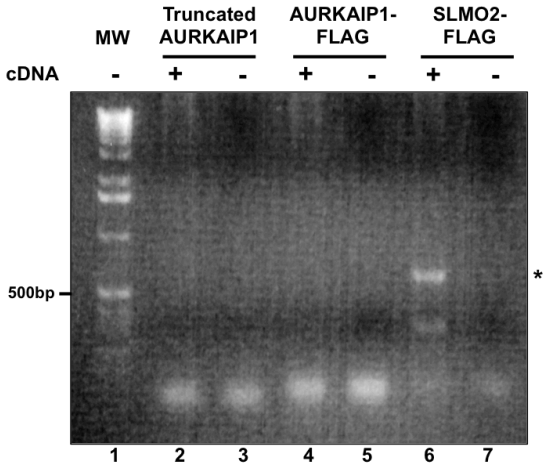

Figure 3.1: Initial PCR reactions for AURKAIP1 inserts. PCR was carried out as described in Chapter 2.2.1 using an annealing temperature of 52°C and cDNA from HEK293 cells as a template for both sets of AURKAIP1 primers (lane 2=truncated AURKAIP1 primers, lane 4=AURKAIP1-FLAG primers). SLMO2-FLAG primers were used as a positive control (lane 6). Reactions without template cDNA added were used as negative controls (lanes 3, 5 and 7). * denotes size of the SLMO2-FLAG positive control insert.

As mentioned, these initial PCR attempts were carried out with an annealing temperature of 52°C. Reducing the annealing temperature to 50°C still failed to generate a product for AURKAIP1. The SLMO2 primers and both sets of AURKAIP1 primers had similar melting temperatures, so it seemed unlikely that the annealing temperature was the problem. However, it was possible that the reverse transcription had not produced enough AURKAIP1 cDNA to allow for amplification, whereas there was sufficient SLMO2 cDNA. This would account for the success of the positive control as seen in Figure 3.1.

To address this problem, an AURKAIP1 full length I.M.A.G.E clone (IMAGE ID 5931927/AL50 K6 (M13F)) was instead used as a template for the PCR reactions. The bacteria containing the AURKAIP1 I.M.A.G.E clone were cultured in 5ml LB with 50μg/ml chloramphenicol overnight at 37°C to amplify the plasmid copy number. The plasmid DNA was then extracted by miniprep (2.3.1) and purified by phenol-chloroform extraction and ethanol precipitation (2.3.3). The concentration of plasmid DNA was measured spectrophotometrically using the Nanodrop (2.3.4) and approximately 75ng of plasmid DNA was used as a template for the subsequent AURKAIP1 PCR reactions. These conditions did produce a product of around the

expected 657bp for the AURKAIP1-FLAG PCR (Figure 3.2A) and 466bp for the truncated AURKAIP1 PCR (Figure 3.2B).

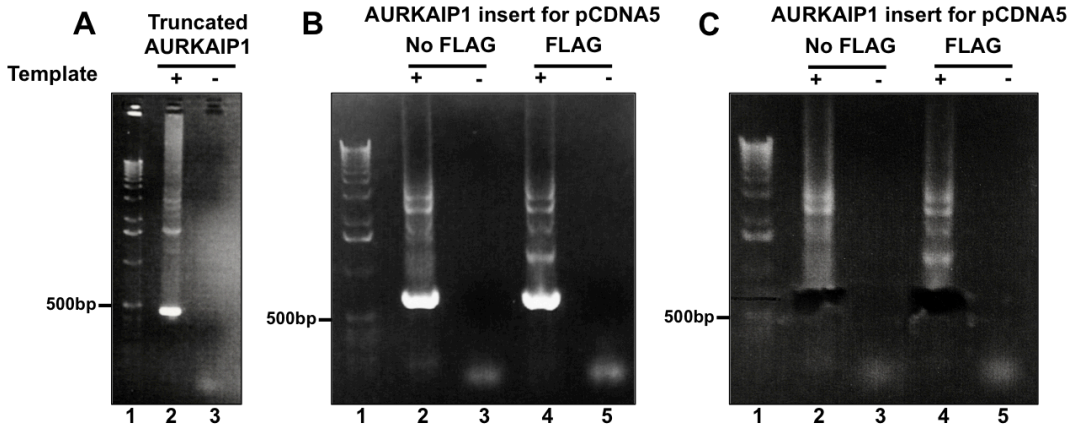

Figure 3.2: Generation of AURKAIP1 PCR Products for Insertion into pGEX-6P-1 and pcDNA^{TM}5/FRT/TO Vectors. A) PCR was performed as described in 2.2.1 with an annealing temperature of 50°C and using AURKAIP1 I.M.A.G.E clone plasmid DNA as a template. An aliquot of 4µl was loaded and separated through a 1% agarose gel. Lane 1 = 1kb DNA ladder, lane 2 = truncated AURKAIP1 PCR reaction and lane 3 = negative control reaction lacking addition of template. **B)** The same procedure as in **A**, but using primers designed to amplify full length *AURKAIP1* gene either with (lane 4) or without (lane 2) a C-Terminal FLAG tag. Negative control reactions that lacked the addition of the AURKAIP1 plasmid DNA were loaded in lanes 3 and 5 respectively. **C)** The bands corresponding to the expected size of the insert were excised from the gel in **B**.

Several annealing temperatures from 45°C to 55°C were tested in order to improve the yield and purity of the PCR products. However, the best annealing temperature for both the AURKAIP1-FLAG insert and the truncated AURKAIP1 insert was found to be 50°C. In both cases the PCR products were not clean enough to proceed with immediately. Though the band of the expected size was by far the most prominent in both cases, both PCR products had additional bands of greater size (Figure 3.2). Therefore the band of approximately the correct size (657bp for AURKAIP1-FLAG) was excised from the gel (Figure 3.2C) and the DNA was extracted from the gel using the QIAquick® Gel Extraction Kit (QIAGEN). Though only the gel excision of the AURKAIP1-FLAG insert is shown in Figure 3.2, the same procedure was carried out for the truncated AURKAIP1 insert.

3.2.1.2 Confirmation of Correct Constructs by Restriction Digests

The purified PCR products (AURKAIP1-FLAG insert and truncated AURKAIP1 insert) were then subjected to restriction digest reactions (2.3.5). As described earlier, both sets of primers had been designed in such a way as to incorporate restriction sites towards the termini of the PCR products (Table 3.1) to facilitate compatibility with the digested recipient vector.

In the case of the vectors, double restriction digests were always followed immediately by dephosphorylation by adding 2µl 1M Tris pH 9.4, 2µl 10% SDS and 0.5µl alkaline phosphatase followed by incubation at 37°C for 30 minutes. This dephosphorylation step is necessary to prevent the empty vector from re-ligating. The ligation reaction requires a 5' phosphate and a 3' hydroxyl group; therefore, removing the phosphate group from the vector encourages ligation of the insert into the vector as only the insert has the necessary 5' phosphate group. After the dephosphorylation incubation, the volume was made up to 50µl with ddH_2O and the mixture was then subjected to phenol-chloroform extraction and ethanol precipitation (2.3.3) in order to isolate the DNA and remove the enzymes.

The same phenol-chloroform extraction and ethanol precipitation was carried out on the truncated AURKAIP1 insert after double digestion because the *Bam*HI restriction endonuclease cannot be heat inactivated and therefore must be removed before proceeding to ligation. However *Hin*dIII and *Xho*I can be heat inactivated at 80°C and 65°C for 20 minutes respectively. Therefore the AURKAIP1-FLAG insert was subjected to incubation at 80°C for 20 minutes to inactivate the restriction enzymes. Though the pcDNA^{TM}5/FRT/TO vector was digested with the same enzymes, phenol-chloroform extraction and ethanol precipitation was still required since alkaline phosphatase cannot be heat inactivated.

3.2.1.3 LIGATION

Once the vectors had been digested, dephosphorylated and purified and the inserts had been digested and purified by gel extraction, both were ready for use in the ligation reaction. DNA concentrations were determined using the Nanodrop (2.3.4) and the following formula was used to determine the relative amounts of vector and insert to be used:

$$\frac{\text{Vector (ng)} \times \text{size of insert (kb)} \times \text{insert:vector molar ratio}}{\text{Size of vector (kb)}} = \text{insert (ng)}$$

The insert to vector molar ratio used was 3:1 and the amount of vector used per ligation reaction was always 50ng, therefore:

AURKAIP1-FLAG construct:

$$\frac{50 \times 0.6 \times 3}{5.1} = 17.6\text{ng of insert}$$

Truncated AURKAIP1 construct:

$$\frac{50 \times 0.4 \times 3}{4.9} = 12\text{ng of insert}$$

The ligation reaction was performed in 10µl total volume containing 1µl 10x T4 ligase buffer, 0.5µl ATP, 1µl T4 ligase and the calculated volumes of vector, insert and ddH_2O. A negative control was always included that lacked the addition of the insert to the reaction. This control was important to ensure the effectiveness of vector dephosphorylation, as no ligation should occur in the absence of a 5' phosphate. The ligation reactions were incubated at 16°C overnight before being used to transform Bioline α-select chemically competent cells (2.2.2), which were subsequently incubated overnight at 37°C on LB-agar plates containing 100µg/ml ampicillin.

If the number of colonies on the control plate was low (<4) and at least a 3-fold increase in colony number seen on the experimental plates, then up to 6 clones were selected for 5ml overnight culture in LBamp media to amplify plasmid copy number. Plasmid DNA was then isolated (2.3.1) and DNA concentrations measured by Nanodrop (2.3.4), before confirming quality and quantity of isolated plasmid DNA by electrophoresis. Several clones were then selected to undergo double restriction digests to test whether the ligation had been successful. Ligation of the AURKAIP1-FLAG insert into the pcDNA^{TM}5/FRT/TO vector was successful (Figure 3.3B) because the vector and insert can both be seen when digested plasmid DNA was separated by agarose gel electrophoresis.

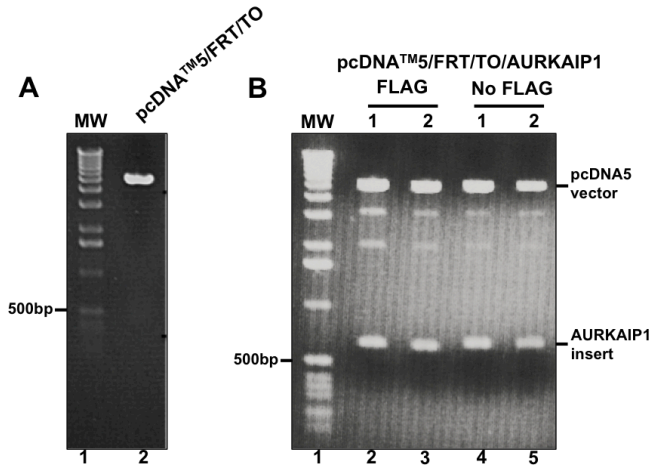

Figure 3.3: Successful cloning of pcDNA™5/FRT/TO/AURKAIP1-FLAG. A) An aliquot of digested pcDNA™5/FRT/TO was subjected to 0.8% agaroge gel electrophoresis **B)** Vector from **A** and gel extracted insert (Figure 3.2C) were ligated and used to transform α-select cells. Several clones were selected for cells transformed with either the FLAG tagged (lanes 2 and 3) or non-FLAG-tagged (lanes 4 and 5) construct. Clones were cultured at 37°C in LBamp and plasmid DNA was extracted by miniprep. Plasmid DNA from the clones were digested with *Hin*dIII and *Xho*I and an aliquot was subjected to 0.8% agarose gel electrophoresis.

3.2.1.4 Overcoming Truncated AURKAP1 pGEX-6P-1 Cloning Problems

The previously described methodology was immediately successful for the production of the pcDNA™5/FRT/TO/AURKAIP1-FLAG construct (Figure 3.3B), but despite several attempts, these methods could not produce successful ligation of the truncated AURKAIP1 construct in pGEX-6P-1. Further attempts at ligation using an increased insert:vector molar ratio of 8:1 were still unsuccessful at producing the desired construct.

To address this problem it was first important to ensure that the restriction endonucleases were digesting the vector and insert correctly. Digestion of the pGEX-6P-1 vector was confirmed by subjecting double digested vector to agarose gel electrophoresis and visualising a single band of approximately 5kb on the gel (Figure 3.4). This showed that the vector had been successfully linearised. However, linearisation could have occurred if only one of the restriction endonucleases were active. Since *Xho*I was also used in the successful generation of the pcDNA™5/FRT/TO/AURKAIP1-FLAG construct, it was only necessary to confirm the activity of the *Bam*HI enzyme. A restriction digest reaction using only the *Bam*HI

enzyme still resulted in successful linearisation of the vector. This proved that the *Bam*HI enzyme used was active.

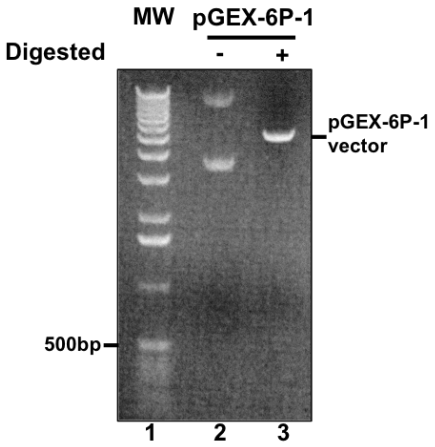

Figure 3.4: Confirmation of pGEX-6P-1 vector linearisation. An aliquot of isolated pGEX-6P-1 vector (lane 2) or pGEX-6P-1 vector digested with *Bam*HI and *Xho*I (lane 3) were subjected to separation through a 0.8% agaroge gel.

Since each of the restriction enzymes were confirmed to linearise the vector, it was more probable that the problem was with the insert. Though there were nucleotides added to the primers downstream of the restriction sites in order to allow endonuclease activity, it was possible that they were insufficient to allow for effective digestion of the inserts. As described earlier, linearisation of the vector was easy to confirm via electrophoresis, but it was impossible to confirm digestion of the insert in the same manner. The few nucleotides that should have been removed from the ends of the insert would have been undetectable by electrophoresis. This reasoning led to the use of the PCR-Script Amp cloning kit (Agilent technologies), which allows any blunt ended PCR product to be cloned into the PCR-Script Amp SK(+) vector. Cloning the truncated AURKAIP1 insert into this vector may improve endonuclease activity and would allow visual confirmation of insert digestion by electrophoresis.

The truncated AURKAIP1 insert was cloned into the PCR-Script Amp SK(+) vector by adding a 100ng aliquot of the PCR product to a 10µl ligation reaction containing 1x PCR Script reaction buffer, 0.5mM rATP, 10ng pre-digested PCR-Script Amp SK(+) vector, 0.5U/µl *Srf*I and 0.4U/µl T4 DNA ligase. The reaction was incubated for 1 hour at room temperature before heating at 65°C for 10 minutes. A 2µl aliquot of the reaction was then used to transform 40µl of Bioline α-select chemically competent cells (2.2.2). Colonies that were transformed by recombinant plasmid were selected by blue/white colour screening after overnight incubation at 37°C on LB-ampicillin agar plates spread

with 100µl of 10mM IPTG and 100µl of 2% X-gal 30 minutes prior to plating the transformation reaction.

Blue/white colony screening is possible due to the presence of a *lacZ'* gene in the PCR-Script Amp SK(+) vector which encodes the α-fragment of β-galactosidase. β-galactosidase is an enzyme that can catalyse X-GAL to 5-bromo-4-chloro-indoxyl, which then spontaneously dimerises and oxidises to form 5,5'-dibromo-4,4'-dichloro-indigo, which is a blue insoluble pigment. Bacterial colonies with functional β-galactosidase will therefore appear blue when grown on agar plates spread with X-GAL. Several *E.coli* strains (including α-select cells) express a mutated form of β-galactosidase, which has an N-terminal deletion and is inactive. Colonies of these bacteria will appear white when grown on agar plates spread with X-GAL due to a lack of β galactosidase activity. The mutated β-galactosidase can have its function restored with expression of the α-fragment, therefore α-select cells transformed with the PCR-Script Amp SK(+) vector would have active β-galactosidase activity. However, since the multiple cloning site of the PCR-Script Amp SK(+) vector is situated within the *LacZ'* gene, ligation of an insert would prevent the expression of the α-fragment of β-galactosidase.

White colonies from the transformation were selected on the basis that they must have been transformed with the PCR-Script Amp SK(+) vector, as this has conferred ampicillin resistance, and that the PCR-Script Amp SK(+) vector must have the insert in the multiple cloning site because there was no β-galactosidase activity. These white colonies were cultured in 5ml LBamp overnight at 37°C in order to amplify the plasmid copy number. Plasmid DNA was then isolated from bacterial lysate (2.3.1) and digested with *Bam*HI and *Xho*I. A 2µg aliquot of the digested construct was subjected to electrophoresis through a 1% agarose gel with 0.2µg/ml ethidium bromide. This technique confirmed that both restriction enzymes had correctly digested the insert because two bands were clearly visible corresponding to the size of the vector and the size of the insert respectively. Only one band with a size consistent with the sum of the sizes of vector and insert would have been seen if only one restriction enzyme had successfully cut the plasmid DNA.

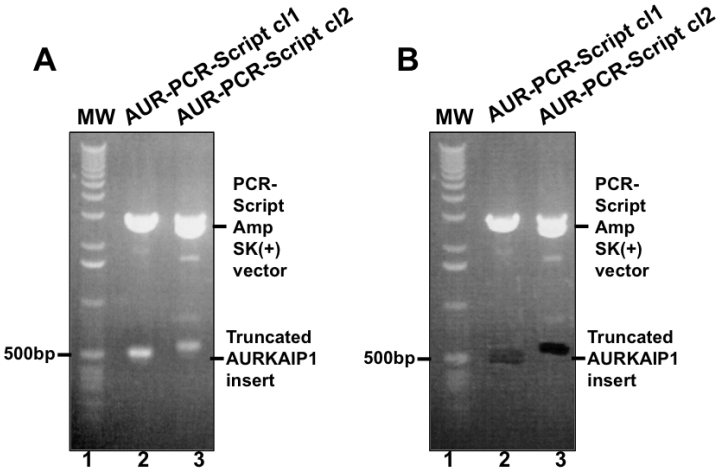

Figure 3.5: Generating Correctly Digested Truncated AURKAIP1 Insert via Cloning into PCR-Script Amp SK(+). A) Two bacterial colonies that were identified as being transformed with PCR-Script Amp SK(+)/truncated AURKAIP1 by blue/white colour colony screening were cultured in LB amp overnight at 37°C. Plasmid DNA was isolated from the bacterial lysate and subjected to double restriction digest with *Bam*HI and *Xho*I. An aliquot of the digestion reactions from two clones were each loaded on a 1.5% GTG low-melt agarose gel (lanes 2 and 3 respectively). **B)** the bands corresponding to the truncated AURKAIP1 insert were excised from the gel for use in subsequent ligation reactions.

Correctly digested pGEX-6P-1 vector and truncated AURKAIP1 insert, as confirmed by electrophoresis were excised and extracted from their respective gels using the QIAquick® Gel Extraction Kit. Further attempts to ligate the vector and insert and subsequently transform α-select cells were carried out. Though some colonies grew on the experimental LB-ampicillin agar plates, plasmid DNA isolation and double digests of all colonies from several ligation and transformation attempts failed to show any evidence of successful construct production.

To overcome this problem, an in-gel ligation reaction was used. The two different clones of the truncated AURKAIP1-PCR-Script construct were digested with *Bam*HI and *Xho*I before a 2μg aliquot was subjected to electrophoresis through a 1.5% GTG low melt agarose gel (Figure 3.5A). The insert was then excised from the gel (Figure 3.5B) and re-melted by placing at 68°C for 10 minutes. The re-melted gel was then placed at 37°C and an extra 10μl of dH_2O was added to prevent re-formation of the gel. The ligation reaction was prepared in a final volume of 25μl with 9μl 10mM Tris-HCL pH 7.5, 2.5μl 10x T4 DNA Ligation buffer, 0.5μl vector, 0.5μl T4 DNA Ligase and 12.5μl of re-melted agarose gel containing insert. The reaction was mixed and incubated

at room temperature for 3 hours. The ligation reaction was then re-melted at 68°C for 10 minutes and a 2μl aliquot was used to transform α-select cells as described previously.

After overnight culture at 37°C on LB-ampicillin plates there were zero colonies on the control plate (from ligation reaction lacking insert), three colonies from the transformation with the truncated AURKAIP1 clone 1 ligation and 15 colonies from the transformation with clone 2. Each of the 3 colonies from the clone 1 plate and 5 colonies from the clone 2 plate were cultured in 5ml LBamp overnight at 37°C and had plasmid DNA isolated by miniprep (2.3.1). Plasmid DNA from each colony was then double digested before an aliquot of each digested plasmid was subjected to electrophoresis through a 1% agarose gel with 0.2μg/ml ethidium bromide (Figure 3.6). The results show that two truncated AURKAIP1 pGEX-6P-1 clones (clones 3 and 4 from ligation with the insert from truncated AURKAIP1-PCR Script clone 2) were successfully produced (Figure 3.6, lanes 7 and 8).

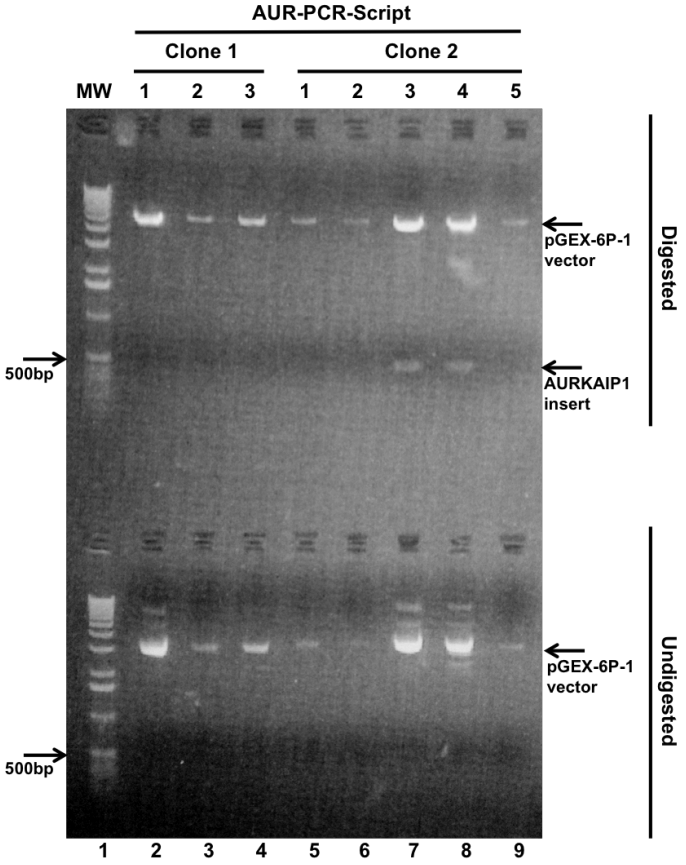

Figure 3.6: Successful Generation of pGEX-6P-1/truncated AURKAIP1 constructs.
Transformed colonies from ligation reactions performed with digested pGEX-6P-1 vector and either digested PCR-Script/AURKAIP1 clone 1 (Figure 3.5B lane 2) or clone 2 (Figure 3.5B lane 3) insert were selected and each cultured at 37°C in LBamp overnight. Plasmid DNA was isolated from each clone and subjected to 1% agarose gel electrophoresis (lower panel). An aliquot of plasmid DNA from each clone was subjected to double restriction digest with *Bam*HI and *Xho*I before separation through a 1% agarose gel (upper panel)

3.2.2 EXPRESSION AND PURIFICATION OF RECOMBINANT PROTEIN FROM BACTERIA

The purpose of generating the truncated AURKAIP1-pGEX-6P-1 construct was to allow expression of the mature form of the AURKAIP1 protein in bacteria for purification and antibody production. To this end, the plasmid construct was isolated from the transformed α-select cells and used to transform Rosetta cells. Rosetta is a strain of *E.coli* derived from BL21 cells. These cells include expression of additional tRNAs that are rare in bacteria, therefore allowing expression of mammalian proteins that would not usually be able to be expressed in bacteria. The AURKAIP1 gene in pGEX-6P-1 is under the control of a T7 promoter, which allowed IPTG induced expression of the GST-AURKAIP1 fusion protein.

Rosetta cells transformed with the truncated AURKAIP1-pGEX-6P-1 construct were cultured overnight at 37°C with aeration in 5ml LBamp. The overnight culture was then added to 500ml LB with appropriate antibiotics and grown at 37°C until OD_{600} of between 0.4 and 0.6 was achieved. IPTG (1mM) was then added to induce the expression of the GST-AURKAIP1 fusion protein and the cultures were incubated for a further 4 hours at 37°C. Aliquots of 5ml were taken to represent the cells both before (uninduced) and after (induced) the IPTG treatment. The cells in these smaller aliquots were pelleted and lysed with cell lytic B (Sigma). After lysis, aliquots of uninduced and induced cells were saved before insoluble and soluble proteins from the induced samples were separated by centrifugation. Finally representative samples of uninduced, induced, soluble and insoluble fractions were separated on a 12% polyacrylamide gel and stained with Coomassie Blue to assess expression and solubility of the protein.

Many iterations of the above protocol were used during experiments as the initial method failed to produce any soluble protein. Incubation at 37°C for 4 hours following IPTG induction produced only insoluble GST-AURKAIP1 fusion protein (Figure 3.7C). It is commonly found that reducing the incubation temperature post-induction can improve the solubility of expressed proteins in bacteria. Therefore the protocol was amended to incubate at 16°C for either 6 hours (Figure 3.7A) or overnight (Figure 3.7B) post IPTG induction. These conditions failed to produce any noticeable induction of the GST-AURKAIP1 fusion protein. It seemed that an incubation temperature of 16°C was insufficient to allow expression, but incubation at 37°C caused the packaging of the

expressed fusion protein into inclusion bodies. Therefore a post-IPTG induction temperature of 23°C was tested to try to encourage soluble expression of the fusion protein. However, though expression of the fusion protein was detectable, it could only be detected in the insoluble fraction (Figure 3.7D).

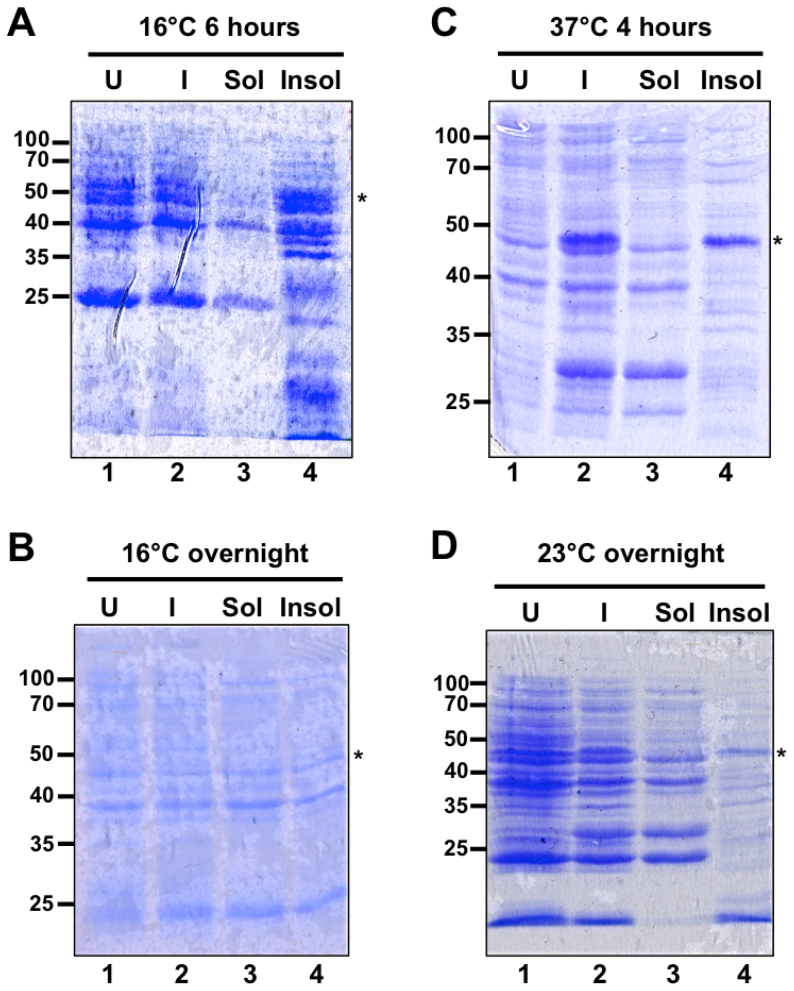

Figure 3.7: Expression of GST-AURKAIP1 Fusion Protein in Rosetta Cells. Rosetta cells transformed with the pGEX-6P-1/truncated AURKAIP1 plasmid were cultured to an OD of 0.4-0.6 before being induced with IPTG followed by incubation at 16°C for 6 hours (A), 16°C overnight (B), 37°C for 4 hours (C) or 23°C overnight (D). Lysate from uninduced cells (U, lanes 1), induced cells (I, lanes 2), soluble fraction of induced cells (Sol, lanes 3) and the insoluble fraction of induced cells (Insol, lanes 4) were subjected to SDS-PAGE through 12% polyacrylamide gels and stained with Coomassie Blue. * Denotes position of the GST-AURKAIP1 fusion protein.

Since lowering the incubation temperature failed to increase solubility of the expressed fusion protein, all further attempts were conducted at 37°C for 4 hours as this temperature allowed for induction most consistently. The next stage of method development led to the use of Tuner cells as host cells rather than the Rosetta cells. Tuner cells have the added benefit of a lac permease (*Lac*Y) mutation that allows

uniform entry of IPTG to the cultured cell population. This means that variations in IPTG concentration will affect the expression levels of the fusion protein. It was possible that low-level expression in this system would increase the solubility of the expressed GST-AURKAIP1 fusion protein. Thus, in the experiments with Tuner cells, IPTG concentrations were varied from 50μM to 500μM.

Expressing the GST-AURKAIP1 fusion protein in Tuner cells improved solubility. Generally, there was still a greater proportion of the fusion protein in the insoluble fraction but in some cases the proportions were roughly equal. Lowering the IPTG levels resulted in a decrease in the expression of the fusion protein as expected. However the relative proportion of soluble to insoluble expressed protein was not increased. An IPTG concentration of 250μM produced an expression level equivalent to using 500μM IPTG but more than 100μM IPTG, therefore 250μM IPTG induction followed by incubation at 37°C for 4 hours became the standard protocol. Despite this, the expression levels and relative proportions were always slightly variable. Figure 3.8 illustrates two examples of induction using the standard protocol in Tuner cells.

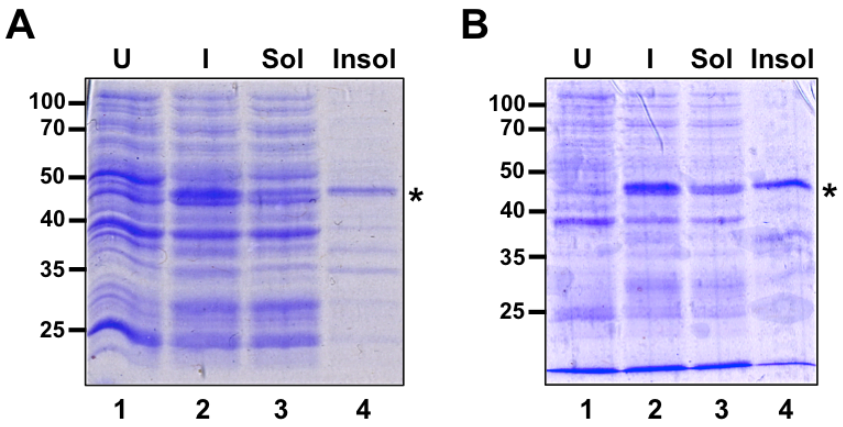

Figure 3.8: Expression of GST-AURKAIP1 Fusion Protein in Tuner Cells. Tuner cells transformed with the pGEX-6P-1/truncated AURKAIP1 plasmid were cultured to an OD of 0.4-0.6 before being induced with 250μM IPTG followed by incubation at 37°C for 4 hours (A and B). Lysate from uninduced cells (U, lanes 1), induced cells (I, lanes 2), soluble fraction of induced cells (Sol, lanes 3) and the insoluble fraction of induced cells (Insol, lanes 4) were subjected to SDS-PAGE through 12% polyacrylamide gels and stained with Coomassie Blue. * Denotes position of the GST-AURKAIP1 fusion protein.

Once conditions for producing as much soluble protein as possible had been optimised, the appropriately induced large (500ml) cultures were subjected to centrifugation at 5000RPM for 15 minutes at 4°C using a Sorvall GSA centrifuge (Rotor code 10). The resulting pellet of cells was frozen at -80°C for at least 2 hours before thawing and resuspending in 10ml PBS supplemented with 1mM PMSF, 1 protease inhibitor tablet

and 1µl Benzonase. The suspension was incubated on ice for 20 minutes before sonicating 15x for 10 seconds with intervals of 10 seconds. The suspension was centrifuged at 30000*g* and the supernatant filtered before this induced soluble fraction was saved for further purification.

The next stage was purification of the soluble GST-AURKAIP1 fusion protein from the rest of the soluble proteins, before cleaving the mature AURKAIP1 from its GST tag. The induced soluble fraction was added to 0.6ml of Glutathione-Sepharose beads in a 10ml BioRad column and incubated overnight at 4°C with agitation. The suspension was then passed through the column and an aliquot of the flow through was stored. The beads were then washed by passing 50ml of PBS (supplemented with 1mM PMSF and 1 protease inhibitor tablet) through the column followed by 50ml of PBS (no supplements). After washing, 750µl PBS with 1mM DTT, 1mM EDTA and 24µl PreScission protease was added to the beads, before incubating overnight at 4°C. The elution from the column was then saved, which contained soluble AURKAIP1 (Figure 3.9).

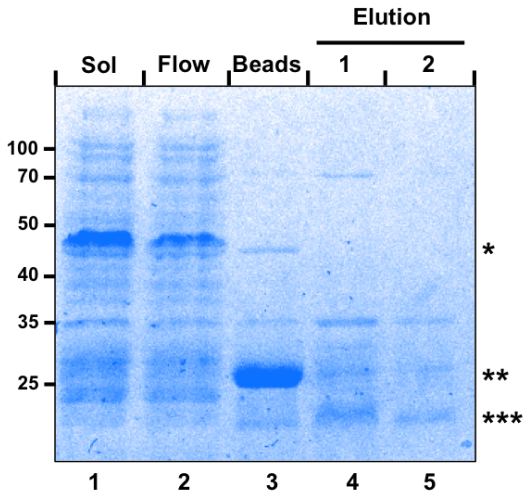

Figure 3.9: Purifying Recombinant Mature AURKAIP1. The soluble fraction was prepared from Tuner cells induced to express GST-AURKAIP1 with IPTG (Sol, lane 1). The soluble fraction was then incubated with Glutathione Sepharose beads overnight at 4°C. The flowthrough (lane 2) was collected before PreScission Protease was added to the beads to cleave between the GST and AURKAIP1. After the incubation with PreScission Protease, the AURKAIP1 was eluted in two fractions (lanes 4 and 5) and a sample of the remaining beads (lane 3) was also collected. Aliquots of the described samples were subjected to SDS-PAGE through a 12% polyacrylamide gel. * Denotes the size of the GST-AURKAIP1 fusion protein, ** denotes the size of GST and *** denotes the size of AURKAIP1.

The elution of AURKAIP1 was not completely clean and produced multiple bands. However there was a clear band corresponding to the size of the mature AURKAIP1 and most of the GST was successfully removed. It was therefore decided to proceed

with antibody production using the eluted fraction. The additional proteins present should not have presented a great problem as polyclonal antibodies were to be produced, meaning that antibodies could be produced to several proteins. Therefore the presence of the additional proteins may produce a less clean antibody, but as long as the antibody was capable of recognising AURKAIP1 it would be useful. Additionally, the extra proteins were bacterial and therefore antibodies raised to them would be unlikely to recognise mammalian proteins, which should mean that when used on mammalian cell lysate, only AURKAIP1 would be recognised by the antibody.

3.2.3 ANTIBODY PRODUCTION

The protein concentration of the soluble AURKAIP1 elution was estimated by Bradford assay. Approximately 1mg of the elution was sent to Eurogentech for use in their speedy 28-day polyclonal antibody production protocol. The polyclonal antibodies were raised in rabbits. Two rabbits were used to produce the antibodies (rabbit 1349 and 1350), both following the same procedure. The animals were immunised with approximately 200μg soluble AURKAIP1 on day 0, day 7, day 10 and day 18 of the protocol and blood was taken on day 0 just before immunisation (pre-immune serum), day 21 (medium bleed) and day 28 (final bleed). Serum from the pre-immune (approximately 2ml), medium bleed (approximately 10ml) and final bleed (approximately 50ml) were sent from Eurogentech to be tested and purified.

The Pre-immune serum, medium bleed and final bleed from each rabbit was used as a primary antibody for immunoblotting (2.5.6). Each blot had protein loaded from the mature AURKAIP1 elution, HEK293 cell lysate and lysate from induced AURKAIP1-FLAG overexpressing HEK293 cells. Pre-immune serum from each rabbit did not detect any cross-reacting material of the correct size. Only the final bleed from rabbit 1349 detected a strong signal from the induced AURKAIP1-FLAG overexpressing HEK293 cells. However the antibody was not clean and there were several non-specific bands. Therefore the final bleed serum from rabbit 1349 was subjected to further purification.

3.2.4 ANTIBODY PURIFICATION

Approximately 900μg of soluble AURKAIP1 in 1.5ml PBS buffer was added to 0.6ml NHS-activated Sepharose 4 fast flow beads that had been pre washed 3 times with 10ml cold 1mM HCL. The beads and protein were left to incubate overnight at 4°C with agitation. The flowthrough was saved and 0.1M Tris/HCL (pH 7.4) was added to the beads and left to incubate overnight at 4°C. The flowthrough was discarded and the beads washed 5 times with PBS. Serum from the final bleed of rabbit 1349 was sequentially filtered through 0.45μm and 0.2μm filters before 7ml was added to the beads along with 3ml PBS and left to incubate overnight at 4°C with agitation. The flowthrough was saved and then the beads were washed twice with 10ml PBS, once with 1x Tris-buffer pH 8.0 (50mM Tris/HCL pH 8.0, 0.1% Triton X-100 and 0.5M NaCl), once with 1x Tris-buffer pH 9.0 (50mM Tris/HCL pH 9.0, 0.1% Triton X-100 and 0.5M NaCl) and once with 1x sodium phosphate buffer pH 6.3 (50mM sodium phosphate pH 6.3, 0.1% Triton X-100 and 0.5M NaCl). Adding 5ml Glycine-buffer pH 2.5 (50mM Glycine pH 2.5, 0.1% Triton X-100 and 0.15M NaCl) then eluted the affinity-purified antibodies where they were immediately neutralised by collecting across 6 tubes with 150μl 1M Tris/HCL pH 9.0 already added.

The collected antibodies were then pooled together and placed inside dialysis tubing. The tubing was sealed and the antibodies were subjected to buffer exchange in 500ml of PBS overnight at 4°C with stirring. This treatment was repeated a further two times by replacing with fresh PBS.

After buffer exchange the antibodies, still in the dialysis tubing, were placed in AQUACIDE II powder (Millipore), which absorbed water through the dialysis tubing, thus concentrating the antibodies. The concentration procedure was monitored over several hours until the volume of the antibodies was approximately 1.5ml. Final concentrations of 10% glycerol and 0.02% sodium azide were then added before the final purified AURKAIP1 polyclonal antibody was aliquoted to avoid repeated freeze-thaw cycles.

The purified antibody was tested against the unpurified final bleed serum to test if the purification had been successful in reducing non-specific binding. Aliquots of 5μg and 10μg of uninduced and induced AURKAIP1-FLAG cell lysate were loaded onto a

single 12% polyacrylamide gel in duplicate. After SDS-PAGE and western blot transfer the membrane was cut in half before blocking with 5% milk in TTBS. The two membrane pieces were then treated separately. One was incubated with unpurified final bleed serum, and the other with purified AURKAIP1 antibody. Each antibody was diluted 1 in 500 in 5% milk in TTBS and incubated with the membrane overnight at 4°C. All subsequent immunoblotting steps were carried out as described in 2.5.6 and detected on the Storm Phosphorimager. The antibody purification (Figure 3.10B) significantly reduced the background and non-specific high MW binding compared to the unpurified serum (Figure 3.10A).

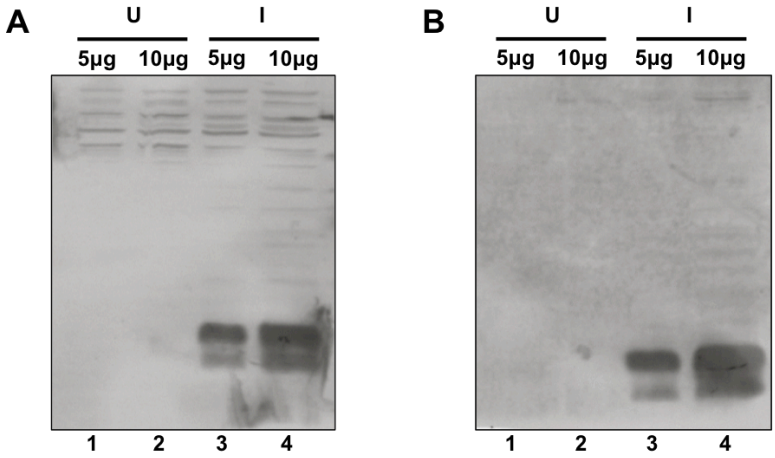

Figure 3.10: Purification of Endogenous AURKAIP1 Antibody. Mitochondrial lysate was prepared from HEK293-AURKAIP1-FLAG cells that had been either induced with 1µg/ml tetracycline (I) or remained uninduced (U) for 3 days. Aliquots of uninduced (5µg, lanes 1 or 10µg, lanes 2) or induced (5µg, lanes 3 or 10µg, lanes 4) mitochondrial lysate were subjected to SDS-PAGE through a 14% polyacrylamide gel and immunoblotted with either unpurified (A) or purified (B) AURKAIP1 antibodies at a 1 in 500 dilution.

The purified endogenous AURKAIP1 antibody was tested further at various dilutions to determine the best working dilution to use for subsequent experiments. Dilution of 1 in 1000 produced similar results to the 1 in 500 dilution, but 1 in 2000 dilution of the antibody produced weaker signal. Therefore a dilution of anti-AURKAIP1 of 1 in 1000 in T-TBS was used for immunoblotting in all subsequent experiments.

3.3 DISCUSSION

The successful generation of the endogenous AURKAIP1 antibody was vitally important for further experiments that will be presented throughout the remaining chapters. The AURKAIP1 antibody recognises overexpressed AURKAIP1-FLAG (Figure 3.10A and B, lanes 3 and 4), but does not appear to recognise the endogenous AURKAIP1 in the uninduced cells (Figure 3.10A and B, lanes 1 and 2). This could indicate low endogenous AURKAIP1 levels in HEK293 cells as the levels in 10μg of uninduced HEK293 mitochondrial lysate cannot be detected by western blot using the produced polyclonal AURKAIP1 antibody (Figure 3.10A and B, lanes 2). Alternatively, the lack of signal could indicate that endogenous AURKAIP1 is not present in the mitochondria. This seems unlikely because the overexpressed AURKAIP1-FLAG is detected in the mitochondrial lysates. These data show that the produced AURKAIP1 antibody recognises overexpressed AURKAIP1-FLAG in human cells, showing the specificity of the antibody. Further, the detection of AURKAIP1-FLAG in mitochondrial lysates is the first indication from my own data to suggest mitochondrial localisation of AURKAIP1. This is in accordance with online prediction tools (TargetP (Emanuelsson et al., 2007), MitoProt II (Claros and Vincens, 1996), Predotar (Small et al., 2004), pTARGET (Guda, 2006) and MultiLoc2 (Blum et al., 2009)) that all strongly predict mitochondrial localisation for AURKAIP1. Therefore, assuming mitochondrial localisation of AURKAIP1, these data suggest endogenous levels of AURKAIP1 are low in HEK293 cells.

Another observation that could indicate low endogenous levels of AURKAIP1 is that no PCR product could be produced when using cDNA from HEK293 cells as a template (Figure 3.1). However, the desired PCR products were obtained when using an AURKAIP1 I.M.A.G.E. clone as a template, which confirmed the primers were appropriate (Figure 3.2). Furthermore, PCR reactions designed to amplify another protein (SLMO2) were successful (Figure 3.1), when using the same cDNA from HEK293 cells. One explanation of these results could be that AURKAIP1 expression levels are very low and that there was insufficient *AURKAIP1* present in the HEK293 cDNA to allow amplification, whereas *SLMO2* is expressed to higher levels and therefore could be amplified from the cDNA template. However, it is also possible that the primers designed for *AURKAIP1* amplification were simply not as efficient as the

primers designed for *SLMO2* amplification despite similar length, G-C content and melting temperature.

Though the focus in this chapter was on generating tools, which were successfully produced, the data presented also provides initial observations that suggest that the endogenous levels of AURKAIP1 are low, at least in HEK293 cells. To confirm this, increased amounts of lysate needed to be loaded onto the gels for western blot and lysates from other cell types also needed to be tested. Further experiments to confirm these early observations and to further characterise the localisation of AURKAIP1 will be the focus of the following chapter.

CHAPTER 4: IS AURKAIP1 A MITOCHONDRIAL PROTEIN?

4.1 INTRODUCTION

The preliminary siRNA screen carried out in my host laboratory strongly suggested that AURKAIP1 is a protein important for mitochondrial function; since depletion of AURKAIP1 caused growth defects in HeLa cells, but not in 143B Rho^0 cells. However, experimental confirmation of the mitochondrial localisation of AURKAIP1 was required. If AURKAIP1 were to be identified as mitochondrial then it would also be crucial to know which of the sub-organellar compartments it is located in.

AURKAIP1 was originally described as a nuclear protein that interacts with Aurora A kinase. In these studies, however, an N-terminal FLAG-tagged protein was used (Lim et al., 2007), which could have resulted in mislocalisation by interfering with the predicted N-terminal mitochondrial targeting sequence of AURKAIP1. According to the Human Protein Atlas (HPA) project, AURKAIP1 has both nuclear and mitochondrial localisation, as determined by immunohistochemistry and fluorescence microscopy (Uhlen et al., 2010). However, these data are unconvincing as only one antibody was used and when the same antibody was used for immunodetection on HEK293 cell lysate, several bands were detected. This casts doubt over the localisation data as the antibody may be binding non-specifically.

During the course of my PhD investigations, two more publications were released that partly addressed the localisation of AURKAIP1. First, a recent publication described the mitochondrial localisation of AURKAIP1 via expression of C-terminal GFP-tagged AURKAIP1 (Szklarczyk et al., 2012). The GFP-tagged AURKAIP1 was shown to co-localise with the mitochondrial specific dye TMRM, indicating that the fusion protein was in, or in the vicinity of mitochondria (Szklarczyk et al., 2012). However, this gives no information as to the sub-localisation of AURKAIP1. A second recent publication suggests that bovine AURKAIP1 is a mitochondrial protein. Koc *et al.* found AURKAIP1 via capLC-MS/MS to be in preparations of bovine mitochondrial ribosomes (Koc et al., 2013). Since this work suggests AURKAIP1 to be a mitoribosomal protein (Koc et al., 2013), it would also imply localisation to the mitochondrial matrix.

However, there are no published data showing that endogenous AURKAIP1 is present in human mitochondria. In this chapter I will present evidence for the intra-mitochondrial localisation of both C-terminal FLAG-tagged and endogenous AURKAIP1 to the matrix, the innermost compartment of the organelle, in human cells.

4.2 METHODS

4.2.1 STABLE TRANSFECTION OF FLP-IN™ TREX™ CELLS

Flp-In™ TREx™ cells (either HEK293 or U2OS, see 2.1.1 for cell line details) were transfected with pcDNA™5/FRT/TO vector (Invitrogen) containing the gene of interest, AURKAIP1 with an in-frame C-terminal FLAG tag (AURKAIP1-FLAG) (see 3.2.1 for details on construct generation). Cells were seeded in a 6 well plate at approximately 50-60% confluency in the morning for an afternoon transfection. For each transfection two ratios of DNA:Superfect (QIAGEN) were used, 1:5 and 1:7.5. 2μg of DNA (0.2μg pcDNA™5/FRT/TO/AURKAIP1-FLAG and 1.8μg pOG44) and either 10μg or 15μg Superfect were added to 100μl DMEM (Sigma) without supplements. After a ten-minute incubation at room temperature, during which time the spent media was aspirated from the cells, 600μl DMEM (with supplements) was added and the whole mix carefully transferred to the wells. After a 3 hour incubation at 37°C the media was replaced with fresh DMEM (with supplements). Selection was initiated after 2 days by supplementing medium with 100μg/ml Hygromycin^{B} (Invitrogen) and 10μg/ml Blasticidin^{S} (Melford). A control well of untransfected cells was always included in the antibiotic treatment. This was to confirm the effects of the antibiotics so that, when all control cells were dead, any remaining in the transfected wells would represent antibiotic resistant populations conferred by successful transfection.

Cells were monitored each day and the media was changed to remove dead cells. Once only antibiotic resistant cells remained the plates were monitored for growth of clonally derived populations, which were subsequently isolated and maintained as independent clonal cell lines. Clonal cell lines were obtained by picking independent colonies that had grown from a single transfectant, and transferring to independent growth vessels. Clones were numbered sequentially, but some clones did not grow well after the selection process. A population was retained, which comprised a mix of the remaining transfectants that had not been clonally selected. These lines were subsequently tested

by subjecting 40μg of cell lysate from uninduced and induced (with 1μg/lm tetracycline for 3 days) cells to 12% SDS-PAGE and western blotting, before immunodetection with an α-FLAG antibody (Sigma). This was to confirm the inducible expression of the AURKAIP1-FLAG protein, which was encoded by the inserted gene.

4.2.2 SUB-MITOCHONDRIAL LOCALISATION

I optimised this technique through several iterations of this protocol in order to generate clean separation of the individual mitochondrial compartments. The following is the final protocol used to generate the data presented in this report.

Mitochondria were isolated as described previously (2.5.2) and the protein concentration was measured by Bradford assay (2.5.3). All of the following steps were carried out at 4°C unless otherwise specified. An aliquot of isolated mitochondria (300 μg) was resuspended in a total volume of 150μl homogenisation buffer. A 12.5μl (25μg) aliquot was taken and an equal volume of 2x dissociation buffer added to form the 'total mitochondrial proteins' fraction. A volume of 1.237ml of 5mM Tris/HCl pH 7.4; 1mM EDTA was added to the remaining isolated mitochondria in homogenisation buffer, before being gently mixed and split into two equal volumes (designated as sample 1 and sample 2). Sample 1 was incubated with 10μg of proteinase K with shaking for 30 minutes at 37°C before 1mM PMSF was added to each sample (1 and 2). Both samples 1 and 2 were pelleted at 8000*g* for 10 minutes at 4°C and washed twice each with 1ml 5mM Tris/HCl pH 7.4; 1mM EDTA. Each pellet was resuspended in 68.7 μl homogenisation buffer. A 12.5μl (25μg) aliquot of sample 1 was taken and an equal volume of 2x dissociation buffer added, which was designated as the 'shaved mitoplast' fraction. A 12.5μl (25μg) aliquot of sample 2 was taken and an equal volume of 2x dissociation buffer added, which was designated as the 'mitoplast' fraction. Homogenisation buffer was then added to each sample to a final volume of 687μl and subsequently centrifuged at 12,000*g* for 10 minutes at 4°C. The supernatants were discarded and the each of the pellets was resuspended in 1.125ml 100mM Na_2CO_3 and incubated for 30 minutes at 4°C. Both samples were pelleted in the bench Beckman Optima TLX ultracentrifuge at 53,000rpm (rotor code TLA 120.2) for 15 minutes at 4°C. Each pellet was finally resuspended in 50μl homogenisation buffer. A 12.5μl (25μg) aliquot of each sample had an equal volume of 2x dissociation buffer added and

was designated the 'Na_2CO_3 extracted proteins' fraction (sample 1, PK-shaved and sample 2, unshaved). An aliquot of each collected fraction (10μg) was then loaded onto 14% SDS:PAGE for subsequent western blot analysis.

Homogenisation buffer (final concentrations)

0.6M Mannitol

10mM Tris/HCl pH7.4

1mM EGTA

Filter sterilised and then stored at 4˚C for no longer than 3 months.

4.3 RESULTS

4.3.1 CONFIRMATION OF AURKAIP1-FLAG EXPRESSION IN FLPIN™ TREX™ CELLS

Clonal AURKAIP1-FLAG overexpressing cell lines were established (both U2OS-AURKAIP1-FLAG and HEK293-AURKAIP1-FLAG lines were produced) and tested to confirm AURKAIP1-FLAG expression. AURKAIP1-FLAG expression was induced by addition of 1μg/ml tetracycline to the cell culture media for 3 days before cells were harvested and lysates analysed by western blotting. When probing with an anti-FLAG antibody, a protein migrating to approximately 15kDa was clearly present in all induced clonal lines tested (Figure 4.1, lanes 4, 6, 8 and 10) that was not present in the uninduced controls (Figure 4.1, lanes 1, 3, 5, 7 and 9). Porin was used as a loading control.

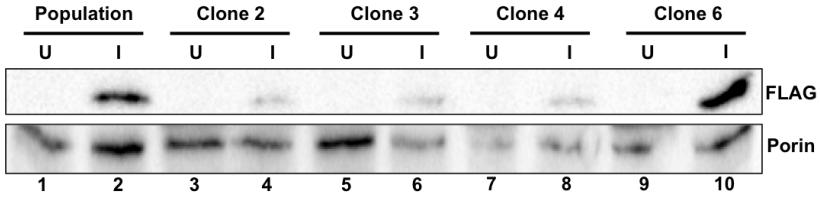

Figure 4.1: Expression of AURKAIP1-FLAG in U2OS Cells. Cell lysates (40μg) from uninduced cells (U) and induced cells (I; grown in presence of 1μg/ml tetracycline for 3 days) were produced from U2OS-AURKAIP1-FLAG cell lines. Several clones (clone 2 = lanes 3 and 4, clone 3 = lanes 5 and 6, clone 4 = lanes 7 and 8, clone 6 = lanes 9 and 10) and the population (lanes 1 and 2) were subjected to 12% SDS-PAGE western blotting using α-FLAG and α-porin antibodies for immunodetection.

The induction of the FLAG-tagged protein confirmed that the production of the stable, inducible cell line was successful. The observed protein size of 15kDa was considerably smaller than the predicted molecular weight of AURKAIP1 (22.4kDa, Figure 4.2B), however, this would be consistent with cleavage of a substantial mitochondrial targeting sequence. Supporting this, if an N-terminal pre-sequence of 76 amino acids (as predicted by TargetP, Figure 4.2A) was removed, the remaining mature protein would be predicted to have a molecular weight of 14.3kDa (Figure 4.2C), which is very close to the size of the observed AURKAIP1-FLAG band on the western blot.

A

Name	Len	mTP	SP	other	Loc	RC	TPlen
AURKAIP1	199	0.815	0.091	0.051	M	2	76

B

```
        10         20         30         40         50         60
MLLGRLTSQL LRAVPWAGGR PPWPVSGVLG SRVCGPLYST SPAGPGRAAS LPRKGAQLEL

        70         80         90        100        110        120
EEMLVPRKMS VSPLESWLTA RCFLPRLDTG TAGTVAPPQS YQCPPSQIGE GAEQGDEGVA

       130        140        150        160        170        180
DAPQIQCKNV LKIRRRKMNH HKYRKLVKKT RFLRRKVQEG RLRRKQIKFE KDLRRIWLKA

       190
GLKEAPEGWQ TPKIYLRGK
```

Predicted MW 22354.2 Da

C

```
        10         20         30         40         50         60
WLTARCFLPR LDTGTAGTVA PPQSYQCPPS QIGEGAEQGD EGVADAPQIQ CKNVLKIRRR

        70         80         90        100        110        120
KMNHHKYRKL VKKTRFLRRK VQEGRLRRKQ IKFEKDLRRI WLKAGLKEAP EGWQTPKIYL


RGK
```

Predicted MW 14349.82 Da

Figure 4.2: Predicted Molecular Weight of AURKAIP1. (A) TargetP prediction of mitochondrial localisation and N-terminal pre-sequence length. The output displays sequence length (len), Final NN scores (on which the final probability is based) for presence of a mitochondrial targeting peptide (mTP), signal peptide (SP) for secretory pathway or any other location (other). The predicted localisation (Loc) based on the NN scores is shown to mitochondria (M). The reliability class (RC) is a measure of the strength of the prediction and values range from 1-5 with 1 being the strongest predictor. The predicted pre-sequence length (TPlen) from the additional cleavage site prediction is also shown (Emanuelsson et al., 2007). **(B)** The full length AURKAIP1 amino acid sequence with the predicted molecular weight as calculated using the ProtParam online tool (Gasteiger et al., 2005). **(C)** The predicted amino acid sequence of mature AURKAIP1 with the predicted 76 amino acid N-terminal targeting sequence removed and the predicted molecular weight.

4.3.2 AURKAIP1 IS A MITOCHONDRIAL MATRIX PROTEIN

To address the question of mitochondrial localisation of AURKAIP1, mitochondria were isolated from HEK293-AURKAIP1-FLAG cells following 3 days induction with 1μg/ml tetracycline and mitochondrial lysates were analysed by immunoblotting with an α-FLAG antibody. The isolated mitochondria had been treated with proteinase K (PK) to degrade cytosolic contaminants or broken mitochondria. Western blot analysis showed that AURKAIP1-FLAG was present in the PK treated mitochondria (data not shown), however, with concomitant addition of triton X-100 added to break up the mitochondrial membrane, less AURKAIP1-FLAG could be detected. This preliminary experiment suggested AURKAIP1-FLAG was present within the mitochondria.

To investigate the mitochondrial localisation of AURKAIP1 further, a sub-localisation protocol was used (illustrated in Figure 4.3A). This allowed separation of mitochondria into the constituent sub-fractions. Mitochondrial fractions were confirmed using antibodies to known markers of the outer membrane (Tom20), inner membrane (NDUFA9), inter membrane space (AIF), matrix (GDH) and post mitochondrial supernatant (S6) (Figure 4.3B). AURKAIP1-FLAG was detected in the same fractions (Figure 4.3B, lanes 2, 3, and 4) as GDH (glutamate dehydrogenase), which is a mitochondrial matrix protein. A small amount of GDH was seen in the membrane fractions. This was to be expected as there are several isoforms of GDH, some of which are membrane-bound (Rajas et al., 1996). There is no detectable signal for AURKAIP1-FLAG in the membrane fractions (Figure 4.3B, lanes 5 and 6), suggesting AURKAIP1 is a soluble protein present in the matrix.

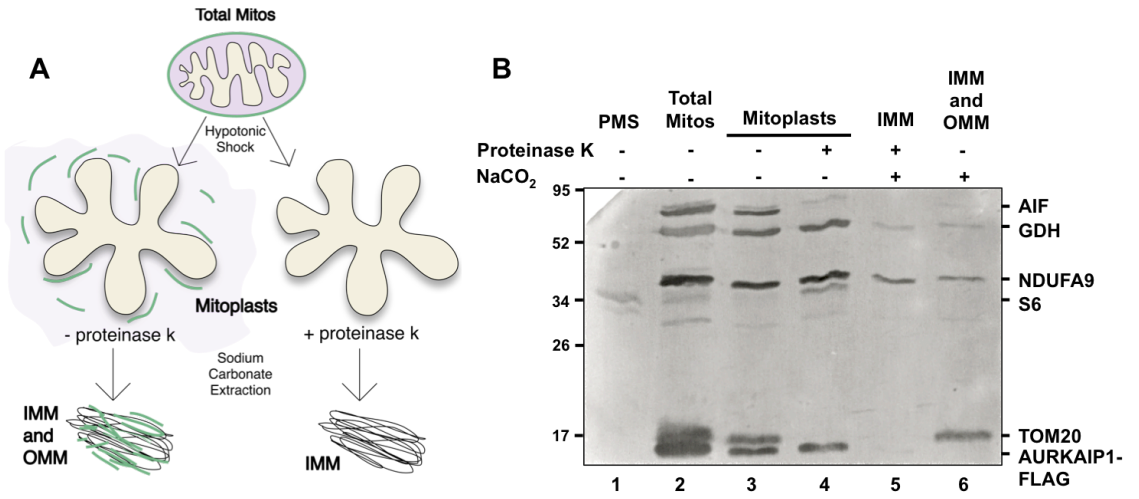

Figure 4.3: AURKAIP1-FLAG is Present In the Mitochondrial Matrix: A) Schematic diagram of the mitochondrial sub-localisation procedure. IMM = inner mitochondrial membrane, OMM = outer mitochondrial membrane **B)** Mitochondria were isolated from AURKAIP1-FLAG Hek-293-Flp-In^{TM} cell lines that were induced for 3 days. Samples (approximately 10μg) of post mitochondrial supernatant (PMS) (lane 1), and total mitochondrial proteins (lane 2) were saved before the isolated mitochondria were further subfractionated by hypotonic shock to form mitoplasts (lane 3) which were treated with proteinase k (PK) to form shaved mitoplasts (lane 4). Membrane proteins were then isolated by sodium carbonate extraction of PK shaved mitoplasts (lane 5) or untreated mitoplasts (lane 6). These were analysed by 14% SDS-PAGE and immunoblotting with antibodies against FLAG and known markers for the outer mitochondrial membrane (Tom20), intermembrane space (AIF), matrix (GDH) and inner mitochondrial membrane (NDUFA9).

4.3.3 Endogenous AURKAIP1

Once the localisation of the AURKAIP1-FLAG protein was established to be predominantly in the mitochondrial matrix, confirmation of the localisation of the endogenous levels of AURKAIP1 was required. The endogenous levels of AURKAIP1 are very low and are not detectable by western blot on 40μg cell lysate from HEK 293 or HeLa cells. To detect endogenous AURKAIP1 it was necessary to load 50μg of isolated mitochondria from 143B cells. Immunodetection was performed using an endogenous α-AURKAIP1 antibody, the production of which was described in Chapter 3. To confirm that the detected band was indeed AURKAIP1 and was not due to non-specific binding of the antibody, cells were depleted of AURKAIP1 via siRNA. AURKAIP1 siRNA was able to deplete overexpressed AURKAIP1-FLAG in HEK293 cells (Figure 4.4A, lanes 2, 4 and 6) and endogenous AURKAIP1 in 143B cells (Figure 4.4B, lane 3) relative to control cells transfected with non-targeting siRNA (Figure 4.4B lane 1). These data confirm: i) the ability of the produced AURKAIP1 antibody to detect endogenous AURKAIP1, ii) the specificity of the AURKAIP1 siRNA for its target, iii) endogenous AURKAIP1, although at low levels, is present in mitochondria.

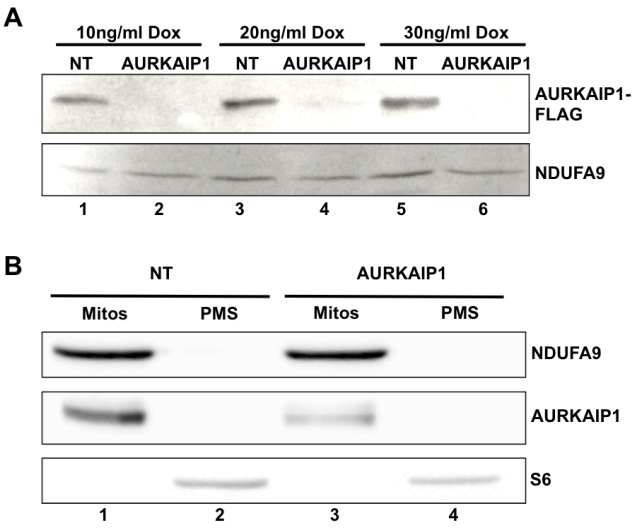

Figure 4.4: AURKAIP1 siRNA can Deplete Both Expressed and Endogenous AURKAIP1 A) HEK293-AURKAIP1-FLAG cells were subjected to transfection with either non targeting (NT) or AURKAIP1 siRNA and induced with several concentrations of doxycycline (Dox) for 3 days. Cell lysate (40μg) was subjected to 12% SDS-PAGE and western blot followed by immunodetection with α-FLAG and α-NDUFA9 antibodies. **B)** Mitochondrial lysate (50μg) and post-mitochondrial supernatant (PMS, 50μg) from 143B cells transfected with either non-targeting (NT) or AURKAIP1 specific siRNA for 4 days was subjected to 14% SDS-PAGE and western blotting. Immunodetection was performed using antibodies against AURKAIP1, NDUFA9 (mitochondrial inner membrane) and S6 (cytosolic ribosomal protein).

Endogenous levels of AURKAIP1 in HEK293, HeLa and U2OS cells are lower than in 143B cells and as such cannot be detected by western blotting when loading 50μg of mitochondrial lysate. It was important to confirm that the endogenous AURKAIP1 was present in the matrix, to verify the findings obtained using AURKAIP1-FLAG. Western blot analysis of approximately 200μg of PK-shaved mitoplasts (performed by Dr Hornig-Do) allowed detection of signal for AURKAIP1 (Figure 4.5C), thus confirming that endogenous levels of AURKAIP1 are present in the mitochondrial matrix.

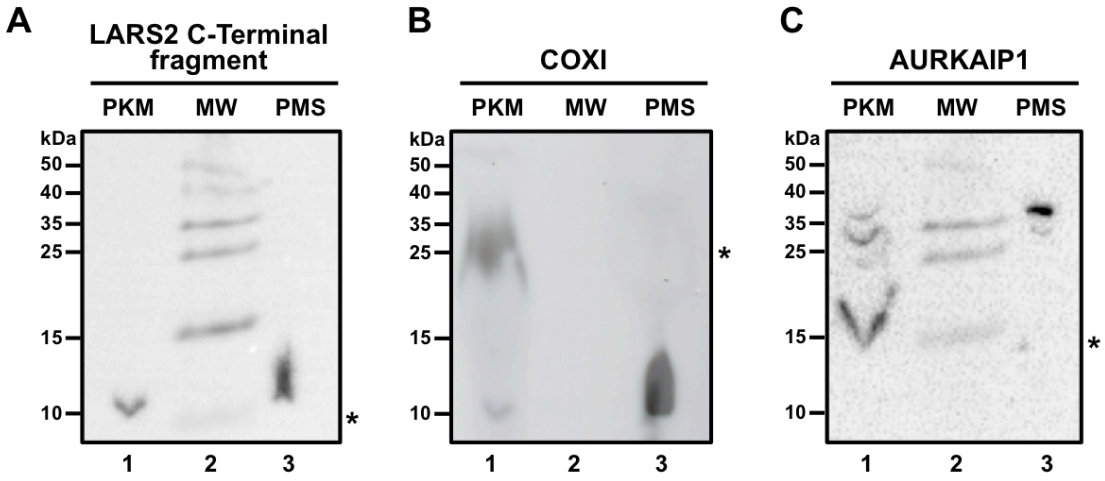

Figure 4.5: Endogenous AURKAIP1 is Detectable in PK Shaved Mitoplasts from HEK293 Cells. Approximately 200μg of Proteinase K (PK) shaved mitoplasts (PKM, lane 1) and post-mitochondrial supernatant (PMS, lane 3) were separated by 15% SDS-PAGE and western blotting by Dr Hornig-Do. (A) Dr Hornig-Do performed immunoblotting antibodies against FLAG to detect the expressed FLAG-tagged C-terminal LARS2 fragment and (B) COXI. I then immunoblotted with the custom polyclonal α-AURKAIP1 antibody **(C)**. A molecular weight marker (MW) was loaded in lane 2.

4.4 DISCUSSION

I have shown that AURKAIP1 is predominantly a mitochondrial matrix protein. Sub-mitochondrial localisation experiments showed that overexpressed C-terminal FLAG-tagged AURKAIP1 is present in the mitochondrial matrix (Figure 4.3B). Furthermore, endogenous AURKAIP1 is detected in PK-shaved mitoplasts of HEK293 cells (Figure 4.5) and in mitochondrial lysates of 143B cells (Figure 4.4B). These data are in agreement with recent reports, published during the course of my PhD investigations that have also suggested the mitochondrial localisation of AURKAIP1. Szklarczyk *et al.* demonstrated that C-terminal GFP-tagged AURKAIP1 co-localises with the mitochondrial marker TMRM via fluorescence microscopy (Szklarczyk et al., 2012). Additionally, another study has suggested that AURKAIP1 is present in preparations of bovine mitochondrial ribosomes (Koc et al., 2013). This work implies mitochondrial matrix localisation as it identifies AURKAIP1 by mass spectrometry as associated with mitoribosomes (Koc et al., 2013). However, the work of Koc *et al.* was conducted in bovine tissue (Koc et al., 2013) and the fluorescent microscopy studies with GFP-tagged AURKAIP1 only indicates co-localisation with mitochondria (Szklarczyk et al., 2012). I believe, therefore, that the work presented in this chapter is the first to conclusively demonstrate that AURKAIP1 is present in the mitochondrial matrix of human cells.

The C terminal FLAG-tagged AURKAIP1 that is detected in the mitochondrial matrix is considerably shorter (approximately 15 kDa, Figure 4.3B) than the predicted full length AURKAIP1 protein (22.4kDa, Figure 4.2B). Since the C-terminal FLAG tag remains intact, these data strongly suggest that the full length AURKAIP1 protein has an N-terminal mitochondrial targeting sequence, which is cleaved upon import into mitochondria. Furthermore, endogenous AURKAIP1 detected in the mitochondrial preparations of 143B cells and in PK-shaved mitoplasts of HEK293 cells was also approximately 15kDa in size (Figure 4.5C, lane 1). These data suggest that the endogenous protein is also cleaved upon on import into the mitochondria and indicate that the addition of the C-terminal FLAG tag had no significant effect on either localisation or size of the expressed protein.

Therefore, these data supporting AURKAIP1 having an N-terminal mitochondrial targeting sequence are in agreement with bioinformatic approaches, and with the

prediction programs, Target P (Emanuelsson et al., 2000; 2007), Predotar (Small et al., 2004), MitoProt II (Claros and Vincens, 1996), pTARGET (Guda, 2006) and MultiLoc2 (Blum et al., 2009), all of which predict mitochondrial localisation. MitoProt II (Claros and Vincens, 1996) predicts AURKAIP1 to have a 54 amino acid N-terminal targeting sequence. If this were correct the predicted molecular weight of mature AURKAIP1 would be 16.8kDa (Gasteiger et al., 2005). The removal of a 76 amino acid N-terminal targeting sequence, as predicted by the TargetP program (Emanuelsson et al., 2007), would produce a mature protein with a predicted molecular weight of 14.3kDa (Figure 4.2C). This is more similar to the observed size of AURKAIP1, as the observed size of AURKAIP1 on western blots is approximately 15kDa. However, the observed size of proteins subjected to SDS-PAGE can vary slightly, preventing accurate estimates of the actual molecular weight. It is, therefore, not possible from my work to predict the exact cleavage site with confidence, but it is probable that the N-terminal pre-sequence of AURKAIP1 is between 54 and 76 amino acids. This is a relatively long pre-sequence, especially as a proportion of the length of the protein, as typical mitochondrial targeting sequences usually range from 15-50 amino acids, although pre-sequence lengths up to ~100 have been described (Chacinska et al., 2009).

Studies by Lim *et al.* have described AURKAIP1 as a nuclear protein that binds to Aurora A kinase and promotes Aurora A degradation (Lim et al., 2007; Kiat, 2002). These studies describe the localisation of AURKAIP1 to be entirely nuclear, however overexpressed N-terminally FLAG-tagged AURKAIP1 was used. This approach has the potential to mislocalise the AURKAIP1 protein, as the FLAG tag at the N-terminal would interfere with the mitochondrial targeting sequence. Indeed, the current data shows that C-terminal rather than N-terminal FLAG-tagged AURKAIP1 is localised to mitochondria (Figure 4.3B). AURKAIP1-FLAG was not detected in the post mitochondrial supernatant of cells (Figure 4.3B), which comprises the cytosolic fraction, as it is collected after the initial centrifugation to remove nuclei and unbroken cells, and after the centrifugation to isolate mitochondria. This suggests there is no detectable expression of AURKAIP1-FLAG in the cytosol, but does not rule out nuclear localisation. Nuclear isolation protocols were attempted during my investigations, but I was unable to produce nuclear and cytosolic fractions that were free of any contamination with the other fraction. However, overexpressed AURKAIP1-FLAG was never detected in any of the nuclear fractions that were prepared, but was always

present in mitochondrial lysates. This indicates AURKAIP1-FLAG does not localise to the nucleus, which is in accordance with data from Szklarczyk *et al.,* that did not identify nuclear localisation of C-terminal GFP-tagged AURKAIP1 by fluorescence microscopy (Szklarczyk et al., 2012). Therefore, although some nuclear localisation of endogenous AURKAIP1 cannot be ruled out by my investigations, all of data presented indicate that AURKAIP1 is predominantly a mitochondrial matrix protein.

The majority of AURKAIP1-FLAG is present in the mitochondrial matrix (Figure 4.3B). However, the proportions of AURKAIP1-FLAG in the PK-shaved mitoplasts (4.3B lane 4) relative to the total mitochondrial proteins (lane 2) were slightly lower than the respective proportions of the mitochondrial matrix protein GDH. This may have been due to a small fraction of IMS located AURKAIP1-FLAG, that was degraded by the PK. It is, therefore, not possible to rule out that a small amount of AURKAIP1-FLAG may have been present in the IMS. Although, any IMS located protein could only account for a small percentage since there was only a slight reduction in AURKAIP1 signal between the untreated mitoplasts (Figure 4.3 lane 3) and the PK-shaved mitoplasts (lane 4), whereas the IMS protein AIF was undetectable in the PK-shaved mitoplasts. It is difficult conclude IMS localisation for AURKAIP1 from these data, as overexpression of AURKAIP1-FLAG was used, where there is the possibility that the potential IMS localisation could be explained by saturation of the matrix with imported AURKAIP1-FLAG. This may occur since the endogenous AURKAIP1 levels are very low and therefore the overexpression may represent an unusual challenge to the import machinery and any interacting proteins. What is clear, however, is that AURKAIP1-FLAG is a soluble protein as there was no signal detected in either of the sodium carbonate extracted fractions, which contained membrane proteins (Figure 4.3B lanes 5 and 6). A proportion of the signal for the matrix protein GDH was seen in the inner membrane fraction, which validates the stringency of the sub-localisation protocol because certain isoforms of GDH are tightly associated with the inner mitochondrial membrane (Rajas et al., 1996). Therefore AURKAIP1-FLAG can be confidently described as a soluble protein, predominantly located to the matrix.

Endogenous AURKAIP1 is also present in PK-shaved mitoplasts from HEK293 cells (Figure 4.5), indicating mitochondrial matrix localisation. However inner membrane localisation cannot be completely ruled out, as mitochondrial sub-localisation studies were not conducted due to low endogenous levels of AURKAIP1.

Endogenous AURKAIP1 was detected using the custom AURKAIP1 polyclonal antibody (the production of which is described in Chapter 3). Depletion of AURKAIP1-FLAG (Figure 4.4A) in HEK293-AURKAIP1-FLAG cells and endogenous AURKAIP1 (Figure 4.4B) in 143B cells was confirmed using this antibody. This shows that the antibody and siRNA used in this study were specifically targeting AURKAIP1 and AURKAIP1-FLAG. The depletion of AURKAIP1-FLAG was more efficient than depletion of endogenous AURKAIP1 (Figure 4.4). This is likely to be due to the transfection efficiency rather than differential effects of the siRNA on the endogenous and FLAG-tagged *AURKAIP1* transcripts. The depletion of AURKAIP1-FLAG was performed in 6 well plates using the standard protocol for 3 days (2.1.6) and 40μg of cell lysate was analysed. However, 50μg of isolated mitochondrial lysate was required to detect endogenous AURKAIP1, therefore, larger scale depletion experiments were set up (3x 75cm^2 flasks) for four days to permit mitochondrial isolation. It is possible that the transfection efficiency was lower in the 75cm^2 flasks compared to transfections carried out in 6 well plates. Another possibility is that AURKAIP1 depletion inhibits cell growth. If this were true, there would be a selection pressure favouring untransfected cells, thus a prolonged (extra 24-hour) incubation with siRNA would be expected to result in a greater proportion of cells that were not transfected with the siRNA. This may explain why the siRNA depletion of endogenous AURKAIP1 depletion appeared to be less efficient than siRNA depletion of overexpressed AURKAIP1-FLAG. To address this issue, the effects of AURKAIP1 depletion on cell growth were investigated and will be presented in the following chapter.

CHAPTER 5: STUDYING THE MORPHOLOGICAL EFFECTS OF AURKAIP1 DEPLETION

5.1 INTRODUCTION

Mitochondrial gene expression encompasses a range of processes as outlined in the general introduction (Section 1.7). I wished to determine whether AURKAIP1 plays a role in any of these processes, as at the time of my investigations, there was no published data to suggest a functional role for AURKAIP1 in mitochondria. AURKAIP1 depletion could potentially affect mtDNA levels, transcription, translation, dynamics, protein import or several other processes, which could lead to reduced mitochondrial gene expression. Due to this range of possibilities, initial studies were conducted using imaging techniques to assess the effects of AURKAIP1 depletion on multiple aspects of mitochondrial morphology. These experiments allowed estimation of changes to mitochondrial membrane potential (Ψ_m), analysis of mitochondrial shape and visualisation of mtDNA.

Fluorescence microscopy has long been established as a method to estimate relative changes in Ψ_m by quantifying changes in uptake of one of the several lipophilic cationic probes that are selectively accumulated within the mitochondria (Johnson et al., 1981). Fluorescent rhodamine derivatives such as rhodamine 123, tetramethylrhodamine ethyl ester (TMRE) and tetramethylrhodamine methyl ester (TMRM) are examples of cationic probes used to estimate Ψ_m (Scaduto and Grotyohann, 1999). TMRM, unlike other rhodamine derivatives, has the added benefit of not inhibiting respiration when used at low concentrations (Scaduto and Grotyohann, 1999). Thus, TMRM is commonly used to visualise mitochondria and estimate Ψ_m (Gerencser et al., 2012; Ashley and Poulton, 2009; Scaduto and Grotyohann, 1999; Nicholls and Ward, 2000; Szklarczyk et al., 2012; Frezza et al., 2006) including work from my host laboratory (Bruni et al., 2013). Under non-saturating conditions (defined as non-quench mode, see (Nicholls and Ward, 2000 for review), the fluorescence intensity emitted by TMRM is proportional to Ψ_m allowing relative measurements of Ψ_m to be made in live cells. The experimental measurements are always relative to controls and are presented in arbitrary

fluorescence units, because absolute measurements of Ψ_m (in mV) are not possible using this technique. However, a recent publication has outlined a method of absolute quantification of Ψ_m using TMRM via a combination of fluorescence imaging and voltage clamp (Gerencser et al., 2012).

Inhibitors of electron transport such as antimycin A (Complex III) and rotenone (Complex I) diminish Ψ_m. Inhibition of the ATP synthase increases Ψ_m whilst inhibition of mitochondrial protein synthesis with chloramphenicol has no effect (Johnson et al., 1981). Therefore, changes in Ψ_m upon AURKAIP1 depletion may indicate a role for AURKAIP1.

In addition to acting as an indicator of Ψ_m, the accumulation of TMRM in mitochondria allows visualisation of the morphology of the mitochondrial network and any changes in the morphology to be assessed. Particularly elongated mitochondria can indicate a disruption of mitochondrial fission, as in cells depleted of Drp1 (Parone et al., 2008), or overactive fusion, as in OPA1 overexpression (Cipolat et al., 2004). If cells contain punctate mitochondria then this may indicate overactive fission, as in Drp1 overexpression (Cipolat et al., 2004), or a fusion defect, as observed in OPA1 null cells (Song et al., 2007). Therefore, TMRM staining can be useful to indicate altered mitochondrial dynamics, in addition to effects on Ψ_m. It is worth noting that mitochondrial dynamics and Ψ_m can influence each other, for example, loss of Ψ_m promotes punctate mitochondria by causing an increase in OPA1 cleavage, thus impairing mitochondrial fusion (Ishihara et al., 2006; Song et al., 2007).

PicoGreen (PiGr) is a dsDNA specific intercalating dye that has been commonly used to visualise mtDNA nucleoids since the technique was first established in living human cells (Ashley et al., 2005). PiGr staining allows nucleoid morphology to be assessed in addition to estimations of mtDNA depletion (Ashley et al., 2005). Furthermore, PiGr and TMRM can be used to co-stain live cells (Ashley and Poulton, 2009; Bruni et al., 2013), allowing visualisation of mitochondrial morphology, estimation of mitochondrial membrane potential and visualisation of mtDNA nucleoids in the same cell. Therefore, PiGr and TMRM co-staining was selected as a method to allow the consequences of AURKAIP1 depletion on mitochondrial morphology to be assessed. However, it was necessary to first establish and confirm the most efficient and specific siRNA sequences with which to accomplish this.

As mentioned earlier, preliminary data from my host laboratory had identified potential involvement of AURKAIP1 in mitochondrial gene expression. This was initially determined through a bioinformatics approach and then preliminary laboratory data from siRNA mediated depletion of AURKAIP1 in HeLa and Rho^0 cells. In the latter, there were negligible effects of AURKAIP1 depletion after 3 days. When conducting siRNA depletion experiments it is important to be mindful of potential off-target effects. To this end, the preliminary experiments were carried out using siRNAs that targeted three different regions of *AURKAIP1* mRNA. The rationale for this is that if all three siRNAs have similar effects, then it is much more likely that any phenotype seen is due to depletion of the target protein rather than non-specific off-target effects. Cells were transfected with each siRNA independently and cultured for 3 days in media containing glucose. Cell growth was monitored to assess the effects of each AURKAIP1 siRNA. Three days post-transfection the cells were subjected to MTT assay (3-(4,5-Dimethylthiazol-2-yl)-2,5-diphenyltetrazolium bromide, Sigma) to measure relative cell viability between AURKAIP1 depleted and non-targeting siRNA treated cells. MTT is reduced to an insoluble purple formazan in living cells and, as such, accumulation of formazan can be used as an estimation of cell growth (as measured by absorbance at 550nm). In these preliminary experiments with HeLa cells, growth of AURKAIP1 depleted cells treated with siRNA1, 2 and 3 was 90%, 40% and 50% respectively of the growth of control cells. However, the growth of Rho^0 cells treated with any of the three AURKAIP1 siRNAs was 100% of the growth of control cells. Therefore all three siRNAs were causing growth retardation to different degrees in HeLa cells, but no growth defect was observed in the Rho^0 cells.

Since the growth retardation phenotype in AURKAIP1 depleted HeLa cells was most prominent when using siRNA2, it was probable that siRNA2 most efficiently depleted *AURKAIP1* transcripts. For this reason, one of the first objectives of my investigations was to test the effects of each siRNA in more detail and to confirm the findings of the preliminary data.

5.2 MATERIALS AND METHODS

General cell culture methods (2.1.1), cell counts (2.1.3) and details of siRNA depletions (2.1.6) are in the General Materials and Methods (Chapter 2).

5.2.1 IMAGING THE MITOCHONDRIAL NETWORK AND NUCLEOIDS

Cells were seeded in WillCo glass-bottomed wells (GWst 3522). Cell numbers, treatment and incubation time varied depending on the experiment and cell type used. Images were captured with an inverted fluorescent microscope (Axiovert 200 M, Carl Zeiss) with FITC and Texas Red filters, using the 63X magnification oil immersion lens. This equipment and the fluorescent lamp were switched on at least 30 minutes prior to image acquisition to allow the light intensity to stabilise. A 3µl PiGr aliquot (undiluted, Quant-iT^{TM}, Invitrogen, cat. no. P7581 stored at -20°C and shielded from light) was added per ml of media and cells were incubated as normal at 37°C for 50 minutes. TMRM (Sigma, cat. no. T5428. Stocks prepared in 100% methanol at 5µM concentration, stored at -20°C and shielded from light) to a final concentration of 5nM was then added to the media and incubated at 37°C for a further 10 minutes. Cells were then washed twice with 1ml KRB buffer (135mM NaCl, 5mM KCl, 0.4mM KH_2PO_4, 1mM $MgSO_4$, 20mM HEPES pH 7.4 filter sterilised and stored at 4°C,) to remove dead cells before adding 1ml of supplemented KRB buffer (KRB supplemented with 5.5mM glucose, 1.3mM Ca^{2+} (from 2M $CaCl_2$ stock) and 5nM TMRM prior to each experiment) and shielding from light. The cells were then ready for imaging.

Exposure times for image capture varied between different experiments, but were always the same for all samples within a single experiment. Signal from the PiGr dye was captured using the FITC channel (Excitation 495nm, emission 519nm) and signal from TMRM dye was captured using the Texas Red channel (excitation 589nm, emission 615). Each field was imaged using Z-stacks set to produce ten images with focal points 0.4µm apart. Each imaged field was as far apart from each other as possible by imaging across the whole area of the well in order to reduce photo-bleaching. Transmission light (bright field) images were also taken for each field to document cellular morphology. Transmission light images were also used to define cellular area when processing the images so that no user bias was introduced by selecting cells based on the fluorescent images.

5.2.2 Analysing Nucleoid Size

Quantification was performed on all fields imaged for each experimental condition using the ImageJ program (http://imajej.nih.gov/ij). The image with the most nucleoids in focus from the Z-stacked images from each field was selected to analyse. The background was subtracted using a 5-pixel rolling ball radius and then setting an appropriate threshold. The image was then subjected to watershed to separate any overlapping particles (using Euclidean distance mapping algorithms (Danielsson, 1980; Russ, 2011)). A representative section of each image was then subjected to particle analysis, which measured the area of each nucleoid. This data was then exported to Microsoft Excel for further analysis.

5.2.3 Analysing Mitochondrial Network Fragmentation

Quantification of mitochondrial network fragmentation was carried out in a similar way to the nucleoid size. The most in-focus Z-stack slice was selected and particles analysed. This analysis was kindly performed in collaboration with Dr Jorge Oliveira (University of Porto) whilst a visiting scholar.

5.2.4 Measuring Mitochondrial Membrane Potential

Cells were prepared as described in 5.2.1, but images were taken using the 10x objective without Z-stacks. A transmission light image was taken to ensure correct focus before a total of 40 fluorescent images were taken at 30-second intervals using the Texas Red channel. After seven images were taken, 2μM FCCP was added to abolish the mitochondrial membrane potential. The time-lapse images for each experimental condition were analysed in ImageJ. The transmission light image was used as a guide to draw regions of interest (ROI) around a selection of over 20 cells within the field. These defined ROIs were transferred to the fluorescent images. The fluorescence intensity of each ROI was measured and the non-mitochondrial fluorescence (intensity measurement from image 40) was subtracted from the total fluorescence (intensity measurement from image 1) to give an approximation of the mitochondrial membrane potential. The measurements are in arbitrary units but since all images for each experiment were acquired with the same exposure settings the values obtained between different experimental conditions can be compared to each other, therefore the average

membrane potential in a particular experimental condition was presented as a percentage of the average membrane potential of the control condition.

5.3 RESULTS

5.3.1 EFFECTS OF AURKAIP1 DEPLETION ON CELL GROWTH

To ensure the preliminary data was replicable it was necessary to test the effects of each of the three AURKAIP1 siRNAs. HeLa cells were therefore subjected to depletion with each of the three siRNAs independently or with non-targeting control siRNA and cells counted after two, three and four days (Figure 5.1).

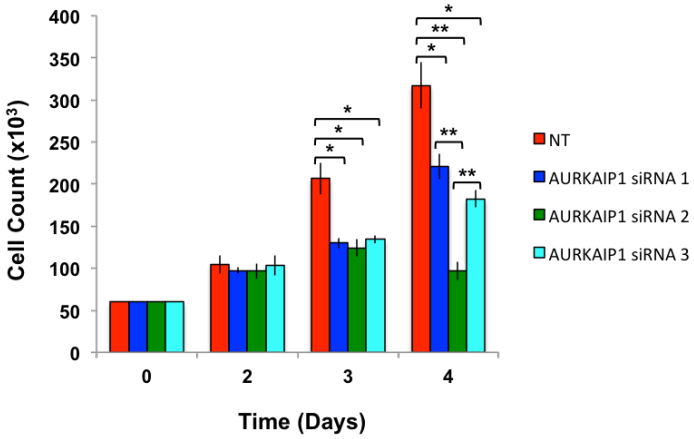

Figure 5.1: The Effects of AURKAIP1 Depletion on HeLa Cell Growth. HeLa cells were transfected with siRNA that were non-targeting (NT, red) or targeted to AURKAIP1 (siRNA1-blue, siRNA2-green, siRNA3-cyan) and incubated for either 2, 3 or 4 days before cells were harvested and counted. Error bars show the SEM (standard error mean) of data from three independent experiments for each condition. Statistical significance was determined by T-tests on the raw data for each siRNA within each time point. * denotes p-values <0.05, ** denotes p-values <0.005, *** denotes p-values <0.0005 n=3.

Two days post-transfection, there was no difference between non-targeting treated cells and AURKAIP1 depleted cells. After three days there was significant growth retardation in all AURKAIP1 depleted HeLa cells (p-values (vs. NT) - siRNA1=0.018, siRNA2=0.018, siRNA3=0.02). This trend continued after four days of siRNA treatment (p-values – siRNA1=0.037, siRNA2=0.0018, siRNA3=0.01). However, the growth of cells treated with siRNA2 was significantly lower than cells treated with either siRNA1 (p=0.0025) or siRNA3 (p=0.0045). The number of cells after four days of growth post-transfection with siRNA2 was lower than after 3 days, suggesting cell death rather than reduced growth. These data confirm that depletion using siRNA2 has the strongest inhibitory effect on cell growth in HeLa cells, with cell number reduced to 30% of control NT values, compared to 70% with siRNA1 and 58% with siRNA3.

Therefore siRNA2 was used to deplete AURKAIP1 in HEK293 and 143B cells to investigate the effect on growth in other cell types and caused similar growth retardation to HeLa cells, with a reduced growth rate evident on day 3, and evidence of cell death after 4 days of depletion (Figure 5.2).

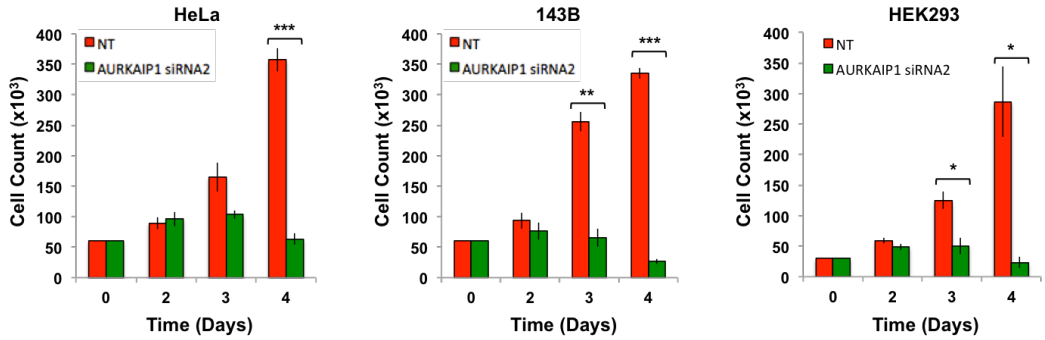

Figure 5.2: AURKAIP1 Depletion Affects Cell Growth in Multiple Cell Types. HeLa, 143B and HEK293 cells (labelled) were transfected with either non-targeting (NT) siRNA (red) or AURKAIP1 siRNA2 (green) and incubated for either 2, 3 or 4 days before cells were harvested and counted. Error bars show the SEM of data from three independent experiments for each condition. Statistical significance was determined using T-tests on the raw data for each siRNA within each time point. * denotes p-values <0.05, ** denotes p-values <0.005, *** denotes p-values <0.0005.

The effects of AURKAIP1 depletion on cell growth were more severe in 143B cells (8% of NT after 4 days p=0.00007, 26% after 3 days p=0.0009) and HEK293 cells (8% of NT after 4 days p=0.01, 40% after 3 days p=0.02) compared to HeLa cells (18% of NT after 4 days p=0.00015, 63% after 3 days p=0.07).

Cells depleted of AURKAIP1 were visualised by light microscopy. There was clear evidence of cell death after 4 days of AURKAIP1 depletion. There were many cells that had detached and, of those that were still attached to the culture vessel, most displayed a clear morphological change. These cells were more rounded compared to cells treated with non-targeting siRNA that had a more irregular angular shape (Figure 5.3).

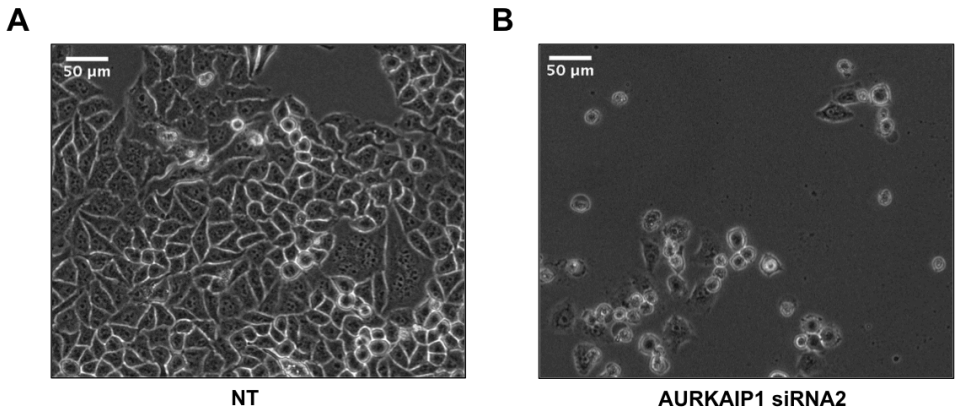

Figure 5.3: Effects of AURKAIP1 Depletion on Cell Morphology. HeLa cells were transfected with either non targeting (NT) siRNA **(A)** or AURKAIP1 siRNA **(B)** and incubated for four days before being visualised by light microscopy.

5.3.2 Effects of AURKAIP1 Depletion on Mitochondrial and Nucleoid Morphology

It was clear that AURKAIP1 depletion was causing growth retardation in a range of different human cell lines (Figure 5.2) and the lack of an effect in Rho^0 cells (preliminary data as described in 5.1) is suggestive of a mitochondrial role for AURKAIP1. Therefore, in order to assess the effects of AURKAIP1 depletion on mitochondria, depleted cells were treated with PiGr and TMRM to fluorescently stain double-stranded DNA (including mtDNA) and the mitochondrial network respectively.

AURKAIP1 depletion with siRNA2 appeared to increase the size of mitochondrial nucleoids in HeLa cells compared to controls (Figure 5.4). Evidence of large nucleoids was clearly visible in the majority of images of AURKAIP1 depleted cells but not in those treated with non-targeting siRNA. However there was no difference between AURKAIP1 depleted and NT control cells with respect to mitochondrial morphology or membrane potential on the basis of TMRM staining.

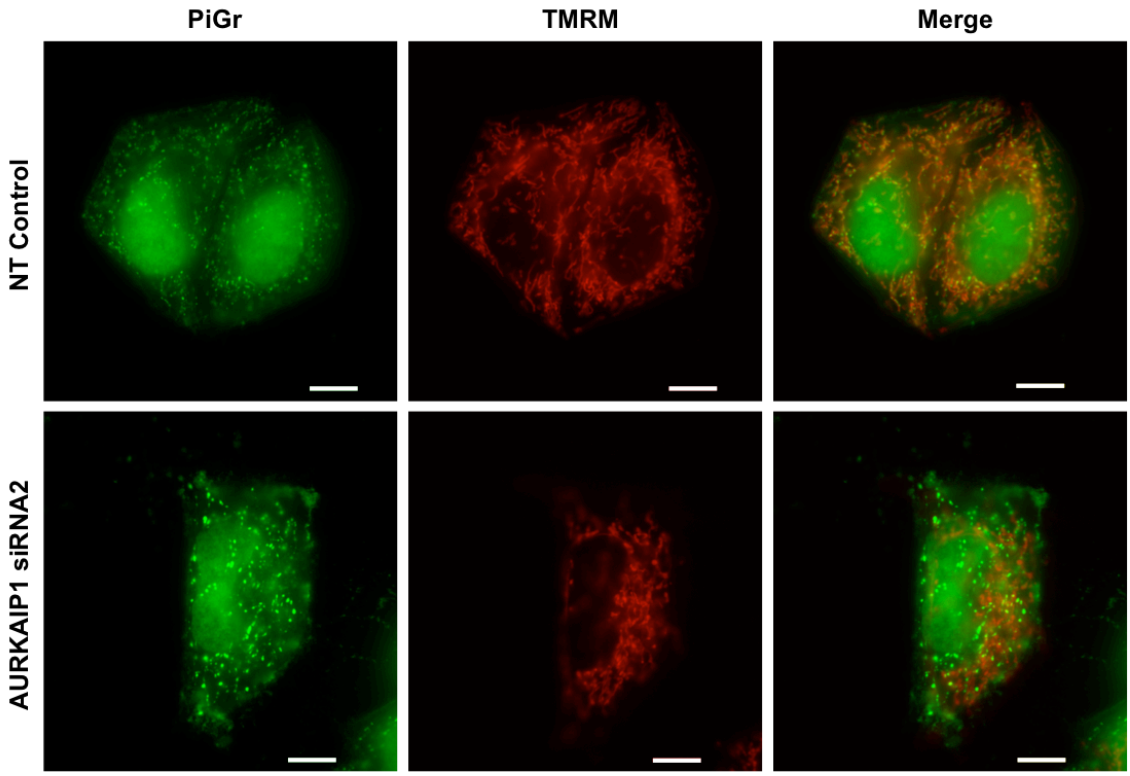

Figure 5.4: Effects of AURKAIP1 Depletion on Mitochondrial Morphology in HeLa Cells. HeLa cells were transfected with either non-targeting (NT) siRNA or AURKAIP1 siRNA1 for 4 days. Cells were treated with TMRM to stain the mitochondrial network (red) and PicoGreen (PiGr) to stain the double-stranded DNA (green) and live-cell fluorescence microscopy was performed. Scale bar = 10μm.

These mitochondrial imaging experiments were repeated in 143B, HEK293 and U2OS cells and produced similar results. Depletion with siRNA1 and siRNA3 were also carried out to confirm that the phenotype was not specific to siRNA2. To illustrate this, depletion of AURKAIP1 with siRNA1 in 143B cells is presented in Figure 5.5 and the same enlarged nucleoid phenotype can be seen. The same phenotype was observed with all 3 siRNAs, indicating that these enlarged nucleoids are likely to be a specific effect of AURKAIP1 depletion.

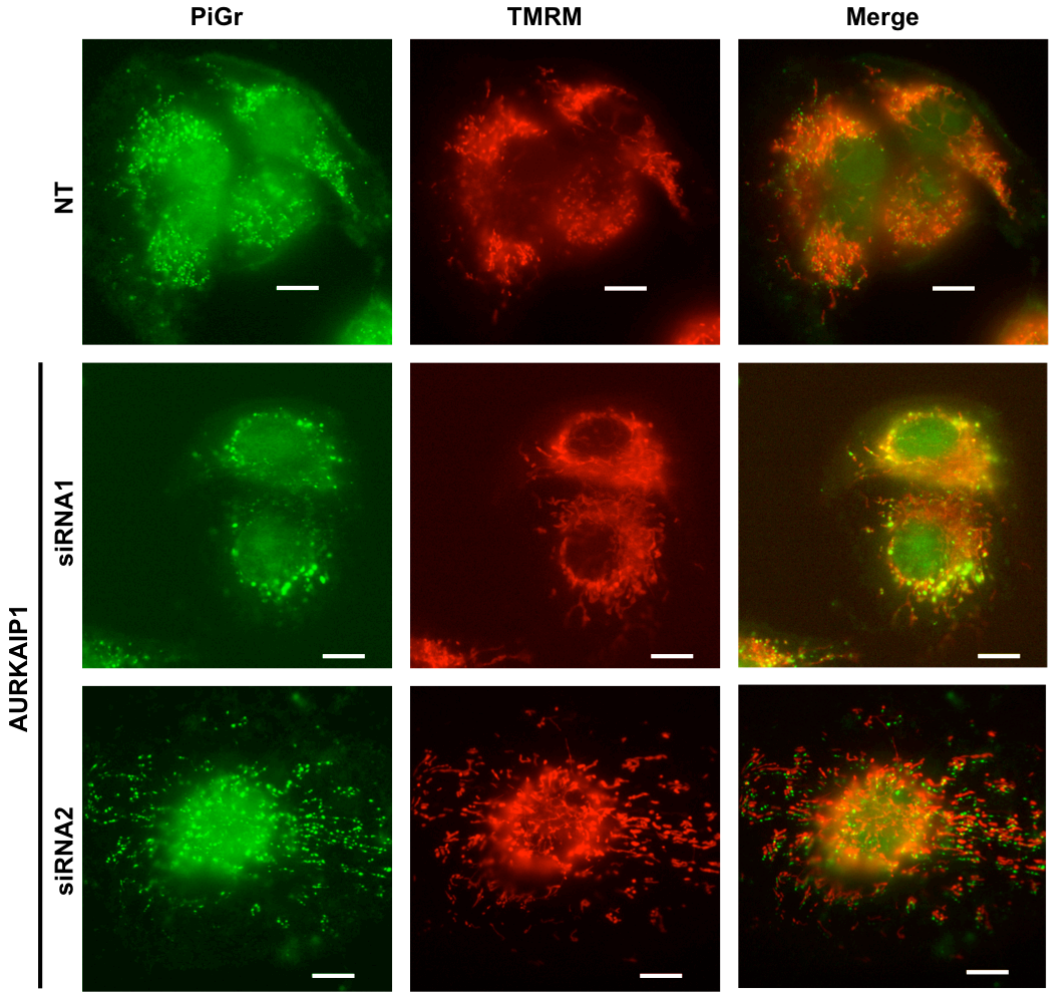

Figure 5.5: Effects of AURKAIP1 Depletion on Mitochondrial Morphology in 143B Cells. HeLa cells were transfected with non-targeting (NT) siRNA, AURKAIP1 siRNA1 or AURKAIP1 siRNA2 for 4 days. Cells were treated with TMRM to visualise the mitochondrial network (red) and PicoGreen (PiGr) to stain double-stranded DNA (nucleus and mtDNA nucleoids, green) and live-cell fluorescence microscopy was performed. Scale bar = 10μm.

Depletion of AURKAIP1 in HEK293 cells produced similar phenotypes with larger nucleoids than in control cells (data not shown). However, the cellular morphology of HEK293 cells appears to be more affected by AURKAIP1 depletion than HeLa cells or 143B cells. Healthy HEK293 cells are more rounded and smaller than the other cell types used, and thus it was not possible to visualise features within the cytoplasm as easily. Larger and flatter cells produce better images as they have a larger proportion of their mitochondria in focus on a single focal plane. For this reason, quantification of the increased nucleoid size phenotype was performed on images of both HeLa cells and U2OS cells, which are also the most adherent of the cells tested.

As U2OS are typically the flattest of the cell type tested, the best quality data could be obtained using this line. Consistent with other cell lines investigated, the enlarged nucleoid phenotype produced by AURKAIP1 depletion was also evident in U2OS cells (Figure 5.6).

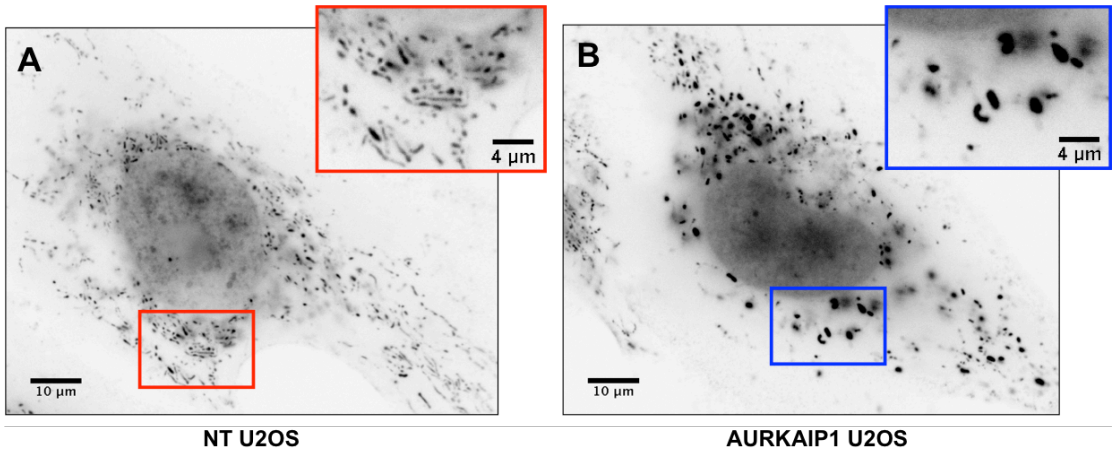

Figure 5.6: Enlarged Nucleoids are seen in U2OS cells depleted of AURKAIP1. Representative images of U2OS cells that were transfected with either non-targeting (NT) siRNA **(A)** or AURKAIP1 siRNA1 **(B)** and grown for 3 days before being stained with PicoGreen to detect double-stranded DNA and imaged using live-cell fluorescence microscopy.

To evaluate the observation of size difference in nucleoids between control and AURKAIP1 depleted cells in the PiGr images, the signals detected using the FITC channel were subjected to processing to remove background and nuclear staining to leave only the signal from nucleoids. Particle analysis was then performed to measure the size of each nucleoid. The measurements were then plotted on a histogram to compare nucleoid sizes. Larger nucleoids were relatively common in U2OS cells depleted of AURKAIP1, but very rare in control cells (Figure 5.7A). When comparing the relative proportions of large nucleoids (defined as $>0.4\mu m^2$) to small nucleoids (defined as $<0.4\mu m^2$) there was a clear shift between non-targeting and AURKAIP1 siRNA treated cells. Analysis showed that in U2OS cells depleted of AURKAIP1 42% of nucleoids were large compared to 22% in non-targeting treated control cells ($p=0.0024$, Figure 5.7C). Visual inspection of other cell types depleted of AURKAIP1 suggested a similar trend towards enlarged nucleoids (Figure 5.4 and 5.5). Therefore, for improved scientific rigour, the phenotype was also quantified in HeLa cells (Figure 5.7B). The results were strikingly similar between experiments performed in U2OS and HeLa cells. HeLa cell depleted of AURKAIP1 had 40% of nucleoids designated as

large (>40μm^2) compared to only 17% in non-targeting controls (p=0.0003, Figure 5.7C).

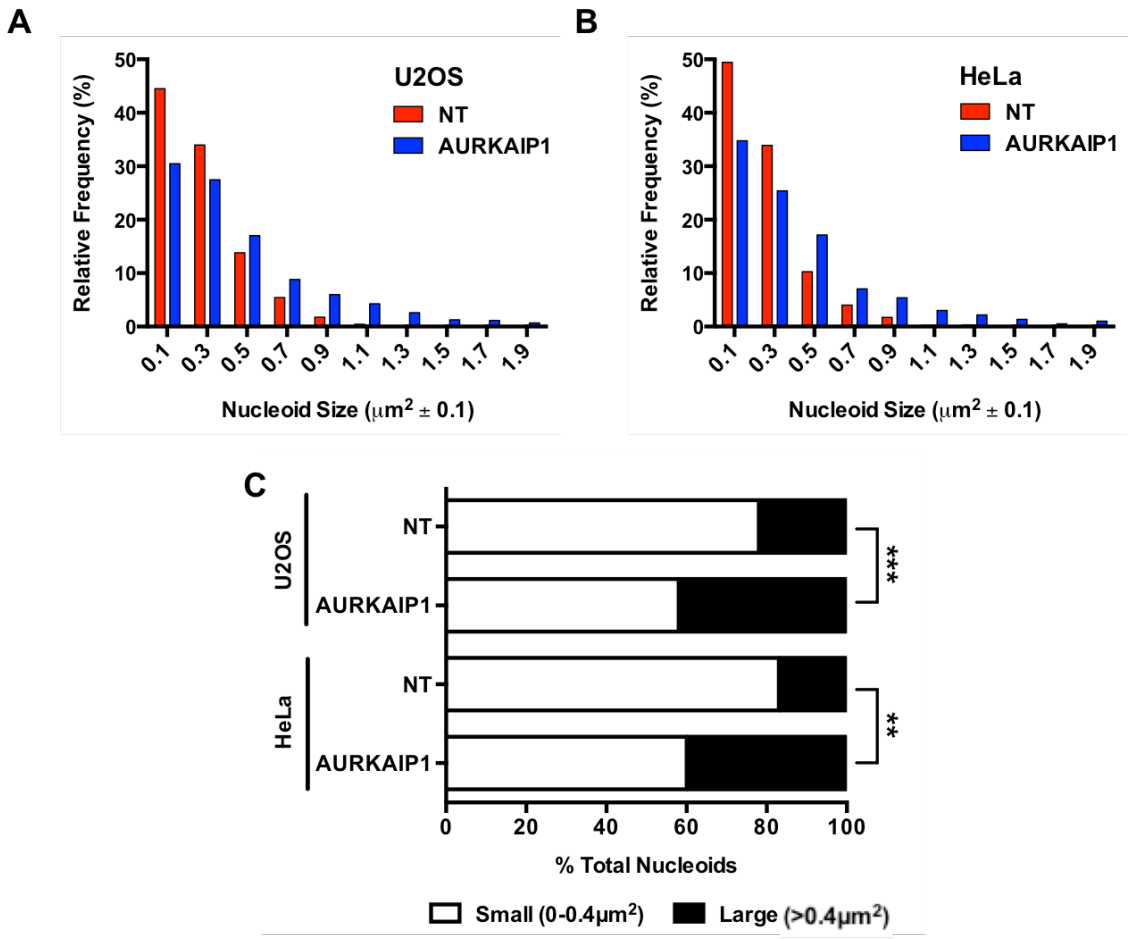

Figure 5.7: Quantification of Nucleoid Size in AURKAIP1 Depleted U2OS and HeLa Cells. Images such as those depicted in Figure 5.6 were subjected to background removal to remove the nuclear signal. The areas of each remaining nucleoid were measured in images from cells treated with NT siRNA (red) and AURKAIP1 siRNA1 (blue) and plotted on a histogram. Results are shown from images of experiments performed in U2OS cells **(A)** and HeLa cells **(B)**. The relative frequency of large nucleoids (>0.4μm^2, black) to small nucleoids (0-0.4μm^2, white) is depicted in **(C)**. * denotes p-values <0.05, ** denotes p-values <0.005 and *** denotes p-values <0.0005. Number of nucleoids analysed (from 10 fields of each condition): U2OS NT n=1310, U2OS AURKAIP1 n=1034, HeLa NT n=1325, HeLa AURKAIP1 n=595.

The enlarged nucleoid phenotype upon AURKAIP1 depletion was remarkably consistent. Large nucleoids were seen in images of all cell types tested and with all siRNAs tested. However, this phenotype was not as marked using siRNA3 compared to siRNA1 (Figure 5.8). Although the relative percentage of large nucleoids was greater in AURKAIP1 siRNA3 treated cells (25%) compared to non-targeting controls (17%), this effect was not statistically significant (p=0.164). Large nucleoids represented 40% of

the total in AURKAIP1 siRNA1 treated cells, which was statistically significant (p=0.0003). Despite the less striking phenotype in cells treated with siRNA3, very large nucleoids (>1μm^2) were detected in AURKAIP1 depleted cells with either siRNA (10% of nucleoids for siRNA1, n=595; 4% of nucleoids for siRNA3, n=1047), but not in non-targeting siRNA treated controls (0% of nucleoids, n=1325).

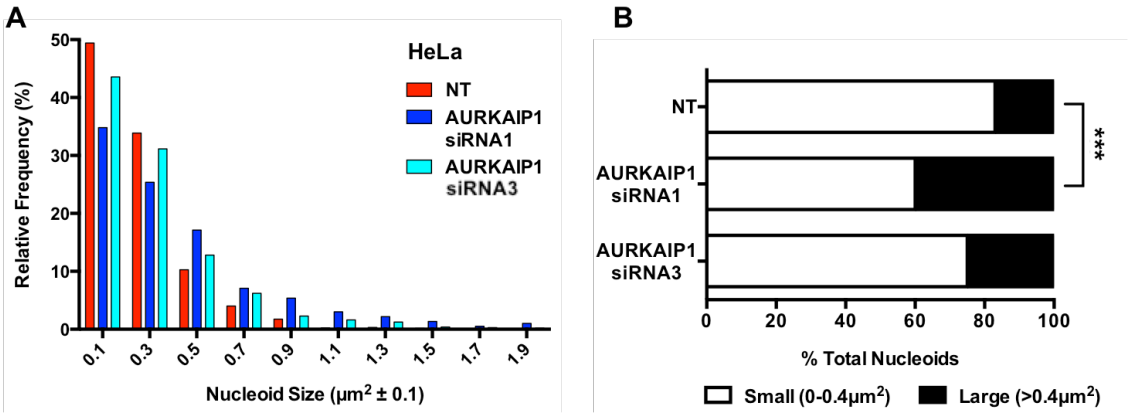

Figure 5.8: Comparison of Nucleoid Enlargement with Different AURKAIP1 siRNAs. Images such as those depicted in Figure 5.6 were subjected to background removal to remove the nuclear signal. The areas of each remaining nucleoid were measured in images from cells treated with NT siRNA (red), AURKAIP1 siRNA1 (blue) and AURKAIP1 siRNA3 (cyan) plotted on a histogram **(A).** The relative frequency of large nucleoids (>0.4μm^2, black) to small nucleoids (0-0.4μm^2, white) is depicted in **(B)**. *** denotes p-value <0.0005. n values given in text.

5.3.3 Effects of AURKAIP1 Depletion on Mitochondrial Membrane Potential

TMRM is a lipophilic cationic dye that is accumulated by mitochondria due to the electrochemical gradient present across the mitochondrial membranes. Thus, at non-saturating concentrations of TMRM (5nM, non-quench mode), the fluorescence intensity is directly proportional to Ψ_m.

Initial comparisons of mitochondrial membrane potential can be gathered from the images taken at 63x magnification on the Texas Red channel, which detects TMRM fluorescence. All images of AURKAIP1 depleted and control cells were all taken with the exact same exposure times, to allow the intensity of TMRM signal to be compared between the two conditions. The analysis performed on AURKAIP1 depleted cells and non-targeting treated controls showed that there was no significant difference in membrane potential between the two conditions (Figure 5.9). However, the range of intensities was much greater in the AURKAIP1 depleted cells, with a population of

cells displaying lower membrane potential and another population displaying higher membrane potential than any of the non-targeting controls (Figure 5.9).

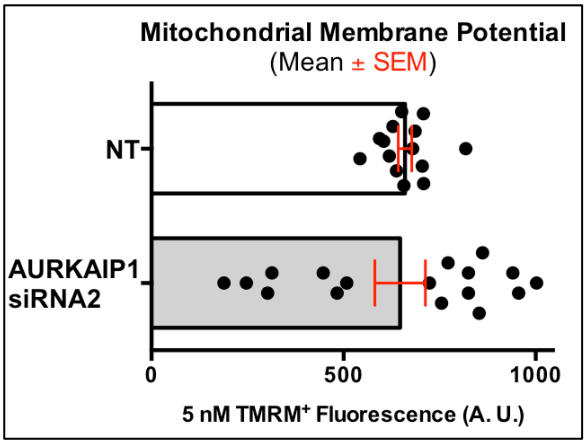

Figure 5.9: Effects of AURKAIP1 Depletion on Mitochondrial Membrane Potential. HeLa cells were treated with either non-targeting (NT) siRNA or AURKAIP1 siRNA2 for 3 days. Cells were imaged and the average fluorescence intensity per cell was calculated using ImageJ software. Fluorescence intensity is presented in arbitrary units (A. U.).

5.4 DISCUSSION

The data presented in this chapter shows that AURKAIP1 depletion, with all three siRNAs targeting different regions of the transcript, is detrimental to all cell types tested. This suggests that the resulting phenotype is not an off-target effect, as it would be very unlikely that the same phenotype could be produced via off-target effects from three different siRNAs. Changes in nucleoid morphology (Figures 5.4-5.8) upon AURKAIP1 depletion corresponded with growth retardation (Figures 5.1 and 5.2). Together, these data suggest that the detrimental effects of AURKAIP1 depletion are, at least in part, due to effects on the mitochondria.

Depletion of AURKAIP1 appeared to be more efficient with the use of siRNA2 since this showed the strongest growth retardation and caused cell death four days post-transfection (Figure 5.1). This cell death was not evident from the growth curve data of cells transfected with siRNA1 and siRNA3. However, when inspecting the cells visually, there was evidence that cell death was occurring after siRNA1 and siRNA3 treatment, but to a lesser degree than with siRNA2. Perhaps this lower level of depletion with siRNA1 or siRNA3 could be due to reduced annealing to the *AURKAIP1* mRNA, thus resulting in less RISC-mediated degradation. Since the same reagents and concentration of each siRNA was used for transfection, it is unlikely that the discrepancy in phenotype was due to differences in siRNA uptake. It was concluded that siRNA2 was likely to be the most effective in binding *AURKAIP1* mRNA and triggering RISC-mediated degradation of the transcript, with a consequent loss of

protein synthesis. These data, consistent with the results from the preliminary experiments (conducted by Dr P. M. Smith), indicated that siRNA2 was the most appropriate to mediate AURKAIP1 depletion.

The efficacy of AURKAIP1 protein depletion was not readily determined by western blot, as the endogenous levels of AURKAIP1 are too low to allow detection in cell lysates, as discussed previously. Other methods to determine the efficiency of AURKAIP1 depletion will be discussed in the following chapter.

Irrespective of relative differences in siRNA potency, it was clear that the increased size of mitochondrial nucleoids was consistent using any of the three AURKAIP1 siRNAs, in all of the tested cell types (Figures 5.4-5.7). This nucleoid enlargement was very robust and reproducible, but what it suggests about the function of AURKAIP1 is unclear. Similar enlarged nucleoid phenotypes have been reported with knockdown of TFAM (Kasashima et al., 2011), Drp1 (Ban-Ishihara et al., 2013) and REXO2 (Bruni et al., 2013), in addition to overexpression of POLGβ (Di Re et al., 2009) and mutant TWINKLE (Goffart et al., 2009).

When drawing conclusions based on the nucleoid enlargement, it is important to consider that PiGr will stain any double-stranded DNA, but it will bind significantly less well to supercoiled DNA. This was demonstrated by a reduction in PiGr staining for nucleoids following ATAD3 depletion (He et al., 2007), a protein associated with nucleoids (Wang and Bogenhagen, 2006). The authors attribute the reduced PiGr signal to an increase in negative supercoiling, since the mtDNA levels were only marginally reduced and nucleoids could still be seen in fixed cells by immunocytochemistry using anti-DNA antibodies (He et al., 2007). Unpublished data from the same group showing an increase in PiGr staining upon relaxation of supercoiled plasmid DNA *in vitro* was cited to support the notion that PiGr staining is not necessarily an accurate measure of mtDNA mass (He et al., 2007).

It is possible that the appearance of larger nucleoids in AURKAIP1 depleted cells could be explained by the partial or full unwinding of mtDNA. This would cause an increased signal from PiGr, which, at the resolution of fluorescence microscopy, may appear to have a greater area. This is due to ‘halo’ effects, which are common imaging artefacts when visualising intense signal or signals from rounded or thick cells. An unwinding of mtDNA would occur during replication, therefore, nucleoids containing replicating

mtDNA could potentially produce more intense staining. The unwinding of mtDNA is solely carried out by the helicase TWINKLE (Milenkovic et al., 2013). Overexpression of several mutated forms of TWINKLE have been shown to increase nucleoid size (Goffart et al., 2009). However, this increase in size is not due to TWINKLE unwinding DNA resulting in increased intensity of PiGr staining, as nucleoids were visualised with an anti-DNA antibody by immunocytochemistry in this study (Goffart et al., 2009). Additionally, overexpression of wild-type TWINKLE did not affect nucleoid morphology (Goffart et al., 2009). Instead, the replication stalling events dictated by mutant TWINKLE may have resulted in a failure to divide nucleoids, thus leading the enlarged nucleoid phenotype (Goffart et al., 2009). If this effect is also the cause of the enlarged nucleoids with AURKAIP1 depletion, then AURKAIP1 may be implicated in mtDNA replication or transcription and in the absence of AURKAIP1, there is a stalling of these processes, resulting in enlarged nucleoids.

If not involved in replication stalling, AURKAIP1 may be involved in nucleoid dynamics. Since mitochondrial nucleoids are not static packages of mtDNA, nucleoid enlargement could be the result of aberrant nucleoid separation and an accumulation of multiple mtDNA molecules per nucleoid. This could be possible without the replication stalling seen with mutant TWINKLE overexpression (Goffart et al., 2009). However, this explanation seems unlikely, as recent data has estimated that there are only 1.4 copies of mtDNA per nucleoid on average (Kukat et al., 2011). This study used STED super resolution microscopy that gives resolution down to ~50nm compared to only ~260nm with confocal microscopy. Using this technique Kukat *et al.* showed that larger nucleoids as identified by confocal microscopy were actually clusters of discrete nucleoids of approximately equal size (Kukat et al., 2011), rather than a single nucleoid containing more copies of mtDNA.

This could also be the case with the nucleoid distribution following AURKAIP1 depletion, as the apparently larger nucleoids could actually be due to increased clustering of nucleoids. Indeed, impaired segregation of mtDNA was claimed to be the reason for the presence of enlarged nucleoids in TFAM depleted cells (Kasashima et al., 2011). Furthermore, nucleoid clustering has been described in Drp1 depleted cells, showing that mitochondrial fission is an important factor in allowing correct nucleoid distribution (Ban-Ishihara et al., 2013). This is also supported by data that showed loss of mitochondrial fusion by OPA1 depletion prevented the formation of enlarged

nucleoids mediated by DNA intercalators (Ashley and Poulton, 2009). Together, these data may implicate a role for AURKAIP1 in mitochondrial fission. However, there was no evidence of overly elongated mitochondria in AURKAIP1 depleted cells on the basis of TMRM staining (Figures 5.4 and 5.4).

In fact, TMRM staining did not produce any strong indicator of mitochondrial function. There was no clear effect on mitochondrial fission or fusion in any of the cell types tested. Furthermore, there was no shift in the mean mitochondrial membrane potential (Figure 5.9). However, this may be an oversimplification, as the range of estimated membrane potential readings in AURKAIP1 depleted cells was much wider than in non-targeting controls (Figure 5.9). There is a clear population of AURKAIP1 depleted cells displaying reduced membrane potential and another population displaying increased membrane potential relative to non-targeting controls. This could suggest a sequential process of increased membrane potential, as seen in ATP synthase inhibited cells (Johnson et al., 1981), followed by collapse, which can be caused by many insults. Membrane potential collapse has been shown to be linked to apoptosis (reviewed in Ly et al., 2003). Since cell death is apparent in AURKAIP1 depleted cells, perhaps the subset of cells displaying membrane potential collapse (Figure 5.9) were about to undergo apoptosis. Though an intriguing possibility, this is speculative and it is impossible to ascertain the causality of this effect from the presented data. Respiratory dysfunction can lead to apoptosis (reviewed in Helling et al., 2012). Therefore, since the preliminary data from AURKAIP1 depleted cells suggested respiratory dysfunction, further studies into the effects of AURKAIP1 depletion on mitochondrial gene expression were prioritised over estimation of apoptosis levels, due to time constraints.

Whether the enlarged nucleoid phenotype upon AURKAIP1 depletion was due to an increase of mtDNA copy number within a single nucleoid, the clustering of several nucleoids in close proximity or the increase in signal intensity due to relaxation of supercoiled mtDNA needed to be addressed. If enlarged nucleoids were a result more replication events, AURKAIP1 depletion would be expected to lead to an increase in mtDNA copy number per cell. If replication stalling were the reason for observing enlarged nucleoids, then mtDNA levels would be expected to be reduced, as was seen in cells overexpressing mutant TWINKLE (Goffart et al., 2009). Disruption of nucleoid distribution would not be expected to alter mtDNA copy number, as was the case with Drp1 depletion (Ban-Ishihara et al., 2013). It was therefore important to measure the

mtDNA copy number, the results of which will be presented alongside further biochemical characterisation of the effects of AURKAIP1 depletion in the following chapter.

It would be interesting to use of STED super resolution microscopy to investigate the effects of AURKAIP1 depletion on nucleoids. The enhanced resolution microscopy would allow distinction between enlarged nucleoids and clustered nucleoids (Kukat et al., 2011). However, due to time constraints these studies were not conducted during my investigations.

CHAPTER 6: IS AURKAIP1 REQUIRED FOR OXIDATIVE PHOSPHORYLATION?

6.1 INTRODUCTION

Thus far, my work has shown that AURKAIP1 is a mitochondrial protein (Chapter 4, Figure 4.3) and that depletion of AURKAIP1 impairs cell growth (Chapter 5, Figure 5.1) and leads to an enlarged nucleoid morphology (Chapter 5, Figures 5.5-5.8). These data are consistent with the preliminary screen conducted in my host laboratory, which indicated that AURKAIP1 depletion caused growth defects in HeLa cells but not in Rho^0 cells.

Preliminary data from this screen further suggested a role for AURKAIP1 in mitochondrial gene expression as mitochondrial mRNA, protein synthesis and oxygen consumption were reduced after depletion of AURKAIP1. However, this preliminary data was generated alongside several candidate proteins in a medium/high throughput screen. The preliminary nature of the screen meant that estimations of mitochondrial mRNA levels were based on qPCR for *MT-CO1* only, rather than northern blotting. Similarly, measurement of mitochondrial protein synthesis, via [^{35}S] labelled methionine incorporation into nascent polypeptides, was estimated based on relative radioactivity (counts per second ratio) between AURKAIP1 siRNA treated cells and non-targeting siRNA treated controls, rather than visualisation of the translation products by SDS-PAGE. Whilst these preliminary findings were useful to implicate the involvement of AURKAIP1 in mitochondrial gene expression, there was a requirement to confirm reproducibility of these findings using more stringent methods. Therefore, this chapter will describe the characterisation of the biochemical phenotype resulting from AURKAIP1 depletion, including analysis of mtDNA levels, mt-RNA levels, mitochondrial protein synthesis and steady state levels of mtDNA-encoded proteins.

6.2 METHODS

6.2.1 [^{35}S]-METABOLIC LABELLING OF MITOCHONDRIAL PROTEINS

These experiments were performed with the assistance of Dr Francesco Bruni and Dr Hue Tran Hornig-Do. All cells were grown in 25cm^2 flasks for three days until a confluency of 50-60% was achieved. At this point, normal growth medium was then replaced with 2.5ml pre-warmed DMEM free of methionine and cysteine (Sigma, D0422) and incubated for 10 minutes at 37°C. Two further met/cys wash out incubations were performed, before the media was removed and replaced with 3ml methionine/cysteine free DMEM supplemented with 10% dialysed FCS (Sigma, F0392) and 100µg/ml emetine dihydrochloride (Sigma, E2375). Following a 10 minute incubation at 37°C, 20µl of [^{35}S]-methionine/cysteine mix (Perkin-Elmer Easy Tag Express protein labelling mix, NEG-772, specific activity: >1000Ci(37.0TBq)/mmol) was added and the cells were incubated at 37°C for a further 45 minutes. Cells were then washed with normal growth media containing methionine, harvested in 1ml PBS-EDTA and pelleted by centrifugation at 200*g* for 4 minutes. The cell pellets were washed three times with PBS (10ml supplemented with one protease inhibitor tablet and 1mM PMSF) before preparing cell lysates (2.5.1).

A 50µg aliquot from each sample was subjected to electrophoresis through a 15% SDS polyacrylamide gel (using the Hoefer system). The gel was stained with Coomassie for 10 minutes and destained for 15 minutes. The stained gel was then fixed for 4 hours in 30% methanol, 10% acetic acid and 3% glycerol and vacuum-dried for 4 hours at 70°C. The gel was exposed to a PhosphorImage screen for 5 days before the signal on the screen was visualised using the Typhoon FLA 9500 system and ImageQuant software (GE Healthcare).

6.2.2 COMPLEX ACTIVITY ASSAY

This assay was performed with the assistance of Dr Hue Tran Hornig-Do, according to the protocol outlined in (Rustin et al., 1994). Complex activity measurements were normalised using total protein concentration as determined by Bradford assay (2.5.3).

6.2.3 SITE DIRECTED MUTAGENESIS

Primers were designed to allow alteration of the sequence of AURKAIP1 in the region that was targeted by AURKAIP1 siRNA1 (Table 6.1). Specific mutations were incorporated into the primers so that the third base of three consecutive codons were changed, but that the codons would encode the same amino acids. These silent mutations were incorporated into the pcDNA^{TM}5/FRT/TO/AURKAIP1-FLAG plasmid using the QuickChange II site directed mutagenesis kit (Agilent Technologies, 200523) according to manufacturer's guidelines. Following sequence confirmation of the resulting plasmid, this was used to transfect HEK293 cells (as described in 4.2.1) to allow expression of siRNA resistant AURKAIP1-FLAG.

Table 6.1: Primers for Site-Directed Mutagenesis.

Name	Sequence (5'-3')
silAURKAIP1 siRNA1	CGG AAG ATG AAC CA**T** CA**T** AA**A** TAC CGG AAG CTG GT
silAURKAIP1 siRNA2	CAC CAC AAG TAC CG**T** AA**A** CT**C** GTG AAG AAG ACG CG

Key: Blue highlight depicts sequence targeted by the respective siRNAs. Bold and underlined bases represent the altered nucleotides relative to the WT AURKAIP1 sequence.

6.3 RESULTS

6.3.1 EFFECTS OF AURKAIP1 DEPLETION ON MTDNA LEVELS

Since the nucleoid morphology of cells was altered upon AURKAIP1 depletion (Chapter 5, Figures 5.4-8), it was important to ascertain whether this was a consequence of a change in the levels of mtDNA within the cells. To investigate this, qPCR was carried out on DNA isolated from HeLa cells treated with either AURKAIP1 or non-targeting siRNA for three days. The levels of *MT-ND4*, which is a mtDNA-encoded gene, were analysed relative to the nuclear-encoded gene for 18S rRNA as described in Section 2.3.11.

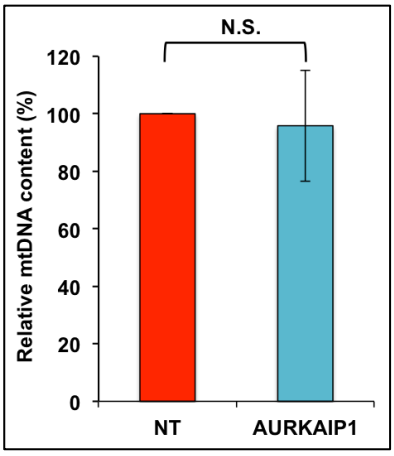

Figure 6.1: The Effects of AURKAIP1 Depletion on mtDNA Copy Number. Graph shows data from qPCR experiments conducted in HeLa cells treated with non-targeting (NT) siRNA or AURKAIP1 siRNA1 for 4 days. DNA was extracted and qPCR performed using *MT-ND4* and *18S* primers. The relative quantification of mtDNA (*MT-ND4*) to nuclear DNA (*18S*) was calculated using the normalised expression ratio ($2^{\Delta Cq}$) method. The $2^{\Delta Cq}$ values from AURKAIP1 depleted cells were normalised to the data from NT controls. Statistical significance was determined by t-test (n=6).

These data show that there was no significant change in mtDNA copy number in cells depleted of AURKAIP1 (average 95.8% relative to non-targeting control, p=0.45 n=5, Figure 6.1). Thus, the enlarged nucleoid phenotype seen in AURKAIP1 depleted cells (Figures 5.4-5.7) was unlikely to be due to increased mtDNA replication or replication stalling, as those conditions would be expected to lead to increased and decreased mtDNA copy number respectively. Consequently, it is most likely that AURKAIP1 depletion interferes with nucleoid distribution, as nucleoid clustering would account for the observed phenotype, but would not be expected to affect mtDNA copy number.

6.3.2 Effects of AURKAIP1 Depletion on Mitochondrial RNA Levels

Since mtDNA levels were unaffected, I next wanted to assess whether AURKAIP1 could be involved in mitochondrial transcription or RNA processing/regulation. To this end, the levels of mitochondrial RNA following AURKAIP1 depletion were analysed by northern blot. After 3 days siRNA treatment there was a slight decrease in *MT-CO1* and *MT-RNR1* (12S rRNA) levels, but an increase in the levels of *MT-ND1* (Figure 6.2). A general defect in mitochondrial transcription should affect all transcripts equally since mtDNA is transcribed from promoters found solely in the non-coding region and thus forms large polycistronic units (as discussed in 1.7.2). Therefore, these data indicated that AURKAIP1 depletion altered the levels of some mitochondrial RNAs, but was unlikely to be affecting transcription.

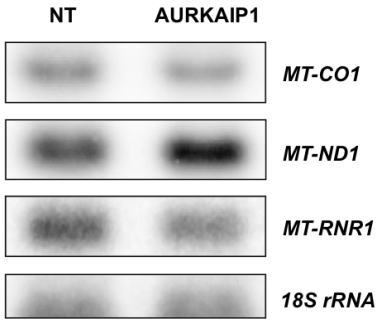

Figure 6.2: Effects of AURKAIP1 Depletion on Mitochondrial RNA levels. HeLa cells were treated with either non-targeting (NT) siRNA or AURKAIP1 siRNA1 for 3 days. RNA was extracted and purified, before being subjected to northern blot analysis. The blot was analysed using probes for mitochondrial mRNAs *MT-CO1* and *MT-ND1*, mitochondrial 12S rRNA and cytosolic 18S rRNA.

6.3.3 Effects of AURKAIP1 Depletion on Mitochondrial Protein Synthesis

To see whether the changes in RNA levels upon AURKAIP1 depletion corresponded to changes in mitochondrial protein synthesis, HeLa cells were depleted of AURKAIP1 for three days and nascent mitochondrial proteins were radiolabelled with [^{35}S]met. It was clear that the synthesis of some mtDNA-encoded proteins was reduced in AURKAIP1 depleted cells, most notably, COXI (Figure 6.3). However, the synthesis of several proteins, for example ND2, remained unchanged (Figure 6.3). Quantification was performed on the COXI, ND2 and cyt *b* signal from two independent experiments and analysed by T-test. COXI synthesis was reduced to 44% in cells treated with AURKAIP1 siRNA1 compared to controls ($p=0.00063$), whereas there was no significant change in ND2 (100% $p=0.5$) or cyt *b* (104%, $p=0.36$) synthesis relative to non-targeting controls.

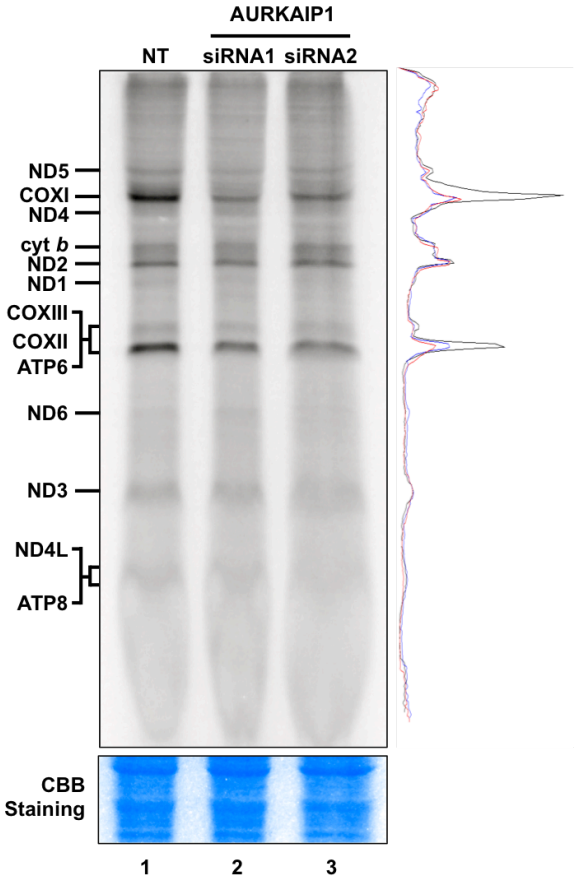

Figure 6.3: The Effects of AURKAIP1 depletion on Mitochondrial Protein Synthesis. HeLa cells were treated with either non-targeting (NT, lane 1) siRNA or AURKAIP1 siRNA1 (lane 2) or siRNA2 (lane3) for 3 days. Nascent mitochondrial polypeptides were labelled with [^{35}S]-methionine, subjected to 15% SDS-PAGE and detected using the Typhoon FLA 9500 system and ImageQuant software. The presented data is representative of two independent repeats. Quantification of signal intensity was performed using ImageQuant software and a trace representing this is presented with NT shown in black, AURKAIP1 siRNA1 shown in red and AURKAIP1 siRNA2 shown in blue.

The phenotype produced by AURKAIP1 depletion was far from a generalised defect in mitochondrial translation. Unexpectedly, 3 days of AURKAIP1 depletion slightly reduced the synthesis of ND1 over the 45-minute time course of [^{35}S]met incorporation, despite a substantial increase in mRNA levels (Figure 6.2). There was not adequate separation to allow distinct bands corresponding to ATP6 and COXII to be identified, though it was clear that there was a reduction in signal from the co-migrating band after AURKAIP1 depletion with either siRNA (approximately 57% and 53% of NT for siRNA1 and siRNA2 respectively, Figure 6.3). Whether this reduction reflects reduced synthesis of ATP6, COXII or both cannot be discerned. What is apparent is that depletion of AURKAIP1 with either siRNA1 or siRNA2 produced the same results, which strengthens the validity of these observations.

6.3.4 Effects of AURKAIP1 Depletion on Steady State Levels of mtDNA-Encoded Proteins

Since there was a clear effect of AURKAIP1 depletion on mitochondrial protein synthesis, it was important to assess the steady state levels of mtDNA-encoded proteins

in these cells. To this end, 4-day AURKAIP1 depletion with siRNA2 was conducted in HeLa and 143B cells respectively. The depletion of AURKAIP1 led to reduced signal for COXII (Figure 6.4A) as assessed by immunoblotting. Depleting HeLa cells of AURKAIP1 with each of the AURKAIP1 siRNAs resulted in a reduction in steady state levels of COXI and COXII relative to non-targeting controls (Figure 6.4B). These data once again demonstrated that each siRNA was producing similar phenotypes.

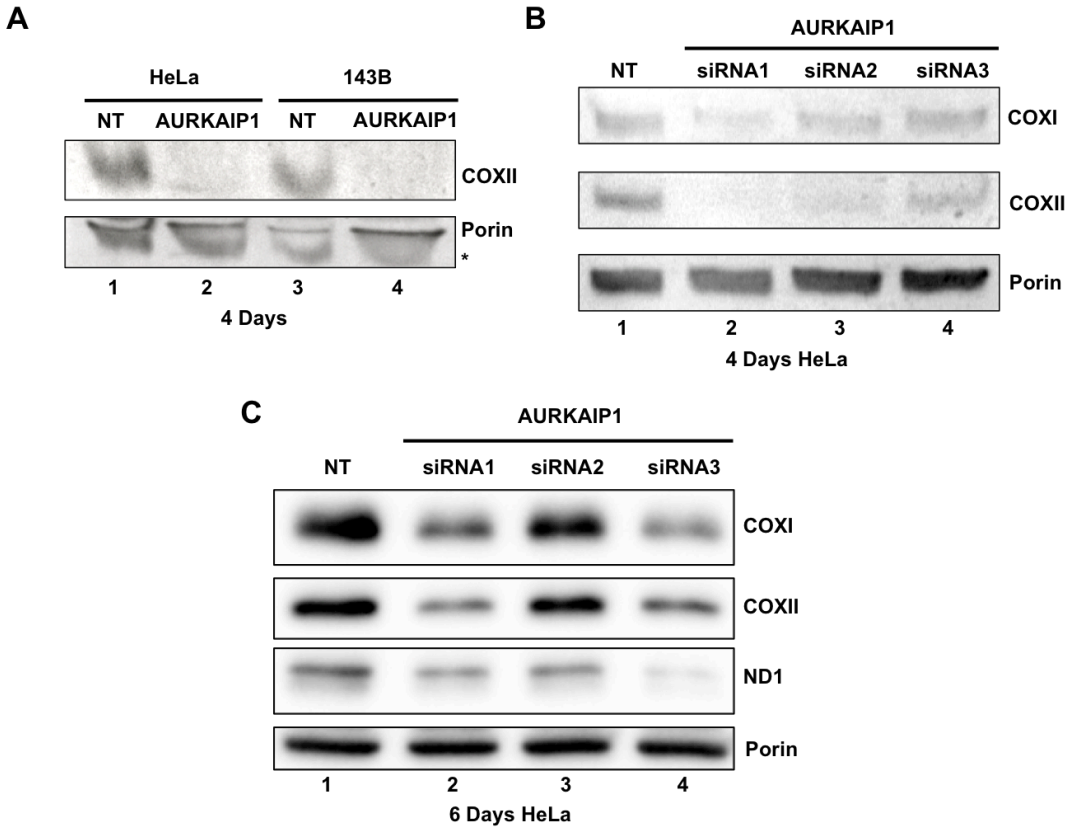

Figure 6.4: Effects of AURKAIP1 Depletion on Steady State Levels of mtDNA-encoded Proteins. A) HeLa cells (lanes 1 and 2) and 143B cells (lanes 3 and 4) were treated with either non-targeting (NT) siRNA (lanes 1 and 3) or AURKAIP1 siRNA2 (lanes 2 and 4) for 4 days. Cell lysates were produced and 40μg aliquots were subjected to western blot analysis and immunoblotted with α-COXII and α-porin antibodies. **B)** HeLa cells were treated as in **A**, but AURKAIP1 siRNA1 (lane 2), siRNA2 (lane 3) and siRNA3 (lane 4) were each used for AURKAIP1 depletion and compared to treatment with NT siRNA (lane1). Additionally α-COXI was also used for immunoblotting. **C)** HeLa cells treated as in B, but siRNA treatment lasted 6 days and α-ND1 was also used for immunoblotting.

Increasing the length of treatment with siRNA to 6 days also showed a clear reduction in the steady state levels of COXI, COXII and ND1 with all of the siRNAs tested (Figure 6.3C). However, after 6 days of AURKAIP1 depletion, the reduction of COXI and COXII levels was less striking. This was particularly evident in cells depleted of AURKAIP1 with siRNA2. This may be explained by the more severe effect of siRNA2 on cell growth (as discussed in Chapter 5, Figure 5.1). It was likely that after 6 days of

depletion, most cells transfected with AURKAIP1 siRNA 2 had died. Thus, the majority of the remaining cells were probably those that were either not transfected or poorly transfected, which would account for the less severe phenotype seen.

The data presented in Figure 6.3 are representative depictions of AURKAIP1 depletions after 4 and 6 days and it was consistently found that 4-day AURKAIP1 depletions using siRNA1 displayed the clearest reduction in mtDNA-encoded proteins and least cell death. For this reason, AURKAIP1 siRNA1 was predominantly used for depleting AURKAIP1.

It was difficult to assess the relative effects of each siRNA on AURKAIP1 protein levels directly since the endogenous levels of AURKAIP1 are very low. Depletion of endogenous AURKAIP1 by siRNA1 was confirmed by western blot analysis of 143B mitochondrial lysate as discussed in Chapter 4 (Figure 4.4B). Overexpressed AURKAIP1-FLAG was also efficiently depleted in cells treated with AURKAIP1 siRNA2 (Figure 4.4A). To confirm that AURKAIP1 depletion coincided with the reduction of steady state levels of mtDNA-encoded proteins, HEK293-AURKAIP1-FLAG cells were simultaneously induced with 10ng/ml doxycycline to allow low levels of AURKAIP1-FLAG overexpression, and treated with AURKAIP1 siRNA1 for 4 days. This allowed depletion of overexpressed AURKAIP1-FLAG, which can be seen in Figure 6.5. Furthermore, the COXII signal was also reduced in the AURKAIP1 depleted cells, thus providing further evidence that the effects of AURKAIP1 siRNA treatment are indeed mediated by AURKAIP1 depletion and not due to off-target effects.

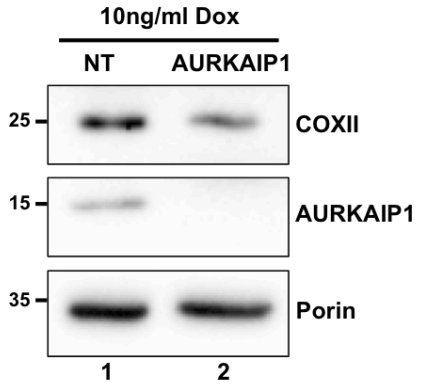

Figure 6.5: AURKAIP1 siRNA can Deplete Expressed AURKAIP1-FLAG. HEK293-AURKAIP1-FLAG cells were subjected to transfection with either non-targeting (NT) siRNA or AURKAIP1 siRNA1. Cells were then induced to express AURKAIP1-FLAG at low levels by the addition of 10ng/ml doxycycline (Dox) to the culture media. The treated cells were then incubated for 4 days under normal growth conditions before cell lysates were prepared and subjected to 12% SDS-PAGE and immunoblotting with α-COXII, α-AURKAIP1 and α-porin antibodies.

6.3.5 DOES AURKAIP1 DEPLETION AFFECT THE ACTIVITY OF RESPIRATORY COMPLEXES?

Next, it was decided to see if the reduction in mtDNA-encoded protein expression corresponded to a reduction in activity of the respiratory complexes. COXI and COXII are subunits of Complex IV and ND1 is a subunit of Complex I. Since the steady state levels of these proteins were reduced upon AURKAIP1 depletion, it would be expected that AURKAIP1 depletion would inhibit the activity of these complexes. Indeed, AURKAIP1 siRNA1-mediated depletion led to a reduction in Complex I (Figure 6.6A) and Complex IV (Figure 6.6B) activity to 59% (p=0.039) and 72% (p=0.04) respectively.

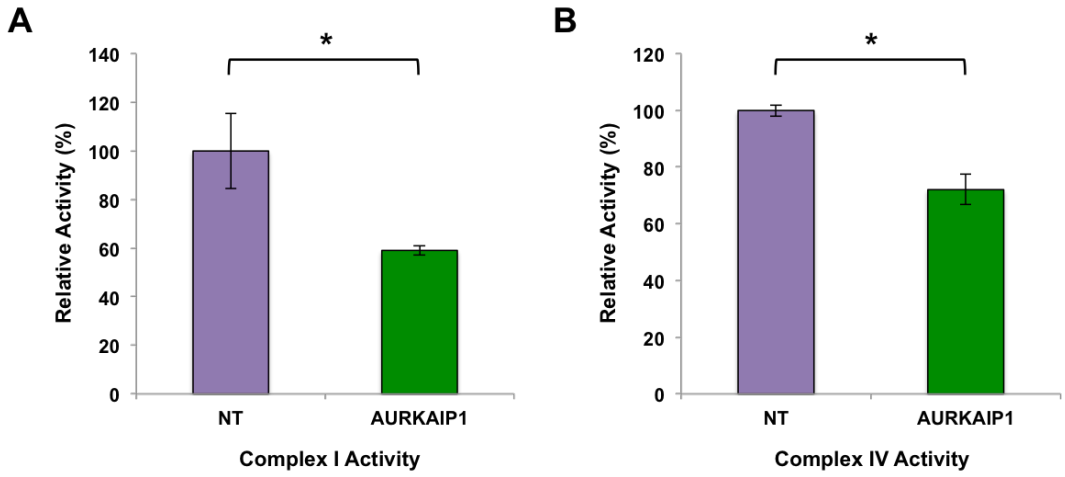

Figure 6.6: The Effects of AURKAIP1 Depletion on Respiratory Complexes. HeLa cells were treated with either non-targeting (NT) siRNA or AURKAIP1 siRNA1 (AUR1) for 4 days. **A)** Complex I (CI) and **B)** Complex IV (CIV) activity were measured spectrophotometrically as described in (Rustin et al., 1994). These experiments were conducted with the help of Dr Hornig-Do. Data represents two independent experiments, error bars=SEM. * denotes $p<0.05$.

6.3.6 CAN EXPRESSION OF SIRNA RESISTANT AURKAIP1 RESCUE THE PHENOTYPE OF AURKAIP1 DEPLETION?

From the previous experiments it was clear that AURKAIP1 depletion was inhibiting mitochondrial gene expression. It has also been shown that AURKAIP1 siRNA could deplete both expressed AURKAIP1-FLAG (Figure 4.4A and 6.4) and the endogenous AURKAIP1 protein (Figure 4.4B). All three siRNAs can deplete AURKAIP1 and produce similar mitochondrial phenotypes such as enlarged nucleoids (Figures 5.4-5.8), reduced mitochondrial protein synthesis (Figure 6.3) and steady state levels of mtDNA-encoded proteins (Figure 6.4 B and C). Together, these data suggest that these

phenotypes are due to AURKAIP1 depletion and not off-target effects. However, to conclusively demonstrate that the phenotype was due to AURKAIP1 depletion alone, it was important to rescue the phenotype of AURKAIP1 depletion. To this end, site directed mutagenesis was performed to allow expression of a modified version of AURKAIP1-FLAG with silent mutations (silAURKAIP1-FLAG). The silent mutations altered the nucleotide sequence so that the third base of three consecutive codons in the siRNA1-binding region of the AURKAIP1 ORF were altered. Crucially, the amino acid encoded by each mutated codon remained unchanged from the wild-type sequence (Figure 6.7A). This allowed for expression of AURKAIP1-FLAG that was resistant to depletion with AURKAIP1 siRNA1. The pcDNA^{TM}5/silAURKAIP1-FLAG plasmid was used to transfect HEK293 cells to produce stable cell lines (HEK293-silAURKAIP1-FLAG) as described in 4.2.1.

HEK293-silAURKAIP1-FLAG cells were treated with non-targeting siRNA or depleted of AURKAIP1 with siRNA1 for 48 hours before inducing the cells with 1μg/ml tetracycline for a further 48 hours. Since reduction of steady state protein levels of COXII and COXI was a consistent observation after 4 days of AURKAIP1 depletion, it was these parameters that were to be assessed in the 'rescued' cells.

Surprisingly, steady state levels of COXI and COXII were reduced in the cells expressing silAURKAIP1-FLAG, regardless of AURKAIP1 depletion (Figure 6.7B). Strikingly, the depletion of COXI and COXII levels after overexpression was more severe than was seen in AURKAIP1 depleted cells (Figure 6.4). These data suggest that precise AURKAIP1 levels are vital for mitochondrial gene expression as AURKAIP1 overexpression and AURKAIP1 depletion can each lead to a reduction in steady state levels of mtDNA-encoded proteins.

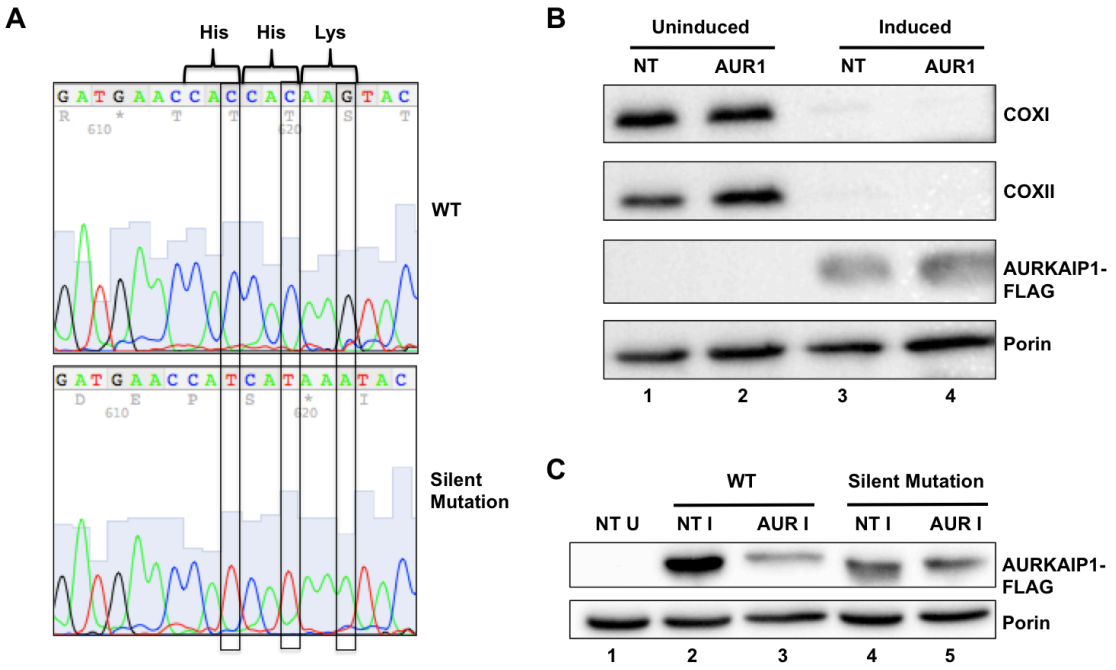

Figure 6.7: Expressing siRNA Resistant AURKAIP1 to attempt to Rescue the Phenotype of AURKAIP1 Depletion. A) Sequencing data illustrating the silent mutations made to the pcDNA™5/AURKAIP1-FLAG plasmid by site-directed mutagenesis. The shown sequence represents the siRNA1-binding region. Two C-T mutations result in change from a CAC codon to a CAT codon, both of which encode histidine. A further G-A mutation changes n AAG codon to an AAA codon, both of which encode lysine. The upper panel shows the wild-type (WT) sequence and the lower panel shows the silent mutated sequence. **B)** HEK293-silAURKAIP1-FLAG cells were transfected with either non-targeting (NT) siRNA (lanes 1 and 3) or AURKAIP1 siRNA1 (AUR1) for 48 hours. Cells were either left for another 48 hours (uninduced, lanes 1 and 2) or treated with 1μg/ml tetracycline (induced, lanes 3 and 4). Aliquots of cell lysate (40μg) from cells subjected to each condition were analysed by SDS-PAGE and western blotting. α-COXI, α-COXII, α-FLAG and α-porin antibodies were used for immunoblotting. **C)** HEK293-AURKAIP1-FLAG (WT) or HEK293-silAURKAIP1-FLAG (Silent Mutation) cells were subjected to combinations of siRNA treatment and tetracycline induction as in **B**. Cell lysate (40μg) from uninduced WT cells treated with NT siRNA (NT U, lane 1), induced NT treated WT cells (WT, NT I, lane 2), induced WT cells treated with AURKAIP1 siRNA1 (WT, AUR I, lane 3), NT treated, induced silent mutation cells (lane 4) or AURKAIP1 siRNA1 treated, induced silent mutation cells (lane 5) were subjected to SDS-PAGE and western blotting. α-FLAG and α-porin antibodies were used for immunoblotting. Quantification of signal intensity was performed in Image Lab.

The effects of AURKAIP1 siRNA1 on expression of AURKAIP1-FLAG and silAURKAIP1-FLAG were assessed to ensure the silAURKAIP1-FLAG expression was successful. It was clear that when HEK293-AURKAIP1-FLAG cells were treated with AURKAIP1 siRNA1, the expression of AURKAIP1-FLAG was greatly diminished (approximately 19% compared to uninduced controls). In contrast, HEK293-silAURKAIP1-FLAG cells treated with AURKAIP1 siRNA1 expressed silAURKAIP1-FLAG to similar levels as cells treated with non-targeting siRNA (approximately 82% of uninduced controls) (Figure 6.7C).

6.4 DISCUSSION

The data presented in this chapter clearly show that AURKAIP1 depletion negatively affects mitochondrial gene expression. The effects are not due to reduction in the mtDNA itself, as qPCR analysis did not show a change in mtDNA copy number after AURKAIP1 depletion (Figure 6.1). Coupled with the enlarged nucleoid phenotype seen in AURKAIP1 depleted cells (Figures 5.4-5.8), these data may indicate that AURKAIP1 plays a role in nucleoid distribution. TFAM depleted cells show similar nucleoid enlargement, which was attributed to a role for TFAM in nucleoid distribution between daughter cells during mitosis (Kasashima et al., 2011). In addition, depletion of the mitochondrial AAA protease ClpX produces a similar nucleoid enlargement phenotype (Kasashima et al., 2012). This effect was dependent on TFAM and ClpX was hypothesised to function as a chaperone rather than a protease to maintain nucleoid distribution through TFAM (Kasashima et al., 2012). Mitochondrial fission has also been implicated in nucleoid distribution as depletion of Drp1 also results in enlarged nucleoids, without any change in mtDNA copy number (Ban-Ishihara et al., 2013). It is difficult to say whether effects on nucleoid distribution are a primary effect of depletion of these proteins, or a consequence of another effect. Very little is currently understood regarding nucleoid distribution and its importance for mitochondrial gene expression. Nonetheless, a potential role for AURKAIP1 in the process will be an interesting topic for future investigations.

Though the levels of mtDNA remain unchanged, there were effects on the steady state levels of mitochondrial RNAs after AURKAIP1 depletion. This may implicate AURKAIP1 as a modulator of transcription or in an RNA processing or maturation process. Levels of *MT-CO1* and 12S rRNA (*MT-RNR1*) were slightly reduced in AURKAIP1 depleted cells, but *MT-ND1* levels were increased (Figure 6.1). These data suggest AURKAIP1 is unlikely to play a role in mitochondrial transcription as there was not a generalised reduction in mitochondrial RNA levels as would be expected if transcription was inhibited. Perhaps AURKAIP1 has a role in stabilising *MT-CO1* mRNA. This could explain the reduction in *MT-CO1* mRNA relative to *MT-ND1* mRNA. AURKAIP1 shares a conserved DUF1713 domain (conserved domain search for AURKAIP1 was carried out using the Conserved Domain Database (Marchler-Bauer et al., 2011) with the yeast Cox24 protein, which is expressed in *Schizosaccharomyces pombe* (Wood et al., 2002) and *Saccharomyces cerevisiae* (Huh

et al., 2003). Cox24 has been shown to be involved in *COXI* mRNA splicing in *S.cerevisiae* (Barros et al., 2006). This shared DUF1713 domain also led to AURKAIP1 appearing on a bioinformatic screen searching for Complex IV assembly factors (Szklarczyk et al., 2012). However, there are no introns in the human mitochondrial genome, unlike in yeast mtDNA. Therefore, *MT-CO1* mRNA does not require splicing, unlike *COXI* mRNA in yeast (Barros et al., 2006). A notable difference between yeast Cox24 and AURKAIP1 is that Cox24 is a mitochondrial inner membrane protein (Barros et al., 2006), whereas I have shown AURKAIP1 to be a matrix protein (Figure 4.3B). Nevertheless, this conservation of domains was of interest and was pursued during the course of my investigations, however, no RNA binding activity was seen with AURKAIP1-FLAG using CLIP (cross-linking and immunoprecipitation, as described in (Ule et al., 2005) (data not shown).

The importance of AURKAIP1 for mitochondrial translation was determined by [^{35}S] labelling of nascent polypeptides (Figure 6.2). The synthesis of some mitochondrial proteins (most notably COXI) was significantly reduced, though the synthesis of most proteins (such as ND2 and cyt *b*) was similar to non-targeting controls. Since there was not a general effect on the synthesis of all mtDNA-encoded protein, these data suggest that AURKAIP1 is not involved in critical translation processes such as elongation. However, there may be a modulatory role for AURKAIP1, perhaps as a translational activator for COXI. It may also be possible that AURKAIP1 associates with a subset for mitoribosomes and affects which mRNAs are loaded. Alternatively, the reduction in protein synthesis for COXI could simply be due to the reduced mRNA levels of *MT-CO1*. This is unlikely because the effect on COXI synthesis was more profound than the reduction of *MT-CO1* mRNA. Moreover, synthesis of ND1 was reduced in AURKAIP1 depleted cells (Figure 6.3), whereas *MT-ND1* mRNA levels were increased (Figure 6.2), suggesting the effects on mitochondrial translation cannot be explained by altered mRNA levels alone. The discrepancy between *MT-ND1* mRNA levels and protein synthesis of ND1 is interesting, but this effect is not unique. Other data from my host laboratory has also shown an increase in *MT-ND1* mRNA, with an accompanying reduction of ND1 protein levels in patient cell lines harbouring a mutation in mtPAP (Dr W. C. Wilson *personal communication*). The mechanisms underlying this phenotype remain unclear.

Steady state levels of mtDNA-encoded proteins are in accordance with the observed effects on protein synthesis in AURKAIP1 depleted cells. For example, COX1 and ND1 protein levels are both reduced in cells lacking AURKAIP1 (Figure 6.3C). The steady state levels of COXII are also reduced. This may suggest that a reduction in COXII protein synthesis. From the [^{35}S] labelling of nascent proteins, it was difficult to determine the effects of AURKAIP1 depletion on COXII synthesis as COXII and ATP6 were not separated by the 15% polyacrylamide gel. There was a clear decrease in the intensity of the co-migrating band, but from the presented data alone it was impossible to suggest whether reduced synthesis of COXII, ATP6 or both was the cause of this observation. Since steady state levels of COXII are dramatically reduced after AURKAIP1 depletion, it is more likely that COXII synthesis was impaired. Although, low COXI levels would affect Complex IV stability, potentially leading subsequent COXII degradation, which could also explain for the observed reduction in steady state COXII levels.

The most surprising observation presented in this chapter is the dramatic reduction in steady state levels of COXI and COXII after overexpression of silAURKAIP1-FLAG (Figure 6.7B). Far from rescuing the phenotype of AURKAIP1 depletion, overexpression of silAURKAIP1-FLAG resulted in a more pronounced reduction of COXI and COXII steady state levels. Moreover, AURKAIP1 depletion did not reduce the mtDNA-encoded protein levels in HEK293-silAURKAIP1-FLAG cells (Figure 6.6B lane 2). The most likely explanation for this is 'leaky' expression of silAURKAIP1-FLAG in the uninduced cells. The FlpIn^{TM}TREx^{TM} system relies on expression of the tet-repressor to prevent expression of the inserted gene in the absence of tetracycline. However, there is almost always a very small amount of 'leaky' expression of the inserted gene in the absence of tetracycline (Prof R. N. Lightowlers, unpublished observation, *personal communication*). Therefore, it is probable that there was low-level expression of silAURKAIP1-FLAG in the uninduced cells that was not detectable on the western blot (Figure 6.7B lanes 1 and 2). Since the endogenous levels of AURKAIP1 in 40μg of cell lysate are also undetectable by western blot, and that silAURKAIP1-FLAG is resistant to AURKAIP1 siRNA1 treatment (Figure 6.7C), it is possible that the 'leaky' expression of silAURKAIP1-FLAG is sufficient to prevent the conditions of AURKAIP1 depletion. This explanation is consistent with data showing that AURKAIP1 depletion led to a reduction in COXII protein levels in HEK293-

AURKAIP1-FLAG cells (Figure 6.5, lane 2), but not in HEK293-silAURKAIP1-FLAG cells (Figure 6.7B, lane 2), as the wild-type AURKAIP1-FLAG was depleted by the siRNA (Figure 6.5, lane 2), but silAURKAIP1-FLAG was resistant to depletion (Figure 6.7C, lane 5).

The 'leaky' expression of silAURKAIP1-FLAG cannot be said with certainty to account for the apparent rescue of the effects of AURKAIP1 siRNA treatment, as the potential 'leaky' expression could not be detected by western blot. However, this hypothesis best explains the observed data and would suggest that AURKAIP1 siRNA mediates its effects by specific AURKAIP1 depletion rather than off-target effects. The fact that AURKAIP1 depletion with each siRNA produces very similar phenotypes in terms of morphology changes (Chapter 5), and impairment of mitochondrial gene expression (this Chapter), further supports this conclusion.

The most striking aspect of the AURKAIP1 overexpression phenotype is that it is similar to the AURKAIP1 depletion phenotype in that COXI and COXII protein levels are reduced by each condition. This creates a conundrum as to how excessively high or extremely low levels of a single protein can exhibit similar, rather than opposite effects. To address this issue, further characterisation of the AURKAIP1 overexpression phenotype will be the focus of the following chapter.

CHAPTER 7: STUDYING AURKAIP1 OVEREXPRESSION

7.1 INTRODUCTION

In the preceding chapter I showed that AURKAIP1 overexpression, as well as AURKAIP1 depletion, disrupted mitochondrial gene expression as measured by COXI and COXII steady state protein levels (Figure 6.6B). Therefore, it was important to further investigate the effects of AURKAIP1 overexpression on mitochondrial gene expression. To this end, studies were conducted to characterise the effects of AURKAIP1 overexpression on cell and mitochondrial morphology, mtDNA levels, mitochondrial RNA levels and mitochondrial protein synthesis. Of particular interest was determining the similarities and differences between the phenotypes exhibited by AURKAIP1 overexpression and AURKAIP1 depletion. In this way, AURKAIP1 overexpression was used as an additional tool to allow further investigation of the function of AURKAIP1 in human mitochondria.

The role of AURKAIP1 may be hinted by identifying binding partners. Towards this goal, immunoprecipitation studies were conducted. Co-immunoprecipitation (Co-IP) is the method of precipitating a known protein, along with any proteins that are bound to it, out of a solution using an antibody that specifically binds the known protein. The precipitated protein complex can then be eluted and analysed by various methods including western blot analysis and mass spectrometry. Western blot analysis should be used when testing for specific interactions, and requires antibodies to each protein that is to be assessed. Mass spectrometry analysis, on the other hand, allows identification of unknown proteins based on the mass-charge ratio of their constituent molecules. Since there were no published data regarding binding partners of AURKAIP1 at the time of my investigations, mass spectrometry was a useful technique to use. There are many types of mass spectrometry, but of particular relevance to my work is MALDI-TOF (matrix-assisted laser desorption/ionisation with time of flight), which coupled with peptide mass fingerprinting is commonly used for identification of proteins. MALDI refers to the method of breaking up and charging the analyte and TOF refers to the method of detection (Vorm et al., 1994). Put simply, when used to analyse peptides, the analyte is charged by MALDI, before the application of a voltage causes acceleration of

the constituent molecules based on their charge. The molecules then pass though a defined space to a detector, with the time of flight being proportional to the mass of the molecule (Wollnik, 1993). Peptide mass fingerprinting involves the protein being cleaved into smaller peptides, the masses of which are determined by MALDI-TOF. The resulting masses are compared to those produced by known proteins in a large database. The best match is determined statistically and the identified protein can then be confirmed using western blotting.

AURKAIP1 overexpression allowed Co-IP studies to be conducted via the FLAG moiety. For this reason, Co-IP experiments will be presented in this chapter alongside the biochemical characterisation of the effects of AURKAIP1 overexpression.

7.2 METHODS

7.2.1 ISOKINETIC SUCROSE GRADIENT

Before harvesting cells, gradient buffer was prepared (50mM Tris/HCl pH 7.2, 10mM MgOAc, 40mM NH_4Cl, 100mM KCl, 1mM PMSF and 50μg/ml chloramphenicol), filter sterilised and left on ice. A total of 0.5g and 1.5g of sucrose was added to 5ml gradient buffer to produce 10% and 30% sucrose solutions respectively. An aliquot of 500μl of the 10% sucrose solution was added to a Beckman Ultracentrifuge tube (Beckman Coulter, 343778). Then, using a 1ml syringe and needle, 500μl of the 30% sucrose solution was carefully injected under the 10% solution, so as to produce two distinct layers. The tubes were sealed with a rubber plug and placed onto the Biocomp Gradient Maker 107 instrument. A linear gradient was produced by running the TL55 program (short sucrose, 10-30% S1/1 0:55/85.0/22) and then incubating at 4°C on a flat surface for 1 hour.

Cells were harvested and lysed in Sigma lysate buffer (as for immunoprecipitation described below, 7.2.2) and incubated at 4°C for 30 minutes with rotation. The lysates were centrifuged at 12,000*g* for 10 minutes before the supernatant was collected and protein concentration measured by Bradford assay (2.5.3). An aliquot of 800μg (in a 100μl volume) of lysate was carefully loaded onto the gradient so as not to disturb the gradient. The loaded gradient(s) were then centrifuged at 100,000*g* for 2 hours 15 minutes at 4°C (Beckman Optima TLX ultracentrifuge, acceleration-1, deceleration-4).

The gradient(s) were carefully removed from the ultracentrifuge and eleven 100µl fractions were sequentially taken, removing the uppermost layer of the remaining gradient each time. The first fraction taken from the top of the gradient was designated fraction 1 and all subsequent fractions named sequentially, until finally fraction 11 was taken. The gradient fractions were either snap frozen in liquid nitrogen and stored at -80°C or aliquots of 10µl (with the addition of 2.5µl 5x SB) were subjected to SDS-PAGE.

7.2.2 CO-IMMUNOPRECIPITATION VIA THE FLAG MOIETY

Co-Immunoprecipitaiton (Co-IP) via the FLAG moiety was carried out on mitochondrial preparations from HEK293-AURKAIP1-FLAG or U2OS-AURKAIP1-FLAG cells that had been grown in 300cm^2 flasks and induced with tetracycline for 3 days. Mitochondrial pellets were resuspended in homogenisation buffer (2.5.2) and the protein concentration was measured by Bradford assay (2.5.3). A known quantity (varied between experiments depending on amount of material available, generally 0.5-1mg) of mitochondria were once again pelleted at 11,000*g* for 10 minutes at 4°C before the supernatant was discarded and the mitochondrial pellet was lysed by the addition of 500µl Sigma lysis buffer (50mM Tris/HCl pH 7.4, 150mM NaCl, 1mM EDTA, 1% Triton X-100 and supplemented with 10mM $MgCl_2$ and 1mM PMSF) and incubating at 4°C for 30 minutes with rotation.

The Co-IP was carried put using the FLAG® immunoprecipitation kit (Sigma, FLAGIPT-1). A 40µl aliquot of the ANTI-FLAG® affinity gel, which equates to approximately 20µl volume of packed gel resin, was centrifuged at 5000*g* for 30 seconds in a hydrophobic microcentrifuge tube. The supernatant was discarded and the packed gel washed 3 times with 1ml of 1x wash buffer (50mM Tris/HCl pH 7.4 and 150mM NaCl supplemented with 10mM $MgCl_2$, 1x protease inhibitor cocktail and 1mM PMSF). Wash buffer was removed without discarding any resin.

After the 30-minute incubation, the mitochondrial lysate was centrifuged at 12,000*g* for 10 minutes at 4°C before removing the supernatant into a new tube and performing a Bradford assay (2.5.3). Typically, 800µg of mitochondrial proteins in 500µl Sigma lysate buffer was added to the washed resin and incubated at 4°C for 3 hours with rotation. The resin was pelleted by centrifugation at 5000*g* for 30 seconds and the

supernatant (flowthrough fraction) was saved. The resin was then washed 3 times with supplemented wash buffer. To elute, the resin was resuspended in 100µl supplemented wash buffer with 250ng/µl final concentration of 3x FLAG® peptide and incubated at 4°C for 45 minutes with rotation. The resin was pelleted by centrifugation at 5000*g* for 30 seconds and the supernatant (elution fraction) saved for analysis by SDS-PAGE and either western blotting (2.5.6) or InstantBlue Coomassie staining (2.5.5).

7.2.3 Co-Immunoprecipitation via Antibodies to Endogenous Proteins

Typically 20µl of magnetic beads (Dynabeads Protein G, Life Technologies, 10003D) were used per Co-IP reaction. The beads were prepared by washing 3 times with 1ml 100mM sodium phosphate buffer pH 8.1 (Na-P) and pelleted after each wash by placing in a magnetic rack. The beads were resuspended in a final volume of 100µl antibody mix (10µl for commercial antibodies (mtPAP, MNK1, p32) and 30µl for in-house generated antibodies (AURKAIP1 and MRPL12) made up to 100µl with Na-P) and incubated for 1 hour at room temperature with rotation. This allowed the formation of a Protein G-antibody complex, which was subsequently washed 3 times with 1ml chilled Sigma lysate buffer before the addition of the lysed mitochondrial fraction (prepared in the same manner as for α-FLAG Co-IP, see 7.2.2 above). The reaction was incubated for 3 hours at 4°C with rotation. The beads (now complexed with antibody and antigen) were once again pelleted in a magnetic rack and washed 5 times with chilled lysate buffer. The antigens were eluted from the beads by the addition of 25µl Sigma lysate buffer and 6.25µl 5x sample loading buffer (as for western blotting, 2.5.6) and heating at 95°C for 3 minutes with 1000rpm shaking in an Eppendorf Thermomixer. The beads were pelleted in a magnetic rack and the elution (supernatant) transferred to a fresh tube and either stored at -80°C or immediately subjected to SDS-PAGE (2.5.4).

When performing Co-IP using the endogenous AURKAIP1 antibody, 800µg of proteinase K shaved mitoplasts were used rather than crude mitochondrial lysate. Preparation of the mitoplast fraction was performed as for the mitochondrial sub-localisation protocol (4.2.2).

7.2.4 MASS SPECTROMETRY ANALYSIS

Approximately half of the α-FLAG Co-IP elution from HEK293-AURKAIP1-FLAG isolated mitochondria was subjected to SDS-PAGE (2.5.4) and stained using SimplyBlue™ SafeStain (2.5.5). Bands were excised using a sterile scalpel and sent to Pinnacle (Newcastle University) for MALDI-TOF mass spectrometry analysis.

7.3 RESULTS

7.3.1 DOES AURKAIP1 OVEREXPRESSION AFFECT MITOCHONDRIAL MORPHOLOGY?

AURKAIP1-FLAG overexpression did not produce a striking growth retardation or cell morphology change even after 7 days of treatment (Figure 7.1). This observation contrasts with the effects of AURKAIP1 depletion, where treated cells exhibited clear growth retardation (Figure 5.3).

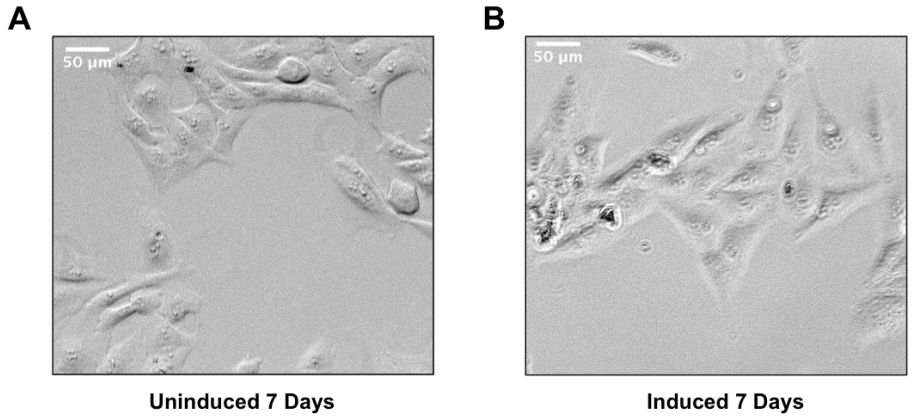

Figure 7.1: Effects of AURKAIP1 Overexpression on Cell Morphology. Equal numbers of U2OS-AURKAIP1-FLAG cells were seeded in Wilco glass bottomed dishes and cultured as normal (uninduced, **A**) or with 1µg/ml tetracycline (induced, **B**) for 7 days and visualised by light microscopy.

There was a distinctive enlarged nucleoid phenotype in AURKAIP1 depleted cells as discussed in Chapter 5. This is likely due to improper nucleoid distribution. To see if AURKAIP1 overexpression had the opposite effect, fluorescence microscopy was performed on AURKAIP1-FLAG overexpressing cells. Since HEK293 cells do not provide good images, U2OS-AURKAIP1-FLAG cells were used for imaging.

Surprisingly, cells overexpressing AURKAIP1-FLAG also displayed an enlarged nucleoid phenotype (Figure 7.2). However this effect differs from AURKAIP1 depleted cells in that and there were very few nucleoids, almost all of which were enlarged.

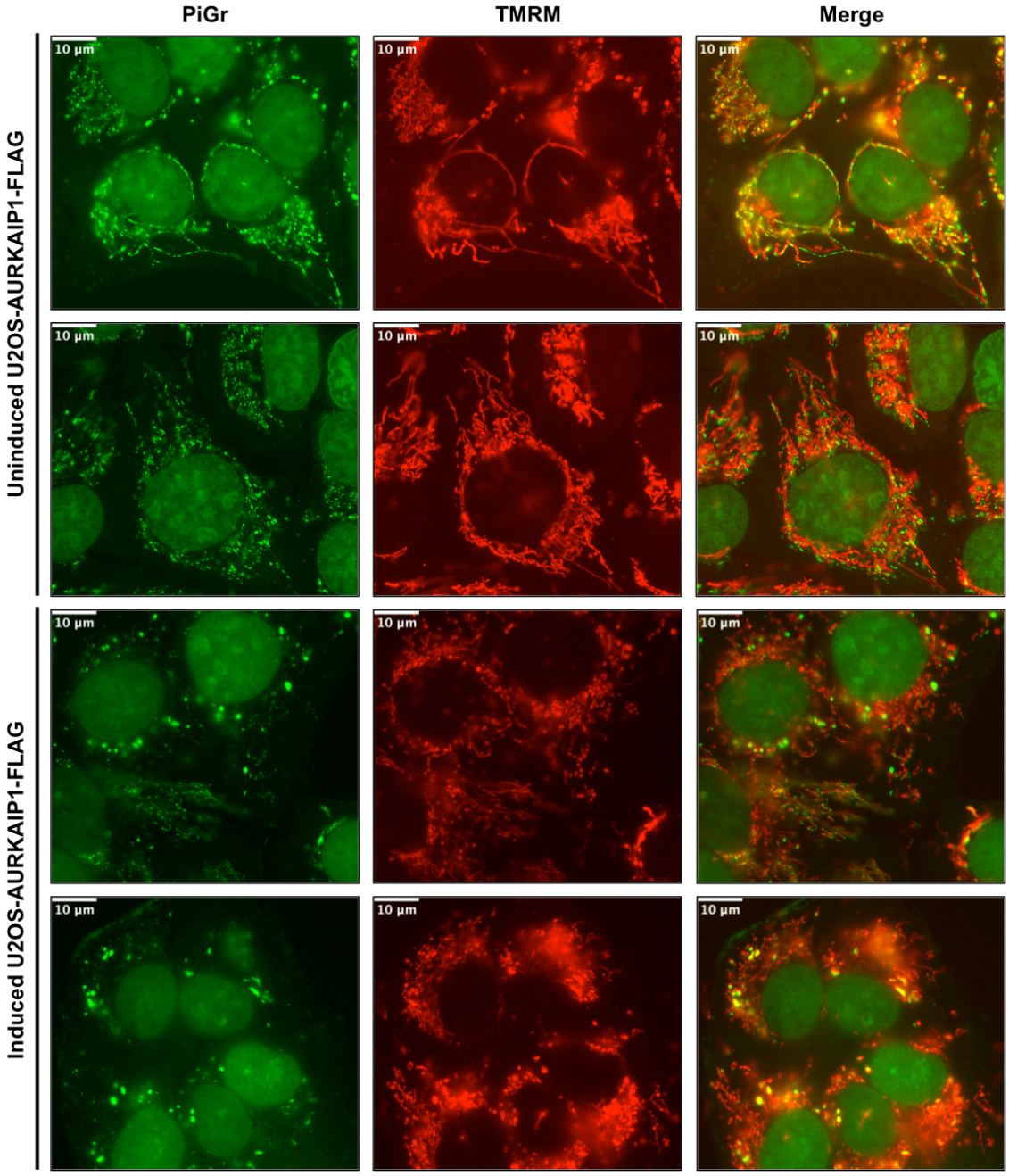

Figure 7.2: Effects of AURKAIP1 Overexpression on Mitochondrial Morphology. U2OS-AURKAIP1-FLAG cells either grown as normal (uninduced) or treated with 1µg/ml tetracycline (induced) for 4 days. Cells were stained with TMRM to visualise the mitochondrial network (red) and PicoGreen (PiGr) to stain double-stranded DNA (nucleus and mtDNA nucleoids, green) and live-cell fluorescence microscopy was performed. Scale bar = 10µm.

The mitochondria, as visualised by TMRM staining and fluorescent microscopy, appeared more punctate in AURKAIP1-FLAG overexpressing cells, with fewer

elongated mitochondria. This could indicate an increase in mitochondrial fission, or impaired mitochondrial fusion in AURKAIP1-FLAG overexpressing cells. Quantification of this phenotype showed on average fragmented mitochondria (defined as <1μm particles with a circularity between 0.5 and 1) accounted for 25% of the total mitochondrial mass in AURKAIP1-FLAG overexpressing cells, which was significantly more than in uninduced controls (13.6%, p=0.0221, n=7 fields, further details in the following chapter, Figure 8.6A).

7.3.2 Effects of AURKAIP1 Overexpression on Mitochondrial Gene Expression

The data presented in the preceding chapter clearly showed a strong reduction of COXI and COXII after AURKAIP1-FLAG overexpression (Figure 6.7B). It was crucial to ensure that this effect was not simply due to the addition of tetracycline. To this end, several clones of HEK293-AURKAIP1-FLAG cells were induced with tetracycline alongside untransfected HEK293 cells. These data showed that tetracycline did not deplete the steady state levels of COXII in wild-type HEK293 cells (Figure 7.3A, lane 2), but that all HEK293-AURKAIP1-FLAG clones exhibited reduced COXII levels upon tetracycline-mediated induction (Figure 7.3A, lanes 4, 6 and 8). Additionally, AURKAIP1-FLAG overexpression produced the same phenotype in U2OS-AURKAIP1-FLAG cells (Figure 7.3B), which showed that these effects were not cell type dependent. It is also worth noting that depletion of mtDNA-encoded proteins was not seen with the induction of any other overexpressed protein within our laboratory using the same FlpIn^{TM}TREx^{TM} (HEK293) system (data from other lab members not shown). Together, these data strongly suggest that it is the overexpression of AURKAIP1-FLAG that is causing the reduction in COXI and COXII levels.

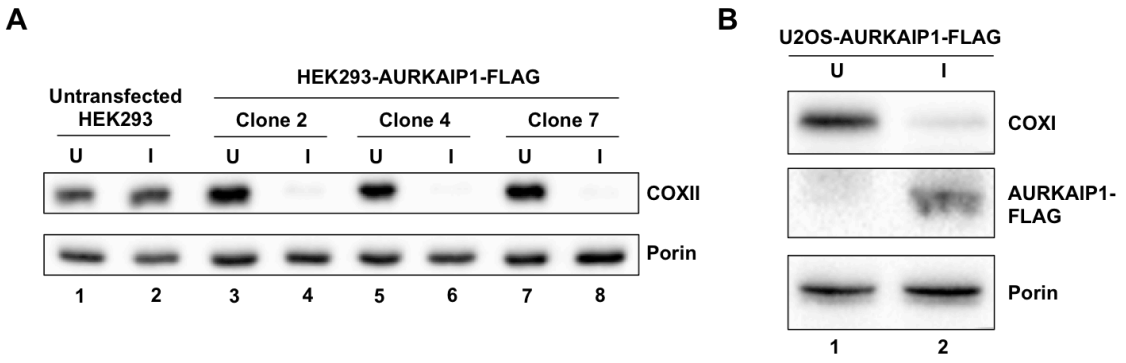

Figure 7.3: AURKAIP1 Overexpression Causes Depletion of COXI and COXII. (A) Untransfected HEK293 cells (lanes 1 and 2), and three independent HEK293-AURKAIP1-FLAG clones (lanes 3-8) were either grown as normal (uninduced) or with 1μg/ml tetracycline (induced) as indicated for 3 days. Cell lysate (40μg) from each sample was subjected to SDS-PAGE and western blotting. **(B)** U2OS-AURKAIP1-FLAG cells were treated as described in **A**. α-COXI, α-COXII, α-porin and α-FLAG antibodies were used for immunoblotting.

As was the case when studying the effects of AURKAIP1 depletion, it was important to test mtDNA copy number to see if there was an effect that may allow explanation of the enlarged nucleoid phenotype. There was a small, but statistically significant reduction in mtDNA copy number after 3 days of AURKAIP1-FLAG overexpression (85.3% of NT controls, p=0.012, n=6, Figure 7.4).

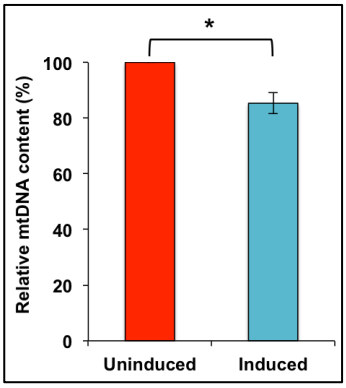

Figure 7.4: The Effects of AURKAIP1 Overexpression on mtDNA Levels. Graph shows data from qPCR experiments conducted in U2OS-AURKAIP1-FLAG cells. Uninduced cells or cells treated with 1μg/ml tetracycline (induced) were grown for three days. DNA was extracted and qPCR performed using *MT-ND4* and *18S* primers. The relative quantification of mtDNA (*MT-ND4*) to nuclear DNA (*18S*) was measured using the normalised expression ratio ($2^{\Delta Cq}$) method. The $2^{\Delta Cq}$ values for the induced samples were normalised to be expressed as a percentage of the uninduced controls. Statistical significance was determined by t-test (p=0.012, n=6). * denotes $p<0.05$. Error bars indicate SEM.

Again, these data showed similarities between the effects of AURKAIP1 depletion and AURKAIP1-FLAG overexpression in that only modest reduction in mtDNA levels was seen (95.8% and 85.3% respectively). However, the results were only statistically significant with AURKAIP1-FLAG overexpression.

Next, the effects of AURKAIP1-FLAG overexpression on mitochondrial RNA levels were assessed by northern blot. The levels of *MT-CO1* and 12S rRNA (*MT-RNR1*) were clearly reduced with AURKAIP1-FLAG overexpression, but the levels of *MT-ND1*

mRNA remained unchanged (Figure 7.5). Once again, this is consistent with AURKAIP1-FLAG overexpression providing a more severe biochemical phenotype compared to AURKAIP1 depletion.

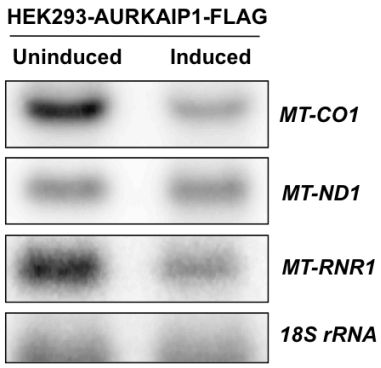

Figure 7.5: The Effects of AURKAIP1 Overexpression on Mitochondrial RNA levels. HEK293-AURKAIP1-FLAG cells were either grown as normal (uninduced) or treated with 1μg/ml tetracycline (induced) for three days. RNA was extracted and purified, before being subjected to northern blot analysis. The blot was analysed using probes for mitochondrial mRNAs (*MT-CO1* and *MT-ND1*), mitochondrial 12S rRNA (*MT-RNR1*) and cytosolic 18S rRNA as a loading control.

In keeping with previous observations of AURKAIP1-FLAG overexpression causing a more dramatic biochemical phenotype than AURKAIP1 depletion; a more severe reduction of Complex I and Complex IV activity was seen in AURKAIP1-FLAG overexpressing cells (Figure 7.6). Average Complex I and Complex IV activities were reduced (to 49.7% and 47.8% respectively) in AURKAIP1-FLAG overexpressing cells compared to uninduced controls.

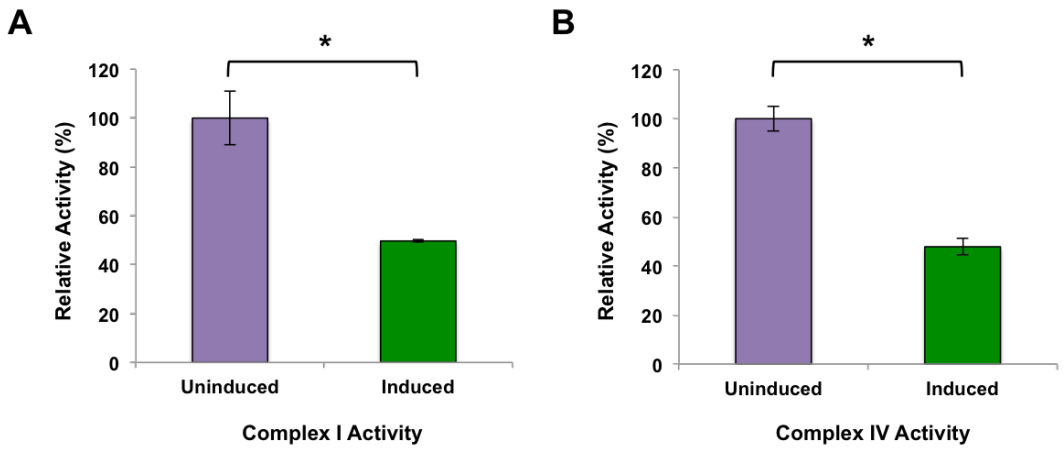

Figure 7.6: The Effects of AURKAIP1 Overexpression on Respiratory Chain Complexes. HEK293-AURKAIP1-FLAG cells were either grown as normal (uninduced) or treated with 1μg/ml tetracycline (induced) for 4 days. **A)** Complex I (CI) and **B)** Complex IV (CIV) activities were measured spectrophotometrically as described in (Rustin et al., 1994). These experiments were conducted with the assistance of Dr Hornig-Do. * denotes $p<0.05$. Statistics were performed on data from two independent repeats using T-test. CI – $p=0.044$. CIV – $p=0.013$.

Next, it was important see if the effects of AURKAIP1-FLAG overexpression on steady state levels of mtDNA-encoded proteins and RNA were consistent with an impairment of mitochondrial protein synthesis. To this end, [^{35}S] labelled methionine incorporation studies were conducted as described in Section 6.2.1. As expected, protein synthesis was more severely impaired with AURKAIP1-FLAG overexpression compared to AURKAIP1 depletion (Figure 7.7). Notably, AURKAIP1-FLAG overexpression severely reduced the synthesis of all mtDNA-encoded proteins (Figure 7.7, lane 4), whereas AURKAIP1 depletion only reduced the synthesis of COXI (46% of NT control) and COXII (60% of NT control) clearly (Figure 7.7 lane 2, Chapter 6), suggesting that AURKAIP1 depletion and overexpression mediate their effects by different mechanisms.

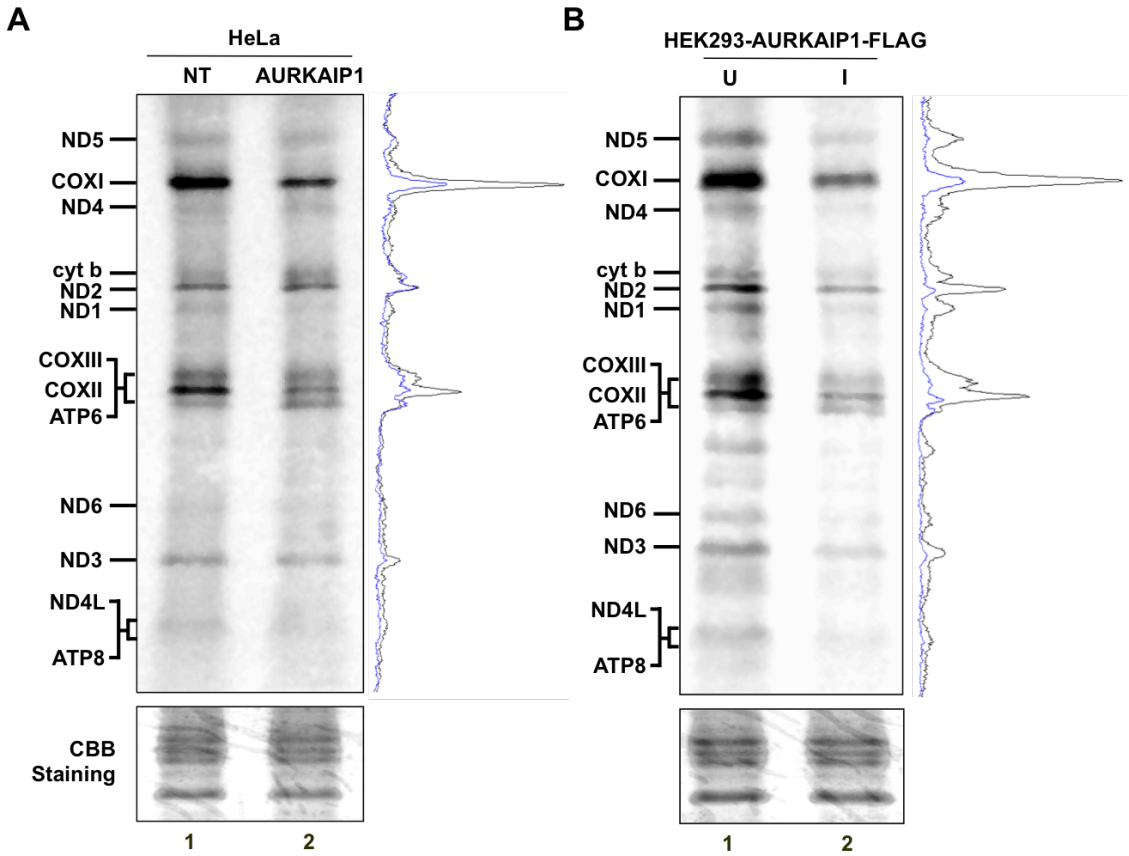

Figure 7.7: The Effects of AURKAIP1 Depletion and Overexpression on Mitochondrial Protein Synthesis. (A) HeLa cells were treated with non-targeting (NT, lane 1) or AURKAIP1 siRNA1 (lane 2) for 3 days. Nascent mitochondrial polypeptides were labelled with [^{35}S] methionine and subjected to SDS-PAGE (15-20% polyacrylamide gel) and detected using the Typhoon FLA 9500 system and ImageQuant software. Graphical representation of NT = black and AURKAIP1 siRNA1 = blue. **(B)** Same technique performed In parallel with **A**, but using HEK293-AURKAIP1-FLAG cells either grown as normal (uninduced, U, lane 1, black trace) or treated with 1μg/ml tetracycline (induced, I, lane 2, blue trace) for 3 days. ([^{35}S] radiolabeling and SDS-PAGE were performed in collaboration with Dr Francesco Bruni). Designation of which mtDNA-encoded protein corresponded to each signal was determined with reference to (Chomyn, 1996). After detection of the radioactive signal, the gel was rehydrated and stained with Coomassie Brilliant Blue (CBB) to ensure equal loading.

7.3.3 ARE MTDNA-ENCODED PROTEINS ACTIVELY DEGRADED UPON AURKAIP1 OVEREXPRESSION?

AURKAIP1-FLAG overexpression led to depletion of COXI and COXII steady state protein levels after just 3 days (Figure 7.3). In contrast, depletion of AURKAIP1 was required for at least 4 days before changes in COXI and COXII levels were detectable. Both COXI and COXII are highly hydrophobic integral membrane components of Complex IV and, as such, are fairly stable. Indeed, the half life of COXI has been shown to be 5 days in liver tissue (Ip et al., 1974). If this were the case in cultured cells, inhibition of translation would not dramatically affect the levels of COXI after 3 days, as the mature protein would not degrade rapidly.

Since I have already shown that AURKAIP1-FLAG overexpression inhibits mitochondrial protein synthesis (Figure 7.7), I wanted to investigate whether inhibition of translation alone could account for the rapid and severe depletion of COXI and COXII seen in the induced AURKAIP1-FLAG expressing cell lines, or whether these proteins were being actively degraded, perhaps as a consequence of Complex IV disassembly. Towards this goal, the effects of AURKAIP1-FLAG overexpression via induction with tetracycline were investigated alongside the effects of chloramphenicol-mediated inhibition of translation. The stocks of chloramphenicol and tetracycline were each dissolved in ethanol. Therefore, uninduced control cells were treated with equal volumes of ethanol to exclude any potential contribution to the phenotype. Cells incubated with each treatment were harvested after 2, 3, 4, 5 and 6 days and cell lysates were analysed by western blotting and immunodetection (Figure 7.8).

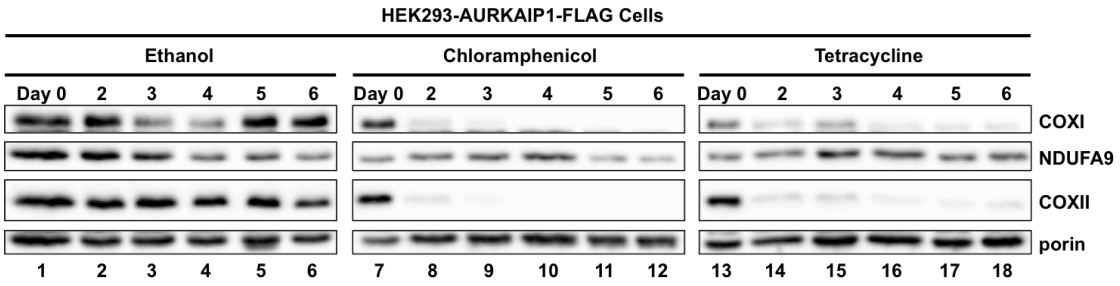

Figure 7.8: Is COXI and COXII Depletion Upon AURKAIP1 Overexpression More Rapid than is Possible by Inhibiting Mitochondrial Translation Alone? HEK293-AURKAIP1-FLAG cells were treated with 1μl 100% ethanol, 50μg/ml chloramphenicol or 1μg/ml tetracycline for 2, 3, 4, 5 and 6 days. Cell lysate was prepared from cells subjected to each treatment at each time point and also cells harvested before any treatment (Day 0). Aliquots (40μg) of the cell lysates were subjected to SDS-PAGE and western blotting. Antibodies to mtDNA-encoded Complex IV subunits (COXI and COXII), nuclear-encoded Complex I subunit (NDUFA9) and porin (loading control) were used for immunoblotting.

It was clear that COXI and COXII protein levels were reduced after only 2 days of translation inhibition via chloramphenicol treatment (Figure 7.8, lanes 8-12). The same effect was seen after tetracycline-mediated AURKAIP1-FLAG overexpression (Figure 7.8, lanes 14-18), but not in ethanol treated control cells (lanes 1-6). These data indicate that the reduction in the steady state levels of COXI and COXII in AURKAIP1-FLAG overexpressing cells can be explained by inhibition of mitochondrial protein synthesis alone. Furthermore, NDUFA9 (a nuclear-encoded subunit of Complex I) levels are neither affected by mitochondrial translation inhibition via chloramphenicol treatment nor AURKAIP1-FLAG overexpression, thus suggesting that AURKAIP1-FLAG overexpression may specifically deplete only mtDNA-encoded protein levels. Together, these data are consistent with AURKAIP1-FLAG overexpression inhibiting mitochondrial protein synthesis.

7.3.4 DOES AURKAIP1 INTERACT WITH THE MITORIBOSOME?

Since AURKAIP1-FLAG overexpression impaired mitochondrial protein synthesis (Figure 7.7), it was important to see if these effects were mediated by interfering with the assembly of the mitoribosome. To investigate this possibility, sucrose gradient studies were conducted to investigate the potential of AURKAIP1 to interact with the mitoribosome and assess whether AURKAIP1-FLAG overexpression alters ribosome assembly (Figure 7.9).

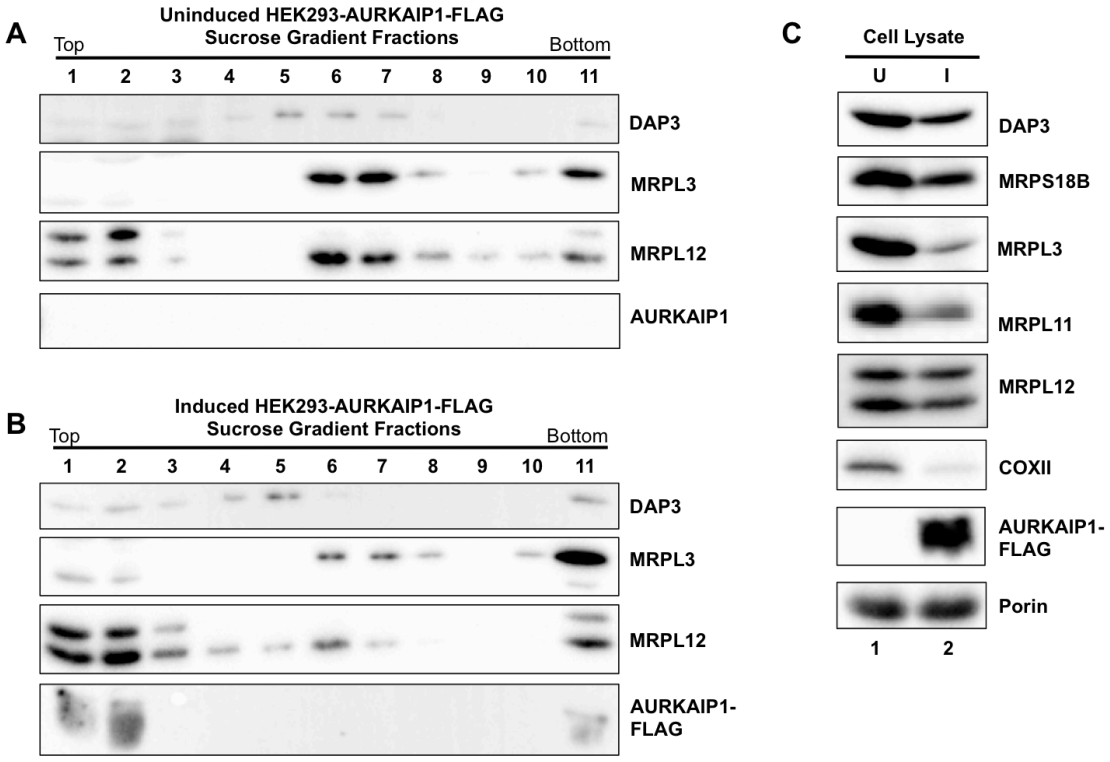

Figure 7.9: Does AURKAIP1 Overexpression Affect the Mitoribosome? Aliquots (800μg) of cell lysate from uninduced **(A)** or induced (with 1μg/ml tetracycline for 3 days **(B)**) HEK293-AURKAIP1-FLAG cells were separated on 10-30% sucrose gradients. Fractions of equal (100μl) volume were collected from the top of the gradient (fraction 1) sequentially to the bottom (fraction 11). An aliquot of 10% of each fraction was subjected to SDS-PAGE and western blotting was performed. The displayed images are compiled from two blots per condition, loaded with the same amount of material from the same sucrose gradient fractions. **(C)** An aliquot of 40μg of cell lysate from the same uninduced (lane 1) or induced (lane 2) cells prior to sucrose gradient centrifugation were subjected to SDS-PAGE and western blotting The displayed images are a compilation of signals from several blots each loaded with equal amounts of lysate from the same preparation. Antibodies to DAP3, MRPS18B, MRPL3, MRPL11, MRPL12, COXII, AURKAIP1 (**A** only), FLAG (**B** and **C**) and porin were used for immunoblotting.

AURKAIP1-FLAG was predominantly found in the least dense fractions of the sucrose gradient (Figure 7.9B fractions 1 and 2), whereas MRPL3 was present in fractions 6 and 7 and DAP3 predominantly detected in fraction 5, indicating the expected positions of the mitoribosomal 39S LSU and 28S SSU respectively. These data suggest that AURKAIP1-FLAG does not associate with the mitoribosome and implies that AURKAIP1-FLAG is mostly 'free' with a small proportion present in aggregates in the densest fraction (Figure 7.9B fraction 11).

Mitoribosomal proteins (MRPs) were affected by AURKAIP1-FLAG overexpression. MRPL12 is present in the large subunit of the mitoribosome and, in uninduced cells, was found in fractions 6 and 7 (Figure 7.9A). However, it is known that there is a pool of 'free' MRPL12 in cells (Surovtseva et al., 2011), which was seen in the least dense gradient fractions (Figure 7.9A fractions 1 and 2). AURKAIP1-FLAG overexpression

caused the relative amounts of MRPL12 to shift dramatically toward the less dense fractions, indicating a reduction in LSU-associated MRPL12 (Figure 7.9B) compared to uninduced controls (Figure 7.9A). The relative levels of LSU-associated MRPL3 (fractions 6 and 7) were also lower in AURKAIP1-FLAG overexpressing cells, however, the position of MRPL3 shifted toward the most dense fractions (fraction 11). MRPL3 also appeared to be present at lower levels in the induced cells (Figure 7.9B). To assess the steady state levels of MRPs after AURKAIP1-FLAG overexpression more stringently, 40μg of cell lysate from uninduced and induced HEK293-AURKAIP1-FLAG cells (without sucrose gradient separation) were analysed by immunoblotting. These data showed that steady state levels of MRPL3, MRPL11, MRPS18B and DAP3 were all reduced after AURKAIP1-FLAG overexpression. The only MRP tested that was not reduced was MRPL12. This is probably due to the fact that a certain amount of MRPL12 is 'free' (Surovtseva et al., 2011), indicating stability when separate from the mitoribosome. Other MRPs may not be as stable as MRPL12 and perhaps they are degraded when not bound to the mitoribosome. If this is true, then the data presented in Figure 7.9C may be explained by AURKAIP1-FLAG overexpression causing disassembly of the mitoribosomes and that MRPs are subsequently degraded.

The reduction of MRP levels upon AURKAIP1-FLAG overexpression was intriguing. To see if ribosome stalling protected the MRPs from degradation, HEK293-AURKAIP1-FLAG cells were pre-treated for 24 hours with 50μg/ml chloramphenicol to stall mitoribosomes before inducing the cells with 1μg/ml tetracycline for a further 3 days (still in the presence of chloramphenicol). In ethanol treated control cells, AURKAIP1-FLAG overexpression lead to reduced MRP levels (Figure 7.10, lane 2). However, the results showed that chloramphenicol-mediated ribosome stalling reduced AURKAIP1-FLAG-mediated MRP depletion (Figure 7.10, lane 4). These data may indicate that an actively translating ribosome is required for AURKAIP1-FLAG overexpression to mediate its effects.

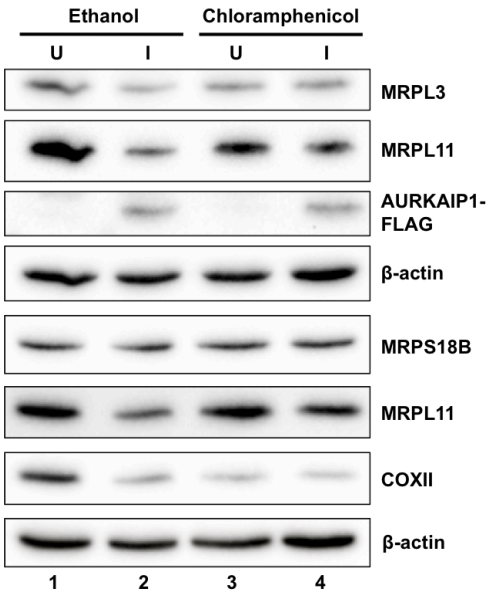

Figure 7.10: Can Mitoribosome Stalling Protect MRPs from AURKAIP1-FLAG Overexpression Mediated Depletion? HEK293-AURKAIP1-FLAG cells were either treated with chloramphenicol (50μg/ml) or an equivalent volume of ethanol for 24 hours. After this incubation an aliquot of ethanol treated cells remained uninduced (U, lane 1) and another aliquot induced (I) with 1μg/ml tetracycline for further 3 days (lane 2). Chloramphenicol treated cells were also either left uninduced (lane 3) or tetracycline induced (lane 4), with chloramphenicol treatment persisting for the further 3 days. Cell lysate (40μg) from each treatment was subjected to SDS-PAGE and western blotting. The displayed images were compiled from two independent western blots carried out in an identical fashion with the same material. Antibodies to MRPL3, MRPL11, MRPS18B, COXII, FLAG and β-actin were used for immunoblotting. Signal for MRPL11 and β-actin is shown from each blot.

A recent study has been published proposing that AURKAIP1 is a small subunit MRP and should be renamed MRPS38 (Koc et al., 2013). My data strongly indicated that this is not the case as AURKAIP1 levels are too low to have 1:1 stoichiometry with mitoribosomes. Furthermore, AURKAIP1-FLAG was not detected in sucrose gradient fractions corresponding to the SSU (Figure 7.9B, fraction 5) and overexpression resulted in reduced steady state levels of MRPs (Figure 7.9C). These data do not support the notion of AURKAIP1 being a *bona fide* MRP. To address this issue, a commercial antibody to AURKAIP1 that was used in the study by Koc *et al.* was purchased (Sigma α-AURKAIP1). Immunoblotting with Sigma α-AURKAIP1 did not allow detection of signal from endogenous AURKAIP1 at the correct size (approximately 15kDa) in the uninduced sucrose gradient fractions (Figure 7.11A). This was to be expected due to low endogenous AURKAIP1 levels. Figure 7.11A shows signal from an entire blot containing the sucrose gradient fractions from uninduced cells in order to show all of the signal from the Sigma α-AURKAIP1 antibody, which was the first primary antibody incubated with this blot. These data show that although no signal of the correct size was detectable, a non-specific band of approximately 25kDa was seen in fraction 4, which would correspond to the small subunit of the mitoribosome (Figure 7.10A). This signal does not correspond with the size of AURKAIP1-FLAG detected in cell lysate (Figure 7.10B).

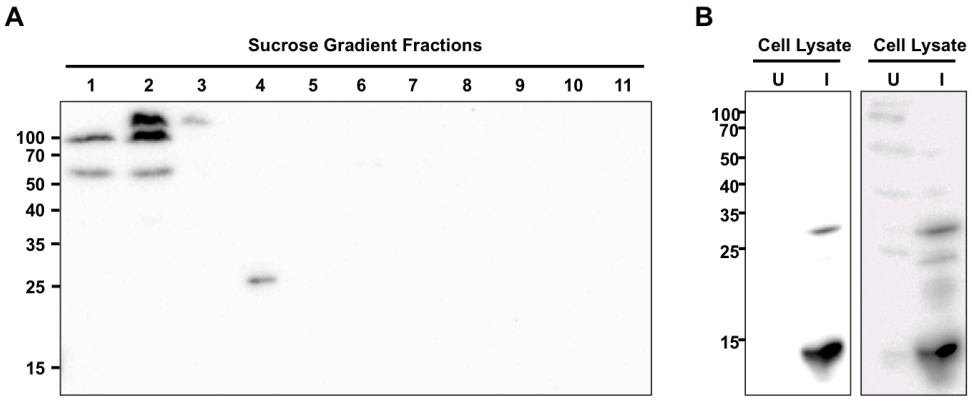

Figure 7.11: Does Endogenous AURKAIP1 Bind to the Mitoribosome? Sucrose gradient analysis was performed as in Figure 7.9. **(A)** shows an entire blot from sucrose gradient western blot analysis of uninduced HEK293-AURKAIP1-FLAG cell lysate after immunoblotting with Sigma α-AURKAIP1 only. **(B)** Shows an entire blot from western blot analysis of 40μg cell lysate from uninduced (U) or tetracycline induced (I) cells after only immunoblotting with the Sigma α-AURKAIP1 antibody with different exposure settings.

The Sigma α-AURKAIP1 antibody has a degree of non-specific binding, as does the in-house produced α-AURKAIP1 antibody. However, the Sigma antibody does bind to AURKAIP1 as it produced similar signal as the in-house produced α-AURKAIP1 antibody or α-FLAG antibody (Figure 7.9C) when tested on induced cell lysate from HEK293-AURKAIP1-FLAG cells (two different exposures shown in Figure 7.11B).

In summary, the data presented in this section do not support the notion of AURKAIP1 being a small subunit MRP as no evidence of endogenous or overexpressed AURKAIP1 associating with the mitoribosome was detected (Figures 7.9A, 7.9B and 7.11A). However, this does not exclude the possibility that AURKAIP1 transiently associates with some MRPs, which may account for the identification of AURKAIP1 by mass spectrometry in bovine mitoribosomal preparations (Koc et al., 2013). For this reason, immunoprecipitation studies were carried out to assess any AURKAIP1 binding partners (including MRPs) with more stringency, which I will outline below.

7.3.5 Identifying Binding Partners of AURKAIP1

As another tool to understand the role of AURKAIP1 in mitochondrial gene expression it was important to identify proteins that interact with AURKAIP1. Co-IP studies were performed in HEK293-AURKAIP1-FLAG cells, overexpressing AURKAIP1-FLAG, using α-FLAG antibodies (α-FLAG Co-IP). Only two clear bands were detectable by SimplyBlue^{TM} SafeStain of the α-FLAG Co-IP elution, one of which corresponded to the AURKAIP1-FLAG protein (Figure 7.12A).

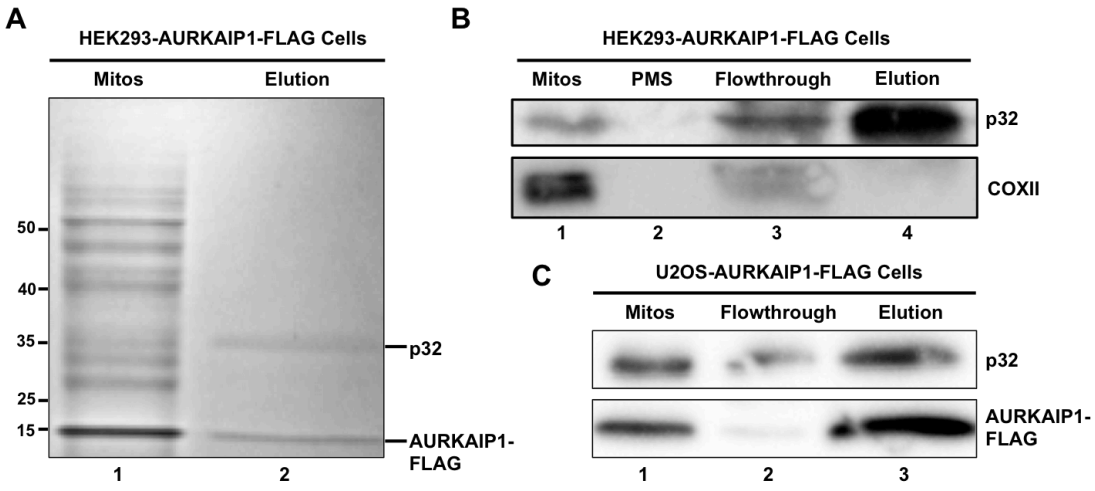

Figure 7.12: Identification a Novel Interaction Between AURKAIP1 and p32. (A) α-FLAG Co-IP was performed on 500μg of mitochondrial lysate from HEK293-AURKAIP1-FLAG cells induced for 3 days with 1μg/ml tetracycline. Half of the elution was analysed alongside 25μg of total mitochondrial lysate by SDS-PAGE and staining with SimplyBlue^{TM} SafeStain. The higher molecular weight band was excised and identified as p32 by mass spectrometry analysis (MALDI-TOF Pinnacle, Newcastle University). **(B)** An aliquot of 25% of the elution described in **A** (lane 4), 35μg of post mitochondrial supernatant (PMS, lane 2) and flowthrough (lane 3) from the same experiment were loaded alongside 10μg of mitochondrial lysate from 143B cells (lane 1) and subjected to SDS-PAGE and western blotting. **(C)** The same α-FLAG Co-IP procedure was carried out (as in **A**) on mitochondrial lysate from U2OS-AURKAIP1-FLAG cells. Aliquots of total mitochondrial proteins (mitos, 25μg, lane 1), flowthrough (25μg, lane 2) and elution (50% of total, lane 3) fractions were subjected to SDS-PAGE and western blotting. Antibodies to p32 (rabbit), FLAG and COXII were used for immunoblotting where indicated.

The unidentified band was excised from the gel and sent for mass spectrometry analysis (MALDI-TOF conducted by Pinnacle, Newcastle University). The protein was identified as p32, a protein that has several aliases, which will be described in detail in the following chapter. Western blotting and immunodetection using α-p32 antibodies allowed confirmation that p32 was immunoprecipitated with AURKAIP1-FLAG as the elution fraction contained strong signal for p32 when α-FLAG Co-IP was performed in either HEK293-AURKAIP1-FLAG (Figure 7.12B) or U2OS-AURKAIP1-FLAG cells (Figure 7.12C).

Further confirmation of the interaction between AURKAIP1 and p32 was sought by performing Co-IP using α-p32 antibodies. Initial attempts at α-p32 Co-IP using a α-p32 antibody raised in rabbit (α-p32 (rabbit), see Table 2.6 for antibody details) failed to immunoprecipitate p32 (data not shown). Therefore, another α-p32 antibody (mouse) was used. Co-IP using α-p32 (mouse) did pull down some p32 as detected by western blot using α-p32 (rabbit) (Figure 7.13). However, the levels of immunoprecipitated p32 were very low relative to the amount of p32 detected in the mitochondrial fraction

(Figure 7.13). Even with this small amount of p32, AURKAIP1-FLAG was also detected in the α-p32 (mouse) Co-IP elution (Figure 7.13), further implicating a strong interaction between AURKAIP1 and p32.

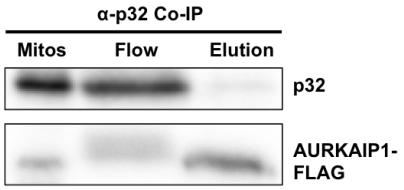

Figure 7.13: Endogenous p32 Immunoprecipitation. Mitochondrial lysates were prepared from tetracycline-induced HEK293-AURKAIP1-FLAG cells and incubated with α-p32 (mouse) antibodies. Aliquots of the mitochondrial lysate before Co-IP (25μg, mitos), the flowthrough (25μg, flow) and the fraction eluted from the antibody (50% of total, elution) were subjected to SDS-PAGE. α-p32 (rabbit) and α-AURKAIP1 antibodies were used for immunoblotting.

Since the α-p32 Co-IP was very inefficient, care must be taken when interpreting these results. To ensure that the problems with α-p32 Co-IPs were due to the antibodies used and not the Co-IP procedure itself, α-MRPL12 Co-IPs were performed. The α-MRPL12 antibody has been shown to successfully Co-IP other MRP proteins (work from Agata Rozanska in my host laboratory, see Serre et al., 2013). Thus, α-MRPL12 Co-IP would allow confirmation of the validity of the Co-IP procedure.

The α-MRPL12 Co-IP was successful in pulling down MRPL3 and DAP3 as expected (Figure 7.14A, lanes 3 and 6). Surprisingly, the α-MRPL12 Co-IP also pulled down AURKAIP1-FLAG in the induced cells (Figure 7.14A, lane 6). Very small amounts of p32 were also co-immunoprecipitated with α-MRPL12 antibodies, which may account for the presence of AURKAIP1-FLAG in the elution (Figure 7.14B).

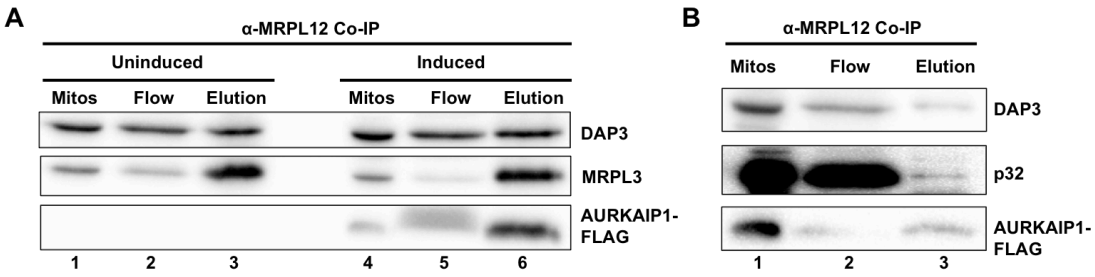

Figure 7.14: Does AURKAIP1 Interact with MRPL12? (A) Endogenous α-MRPL12 Co-IPs were carried out on mitochondrial lysates from HEK293-AURKAIP1-FLAG cells either grown as normal (uninduced) or with 1μg/ml tetracycline (induced). Total mitochondrial lysate (input/mitos), flowthrough and elution fractions were subjected to SDS-PAGE and western blotting. **(B)** Repeat of α-MRPL12 Co-IP described in **A** on induced mitochondrial lysate. Antibodies to DAP3, MRPL3, p32 (mouse) and FLAG were used for immunodetection.

It was important to ensure that AURKAIP1-FLAG was not binding non-specifically to the beads rather than to the antibodies used for Co-IP. To this end, α-mtPAP Co-IP experiments were conducted. The α-mtPAP has been used successfully for Co-IP and did not pull down MRPs (work conducted in my host laboratory by Dr W. C. Wilson, *personal communication*). This is consistent with data presented in Figure 7.15A, which showed that MRPL3 and MRPL12 were not immunoprecipitated by α-mtPAP Co-IP (lane 3). Importantly, AURKAIP1-FLAG was also not present in the elution of α-mtPAP Co-IP (Figure 7.15A, lane 3). This result confirmed that AURKAIP1-FLAG was not binding non-specifically to every antibody or binding the beads used for antibody immobilisation during the Co-IP procedure. Co-IP studies with α-FLAG showed that certain quantities of MRPL3 and MRPL12 were present in the α-FLAG Co-IP elution (7.15B, lane 3), which, coupled with the results from α-MRPL12 Co-IP (Figure 7.14), may suggest a transient association between AURKAIP1 and the mitoribosome.

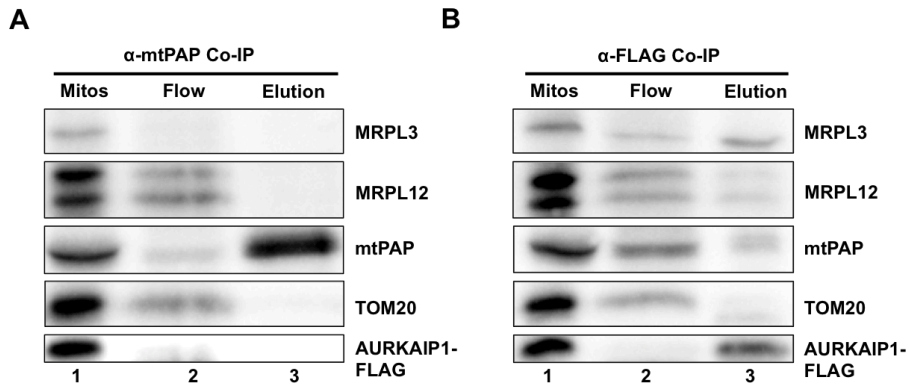

Figure 7.15: Is the Interaction Between AURKAIP1 and MRPL12 Specific? (A) α-mtPAP Co-IP experiments were carried out on mitochondrial lysates from induced HEK293-AURKAIP1-FLAG cells. Total mitochondrial lysate (mitos), flowthrough (flow) and elution fractions were subjected to SDS-PAGE and western blotting. **(B)** α-FLAG Co-IP was performed on the same mitochondrial lysate described in **A**. Antibodies to MRPL3, MRPL12, mtPAP, Tom20 and AURKAIP1 were used for immunodetection.

Despite identifying a novel interaction between AURKAIP1-FLAG and p32 by Co-IP experiments, it was imperative to show that p32 and AURKAIP1 could interact at endogenous levels. This was required in order to rule out the possibility that the interaction observed thus far was mediated by the FLAG tag or by the presence of much higher AURKAIP1 levels in the induced HEK293-AURKAIP1-FLAG cells. Validation of an endogenous interaction between AURKAIP1 and p32 was attempted in several

different ways and proved difficult for several reasons: i) as mentioned, endogenous p32 Co-IP was very inefficient ii) endogenous AURKAIP1 levels are very low and iii) both antibodies to AURKAIP1 produce additional non-specific signal on western blots of cell lysate. To overcome these obstacles, the following observations were considered. First, 143B cells express detectable levels of endogenous AURKAIP1 in mitochondrial lysate (as previously shown in Figure 4.4B). Second, the non-specific signal from the α-AURKAIP1 antibody is predominantly seen in cell lysate and is greatly reduced in mitochondrial lysate. Finally, AURKAIP1 is present in the mitochondrial matrix (as shown in Figure 4.3B and 4.5C). For these reasons, endogenous α-AURKAIP1 Co-IP was conducted in proteinase K-shaved mitoplasts from 143B cells, in order to confirm an endogenous interaction between p32 and AURKAIP1 within the mitochondrial matrix (Figure 7.16). Further, to ensure that p32 was not binding non-specifically, Co-IP was also carried out with control IgG (antibody to cytosolic protein MNK1) as a negative control.

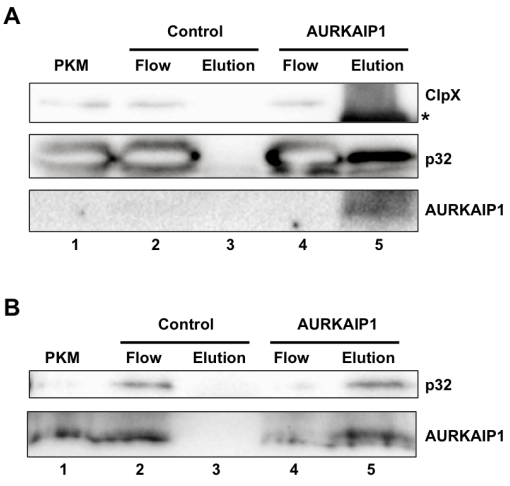

Figure 7.16: Endogenous AURKAIP1 Interacts with p32. **A** and **B** represent independent repeats of the same experiment. Mitoplasts were isolated from 143B cells and treated with proteinase K. The proteinase K-shaved mitoplasts (PKM) were lysed and used as the input for endogenous α-AURKAIP1 Co-IP. Lysates were also subjected to the Co-IP protocol with control IgG (antibody to cytosolic protein MNK1). Aliquots of input PKM (lane 1), flowthrough (lane 2) and elution (lane 3) for control Co-IP and flowthrough (lane 4) and elution (lane 5) from α-AURKAIP1 Co-IP samples were subjected to SDS-PAGE and western blotting. Antibodies to p32 (mouse), ClpX and AURKAIP1 were used for immunodetection. * denotes signal from the heavy chain of the AURKAIP1 antibody.

It was clear that α-AURKAIP1 Co-IP pulled down p32 (Figure 7.16 A and B, lane 5), but that control IgG did not (lane 3). These data showed that endogenous levels of AURKAIP1 interact with p32, thus increasing confidence in data obtained using AURKAIP1-FLAG.

7.4 DISCUSSION

The work presented in this chapter has focused on investigating the role of AURKAIP1 using AURKAIP1-FLAG overexpressing cell lines. The overexpression of AURKAIP1-FLAG is interesting as it leads to a severe reduction in mitochondrial gene expression. This presents a fascinating dilemma because, as discussed in the previous chapter, AURKAIP1 depletion also inhibits mitochondrial gene expression. Quite how depletion and overexpression of AURKAIP1 can each lead to defects in mitochondrial gene expression remains unclear at this stage.

One of the distinguishing features of AURKAIP1 depletion was nucleoid enlargement without a change in mtDNA copy number (Figures 5.8 and 6.1). As discussed earlier, these apparently larger nucleoids, as visualised by fluorescent microscopy, are most likely clusters of similar sized nucleoids that arise as a consequence of aberrant nucleoid distribution. If this were true, it would have been reasonable to assume that AURKAIP1 overexpression would have the opposite effect. This was clearly not the case, however, as AURKAIP1-FLAG overexpression also led to an apparent enlargement of nucleoid size. Potential mechanisms to explain the observed nucleoid enlargement have been discussed in detail in Chapter 5. Nucleoid enlargement has been seen in cells depleted of several proteins with very different functions including the transcription factor TFAM (Kasashima et al., 2011), fission protein Drp1 (Ban-Ishihara et al., 2013), AAA protease ClpX (Kasashima et al., 2012) and exonuclease REXO2 (Bruni et al., 2013). Thus, it is impossible to attribute a function to AURKAIP1 based on the enlarged nucleoid phenotype alone.

Similarities were observed between AURKAIP1 depletion and AURKAIP1-FLAG overexpression regarding mitochondrial RNA levels. Each condition led to a reduction in *MT-CO1* and *MT-RNR1* levels compared to the respective control cells, but *MT-ND1* levels were not reduced. The clearest distinction between AURKAIP1 depletion and AURKAIP1-FLAG overexpression lies in the respective effects on mitochondrial protein synthesis. AURKAIP1-FLAG overexpression has a more dramatic inhibitory effect on translation than AURKAIP1 depletion. This was illustrated by AURKAIP1-FLAG overexpression inhibiting the synthesis of all mtDNA-encoded proteins (Figure 7.7, lane 4), whereas AURKAIP1 depletion only affected the synthesis of a subset of mtDNA-encoded proteins (Figure 7.7, lane 2). Synthesis of COXII was confirmed to be

decreased by AURKAIP1 depletion (Figure 7.7 lane 2), which had been uncertain due to co-migration with ATP6 when analysed using a 15% SDS polyacrylamide gel (Figure 6.3). The improved resolution achieved using 15-20% SDS polyacrylamide gradient gel allowed separation of COXII and ATP6 and showed that synthesis of COXII was reduced (to 60% of the NT controls), whereas synthesis of ATP6 was increased in AURKAIP1 depleted cells (Figure 7.7, lane 2).

The difficulty in directly assessing the relative effects of AURKAIP1 depletion and AURKAIP1-FLAG overexpression on mitochondrial protein synthesis was partly due to the enforced use of different cell types for siRNA depletions and overexpression. Initially only HEK293-AURKAIP1-FLAG stable cell lines were available, which limited AURKAIP1-FLAG overexpression studies to HEK293 cells. However, HEK293 cells are not as robust as HeLa cells, thus depletion studies were carried out in HeLa cells. HeLa cells and other cell types (for example 143B) are known to have slightly different patterns of segregation when analysed by SDS-PAGE (Chomyn, 1996). Thus, more direct comparisons could be made if expressing and depleting AURKAIP1 was possible in a single cell type. This was one of the reasons that U2OS-AURKAIP1-FLAG cells were produced. However, these cells were not available until my investigations were nearing an end. Thus, repeats of the [^{35}S]-methionine studies in U2OS-AURKAIP1-FLAG cells were not conducted within the timeframe of my investigations, as there simply was not sufficient time to repeat all of the work in these cells. Imaging studies using the U2OS-AURKAIP1-FLAG cells were prioritised to assess mitochondrial morphology with AURKAIP1-FLAG overexpression, as these studies were not possible with the HEK293-AURKAIP1-FLAG cells. These studies showed a significant increase in mitochondrial fragmentation with AURKAIP1-FLAG overexpression, which will be discussed in the following chapter.

Another interesting observation with AURKAIP1-FLAG overexpression was the depletion of MRP levels. Interestingly, this depletion of MRP levels occurred after just three days of overexpression. As described earlier, mitochondrial protein synthesis and steady state levels of COXI and COXII are also greatly reduced within this time frame. These effects occur more rapidly than would be expected by simply blocking ribosome biogenesis, as the mitoribosome is very stable. For example, ERAL1 is important for the assembly of 28S small subunit of the mitoribosome, but 3 days of ERAL1 depletion does not impair mitochondrial protein synthesis, nor MRPL3 levels in HEK293 or HeLa

cells, implying that the ribosomes already assembled are stable and able to maintain their levels of protein synthesis (Dennerlein et al., 2010). Recently C7orf30 has been suggested to have a role in biogenesis of the 39S large subunit of the mitoribosome (Rorbach et al., 2012). After 6 days of C7orf30 depletion there was no reduction in the steady state level of MRPL3 (Rorbach et al., 2012), which also implies the stability of the already formed MRPL3. Overexpression of mutated C7orf30 also caused a shift of MRPL3 toward less dense fractions after 3 days, but there was no report of MRPL3 levels being reduced at steady state (Rorbach et al., 2012). Together the data from ERAL1 and C7orf30 suggest that inhibition of ribosome biogenesis is not sufficient to dramatically reduce levels of MRPL3. AURKAIP1-FLAG overexpression reduces MRPL3 steady state levels after 3 days Figure 7.9C), which suggests that AURKAIP1 overexpression causes disassembly of mitoribosomes and subsequent degradation of MRPs, which is sufficient to impair mitochondrial protein synthesis. This hypothesis is consistent with the observed data, which showed reduced levels of many MRPs including MRPL3, MRPL11, MRPS18B and DAP3 (Figure 7.9C). MRPL12 is a notable exception, as steady state levels of this MRP were not significantly reduced. However, as mentioned earlier, there is a pool of 'free' MRPL12 present in normal cells, thus, disassembled MRPL12 may be tolerated without degradation.

Reduced steady state levels of mtDNA-encoded proteins upon AURKAIP1-FLAG overexpression can be explained solely by a translation defect rather than active degradation since inhibiting mitochondrial protein synthesis with chloramphenicol reduces the levels of mtDNA-encoded proteins within the same time frame (2 days) (Figure 7.8). Recent data has shown that 48 hours of chloramphenicol treatment reduced COXI levels to almost undetectable levels (Richter et al., 2013), which is consistent with my observations. Moreover, this publication shows that the antibiotic actinonin has a profound effect on MRP levels after 16 hours, which can be prevented with co-treatment with chloramphenicol (Richter et al., 2013). This is strikingly similar to the data shown with AURKAIP1-FLAG overexpression (Figures 7.9C and 7.10). Actinonin treatment of MEFs led to a severe block of cell proliferation (Richter et al., 2013), however, which was not a feature of AURKAIP1-FLAG overexpression (Figure 7.1).

Perhaps the effects of both overexpression and depletion of AURKAIP1 on mitochondrial protein synthesis can be explained by a role for AURKAIP1 in rescuing stalled ribosomes. If a subset of mtDNA-encoded transcripts i.e. *MT-CO1* and *MT-CO2*

have a tendency to stall mitoribosomes during elongation, the usual release factor, mtRF1a (Soleimanpour-Lichaei et al., 2007) would not be able to resolve the stalling event. If AURKAIP1 could allow the recycling of these transcripts and mitoribosomes, then normal protein synthesis could be maintained. Perhaps in the absence of AURKAIP1 these stall events are not resolved, preventing translation of a subset of mtDNA-encoded proteins. If this hypothesis was correct then it would be possible that overexpression of AURKAIP1 could lead to a loss of specificity and thus disassemble non-stalled mitoribosomes, which may account for subsequent degradation of MRPs and general inhibition of translation. The lack of an *in vitro* mitochondrial translation system prevents the direct assessment of this hypothesis at this time, as each transcripts propensity to stall mitoribosomes during elongation cannot be determined. However, optimisation of ribosome profiling techniques may allow insights into this possibility. If a higher percentage of mitoribosomes were stalled with RNA sequences matching *MT-CO1* or *MT-CO2* in AURKAIP1 depleted cells, then this hypothesis would be supported. Thus, ribosome profiling could be an interesting area for further research.

During the course of my investigations, a study was published that identified AURKAIP1 as a protein associated with the mitoribosome (Koc et al., 2013). Moreover, the authors suggested that AURKAIP1 was a SSU MRP and sought to rename the protein MRPS38 (Koc et al., 2013). As discussed earlier, the results of my investigations contrast with this view. I have shown that the majority of AURKAIP1-FLAG does not associate with the mitoribosome (Figure 7.9B) and that no endogenous AURKAIP1 signal corresponding to the correct size was observed in ribosome associated fractions with either of the α-AURKAIP1 antibodies tested (Figures 7.9 and 7.11). However, a transient interaction between AURKAIP1 and the mitoribosome seems likely. Indeed, AURKAIP1-FLAG was immunoprecipitated with α-MRPL12 antibodies (Figure 7.14). Additionally the fact that AURKAIP1-FLAG overexpression caused depletion of MRPs is consistent with AURKAIP1 interacting with the subunits of the mitoribosome, perhaps to actively disassemble the ribosome or target some MRPs for degradation. The exact mechanisms to explain the effects of AURKAIP1-FLAG overexpression are currently unknown, but it is probable that there is some interaction with the mitoribosome, either directly or indirectly. This would be consistent with the Co-IP data presented in this chapter and with the identification of AURKAIP1 in preparations of bovine mitoribosomes (Koc et al., 2013).

What is clear is that any potential interaction of AURKAIP1-FLAG with the mitoribosome is weaker or more transient than the interaction between AURKAIP1 and p32. This is apparent since p32 was the only protein to be co-immunoprecipitated with AURKAIP1-FLAG in high enough quantities to be seen via SimplyBlue^{TM} SafeStain (Figure 7.12A). It is even possible that the weak or transient interaction seen between AURKAIP1 and MRPL12 could be mediated through the stronger interaction between AURKAIP1 and p32. Indeed, p32 has been shown to interact with many mitoribosomal proteins (Yagi et al., 2012), including MRPL12, as will be discussed in the following chapter. The particular focus of the following chapter will be to address the possibility that overexpression of AURKAIP1-FLAG causes its phenotype via effects on p32.

CHAPTER 8: ARE THE EFFECTS OF AURKAIP1 OVEREXPRESSION MEDIATED VIA EFFECTS ON P32?

8.1 INTRODUCTION

As described in the previous chapter, I have demonstrated a novel interaction between AURKAIP1 and the protein p32. Human p32 is a multifunctional protein that has been known by many aliases. First, p32 was identified as splicing-factor 2 associated protein (Krainer et al., 1991), but p32 itself did not show any splicing activity *in vitro*. Second, p32 was identified as a processed form of TAP (tat associated protein), which consisted of amino acids 71-279 of TAP (Yu et al., 1995). Full length TAP binds HIV-1 tat and possesses a transcriptional activation domain (Yu et al., 1995). The identification of p32 in the two cases described suggest nuclear localisation of p32 (Yu et al., 1995; Krainer et al., 1991), but p32 has also been described as an extracellular protein on the outer surface of the plasma membrane (Deb and Datta, 1996). This study identified a homodimer of p32 as HABP1 (hyaluronic acid-binding protein) (Deb and Datta, 1996). Also, p32 was further reported to be a membrane protein based on an interaction with the globular heads of C1q (complement component 1 q) (Lim et al., 1996; Ghebrehiwet et al., 1996), leading to the aliases C1QBP (complement component 1 Q subcomponent binding protein) and gC1qR (globular C1q receptor).

Functional roles of p32 were not identified through these various interactions and p32 was subsequently shown to be predominantly localised to the mitochondrial matrix and to be required for respiratory function (Muta et al., 1997). Furthermore, recent p32 knockout studies conducted in mice showed that p32 is a vital protein as knockout mice exhibited embryonic lethality (Yagi et al., 2012). This study also isolated mouse embryonic fibroblasts (MEFs) from the p32 knockout embryos and observed a severe impairment in mitochondrial protein synthesis (Yagi et al., 2012). Another recent study suggested that p32 binds to RNaseH1 (important for hydrolysing DNA/RNA hybrids) and MRPP1 (a subunit of RNaseP, involved in 5' tRNA processing in mitochondria) and suggests a role for p32 in mitochondrial pre-RNA processing (Wu et al., 2013). Wu *et al.* propose that these interactions are mediated by DNA or RNA binding rather than protein-protein interactions (Wu et al., 2013). The RNA binding ability of p32 has been

described before (Ponamarev et al., 2005; Yagi et al., 2012). Co-IP studies of overexpressed HA tagged p32 showed that p32 interacts with many MRPs, RNA binding proteins, transcription factors and proteases within mitochondria (Yagi et al., 2012).

Accumulating evidence indicates that the major functional role of p32 takes place in the mitochondria (Muta et al., 1997; Yagi et al., 2012). This is supported by currently unpublished data from my host laboratory that has identified a pathological mutation in p32, via exome sequencing, in a patient with severe mitochondrial disease (Dr M. Olahova, Prof R. W. Taylor, *personal communication*). The patient had compound heterozygous mutations, each of which caused amino acid substitutions in highly conserved residues (c.557G>C predicting p.Cys186Ser and c.612C>G predicting p.Phe204Leu, see supplementary Figure S1). The patient presented with failure to thrive, cardiomyopathy and severe lactic acidosis and died at a few weeks of age. Respiratory chain complex activities (I, III and IV) were markedly decreased in patient muscle. The identification of possible pathogenic mutations in p32 strongly indicates that the major role of p32 is in mitochondrial gene expression. In addition, p32 was one of the proteins included in the initial siRNA screen that led to the study of AURKAIP1. However, p32 was only included in the growth rate screen in HeLa and Rho^0 cells, as only one of the three p32 siRNAs caused a growth defect in HeLa cells. Only proteins that, when depleted with two or more of the siRNAs, impaired HeLa cell growth were investigated further in the initial screen (Section 1.9). Therefore, it was important to test the specificity of the p32 siRNA that did cause a growth defect in HeLa cells by western blot, which was possible as several commercial antibodies to p32 were available.

So far, my work has identified p32 as the major binding partner of AURKAIP1 and that AURKAIP1-FLAG overexpression causes a profound reduction in mitochondrial translation. Since a similarly severe effects on mitochondrial protein synthesis were seen in p32 knockout MEFs (Yagi et al., 2012), this chapter will focus on elucidating the functional relevance of the interaction between p32 and AURKAIP1.

8.2 RESULTS

8.2.1 ARE P32 STEADY STATE PROTEIN LEVELS AFFECTED BY AURKAIP1 DEPLETION OR OVEREXPRESSION?

I have already demonstrated that AURKAIP1-FLAG overexpression impairs mitochondrial protein synthesis and that AURKAIP1 interacts with p32. Since p32 knockout has also been shown to impair mitochondrial translation (Yagi et al., 2012), it was important to see if the overexpression of AURKAIP1-FLAG caused depletion of p32, as this may account for the observed translation defect mediated by AURKAIP1-FLAG overexpression. Additionally, it was of interest to determine whether AURKAIP1 depletion altered p32 protein levels as an increase in p32 levels may indicate that AURKAIP1 acts as a negative regulator of p32.

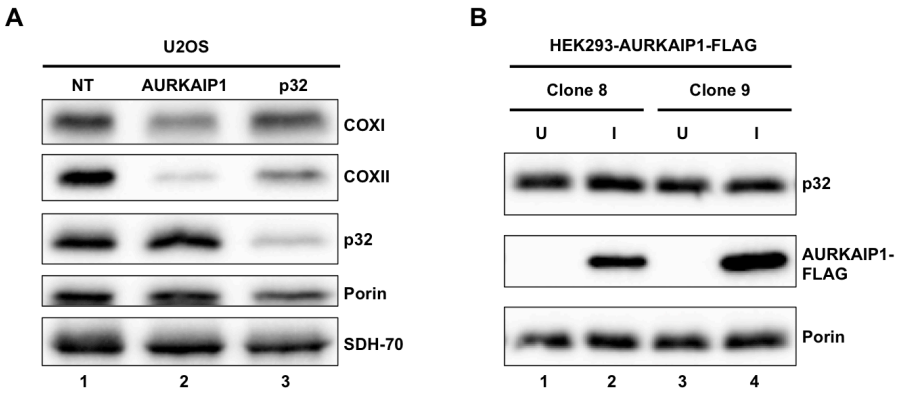

Figure 8.1: Steady State Levels of p32 are not Affected by Changes in AURKAIP1 Protein Levels. (A) U2OS cells were treated for 4 days with non-targeting (NT, lane 1), AURKAIP1 siRNA1 (lane 2) or p32 siRNA (lane 3). Cell lysates (40μg) from cells subjected to each treatment were analysed by SDS-PAGE and western blotting. **(B)** Cell lysates were collected from two independent clones of HEK293-AURKAIP1-FLAG cells that were either uninduced (U) or induced with 1μg/ml tetracycline (I) for 3 days. Each 40μg aliquot of cell lysate was subjected to SDS-PAGE and western blotting. α-COXI, α-COXII, α-p32 (rabbit), α-porin, α-SDH-70 and α-FLAG antibodies were used for immunoblotting.

These results showed that 4-day siRNA depletion of AURKAIP1 (siRNA1) did not affect p32 levels (Figure 8.1A, lane 2), although, the p32 siRNA was specific and depleted p32 protein levels after 4 days (Figure 8.1A, lane 3). Overexpressing AURKAIP1-FLAG for 3 days did not alter the levels of p32 in HEK293-AURKAIP1-FLAG cells (Figure 8.1B). Together, these data suggest that AURKAIP1 does not

regulate the protein levels of p32. However, this does not rule out the possibility that AURKAIP1 functionally impacts p32. Perhaps, when overexpressed, AURKAIP1 sequesters p32 from performing its regular function without modulating the expression or degradation of p32 protein levels. Since the exact function of p32 is unknown, this was difficult to ascertain, but assessing the similarities between the effects of p32 depletion and AURKAIP1-FLAG overexpression was used as a starting point to investigate this hypothesis.

8.2.3 Effects of p32 Depletion, is the Phenotype Similar to that of AURKAIP1 Overexpression?

First, p32 depletions were carried out in HeLa cells for 3 and 6 days respectively. Reduction in steady state levels of mtDNA-encoded proteins COXI and COXII was seen after 6 days of depletion, but not after 3 days (Figure 8.2). Depletion of COXI and COXII was also seen after 4-day p32 depletions in U2OS cells (Figure 8.1A, lane 3).

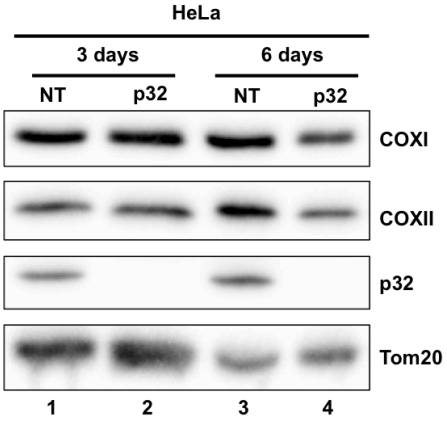

Figure 8.2: Testing the Efficiency and Effects of p32 siRNA Depletion: HeLa cells were treated with either non-targeting (NT) or p32 siRNA for either 3 days or 6 days. Cell lysate (40μg) from cells subjected to each condition were analysed by SDS-PAGE and western blotting. α-COXI, α-COXII, α-p32 (rabbit) and α-Tom20 antibodies were used for immunodetection.

The most striking phenotype of AURKAIP1-FLAG overexpression was the depletion of MRPs. Therefore, HeLa cells were depleted of p32 and levels of MRPs were analysed by immunoblotting (Figure 8.3). The results showed that p32 depletion lead to a reduction in the steady state levels of MRPL3 and MRPL11 (Figure 8.3A, lanes 2,4 and 6). Similar reductions in MRPL3 levels were observed in AURKAIP1-FLAG overexpressing (Figure 8.3B, lane 2) and p32 depleted (Figure 8.3B, lane 4) cells respectively. However, the levels of DAP3 were not depleted in cells lacking p32, whereas they were slightly reduced by AURKAIP1-FLAG overexpression (Figure 8.3B).

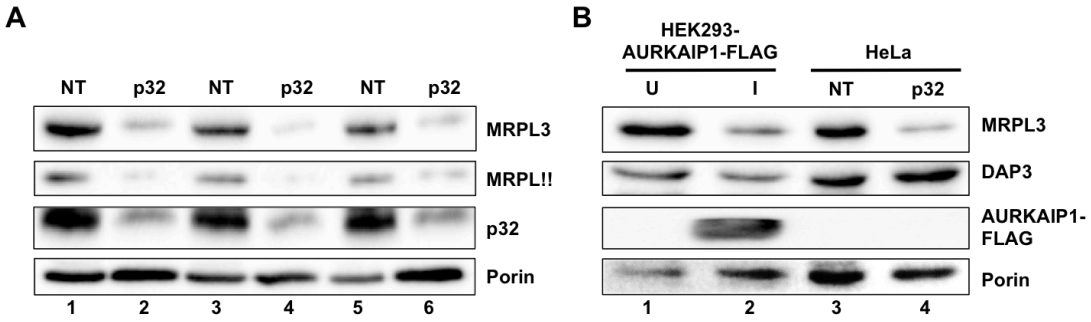

Figure 8.3: The Effects of p32 Depletion on MRP Levels. (A) HeLa cells were treated with 33nM non-targeting (NT, lanes 1,3,5) or p32 siRNA (lanes 2,4,6) for 6 days. Cell lysate (40μg) was subjected to 12% SDS-PAGE and western blotting. Blot shows results from 3 independent experiments **(B)** Uninduced (U, lane 1) HEK293-AURKAIP1-FLAG cells, or those induced with 1μg/ml tetracycline (I, lane 2) were harvested and cell lysates prepared after 3 days. HeLa cells were treated with either non-targeting (NT, lane 3) or p32 siRNA (lane 4) for 6 days. Cell lysates (40μg) from each condition were subjected to 12% SDS-PAGE and western blotting. Immunodetection was performed using α-MRPL3, α-MRPL11, α-p32, αDAP3, α-AURKAIP1 and α-porin antibodies.

Another feature of p32 depletion was poor cell growth and viability. Changes in cellular morphology and growth retardation were clearly visible by light microscopy in HeLa and U2OS cells (Figure 8.4). This was in contrast to the effects of AURKAIP1-FLAG overexpression, which did not noticeably affect the morphology of U2OS cells (as discussed earlier, Figure 7.1).

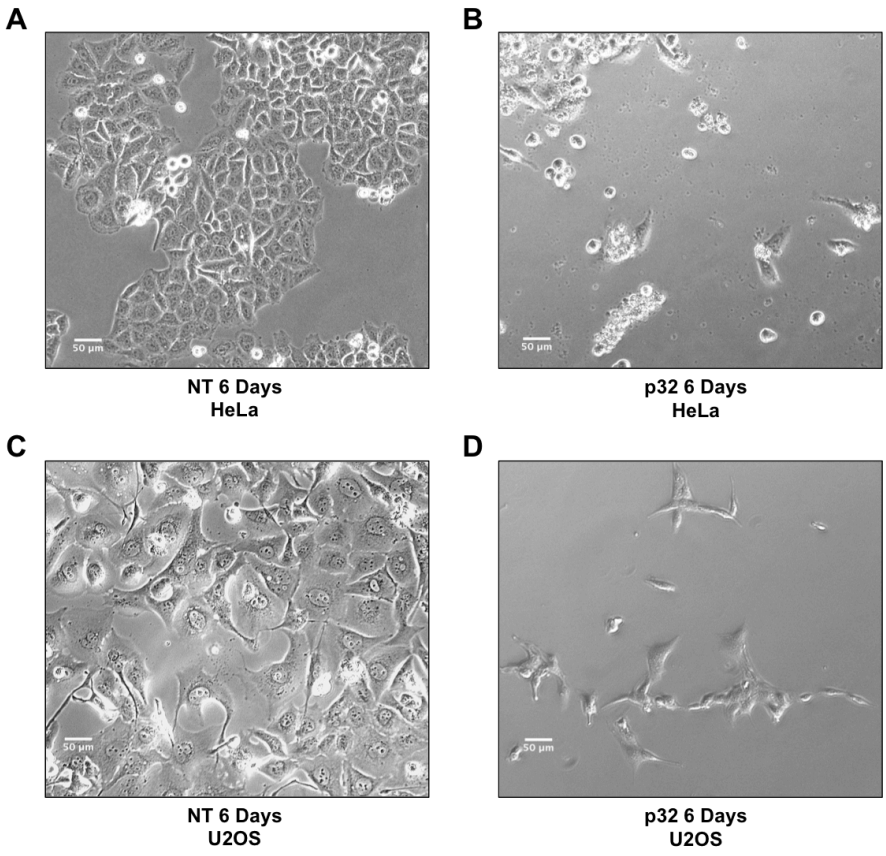

Figure 8.4: Depletion of p32 Inhibits Growth and Alters Cell Morphology. In all cases 30,000 cells were seeded and subjected to siRNA transfection for 6 days, before being visualised by light microscopy. Panels show representative images for: **(A)** HeLa cells treated with non-targeting (NT) siRNA, **(B)** HeLa cells treated with p32 siRNA, **(C)** U2OS cells treated with NT siRNA and **(D)** U2OS cells treated with p32 siRNA.

As shown in the previous chapter, AURKAIP1-FLAG overexpression lead to a greater proportion of punctate, rather than tubular, mitochondria as visualised by TMRM (Figure 7.2). Depletion of p32 has also been shown to increase the proportion of cells with punctate mitochondria (Hu et al., 2013). Therefore, the respective effects of p32 depletion and AURKAIP1-FLAG overexpression with relation to mitochondrial dynamics were compared.

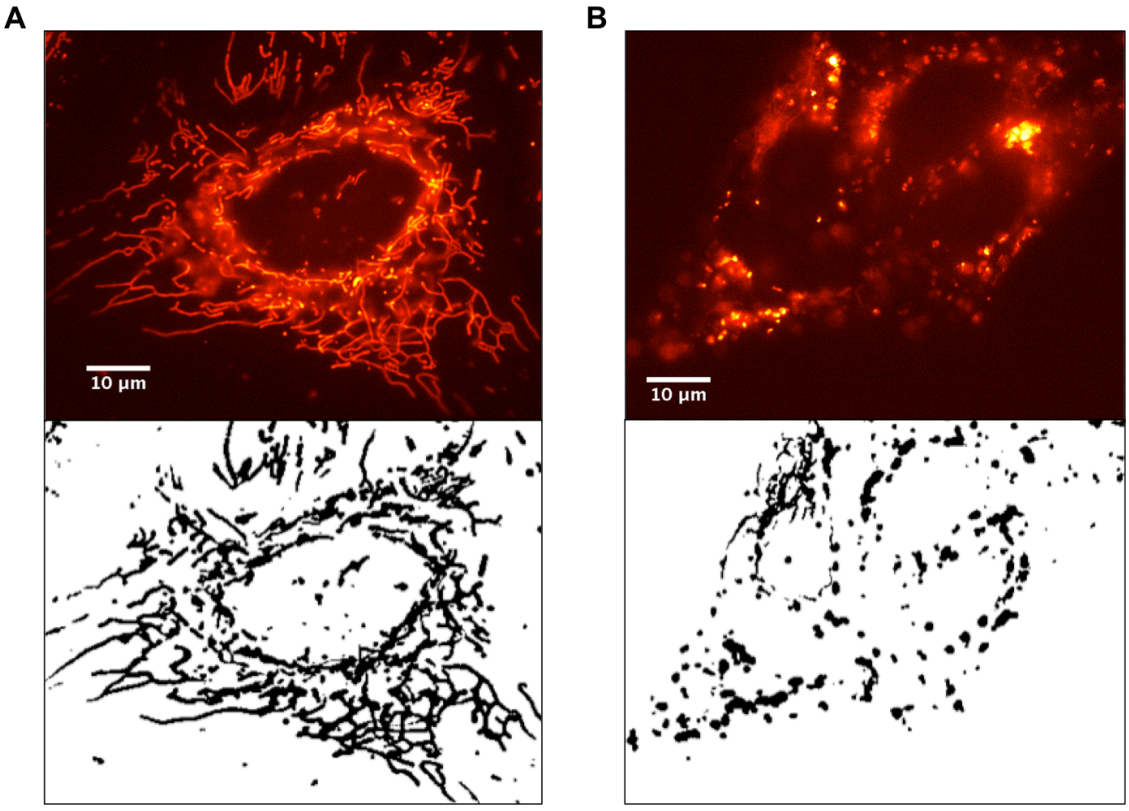

Figure 8.5: Effects of p32 Depletion on Mitochondrial Dynamics. Upper panel shows TMRM stained U2OS cells treated with either non-targeting siRNA **(A)** or p32 siRNA **(B)** and visualised by fluorescent microscopy. Lower panel shows the same field after the image was processed and subjected to thresholding to visualise the shape of the mitochondria without any change in intensity. These are representative images of those used for quantification (Figure 8.6).

Mitochondrial morphology was assessed in p32-depleted cells by TMRM staining. It was clear that p32 depleted cells contained far more punctate and fragmented mitochondria (Figure 8.5B) compared to the normal tubular morphology seen in non-targeting siRNA treated controls (Figure 8.5A). To compare the effects of p32 depletion to the effects of AURKAIP1-FLAG overexpression, the fragmented mitochondria phenotype was quantified (Figure 8.6).

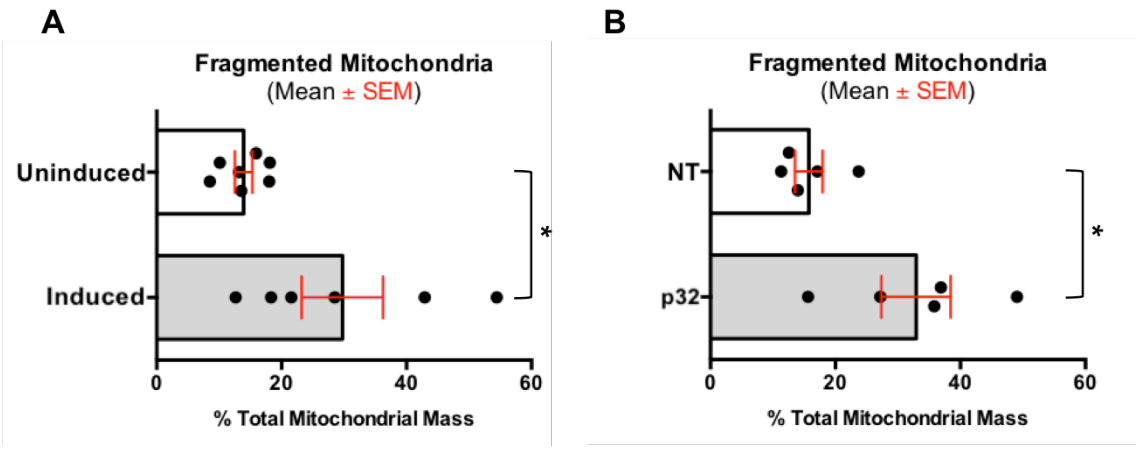

Figure 8.6: Quantification of the Effects of p32 Depletion and AURKAIP1-FLAG Overexpression on Mitochondrial Fragmentation. To allow quantification, images were subjected to thresholding to eliminate changes in intensity (examples seen in Figure 8.5, lower panel). Particle analysis was then performed to quantify fragmented mitochondria, which were defined as small particles (<1μm in diameter) with a circularity value of between 0.5 and 1.0. The total fragmented mitochondrial area was expressed as a percentage of the total mitochondrial area to allow comparisons of approximate mitochondrial fragmentation levels to be made between cells. The proportion of fragmented mitochondria in U2OS-AURKAIP1-FLAG cells that were uninduced or induced with 1μg/ml tetracycline for 3 days is shown in **(A)**. The equivalent data from images of U2OS cells either treated with non-targeting (NT) siRNA or p32 siRNA for 3 days is shown in **(B).** Each point denotes the percentage of fragmented mitochondria per field. Analysis was performed in collaboration with Dr J. M. A. Oliveira. * denotes $p<0.05$ (two-tailed Mann-Whitney U test).

The percentage of mitochondria that were fragmented in uninduced U2OS-AURKAIP1-FLAG cells on average was 13.6%. In cells overexpressing AURKAIP1-FLAG, fragmented mitochondria comprised 25% of the total mitochondrial mass, which was significantly more than in the uninduced controls ($p=0.0221$ $n=7$). Similarly, p32 depletion led to a significant increase in the relative proportion of fragmented mitochondria to an average of 35.8% compared to 14% in non-targeting controls ($p=0.0317$ $n=5$).

8.3 Discussion

The main focus of this chapter was to investigate whether the effects of AURKAIP1-FLAG overexpression could be explained by negatively regulating p32. The data presented in this chapter can neither conclusively confirm nor deny this possibility. It is clear that AURKAIP1 does not regulate the steady state levels of p32, as there was no evidence of a change in p32 levels with either depletion (Figure 8.1A) or overexpression (Figure 8.1B) of AURKAIP1.

It remains possible that AURKAIP1-FLAG overexpression either sequesters or functionally impairs p32 since there is a strong interaction between the two proteins (as

discussed in the previous chapter). Additionally, the phenotype of AURKAIP1-FLAG overexpression has some striking similarities to the phenotype of p32 depletion. For example, the levels of MRPL3 and MRPL11 are reduced in cells overexpressing AURKAIP1-FLAG and in cells depleted of p32 (Figure 8.3). Furthermore, in p32 knockout MEFs, the synthesis of all mtDNA-encoded proteins is inhibited (Yagi et al., 2012), which was also shown in AURKAIP1-FLAG overexpressing cells (Figure 7.7, lane 4). Other similarities include the respective effects of AURKAIP1-FLAG overexpression and p32 depletion on mitochondrial dynamics. Each condition led to a significant increase in fragmented mitochondria (Figure 8.6). Mitochondrial fragmentation in p32 depleted cells has been demonstrated in a recent publication (Hu et al., 2013) and the authors attributed the effects of p32 depletion to a decrease in mitochondrial fusion as the steady state levels of fusion proteins Mfn1 and Mfn2 were reduced in p32 depleted cells (Hu et al., 2013).

On-going work within my research group aims to study the physiological function of p32 in the mitochondria by studying tissue and cell lines from a patient with mitochondrial disease caused by pathogenic mutations in p32 (all work regarding the p32 patient was conducted by Dr Monika Olahova and is presented, with permission, as supplemental material for reference). The specific mutations in the *C1QBP* gene identified in the p32 patient are shown in Figure S.1 (*personal communication M.O.*). Steady state levels of p32 are reduced in patient fibroblasts (Figure S.2A *M.O.*) and virtually absent in muscle tissue (Figure S.2B *M.O.*). Consistent with a role for p32 in mitochondrial gene expression, COX1 steady state levels are reduced in patient muscle tissue (Figure S.3B *M.O.*). However, the biochemical defect is not seen in patient fibroblasts (Figure S.3A *M.O.*). This is likely due to the higher steady state levels of p32 in the patient fibroblasts compared to skeletal muscle (Figure S.2 *M.O.*). Western blot analysis of patient muscle tissue showed a reduction in Mfn2 levels compared to controls (Figure S.4B *M.O.*), which is in accordance with the effects of p32 depletion (Hu et al., 2013). Since AURKAIP1-FLAG overexpression led to mitochondrial fragmentation (Figure 8.6A) it is likely that Mfn levels are be reduced in these cells, though this awaits confirmation.

The similarities between the effects of p32 depletion and AURKAIP1-FLAG overexpression fit with the hypothesis that AURKAIP1-FLAG may elicit a phenotype via sequestration of p32. That being said, there were distinctions between the effects of

AURKAIP1-FLAG overexpression and p32 depletion. For example, cells treated for 3 days with p32 siRNA had comparable COXI and COXII steady state protein levels to non-targeting controls (Figure 8.2, lane 2), however, 3 days of AURKAIP1-FLAG overexpression consistently reduced COXI and COXII levels (Figure 7.3). This was likely due to the time scale and efficiency of p32 depletion. It takes time for siRNA treatment to deplete the target protein levels, as only further expression of the protein is prevented. The mature protein that is present at the time of siRNA transfection may be sufficient for activity for a period of time before it is degraded. This could explain why COXI and COXII steady state protein levels were unaffected after only 3 days of p32 depletion, but were reduced after 4 days (Figure 8.1A, lane 3) and 6 days (Figure 8.2, lane 4) of depletion. Consistent with these data, p32 knockout MEFs have been shown to have undetectable steady state levels of COXI and COXII (Yagi et al., 2012) and analysis of skeletal muscle from the p32 patient also shows marked reduction in COXI levels (Figure S.3B *M.O.*), suggesting that loss of p32 does impair expression of mtDNA-encoded proteins. Perhaps the more rapid reduction in COXI and COXII levels upon AURKAIP1-FLAG overexpression can be explained by the expressed protein functionally inhibiting or sequestering p32, thus effectively subjecting the cell to the effects of p32 loss, without the lag time associated with siRNA-mediated p32 degradation.

Depletion of p32 led to a change in cellular growth and morphology (Figure 8.4), whereas AURKAIP1-FLAG overexpression did not (Figure 7.1). There are several reports linking p32 to apoptosis (Sunayama et al., 2004; Itahana and Zhang, 2008; Hu et al., 2013), but the role of p32 remains somewhat unclear as p32 depletion has been shown to protect against cell death and to cause increased cell death under different stress conditions (Hu et al., 2013). The presence of mitochondrial p32 has been shown to be important for apoptosis mediated via Hrk (Sunayama et al., 2004) and ARF (Itahana and Zhang, 2008). Therefore, depletion of p32 should inhibit apoptosis via these mechanisms. However, p32 depletion causes mitochondrial fragmentation (Figures 8.5-8.6 and (Hu et al., 2013)), which is linked to apoptosis (reviewed in Cleland and Youle, 2011) and as such, the role of p32 in apoptosis remains unclear.

It is likely that p32 has multiple functions within the cell as many interactions have been described, both inside (Hu et al., 2013; Yagi et al., 2012; Itahana and Zhang, 2008) and outside (Krainer et al., 1991; Yu et al., 1995; Deb and Datta, 1996; Lim et al., 1996;

Ghebrehiwet et al., 1996) the mitochondria. It is therefore probable that the proposed sequestering and/or inhibition of p32 in AURKAIP1-FLAG overexpressing cells would inhibit a subset of these functions, whereas p32 depletion would presumably inhibit all p32 mediated functions. This may account for some of the differences in cell growth between the phenotypes caused by AURKAIP1-FLAG overexpression and p32 depletion.

Consistent with data presented in this chapter, p32 knockout MEFs show a decrease in mitoribosomes (Yagi et al., 2012). However, steady state levels of MRPs, including MRPL3 were not reduced (Yagi et al., 2012). In HeLa cells, p32 depletion caused a reduction in the steady state levels of MRPL3 (Figure 8.3), A potential role for p32 in mitoribosome maintenance is an attractive hypothesis given the data presented in this chapter. Interestingly, p32 has recently been implicated in pre-ribosome processing in conjunction with fibrillarin and Nop52 in the nucleolus (Yoshikawa et al., 2011). The authors of this study suggest p32 is important for early processing of pre-rRNAs, thus playing a role in ribosome biogenesis. Perhaps p32 has a similar role within mitochondria. Indeed, the RNA binding capacity of p32 has been suggested to be important (Yagi et al., 2012). Furthermore, p32 has recently been shown to interact with RNaseH1 and depletion of p32 led to an increase in pre-12S/16S rRNA levels (Wu et al., 2013). The authors attribute the increase in pre-12S/16S rRNA to reduced processing by the RNaseP complex in p32 depleted cells (Wu et al., 2013). If this hypothesis were correct, then presumably mature rRNA levels would be reduced, potentially accounting for the observed depletion of mitoribosomes in my investigations. Strangely, levels of mature mitochondrial rRNAs were not shown in this study (Wu et al., 2013). Further, the levels of neither mature mitochondrial rRNAs nor any mature mitochondrial mRNA were reduced in p32 knockout MEFs (Yagi et al., 2012). Quite how translation could be inhibited by accumulation of pre-rRNA without any effect on the mature rRNAs is difficult to fathom.

Further study is clearly required to elucidate the functional role of p32 in human mitochondria. Due to time constraints, the levels of mitochondrial RNA levels were not analysed by northern blot after p32 depletion. However, after AURKAIP1-FLAG overexpression the levels of *12S* rRNA and *MTCO1* mRNA were reduced (Figure 7.5). As discussed earlier, the decrease in *12S* and *MTCO1* are unlikely to be due to reduced transcription, as *MTND1* levels are not depleted. Perhaps inhibition of p32 mediated

pre-rRNA processing could account for the reduction in 12S rRNA levels. This seems unlikely, as I did not observe any increase in pre-rRNA levels. An alternative explanation is that the effects on mitochondrial RNA levels are secondary to the effects on mitochondrial protein synthesis. Perhaps disassembly of the mitoribosome and subsequent degradation of MRPs is the primary effect of AURKAIP1-FLAG overexpression and p32 depletion. If this hypothesis were correct then mitochondrial RNA levels may be degraded more rapidly due to the presence of fewer mitoribosomes to protect them. This hypothesis is interesting as it suggests p32 may have a role in mitoribosomal maintenance rather than biogenesis. Support for this notion comes from data showing that depletion of proteins such as ERAL1 (Dennerlein et al., 2010) and C7orf30 (Rorbach et al., 2012), which are involved in biogenesis of the SSU and LSU respectively, do not show decreased MRP levels after 3 days and 6 days respectively. Together, these data suggest that the half-life of mature mitoribosomes is too long for inhibition of ribosome biogenesis to show an effect on MRP levels after 6 days. I have shown that p32 depletion leads to a significant reduction in MRPL3 levels after 6 days, which may imply that mature ribosomes become disassembled.

If AURKAIP1-FLAG overexpression and p32 depletion cause disassembly of the mitoribosome, then the question of what causes the subsequent degradation of MRPs must be asked. One possibility that is being currently investigated in my host laboratory is that AURKAIP1 may bind p32 activating a latent protease activity, which may lead to MRP degradation. The crystal structure of p32 shows that the protein forms a doughnut-shaped trimer with a pore large enough to allow proteins to pass through (Jiang et al., 1999), indicating protease activity may be feasible. However, the depletion of MRPs in the absence of p32 does not support this hypothesis. Another avenue for future work would be to deplete known matrix proteases, such as ClpP, ClpX, AFG3L2, SPG7 and LonP1 independently before overexpressing AURKAIP1-FLAG. If depletion of any of these proteases could protect MRPs from AURKAIP1-FLAG mediated degradation, then that protease would be implicated MRP degradation. A recent publication showed that actinonin treatment leads to degradation of mitoribosomes (Richter et al., 2013). The authors propose that this degradation is a consequence of actinonin causing mitoribosome stalling, possibly by binding to mitochondrial Pdf (peptide deformylase) and causing Pdfs usually transient binding to the mitoribosome to become permanent (Richter et al., 2013). This could lead to activation of ribosome quality control pathways

being activated (reviewed in Shoemaker and Green, 2012), although these pathways are poorly understood in mitochondria. If these stalled ribosomes cannot be resolved to allow recycling of the assembled SSU and LSU respectively then they may be degraded by the proteasome, as is the case in the cytosol (Shoemaker and Green, 2012). Perhaps AURKAIP1 is involved in a similar pathway and that overexpressed AURKAIP1 binds to p32 causing a change in formation that results in binding and stalling the mitoribosome.

Another avenue being pursued in my host laboratory is the ability of AURKAIP1 to regulate the amount of p32 that exists as trimer. From my investigations it was clear that the steady state protein levels of p32 are not affected by changes in AURKAIP1 levels, however, it is possible that AURKAIP1 may facilitate a change in oligomerisation of p32. It is known that the majority of p32 exists in trimeric form, but that a small proportion is hexameric (Jha et al., 2002). The hexameric form is formed by dimerisation of two trimers via disulphide bond formation (Jha et al., 2002). Perhaps AURKAIP1 facilitates the dimerisation of the p32 trimers. It has been reported that trimeric and hexameric p32 have distinct binding capabilities and possibly independent functions in the extracellular matrix (Jha et al., 2002). If this is also the case in the mitochondria, then the regulation of the two oligomeric forms may allow explanation of why AURKAIP1 depletion and overexpression cause distinct phenotypes. Perhaps depletion of AURKAIP1 prevents the production of hexameric p32, whereas overexpression depletes the required pool of p32 trimer. If evidence for this hypothesis can be gathered using blue native PAGE, then future work will focus on establishing the respective functions of the distinct p32 oligomers.

It is evident from this discussion that there are many more avenues left to explore in order to elucidate the functions of p32 an AURKAIP1 in mitochondria.

CHAPTER 9: GENERAL CONCLUSIONS AND DISCUSSION

The data presented in this thesis has mainly focused on the characterisation of AURKAIP1, a protein about which very little data had been published at the beginning of my investigations. My aims at the outset and the progress I made towards achieving these aims are described below:

- To express and purify recombinant AURKAIP1 to use as an antigen for antibody production

  I successfully overexpressed and purified sufficient recombinant mature AURKAIP1 to allow the production of custom made antisera. I affinity purified the antisera to reduce non-specific binding and characterised that the α-AURKAIP1 antibody was specific to AURKAIP1. Using this tool, I determined that the levels of endogenous AURKAIP1 were too low to be detected in 40μg of cell lysate, but could be identified in 50μg of isolated mitochondrial lysate from 143B cells.

- To produce stable human cell lines capable of expressing C-terminal FLAG-tagged AURKAIP1

  I produced HEK293 cell lines that could inducibly overexpress AURKAIP1 with a C-terminal FLAG tag. I later identified that U2OS cells tolerated siRNA mediated AURKAIP1 depletion better and allowed improved visualisation of mitochondrial morphology by fluorescence microscopy compared to HEK293 cells. For these reasons, I also established U2OS lines capable of inducible AURKAIP1-FLAG expression.

- To use these tools to determine whether AURKAIP1 is mitochondrial, and if so, the sub-mitochondrial localisation

  The α-AURKAIP1 antibody and AURKAIP1-FLAG expressing cell lines were used to show that AURKAIP1 is present in human mitochondria and is predominantly localised to the mitochondrial matrix.

- To characterise the phenotype of AURKAIP1 depletion, with a view to identifying any critical role of AURKAIP1 in mitochondrial gene expression

  I have shown that AURKAIP1 is an essential protein required for cell viability and normal mitochondrial gene expression, as depletion of the protein causes mitochondrial translation defects.

- To identify binding partners of AURKAIP1 via immunoprecipitation to elucidate the potential functions of AURKAIP1

  I have demonstrated a strong novel interaction between AURKAIP1 and p32 using Co-IP techniques. Weaker or more transient interactions were observed between AURKAIP1 and MRPs (MRPL12 and MRPL3), although further investigation would be required to demonstrate that these interactions were direct, rather than mediated by binding of each protein to p32.

Despite extensive study towards my original aims, the precise functional role of AURKAIP1 in human mitochondria remained elusive. One of the difficulties in determining the role of AURKAIP1 lies in the effects resulting from over or under-representational levels of AURKAIP1 protein. This was made apparent by the unexpected observation that AURKAIP1-FLAG overexpression as well as depletion led to an impairment of mitochondrial gene expression. AURKAIP1 depletion and AURKAIP1 overexpression each led to cellular phenotypes that included enlarged nucleoid morphology, reduced steady state levels of 12S rRNA, *MT-CO1* mRNA and also of mtDNA-encoded proteins. Not all the changes were identical, a number of distinctions existed. AURKAIP1-FLAG overexpression caused a generalised defect in mitochondrial translation, whereas depletion of AURKAIP1 reduced the synthesis of only a specific subset of mtDNA-encoded proteins. Only AURKAIP1-FLAG overexpression led to a reduction in steady state levels of mitoribosomal subunits. This strongly suggests that separate signalling pathways underlie the mechanisms that cause the altered cellular phenotype following AURKAIP1 depletion or overexpression. The combination of overlapping and distinct differences in presentation mean that it is difficult to propose a hypothesis to explain all of the observed data at this stage.

It is not possible to say with certainty which of the observed effects following changes in steady state levels of AURKAIP1, are primary and which are secondary. The most striking effect of AURKAIP1-FLAG overexpression was the reduction in MRP levels. This was likely the result of disassembly of mitoribosomes since MRP levels were not reduced upon inhibition of mitoribosome biogenesis, over similar time frames (Dennerlein et al., 2010). The hypothesis that disassembly of the mitoribosome is the primary effect of AURKAIP1-FLAG overexpression offers the best explanation of the observed data, as this could lead to secondary effects of MRP degradation by the proteasome and subsequent impairment of mitochondrial protein synthesis due to the resulting lack of active mitoribosomes. In addition, the reduction in mitochondrial RNA levels may be explained by this hypothesis, as without the MRPs to protect the mRNA transcripts and rRNA, it is possible that they would be more rapidly degraded. Since my data shows that p32 depletion also reduces MRPL3 protein levels and published data has shown that loss of p32 causes a mitochondrial protein synthesis defect (Yagi et al., 2012), an attractive hypothesis is that AURKAIP1 acts to sequester p32 from its function. This may imply that p32 is involved in mitoribosome maintenance. That being said, p32 depletion and AURKAIP1-FLAG overexpression do not have identical phenotypes. This may be explained by p32 being a multifunctional protein. One explanation might be that AURKAIP1-FLAG overexpression blocks only one specific interaction of p32, leading to the impairment of protein synthesis, but other functions of p32 remain unaffected. In contrast p32 depletion would deprive the cells of all p32-mediated functions.

There are several other hypotheses, which may explain the data generated thus far, but further work is required to assess their likelihood. Of particular interest is assessing the nature of the interaction between AURKAIP1 and p32. Studies are currently on-going in my host laboratory, primarily focusing on determining:

- Whether AURKAIP1 can effect the relative amounts of p32 present as a trimer or hexamer and investigating the functional role of each
- Whether p32 and AURKAIP1 can form a complex that has protease activity
- The crystal structure of AURKAIP1 both alone and in complex with p32.

The original aim of these investigations was to study the role of AURKAIP1 in mitochondrial gene expression. Unfortunately, the data described in this thesis is insufficient to conclusively elucidate this. If the effects of AURKAIP1-FLAG overexpression are found not to be mediated by p32, then perhaps studying AURKAIP1 depletion further may be appropriate. The most striking observation upon AURKAIP1 depletion is that synthesis of only a subset of mtDNA-encoded proteins is impaired. Perhaps AURKAIP1 acts to recruit specific mRNAs to the mitoribosome. Alternatively, certain transcripts may have a propensity to stall the mitoribosome during the elongation phase of translation and as such will not be recognised by mtRF1a and subsequently resolved. AURKAIP1 may act to rescue these stalled mitoribosomes, liberating the transcript allowing it to participate in another round of translation. If this were the case, then in AURKAIP1 depleted cells the mitoribosomes may remain stalled on this subset of specific transcripts, resulting in reduced synthesis of the encoded proteins. This hypothesis may also be able to account for the phenotype resulting from overexpression, as high levels of AURKAIP1 may result in a loss of specificity/selectivity and thus disassemble non-stalled mitoribosomes. These ideas are speculative and targeted experiments would be required to test the hypothesis. One approach that could be used to determine if there is a change in the stall profile is ribosome profiling. By performing this technique on mitoribosomes from AURKAIP1 depleted cells, any change in amount or position on transcripts of stall events could be detected and provide data that would challenge or substantiate the hypothesis.

Although the molecular mechanism by which AURKAIP1 contributes to mitochondrial gene expression is not yet clear, my studies have made a contribution to the increasing amounts of data concerning AURKAIP1. Since I have shown that both AURKAIP1 depletion and overexpression affect mitochondrial protein synthesis, I propose that AURKAIP1 plays a role in the regulation mitochondrial translation, potentially mediated though a titrated interaction with p32, however further work is required to confirm this. The identification of pathogenic mutations in p32, the precise function of which is also unknown, leading to mitochondrial disease (*M.O. unpublished, personal communication*) serves to highlight the importance of understanding the fundamental aspects of mitochondrial biology. Better comprehension of mitochondrial processes, in turn provides enhanced understanding of mitochondrial dysfunction, which could lead to advances in treatment strategies for patients suffering from mitochondrial disease.

REFERENCES

Acin-Perez, R. & Enriquez, J. A. (2014) The function of the respiratory supercomplexes: the plasticity model. *Biochimica et biophysica acta*. [Online] 1837 (4), 444–450.

Adams, K. L. & Palmer, J. D. (2003) Evolution of mitochondrial gene content: gene loss and transfer to the nucleus. *Molecular phylogenetics and evolution*. 29 (3), 380–395.

Ahting, U. et al. (2001) Tom40, the pore-forming component of the protein-conducting TOM channel in the outer membrane of mitochondria. *The Journal of Cell Biology*. 153 (6), 1151–1160.

Alexander, C. et al. (2000) OPA1, encoding a dynamin-related GTPase, is mutated in autosomal dominant optic atrophy linked to chromosome 3q28. *Nature*. (26) 211-215.

Anderson, S. et al. (1981) Sequence and organization of the human mitochondrial genome. *Nature*. 290 (5806), 457–465.

Andersson, S. G. et al. (1998) The genome sequence of Rickettsia prowazekii and the origin of mitochondria. *Nature*. [Online] 396 (6707), 133–140.

Ashley, N. & Poulton, J. (2009) Anticancer DNA intercalators cause p53-dependent mitochondrial DNA nucleoid re-modelling. *Oncogene*. [Online] 28 (44), 3880–3891.

Ashley, N. et al. (2005) Detection of mitochondrial DNA depletion in living human cells using PicoGreen staining. *Experimental Cell Research*. [Online] 303 (2), 432–446.

Balsa, E. et al. (2012) NDUFA4 is a subunit of complex IV of the mammalian electron transport chain. *Cell metabolism*. [Online] 16 (3), 378–386.

Ban-Ishihara, R. et al. (2013) Dynamics of nucleoid structure regulated by mitochondrial fission contributes to cristae reformation and release of cytochrome c. *Proceedings of the National Academy of Sciences*. [Online] 110 (29), 11863–11868.

Barrell, B. G. et al. (1980) Different pattern of codon recognition by mammalian mitochondrial tRNAs. *Proceedings of the National Academy of Sciences.* 77(6), 3164-3166.

Barros, M. H. et al. (2006) COX24 codes for a mitochondrial protein required for processing of the COX1 transcript. *The Journal of biological chemistry*. [Online] 281 (6), 3743–3751.

Benz, R. (1994) Permeation of hydrophilic solutes through mitochondrial outer membranes: review on mitochondrial porins. *Biochimica et biophysica acta*. 1197 (2), 167–196.

Berk, A. J. & Clayton, D. A. (1974) Mechanism of mitochondrial DNA replication in mouse L-cells: Asynchronous replication of strands, segregation of circular daughter molecules, aspects of topology and turnover of an initiation sequence. *Journal of Molecular Biology*. [Online] 86 (4), 801–824.

Bhargava, K. et al. (2004) Expression and characterization of isoform 1 of human mitochondrial elongation factor G. *Protein Expression and Purification*. [Online] 37 (2), 368–376.

Bianchetti, R. et al. (1971) Endogenous synthesis of formyl-methionine peptides in isolated mitochondria and chloroplasts. *Biochemical and Biophysical Research Communications*. [Online] 42 (1), 97–102.

Bibb, M. J. et al. (1981) Sequence and gene organization of mouse mitochondrial DNA. *Cell*. [Online] 26 (2), 167–180.

Blum, T. et al. (2009) MultiLoc2: integrating phylogeny and Gene Ontology terms improves subcellular protein localization prediction. *BMC Bioinformatics*. [Online] 10 (1), 274.

Boesch, P. et al. (2008) Mitochondrial DNA and Diseases. *Wiley Online Library*. (Encyclopedia of Life Sciences).

Bogenhagen, D. & Clayton, D. A. (1974) The number of mitochondrial deoxyribonucleic acid genomes in mouse L and human HeLa cells. Quantitative isolation of mitochondrial deoxyribonucleic acid. *The Journal of biological chemistry*. 249 (24), 7991–7995.

Bogenhagen, D. F. (2012) Mitochondrial DNA nucleoid structure. *Biochimica et biophysica acta*. [Online] 1819 (9-10), 914–920.

Bogenhagen, D. F. et al. (2014) Initial steps in RNA processing and ribosome assembly occur at mitochondrial DNA nucleoids. *Cell metabolism*. [Online] 19 (4), 618–629.

Bonn, F. et al. (2011) Presequence-dependent folding ensures MrpL32 processing by the m-AAA protease in mitochondria. *The EMBO Journal*. [Online] 30 (13), 2545–2556.

Bowmaker, M. et al. (2003) Mammalian Mitochondrial DNA Replicates Bidirectionally from an Initiation Zone. *Journal of Biological Chemistry*. [Online] 278 (51), 50961–50969.

Brocks, J. J. et al. (1999) Archean molecular fossils and the early rise of eukaryotes. *Science (New York, NY)*. 285 (5430), 1033–1036.

Bruni, F. et al. (2013) REXO2 Is an Oligoribonuclease Active in Human Mitochondria Paul A Cobine (ed.). *PLoS ONE*. [Online] 8 (5), e64670.

Brzezniak, L. K. et al. (2011) Involvement of human ELAC2 gene product in 3' end processing of mitochondrial tRNAs. *RNA biology*. [Online] 8 (4), 616–626.

Calvo, S. E. et al. (2006) Systematic identification of human mitochondrial disease genes through integrative genomics. *Nature genetics*. [Online] 38 (5), 576–582.

Calvo, S. E. (2010) The mitochondrial proteome and human disease. *Annual review of genomics and human genetics.* 11, 25-44.

Calvo, S. E. (2012) Molecular diagnosis of infantile mitochondrial disease with targeted next-generation sequencing. *Science Translational Medicine.* vol. 4 (118) p. 118ra10

Capaldi, R. A. (1990) Structure and Function of Cytochrome c Oxidase. *Annual Review of Biochemistry*. [Online] 59 (1), 569–596.

Carroll, J. et al. (2006) Bovine Complex I Is a Complex of 45 Different Subunits. *Journal of Biological Chemistry*. [Online] 281 (43), 32724–32727.

Chacinska, A. et al. (2009) Importing Mitochondrial Proteins: Machineries and Mechanisms. *Cell*. [Online] 138 (4), 628–644.

Chang, S. C., Heacock, P. N., Clancey, C. J., et al. (1998b) The PEL1 gene (renamed PGS1) encodes the phosphatidylglycero-phosphate synthase of Saccharomyces cerevisiae. *The Journal of biological chemistry*. 273 (16), 9829–9836.

Chang, S. C., Heacock, P. N., Mileykovskaya, E., et al. (1998a) Isolation and characterization of the gene (CLS1) encoding cardiolipin synthase in Saccharomyces cerevisiae. *The Journal of biological chemistry*. 273 (24), 14933–14941.

Chinnery, P. F. et al. (1997) Molecular pathology of MELAS and MERRF. The relationship between mutation load and clinical phenotypes. *Brain : a journal of neurology*. 120 (Pt 10)1713–1721.

Chipuk, J. E. et al. (2006) Mitochondrial outer membrane permeabilization during apoptosis: the innocent bystander scenario. *Cell death and differentiation*. [Online] 13 (8), 1396–1402.

Chomyn, A. (1996) In vivo labeling and analysis of human mitochondrial translation products. *Methods in enzymology*. 264 (B), 197–211.

Chomyn, A. (2001) Mitochondrial genetic control of assembly and function of complex I in mammalian cells. *Journal of bioenergetics and biomembranes*. 33 (3), 251–257.

Chomyn, A. et al. (1985) Six unidentified reading frames of human mitochondrial DNA encode components of the respiratory-chain NADH dehydrogenase. *Nature*. 314 (6012), 592–597.

Christian, B. E. & Spremulli, L. L. (2009) Evidence for an active role of IF3mt in the initiation of translation in mammalian mitochondria. *Biochemistry*. [Online] 48 (15), 3269–3278.

Christian, B. E. & Spremulli, L. L. (2012) Mechanism of protein biosynthesis in mammalian mitochondria. *Biochimica et biophysica acta*. [Online] 1819 (9-10), 1035–1054.

Christian, B. E. & Spremulli, L. L. (2010) Preferential selection of the 5'-terminal start codon on leaderless mRNAs by mammalian mitochondrial ribosomes. *The Journal of biological chemistry*. [Online] 285 (36), 28379–28386.

Chu, C. T. et al. (2013) Cardiolipin externalization to the outer mitochondrial membrane acts as an elimination signal for mitophagy in neuronal cells. *Nature Cell Biology*. [Online] 15 (10), 1197–1205.

Cipolat, S. et al. (2004) OPA1 requires mitofusin 1 to promote mitochondrial fusion. *Proceedings of the National Academy of Sciences.* 101 (45), 15927-15932.

Claros, M. G. & Vincens, P. (1996) Computational Method to Predict Mitochondrially Imported Proteins and their Targeting Sequences. *European Journal of Biochemistry*. [Online] 241 (3), 779–786.

Clayton, D. A. (1982) Replication of animal mitochondrial DNA. *Cell*. [Online] 28 (4), 693–705.

Cleland, M. M. & Youle, R. J. (2011) 'Mitochondrial Dynamics and Apoptosis', in *Mitochondrial Dynamics and Neurodegeneration*. [Online]. Dordrecht: Springer Netherlands. pp. 109–138.

Cotney, J. & Shadel, G. S. (2006) Evidence for an Early Gene Duplication Event in the Evolution of the Mitochondrial Transcription Factor B Family and Maintenance of rRNA Methyltransferase Activity in Human mtTFB1 and mtTFB2. *Journal of Molecular Evolution*. [Online] 63 (5), 707–717.

Cramer, W. A. et al. (2011) The Q cycle of cytochrome bc complexes: a structure perspective. *Biochimica et biophysica acta*. [Online] 1807 (7), 788–802.

Dang, C. V. (2012) Links between metabolism and cancer. *Genes & Development*. [Online] 26 (9), 877–890.

Danielsson, P.-E. (1980) Euclidean distance mapping. *Computer Graphics and Image Processing*. [Online] 14 (3), 227–248.

Darshi, M. et al. (2011) ChChd3, an Inner Mitochondrial Membrane Protein, Is Essential for Maintaining Crista Integrity and Mitochondrial Function. *Journal of Biological Chemistry*. [Online] 286 (4), 2918–2932.

de Brito, O. M. & Scorrano, L. (2010) An intimate liaison: spatial organization of the endoplasmic reticulum–mitochondria relationship. *The EMBO Journal*. [Online] 29 (16), 2715–2723.

de Kroon, A. I. P. M. et al. (1997) Phospholipid composition of highly purified mitochondrial outer membranes of rat liver and Neurospora crassa. Is cardiolipin present in the mitochondrial outer membrane? *Biochimica et Biophysica Acta (BBA) - Biomembranes*. [Online] 1325 (1), 108–116.

Deb, T. B. & Datta, K. (1996) Molecular cloning of human fibroblast hyaluronic acid-binding protein confirms its identity with P-32, a protein co-purified with splicing factor SF2. Hyaluronic acid-binding protein as P-32 protein, co-purified with splicing factor SF2. *The Journal of biological chemistry*. 271 (4), 2206–2212.

Dee, C. T. & Moffat, K. G. (2005) A novel family of mitochondrial proteins is represented by the Drosophila genes slmo, preli-like and real-time. *Development Genes and Evolution*. [Online] 215 (5), 248–254.

Delettre, C. et al. (2001) Mutation spectrum and splicing variants in the OPA1 gene. *Human genetics*. [Online] 109 (6), 584–591.

Dennerlein, S. et al. (2010) Human ERAL1 is a mitochondrial RNA chaperone involved in the assembly of the 28S small mitochondrial ribosomal subunit. *The Biochemical journal*. [Online] 430 (3), 551–558.

Desmond, E. et al. (2011) On the last common ancestor and early evolution of eukaryotes: reconstructing the history of mitochondrial ribosomes. *Research in microbiology*. [Online] 162 (1), 53–70.

Di Re, M. et al. (2009) The accessory subunit of mitochondrial DNA polymerase γ determines the DNA content of mitochondrial nucleoids in human cultured cells. *Nucleic acids Research.* 37 (17), 5701-5713.

Emanuelsson, O. et al. (2007) Locating proteins in the cell using TargetP, SignalP and related tools. *Nature Protocols*. [Online] 2 (4), 953–971.

Emanuelsson, O. et al. (2000) Predicting Subcellular Localization of Proteins Based on their N-terminal Amino Acid Sequence. *Journal of Molecular Biology.* 300 (4), 1005-1016.

Embley, T. M. & Martin, W. (2006) Eukaryotic evolution, changes and challenges. *Nature Cell Biology*. [Online] 440 (7084), 623–630.

Endo, T. et al. (2011) Structural insight into the mitochondrial protein import system. *Biochimica et Biophysica Acta (BBA) - Biomembranes*. [Online] 1808 (3), 955–970.

Falkenberg, M. et al. (2007) DNA Replication and Transcription in Mammalian Mitochondria. *Annual Review of Biochemistry*. [Online] 76 (1), 679–699.

Falkenberg, M. et al. (2002) Mitochondrial transcription factors B1 and B2 activate transcription of human mtDNA. *Nature genetics*. [Online] 31 (3), 289–294.

Fisher, R. P. et al. (1992) DNA wrapping and bending by a mitochondrial high mobility group-like transcriptional activator protein. *The Journal of biological chemistry*. 267 (5), 3358–3367.

Fontanesi, F. et al. (2006) Assembly of mitochondrial cytochrome c-oxidase, a complicated and highly regulated cellular process. *American journal of physiology. Cell physiology*. [Online] 291 (6), C1129–C1147.

Frezza, C. et al. (2006) OPA1 Controls Apoptotic Cristae Remodeling Independently from Mitochondrial Fusion. *Cell*. [Online] 126 (1), 177–189.

Galkin, A. et al. (2006) The proton pumping stoichiometry of purified mitochondrial complex I reconstituted into proteoliposomes. *Biochimica et biophysica acta*. [Online] 1757 (12), 1575–1581.

Gallerani, R. et al. (1976) Contemporaneous isolation of deoxyribonucleic acid-dependent ribonucleic acid polymerase and poly(A) polymerase from rat liver mitochondria. *The Biochemical journal*. 157 (2), 295–300.

Gandre-Babbe, S. & van der Bliek, A. M. (2008) The novel tail-anchored membrane protein Mff controls mitochondrial and peroxisomal fission in mammalian cells. *Molecular Biology of the Cell*. [Online] 19 (6), 2402–2412.

Gasteiger, E. et al. (2005) '*Protein Identification and Analysis Tools on the ExPASy Server*', in [Online]. Totowa, NJ: Humana Press. pp. 571–607.

Gaur, R. et al. (2008) A Single Mammalian Mitochondrial Translation Initiation Factor Functionally Replaces Two Bacterial Factors. *Molecular cell*. [Online] 29 (2), 180–190.

Gelfand, R. & Attardi, G. (1981) Synthesis and turnover of mitochondrial ribonucleic acid in HeLa cells: the mature ribosomal and messenger ribonucleic acid species are metabolically unstable. *Molecular and cellular biology*. 1 (6), 497–511.

Gerbert, N. et al. (2009) Mitochondrial Cardiolipin Involved in Outer-Membrane Protein Biogenesis : Implications for Bath Syndrome. *Current Biology*. 192133–2139.

Gerencser, A. A. et al. (2012) Quantitative measurement of mitochondrial membrane potential in cultured cells: calcium-induced de- and hyperpolarization of neuronal mitochondria - Gerencser - 2012 - The Journal of Physiology - Wiley Online Library. *The Journal of Physiology.* 590 (12), 2845-2871.

Ghebrehiwet, B. et al. (1996) Identification of functional domains on gC1Q-R, a cell surface protein that binds to the globular ‘heads’ of C1Q, using monoclonal antibodies and synthetic peptides. *Hybridoma*. 15 (5), 333–342.

Ghezzi, D. et al. (2011) Mutations in TTC19 cause mitochondrial complex III deficiency and neurological impairment in humans and flies. *Nature Genetics.* vol. 43 (3) pp. 259-263

Goffart, S. et al. (2009) Twinkle mutations associated with autosomal dominant progressive external ophthalmoplegia lead to impaired helicase function and in vivo mtDNA replication stalling. *Human Molecular Genetics.* 18 (2), 328-340.

Goldstein, A. C. et al. (2013) Mitochondrial disease in childhood: nuclear encoded. *Neurotherapeutics : the journal of the American Society for Experimental NeuroTherapeutics*. [Online] 10 (2), 212–226.

Gray, M. W. et al. (1999) Mitochondrial evolution. *Science (New York, NY)*. 283 (5407), 1476–1481.

Greber, B. J. et al. (2014) Architecture of the large subunit of the mammalian mitochondrial ribosome. *Nature*. [Online] 505 (7484), 515–519.

Greggains, G. D. et al. (2014) Therapeutic potential of somatic cell nuclear transfer for degenerative disease caused by mitochondrial DNA mutations. *Scientific reports*. [Online] 43844.

Guda, C. (2006) pTARGET: a web server for predicting protein subcellular localization. *Nucleic Acids Research*. 34, W210-W213.

Hammarsund, M. et al. (2001) Identification and characterization of two novel human mitochondrial elongation factor genes, hEFG2 and hEFG1, phylogenetically conserved through evolution. *Human genetics*. [Online] 109 (5), 542–550.

Haridas, S. & Gantt, J. S. (2010) The mitochondrial genome of the wood-degrading basidiomycete Trametes cingulata. *FEMS microbiology letters*. [Online] 308 (1), 29–34.

Harris, D. A. & Das, A. M. (1991) Control of mitochondrial ATP synthesis in the heart. *Biochemical journal*. 280, 561-573.

He, J. et al. (2007) The AAA+ protein ATAD3 has displacement loop binding properties and is involved in mitochondrial nucleoid organization. *The Journal of Cell Biology*. 176 (2), 141-146.

Helling, S. et al. (2012) Regulation of mitochondrial respiration and apoptosis through cell signaling: Cytochrome c oxidase and cytochrome c in ischemia/reperfusion injury and inflammation. *Biochimica et Biophysica Acta (BBA)*. 1817, 598-609.

Herrmann, J. M. (2010) Ups delivery to the intermembrane space of mitochondria: a novel affinity-driven protein import pathway. *The EMBO Journal*. [Online] 29 (17), 2859–2860.

Herrmann, J. M. et al. (2013) Control of protein synthesis in yeast mitochondria: the concept of translational activators. *Biochimica et Biophysica Acta*. [Online] 1833 (2), 286–294.

Hiller, S. et al. (2008) Solution Structure of the Integral Human Membrane Protein VDAC-1 in Detergent Micelles. *Science (New York, NY)*. [Online] 321 (5893), 1206–1210.

Hirst, J. (2005) Energy transduction by respiratory complex I--an evaluation of current knowledge. *Biochemical Society Transactions*. [Online] 33 (Pt 3), 525–529.

Hirst, J. et al. (2003) The nuclear encoded subunits of complex I from bovine heart mitochondria. *Biochimica et biophysica acta*. 1604 (3), 135–150.

Hoffmann, B. et al. (1994) The reconstituted ADP/ATP carrier activity has an absolute requirement for cardiolipin as shown in cysteine mutants. *The Journal of biological chemistry*. 269 (3), 1940–1944.

Holland, H. D. et al. (1994) O2 and CO2 in the late Archaean and early Proterozoic atmosphere. *Mineralogical Magazine*. 58A, 424-425.

Holt, I. J. & Reyes, A. (2012) Human mitochondrial DNA replication. *Cold Spring Harbor perspectives in biology*. [Online] 4 (12).

Holt, I. J. et al. (2000) Coupled Leading- and Lagging-Strand Synthesis of Mammalian Mitochondrial DNA. *Cell*. [Online] 100 (5), 515–524.

Holt, I. J. et al. (1989) Deletions of muscle mitochondrial DNA in mitochondrial myopathies: sequence analysis and possible mechanisms. *Nucleic Acids Research*. [Online] 17 (12), 4465–4469.

Hu, M. et al. (2013) p32 protein levels are integral to mitochondrial and endoplasmic reticulum morphology, cell metabolism and survival. *The Biochemical journal*. [Online] 453 (3), 381–391.

Huang, P. et al. (2011) Control of mitochondrial morphology through differential interactions of mitochondrial fusion and fission proteins. *PLoS ONE*. [Online] 6 (5), e20655.

Hughes, T. R. et al. (2000) Functional discovery via a compendium of expression profiles. *Cell.* 102, 109-126.

Huh, W.-K. et al. (2003) Global analysis of protein localization in budding yeast. *Nature Cell Biology*. [Online] 425 (6959), 686–691.

Højlund, K. et al. (2008) Mitochondrial Dysfunction in Type 2 Diabetes and Obesity. *Endocrinology and Metabolism Clinics of North America*. [Online] 37 (3), 713–731.

Ip, M. M. et al. (1974) Turnover of hepatic mitochondrial ornithine aminotransferase and cytochrome oxidase using (14C)carbonate as tracer. *Biochimica et biophysica acta*. 354 (1), 29–38.

Ishihara, N. et al. (2006) Regulation of mitochondrial morphology through proteolytic cleavage of OPA1. *The EMBO Journal*. [Online] 25 (13), 2966–2977.

Itahana, K. & Zhang, Y. (2008) Mitochondrial p32 is a critical mediator of ARF-induced apoptosis. *Cancer cell*. [Online] 13 (6), 542–553.

Jha, B. K. et al. (2002) Disulfide bond formation through Cys186 facilitates functionally relevant dimerization of trimeric hyaluronan-binding protein 1 (HABP1)/p32/gC1qR - Jha - 2003 - European Journal of Biochemistry - Wiley Online Library. *European Journal of Biochemistry.* 269, 298-306.

Jiang, J. et al. (1999) Crystal structure of human p32, a doughnut-shaped acidic mitochondrial matrix protein. *Proceedings of the National Academy of Sciences*. [Online] 96 (7), 3572–3577.

Johnson, L. V. et al. (1981) Monitoring of relative mitochondrial membrane potential in living cells by fluorescence microscopy. *The Journal of Cell Biology.* 88, 526-535.

Jourdain, A. & Martinou, J.-C. (2009) Mitochondrial outer-membrane permeabilization and remodelling in apoptosis. *The International Journal of Biochemistry & Cell Biology*. [Online] 41 (10), 1884–1889.

Kadenbach, B. et al. (1983) Separation of mammalian cytochrome c oxidase into 13 polypeptides by a sodium dodecyl sulfate-gel electrophoretic procedure. *Analytical Biochemistry*. [Online] 129 (2), 517–521.

Kasashima, K. et al. (2011) Human mitochondrial transcription factor A is required for the segregation of mitochondrial DNA in cultured cells. *Experimental Cell Research*. [Online] 317 (2), 210–220.

Kasashima, K. et al. (2012) Maintenance of mitochondrial genome distribution by mitochondrial AAA+ protein ClpX. *Experimental Cell Research*. [Online] 318 (18), 2335–2343.

Katayama, H. et al. (2007) Aurora-A kinase phosphorylation of Aurora-A kinase interacting protein (AIP) and stabilization of the enzyme-substrate complex. *Journal of Cellular Biochemistry* [Online] 102 (5), 1318–1331.

Kemp, J. P. et al. (2011) Nuclear factors involved in mitochondrial translation cause a subgroup of combined respiratory chain deficiency. *Brain.* 134 (Pt 1) pp. 183-195

Kiat, L. S. (2002) Aurora-A Kinase Interacting Protein (AIP), a Novel Negative Regulator of Human Aurora-A Kinase. *Journal of Biological Chemistry*. [Online] 277 (47), 45558–45565.

Kibbe, W. A. (2007) OligoCalc: an online oligonucleotide properties calculator. *Nucleic Acids Research*. [Online] 35 (Web Server), W43–W46.

King, M. & Attardi, G. (1989) Human cells lacking mtDNA: repopulation with exogenous mitochondria by complementation. *Science (New York, NY)*. [Online] 246 (4929), 500–503.

Kinnally, K. W. et al. (2011) Is mPTP the gatekeeper for necrosis, apoptosis, or both? *Biochimica et Biophysica Acta (BBA) - Molecular Cell Research*. [Online] 1813 (4), 616–622.

Kinosita, K. (2012) F(1)-ATPase: a prototypical rotary molecular motor. *Advances in experimental medicine and biology*. [Online] 7265–16.

Kitazaki, K. & Kubo, T. (2010) Cost of Having the Largest Mitochondrial Genome: Evolutionary Mechanism of Plant Mitochondrial Genome. *Journal of Botany*. [Online] 2010 (5950), 1–12.

Knott, A. B. & Bossy-Wetzel, E. (2008) Impairing the Mitochondrial Fission and Fusion Balance: A New Mechanism of Neurodegeneration. *Annals of the New York Academy of Sciences*. [Online] 1147 (1), 283–292.

Koc, E. & Haque, M. (2010) Current Views of the Structure of the Mammalian Mitochondrial Ribosome. *Israel Journal of Chemistry*. 50 (1), 45–59.

Koc, E. C. & Spremulli, L. L. (2002) Identification of mammalian mitochondrial translational initiation factor 3 and examination of its role in initiation complex formation with natural mRNAs. *The Journal of biological chemistry*. [Online] 277 (38), 35541–35549.

Koc, E. C. et al. (2013) Identification and characterization of CHCHD1, AURKAIP1, and CRIF1 as new members of the mammalian mitochondrial ribosome. *Frontiers in physiology*. [Online] 4183.

Kolesnikova, O. A. (2004) Nuclear DNA-encoded tRNAs targeted into mitochondria can rescue a mitochondrial DNA mutation associated with the MERRF syndrome in cultured human cells. *Human Molecular Genetics*. [Online] 13 (20), 2519–2534.

Korhonen, J. A. et al. (2004) Reconstitution of a minimal mtDNA replisome in vitro. *The EMBO Journal*. [Online] 23 (12), 2423–2429.

Korhonen, J. A. et al. (2003) TWINKLE Has 5‘ -> 3’ DNA helicase activity and is specifically stimulated by mitochondrial single-stranded DNA-binding protein. *The Journal of biological chemistry*. [Online] 278 (49), 48627–48632.

Krainer, A. R. et al. (1991) Functional expression of cloned human splicing factor SF2: homology to RNA-binding proteins, U1 70K, and Drosophila splicing regulators. *Cell*. 66 (2), 383–394.

Kukat, C. & Larsson, N.-G. (2013) mtDNA makes a U-turn for the mitochondrial nucleoid. *Trends in cell biology*. [Online] 23 (9), 457–463.

Kukat, C. et al. (2011) Super-resolution microscopy reveals that mammalian mitochondrial nucleoids have a uniform size and frequently contain a single copy of mtDNA. *Proceedings of the National Academy of Sciences*. [Online] 108 (33), 13534–13539.

Kurland, C. G. & Andersson, S. G. E. (2000) Origin and Evolution of the Mitochondrial Proteome. *Microbiology and Molecular Biology Reviews.* 64 (4), 786-820.

Landes, T. & Martinou, J.-C. (2011) Mitochondrial outer membrane permeabilization during apoptosis: The role of mitochondrial fission. *Biochimica et Biophysica Acta (BBA) - Molecular Cell Research*. [Online] 1813 (4), 540–545.

Lang, B. F. et al. (1999) Mitochondrial genome evolution and the origin of eukaryotes. *Annual Review of Genetics*. [Online] 33351–397.

Lesnefsky, E. J. & Hoppel, C. L. (2006) Oxidative phosphorylation and aging. *Ageing research reviews*. 5, 402-433.

Li, L. Y. et al. (2001) Endonuclease G is an apoptotic DNase when released from mitochondria. *Nature*. [Online] 412 (6842), 95–99.

Lill, R. (2009) Function and biogenesis of iron-sulphur proteins. *Nature*. [Online] 460 (7257), 831–838.

Lill, R. & Mühlenhoff, U. (2005) Iron–sulfur-protein biogenesis in eukaryotes. *Trends in biochemical sciences*. 30 (3), 133-141.

Lim, B. L. et al. (1996) The binding protein for globular heads of complement C1q, gC1qR. Functional expression and characterization as a novel vitronectin binding factor. *The Journal of biological chemistry*. 271 (43), 26739–26744.

Lim, S. K. et al. (2007) Aurora-A kinase interacting protein 1 (AURKAIP1) promotes Aurora-A degradation through an alternative ubiquitin-independent pathway. *The Biochemical journal*. [Online] 403 (1), 119.

Lindenboim, L. et al. (2011) Nuclear proteins acting on mitochondria. *Biochimica et Biophysica Acta (BBA) - Molecular Cell Research*. [Online] 1813 (4), 584–596.

Litonin, D. et al. (2010) Human mitochondrial transcription revisited: only TFAM and TFB2M are required for transcription of the mitochondrial genes in vitro. *Journal of Biological Chemistry*. [Online] 285 (24), 18129–18133.

Liu, M. & Spremulli, L. (2000) Interaction of mammalian mitochondrial ribosomes with the inner membrane. *The Journal of biological chemistry*. [Online] 275 (38), 29400–29406.

Liu, X. et al. (2009) Mitochondrial 'kiss-and-run': interplay between mitochondrial motility and fusion–fission dynamics. *The EMBO Journal*. [Online] 28 (20), 3074–3089.

Livak, K. J. & Schmittgen, T. D. (2001) Analysis of relative gene expression data using real-time quantitative PCR and the 2(-Delta Delta C(T)) Method. *Methods*. [Online] 25 (4), 402–408.

Lodeiro, M. F. et al. (2012) Transcription from the second heavy-strand promoter of human mtDNA is repressed by transcription factor A in vitro. *Proceedings of the National Academy of Sciences*. [Online] 109 (17), 6513–6518.

Lopez, M. F. et al. (2000) High-throughput profiling of the mitochondrial proteome using affinity fractionation and automation. *Electrophoresis*. [Online] 21 (16), 3427–3440.

Ly, J. D. et al. (2003) The mitochondrial membrane potential (Δψm) in apoptosis; an update - Springer. *APOPTOSIS*. [Online] 8 (2), 115–128.

Ma, J. et al. (1995) Cloning and sequence analysis of the cDNA for bovine mitochondrial translational initiation factor 2. *Biochimica et biophysica acta*. 1261 (2), 321–324.

Makowska-Grzyska, M. M. et al. (2010) Physical analysis of recombinant forms of the human mitochondrial DNA helicase. *Methods*. 51, 411-415.

Malarkey, C. S. et al. (2012) Transcriptional activation by mitochondrial transcription factor A involves preferential distortion of promoter DNA. *Nucleic Acids Research*. [Online] 40 (2), 614–624.

Manczak, M. et al. (2011) Impaired mitochondrial dynamics and abnormal interaction of amyloid beta with mitochondrial protein Drp1 in neurons from patients with Alzheimer's disease: implications for neuronal damage. *Human Molecular Genetics*. [Online] 20 (13), 2495–2509.

Mannella, C. A. (1992) The 'ins' and "outs" of mitochondrial membrane channels. *Trends in biochemical sciences*. 17, 315-320.

Marchler-Bauer, A. et al. (2011) CDD: a Conserved Domain Database for the functional annotation of proteins. *Nucleic Acids Research*. [Online] 39 (Database issue), D225–D229.

Margulis, L. (1971) *The Origin of Eukaryotic Cells*. Yale University Press.

Marintchev, A. & Wagner, G. (2004) Translation initiation: structures, mechanisms and evolution. *Quarterly reviews of biophysics*. [Online] 37 (3-4), 197–284.

Matsushima, Y. et al. (2005) Drosophila mitochondrial transcription factor B1 modulates mitochondrial translation but not transcription or DNA copy number in Schneider cells. *The Journal of biological chemistry*. [Online] 280 (17), 16815–16820.

Matsushima, Y. et al. (2004) Drosophila mitochondrial transcription factor B2 regulates mitochondrial DNA copy number and transcription in schneider cells. *The Journal of biological chemistry*. [Online] 279 (26), 26900–26905.

Metodiev, M. D. et al. (2009) Methylation of 12S rRNA is necessary for in vivo stability of the small subunit of the mammalian mitochondrial ribosome. *Cell metabolism*. [Online] 9 (4), 386–397.

Micol, V. et al. (1997) Functional Analysis of in Vivo and in Organello Footprinting of HeLa Cell Mitochondrial DNA in Relationship to ATP and Ethidium Bromide Effects on Transcription. *Journal of Biological Chemistry*. 272, 18896-18904.

Mikelsaar, R. (1983) Human mitochondrial genome and the evolution of methionine transfer ribonucleic acids. *Journal of Theoretical Biology*. [Online] 105 (2), 221–232.

Milenkovic, D. et al. (2013) TWINKLE is an essential mitochondrial helicase required for synthesis of nascent D-loop strands and complete mtDNA replication. *Human Molecular Genetics.* 22 (10), 1983-1993.

Miller, C. et al. (2004) Defective mitochondrial translation caused by a ribosomal protein (MRPS16) mutation. *Annals of Neurology*. vol. 56, no. 5, pp. 734–738.

Mitchell, P. (1961) Coupling of phosphorylation to electron and hydrogen transfer by a chemi-osmotic type of mechanism. *Nature*. 191, 144-148.

Mitchell, P. (1975) The protonmotive Q cycle: a general formulation. *FEBS letters*. 59 (2), 137–139.

Mitsuhashi, M. (1996) Technical report: Part 2. Basic requirements for designing optimal PCR primers. *Journal of Clinical Laboratory Analysis*. [Online] 10 (5), 285–293.

Morino, H. et al. (2014) Exome sequencing reveals a novel TTC19 mutation in an autosomal recessive spinocerebellar ataxia patient. *BMC Neurology.* vol. 14 p. 5

Mulkidjanian, A. Y. (2010) Activated Q-cycle as a common mechanism for cytochrome bc1 and cytochrome b6f complexes. *Biochimica et biophysica acta*. [Online] 1797 (12), 1858–1868.

Muta, T. et al. (1997) p32 protein, a splicing factor 2-associated protein, is localized in mitochondrial matrix and is functionally important in maintaining oxidative phosphorylation. *The Journal of biological chemistry*. 272 (39), 24363–24370.

Nagaike, T. et al. (2001) Identification and characterization of mammalian mitochondrial tRNA nucleotidyltransferases. *The Journal of biological chemistry*. [Online] 276 (43), 40041–40049.

Nass, M. M. (1969) Mitochondrial DNA: Advances, Problems, and Goals. *Science (New York, NY)*. [Online] 165 (3888), 25–35.

Nekrasova, O. E. et al. (2011) Vimentin Intermediate Filaments Modulate the Motility of Mitochondria. *Molecular Biology of the Cell*. [Online]

Nicholls, D. G. & Ward, M. W. (2000) Mitochondrial membrane potential and neuronal glutamate excitotoxicity: mortality and millivolts. *Trends in neurosciences*. 23 (4), 166–174.

Nicholls, T. J. & Minczuk, M. (2014) In D-loop: 40years of mitochondrial 7S DNA. *Experimental gerontology*. [Online] In Press.

Nielsen, H. et al. (1997) Identification of prokaryotic and eukaryotic signal peptides and prediction of their cleavage sites. *Protein Engineering Design and Selection*. [Online] 10 (1), 1–6.

Noji, H. et al. (1997) Direct observation of the rotation of F1-ATPase. *Nature*. [Online] 386 (6622), 299–302.

Nolden, M. et al. (2005) The m-AAA protease defective in hereditary spastic paraplegia controls ribosome assembly in mitochondria. *Cell*. [Online] 123 (2), 277–289.

O'Brien, T. W. (2002) Evolution of a protein-rich mitochondrial ribosome: implications for human genetic disease. *Gene*. 286 (1), 73–79.

Ochoa, S. (2006) 'Enzymic Mechanisms in the Citric Acid Cycle', in *Advances in Enzymology and Related Areas of …*. Advances in Enzymology - and Related Areas of Molecular Biology. [Online]. Hoboken, NJ, USA: John Wiley & Sons, Inc. pp. 183–270.

Ojala, D. et al. (1981) tRNA punctuation model of RNA processing in human mitochondria. *Nature*. 290 (5806), 470–474.

Olichon, A. et al. (2003) Loss of OPA1 perturbates the mitochondrial inner membrane structure and integrity, leading to cytochrome c release and apoptosis. *The Journal of biological chemistry*. [Online] 278 (10), 7743–7746.

Oliveira, J. M. A. and Lightowlers, R. N. (2010) Could successful (mitochondrial) networking help prevent Huntington's disease? *EMBO Molecular Medicine*. 2(12): 487–489

Osman, C. et al. (2010) A mitochondrial phosphatase required for cardiolipin biosynthesis: the PGP phosphatase Gep4. *The EMBO Journal*. [Online] 29 (12), 1976–1987.

Osman, C. et al. (2011) Making heads or tails of phospholipids in mitochondria. *The Journal of Cell Biology*. [Online] 192 (1), 7–16.

Osman, C. et al. (2009) The genetic interactome of prohibitins: coordinated control of cardiolipin and phosphatidylethanolamine by conserved regulators in mitochondria. *The Journal of Cell Biology.* 184 (4), 583-596.

Otera, H. et al. (2010) Mff is an essential factor for mitochondrial recruitment of Drp1 during mitochondrial fission in mammalian cells. *The Journal of Cell Biology*. [Online] 191 (6), 1141–1158.

Ou, W. J. et al. (1989) Purification and characterization of a processing protease from rat liver mitochondria. *The EMBO Journal*. 8 (9), 2605–2612.

Pagliarini, D. J. et al. (2008) A mitochondrial protein compendium elucidates complex I disease biology. *Cell*. [Online] 134 (1), 112–123.

Papa, S. et al. (2012) The oxidative phosphorylation system in mammalian mitochondria. *Advances in experimental medicine and biology*. [Online] 9423–37.

Parone, P. A. et al. (2008) Preventing Mitochondrial Fission Impairs Mitochondrial Function and Leads to Loss of Mitochondrial DNA. *PLoS ONE*. [Online] 3 (9), e3257.

Peralta, S. et al. (2012) Mitochondrial transcription: lessons from mouse models. *Biochimica et biophysica acta*. [Online] 1819 (9-10), 961–969.

Pinto, M. and Moraes, C. T. (2014) Mitochondrial genome changes and neurodegenerative diseases. *Biochimica et biophysica acta.* 1842 (8) pp. 1198-1207

Ponamarev, M. V. et al. (2005) Proteomics of bovine mitochondrial RNA-binding proteins: HES1/KNP-I is a new mitochondrial resident protein. *Journal of proteome research*. [Online] 4 (1), 43–52.

Potting, C. et al. (2010) Regulation of mitochondrial phospholipids by Ups1/PRELI-like proteins depends on proteolysis and Mdm35. *The EMBO Journal*. [Online] 29 (17), 2888–2898.

Rabilloud, T. et al. (1998) Two-dimensional electrophoresis of human placental mitochondria and protein identification by mass spectrometry: toward a human mitochondrial proteome. *Electrophoresis*. [Online] 19 (6), 1006–1014.

Rajas, F. et al. (1996) Involvement of a Membrane-bound Form of Glutamate Dehydrogenase in the Association of Lysosomes to Microtubules. *Journal of Biological Chemistry*. 271 (47), 29882-29890.

Rawat, S. & Stemmler, T. L. (2011) Key Players and Their Role During Mitochondrial Iron-Sulfur Cluster Biosynthesis. *Chemistry - A European Journal*. [Online] 17 (3), 746–753.

Reyes, A. et al. (2013) Mitochondrial DNA replication proceeds via a 'bootlace' mechanism involving the incorporation of processed transcripts. *Nucleic Acids Research*. [Online] 41 (11), 5837–5850.

Richter, U. et al. (2013) A Mitochondrial Ribosomal and RNA Decay Pathway Blocks Cell Proliferation. *Current Biology*. [Online] 23 (6), 535–541.

Robberson, D. L. & Clayton, D. A. (1972) Replication of Mitochondrial DNA in Mouse L Cells and Their Thymidine Kinase- Derivatives: Displacement Replication on a Covalently-Closed Circular Template. *Proceedings of the National Academy of Sciences.* 69 (12), 3810-3814.

Roise, D. & Schatz, G. (1988) Mitochondrial presequences. *The Journal of biological chemistry*. 263 (10), 4509–4511.

Rorbach, J. et al. (2012) C7orf30 is necessary for biogenesis of the large subunit of the mitochondrial ribosome. *Nucleic Acids Research*. [Online] 40 (9), 4097–4109.

Rorbach, J. et al. (2008) The human mitochondrial ribosome recycling factor is essential for cell viability. *Nucleic Acids Research*. [Online] 36 (18), 5787–5799.

Rossignol, R. et al. (2003) Mitochondrial threshold effects. *The Biochemical journal*. [Online] 370 (3), 751.

Rossignol, R. et al. (1999) Threshold Effect and Tissue Specificity. *Journal of Biological Chemistry.* 274 (47), 33426-33432.

Rossmanith, W. (2011) Localization of Human RNase Z Isoforms: Dual Nuclear/Mitochondrial Targeting of the ELAC2 Gene Product by Alternative Translation Initiation Bob Lightowlers (ed.). *PLoS ONE*. [Online] 6 (4), e19152.

Russ, J. C. (2011) *The Image Processing Handbook, Sixth Edition*. CRC Press.

Rustin, P. et al. (1994) Biochemical and molecular investigations in respiratory chain deficiencies. *Clinica Chimica Acta*. [Online] 228 (1), 35–51.

Rustin, P. et al. (1997) Inborn errors of the Krebs cycle: a group of unusual mitochondrial diseases in human. *Biochimica et Biophysica Acta (BBA)*. 1361, 185-197.

Rutter, J. et al. (2010) Succinate dehydrogenase - Assembly, regulation and role in human disease. *Mitochondrion*. [Online] 10 (4), 393–401.

Saada, A. et al. (2007) Antenatal mitochondrial disease caused by mitochondrial ribosomal protein (MRPS22) mutation. *Journal of Medical Genetics*. vol. 44, no. 12, pp. 784–786.

Sacconi, S. et al. (2008) A functionally dominant mitochondrial DNA mutation. *Human Molecular Genetics*. [Online] 17 (12), 1814–1820.

Saneto, R. P. & Sedensky, M. M. (2013) Mitochondrial disease in childhood: mtDNA encoded. *Neurotherapeutics : the journal of the American Society for Experimental NeuroTherapeutics*. [Online] 10 (2), 199–211.

Saraste, M. (1999) Oxidative phosphorylation at the fin de siècle. *Science (New York, NY)*. 283 (5407), 1488–1493.

Sazanov, L. A. (2006) Structure of the Hydrophilic Domain of Respiratory Complex I from Thermus thermophilus. *Science (New York, NY)*. [Online] 311 (5766), 1430–1436.

Scaduto, R. C., Jr. & Grotyohann, L. W. (1999) Measurement of Mitochondrial Membrane Potential Using Fluorescent Rhodamine Derivatives. *Biophysical Journal*. [Online] 76 (1), 469–477.

Schaefer, A. M. et al. (2004) The epidemiology of mitochondrial disorders--past, present and future. *Biochimica et biophysica acta*. [Online] 1659 (2-3), 115–120.

Schaffer, S. W. et al. (2014) Role of taurine in the pathologies of MELAS and MERRF. *Amino acids*. [Online] 46 (1), 47–56.

Scheffler, N. K. et al. (2001) Two-dimensional electrophoresis and mass spectrometric identification of mitochondrial proteins from an SH-SY5Y neuroblastoma cell line. *Mitochondrion*.

Schmeing, T. M. & Ramakrishnan, V. (2009) What recent ribosome structures have revealed about the mechanism of translation. *Nature*. [Online] 461 (7268), 1234–1242.

Schwartz, M. & Vissing, J. (2002) Paternal Inheritance of Mitochondrial DNA — NEJM. *New England Journal of Medicine*. 347 (8), 576-580.

Seidel-Rogol, B. L. et al. (2003) Human mitochondrial transcription factor B1 methylates ribosomal RNA at a conserved stem-loop. *Nature genetics*. [Online] 33 (1), 23–24.

Serre, V. et al. (2013) Mutations in mitochondrial ribosomal protein MRPL12 leads to growth retardation, neurological deterioration and mitochondrial translation deficiency. *Biochimica et biophysica acta*. [Online] 1832 (8), 1304–1312.

Sesaki, H. (2006) Ups1p, a conserved intermembrane space protein, regulates mitochondrial shape and alternative topogenesis of Mgm1p. *The Journal of Cell Biology*. [Online] 173 (5), 651–658.

Sharma, M. R. et al. (2003) Structure of the Mammalian Mitochondrial Ribosome Reveals an Expanded Functional Role for Its Component Proteins. *Cell*. [Online] 115 (1), 97–108.

Sheftel, A. et al. (2010) Iron–sulfur proteins in health and disease. *Trends in Endocrinology & Metabolism*. [Online] 21 (5), 302–314.

Shoemaker, C. J. & Green, R. (2012) Translation drives mRNA quality control. *Nature Structural & Molecular Biology*. [Online] 19 (6), 594–601.

Shutt, T. E. & Gray, M. W. (2006) Bacteriophage origins of mitochondrial replication and transcription proteins. *Trends in genetics : TIG*. [Online] 22 (2), 90–95.

Small, I. et al. (2004) Predotar: A tool for rapidly screening proteomes forN-terminal targeting sequences. *PROTEOMICS*. [Online] 4 (6), 1581–1590.

Smeitink, J. A. M. et al. (2006), Distinct clinical phenotypes associated with a mutation in the mitochondrial translation elongation factor EFTs. *American Journal of Human Genetics*, vol. 79, no. 5, pp. 869–877.

Smits, P. et al. (2010) Mitochondrial Translation and Beyond: Processes Implicated in Combined Oxidative Phosphorylation Deficiencies. *Journal of Biomedicine and Biotechnology*. [Online] 20101–25.

Soleimanpour-Lichaei, H. R. et al. (2007) mtRF1a is a human mitochondrial translation release factor decoding the major termination codons UAA and UAG. *Molecular cell*. [Online] 27 (5), 745–757.

Song, Z. et al. (2007) OPA1 processing controls mitochondrial fusion and is regulated by mRNA splicing, membrane potential, and Yme1L. *The Journal of Cell Biology*. 178 (5), 749-755.

Spelbrink, J. N. (2010) Functional organization of mammalian mitochondrial DNA in nucleoids: History, recent developments, and future challenges. *IUBMB Life*. [Online] 62 (1), 19-32

Spencer, A. C. & Spremulli, L. L. (2004) Interaction of mitochondrial initiation factor 2 with mitochondrial fMet-tRNA. *Nucleic Acids Research*. 32 (18), 5464-5470.

Sunayama, J. et al. (2004) Physical and functional interaction between BH3-only protein Hrk and mitochondrial pore-forming protein p32. *Cell death and differentiation*. [Online] 11 (7), 771–781.

Surovtseva, Y. V. et al. (2011) Mitochondrial ribosomal protein L12 selectively associates with human mitochondrial RNA polymerase to activate transcription. *Proceedings of the National Academy of Sciences*. [Online] 108 (44), 17921–17926.

Szklarczyk, R. et al. (2012) Iterative orthology prediction uncovers new mitochondrial proteins and identifies C12orf62 as the human ortholog of COX14, a protein involved in the assembly of cytochrome c oxidase. *Genome Biology*. 13R12.

Takeuchi, N. et al. (2001) Recognition of tRNAs by Methionyl-tRNA transformylase from mammalian mitochondria. *The Journal of biological chemistry*. [Online] 276 (23), 20064–20068.

Tamura, Y. et al. (2010) Mdm35p imports Ups proteins into the mitochondrial intermembrane space by functional complex formation. *The EMBO Journal*. [Online] 29 (17), 2875–2887.

Tamura, Y. et al. (2009) Ups1p and Ups2p antagonistically regulate cardiolipin metabolism in mitochondria. *The Journal of Cell Biology*. [Online] 185 (6), 1029–1045.

Tang, H. L. et al. (2008) Vimentin supports mitochondrial morphology and organization. *The Biochemical journal*. [Online] 410 (1), 141.

Taylor, A. B. et al. (2001) Crystal structures of mitochondrial processing peptidase reveal the mode for specific cleavage of import signal sequences. *Structure (London, England : 1993)*. 9 (7), 615–625.

Taylor, R. W. and Turnbull, D. M. (2005) Mitochondrial DNA mutations in human disease. *Nature Reviews Genetics*. 6(5):389–402.

Taylor, S. W., Fahy, E. & Ghosh, S. S. (2003a) Global organellar proteomics. *Trends in Biotechnology*. [Online] 21 (2), 82–88.

Taylor, S. W., Fahy, E., Zhang, B., et al. (2003b) Characterization of the human heart mitochondrial proteome. *Nature biotechnology*. [Online] 21 (3), 281–286.

Temperley, R. J., Wydro, M., et al. (2010a) Human mitochondrial mRNAs—like members of all families, similar but different. *Biochimica et Biophysica Acta (BBA) - Bioenergetics*. [Online] 1797 (6-7), 1081–1085.

Temperley, R., Richter, R., et al. (2010b) Hungry Codons Promote Frameshifting in Human Mitochondrial Ribosomes. *Science (New York, NY)*. [Online] 327 (5963), 301–301.

Tomasello, F. et al. (2009) Outer membrane VDAC1 controls permeability transition of the inner mitochondrial membrane in cellulo during stress-induced apoptosis. *Cell research*. [Online] 19 (12), 1363–1376.

Tomecki, R. et al. (2004) Identification of a novel human nuclear-encoded mitochondrial poly(A) polymerase. *Nucleic Acids Research*. [Online] 32 (20), 6001–6014.

Tondera, D. et al. (2005) The mitochondrial protein MTP18 contributes to mitochondrial fission in mammalian cells. *Journal of cell science*. [Online] 118 (Pt 14), 3049–3059.

Trifunovic, A. et al. (2004) Premature ageing in mice expressing defective mitochondrial DNA polymerase. *Nature Cell Biology*. [Online] 429 (6990), 417–423.

Tsuboi, M. et al. (2009) EF-G2mt Is an Exclusive Recycling Factor in Mammalian Mitochondrial Protein Synthesis. *Molecular cell*. [Online] 35 (4), 502–510.

Tsukihara, T. et al. (1996) The whole structure of the 13-subunit oxidized cytochrome c oxidase at 2.8 A. *Science (New York, NY)*. 272 (5265), 1136–1144.

Tucker, E. J. et al. (2011) Mutations in MTFMT underlie a human disorder of formylation causing impaired mitochondrial translation. *Cell Metabolism.* vol. 14 (3) pp. 428-434

Uhlen, M. et al. (2010) Towards a Knowledge-Based Human Protein Atlas. *Nature*. [Online] 464 (7291), 1248–1250.

Ule, J. et al. (2005) CLIP: a method for identifying protein-RNA interaction sites in living cells. *Methods*. [Online] 37 (4), 376–386.

Umeda, N. et al. (2005) Mitochondria-specific RNA-modifying enzymes responsible for the biosynthesis of the wobble base in mitochondrial tRNAs. Implications for the molecular pathogenesis of human mitochondrial diseases. *The Journal of biological chemistry*. [Online] 280 (2), 1613–1624.

Valente, L. et al. (2007) Infantile encephalopathy and defective mitochondrial DNA translation in patients with mutations of mitochondrial elongation factors EFG1 and EFTu. *American Journal of Human Genetics*. vol. 80, no. 1, pp. 44–58.

Vaux, D. L. (2011) Apoptogenic factors released from mitochondria. *Biochimica et Biophysica Acta (BBA) - Molecular Cell Research*. [Online] 1813 (4), 546–550.

Veltri, K. L. et al. (1990) Distinct genomic copy number in mitochondria of different mammalian organs. *Journal of Cellular Physiology*. [Online] 143 (1), 160–164.

Vogel, A. et al. (2005) The tRNase Z family of proteins: physiological functions, substrate specificity and structural properties. *Biological chemistry*. [Online] 386 (12), 1253–1264.

Vogel, R. O. et al. (2007) Human mitochondrial complex I assembly: a dynamic and versatile process. *Biochimica et biophysica acta*. [Online] 1767 (10), 1215–1227.

Vorm, O. et al. (1994) Improved Resolution and Very High Sensitivity in MALDI TOF of Matrix Surfaces Made by Fast Evaporation. *Analytical Chemistry*. [Online] 66 (19), 3281–3287.

Wai, T. et al. (2010) The role of mitochondrial DNA copy number in mammalian fertility. *Biology of reproduction*. [Online] 83 (1), 52–62.

Wallace, D. C. (1989) Mitochondrial DNA mutations and neuromuscular disease. *Trends in Genetics*. [Online] 59–13.

Wang, Y. & Bogenhagen, D. F. (2006) Human Mitochondrial DNA Nucleoids Are Linked to Protein Folding Machinery and Metabolic Enzymes at the Mitochondrial Inner Membrane. *Journal of Biological Chemistry*. [Online] 281 (35), 25791–25802.

Wanrooij, S. & Falkenberg, M. (2010) The human mitochondrial replication fork in health and disease. *Biochimica et Biophysica Acta (BBA) - Bioenergetics*. [Online] 1797 (8), 1378–1388.

Wanrooij, S. et al. (2008) Human mitochondrial RNA polymerase primes lagging-strand DNA synthesis in vitro. *Proceedings of the National Academy of Sciences*. [Online] 105 (32), 11122–11127.

Wanrooij, S. et al. (2012) In vivo mutagenesis reveals that OriL is essential for mitochondrial DNA replication. *EMBO reports*. [Online] 13 (12), 1130–1137.

Ward, B. L. et al. (1981) The mitochondrial genome is large and variable in a family of plants (Cucurbitaceae). *Cell*. 25, 793-803.

Weraarpachai, W. et al. (2009) Mutation in TACO1, encoding a translational activator of COX I, results in cytochrome c oxidase deficiency and late-onset Leigh syndrome. *Nature genetics*. [Online] 41 (7), 833–837.

Wollnik, H. (1993) Time-of-flight mass analyzers. *Mass Spectrometry Reviews*. [Online] 12 (2), 89–114.

Wood, V. et al. (2002) The genome sequence of Schizosaccharomyces pombe. *Nature*. [Online] 415 (6874), 871–880.

Wu, H. et al. (2013) Human RNase H1 Is Associated with Protein P32 and Is Involved in Mitochondrial Pre-rRNA Processing Janine Santos (ed.). *PLoS ONE*. [Online] 8 (8), e71006.

Xin, H. et al. (1995) Cloning and expression of mitochondrial translational elongation factor Ts from bovine and human liver. *The Journal of biological chemistry*. 270 (29), 17243–17249.

Xu, D. A. C. (1996) RNA-DNA hybrid formation at the human mitochondrial heavy-strand origin ceases at replication start sites: an implication for RNA-DNA hybrids serving as primers. *The EMBO Journal*. 15 (12), 3135.

Yagi, M. et al. (2012) p32/gC1qR is indispensable for fetal development and mitochondrial translation: importance of its RNA-binding ability. *Nucleic Acids Research*. [Online] 40 (19), 9717–9737.

Yakubovskaya, E. et al. (2014) Organization of the human mitochondrial transcription initiation complex. *Nucleic Acids Research*. [Online]

Yoshida, M. et al. (2001) ATP synthase--a marvellous rotary engine of the cell. *Nature reviews. Molecular cell biology*. [Online] 2 (9), 669–677.

Yoshikawa, H. et al. (2011) Splicing factor 2-associated protein p32 participates in ribosome biogenesis by regulating the binding of Nop52 and fibrillarin to preribosome particles. *Molecular & cellular proteomics : MCP*. [Online] 10 (8), M110.006148.

Yu, L. et al. (1995) Molecular cloning and characterization of a cellular protein that interacts with the human immunodeficiency virus type 1 Tat transactivator and encodes a strong transcriptional activation domain. *Journal of virology*. 69 (5), 3007–3016.

Ziebarth, T. D. et al. (2010) Dynamic effects of cofactors and DNA on the oligomeric state of human mitochondrial DNA helicase. *The Journal of biological chemistry*. [Online] 285 (19), 14639–14647.

Züchner, S. et al. (2004) Mutations in the mitochondrial GTPase mitofusin 2 cause Charcot-Marie-Tooth neuropathy type 2A. *Nature genetics*. [Online] 36 (5), 449–451.

SUPPLEMENTARY FIGURES

All supplementary figures show data generated by Dr Monika Olahova

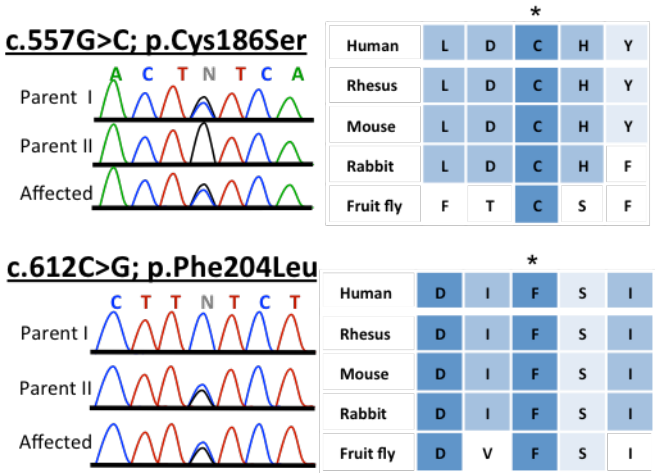

Figure S.1: Genotype For Patient with Compound Heterozygous Mutation in *C1QBP*. Sequencing chromatograms displaying mutations present in the patient. Both allelic variants exhibit base transversions resulting in an amino acid substitution in a conserved residue denoted by *.

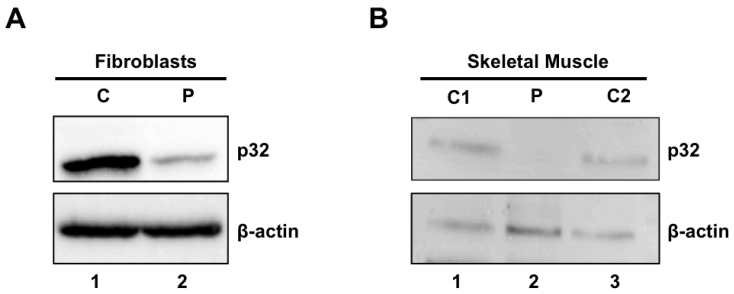

Figure S.2: Reduction of p32 Levels in Patient Derived Fibroblasts and Skeletal Muscle. (A) Cell lysate from control (C, lane 1) and patient (P, lane 2) fibroblasts were subjected to SDS-PAGE and analysed by immunoblotting. **(B)** Lysate from skeletal muscle from patient (P, lane 2) and controls (C1 and C2, lanes 1 and 3) were subjected to SDS-PAGE and western blotting. α-p32 and α-β actin antibodies were used for immunodetection.

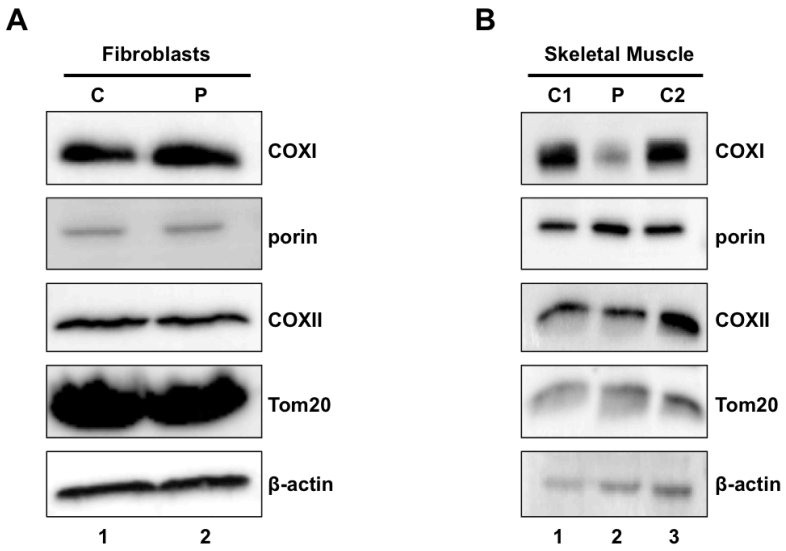

Figure S.3: Effects of p32 Mutation on Steady State Levels of mtDNA-Encoded Proteins in Patient Derived Fibroblasts and Skeletal Muscle Tissue. (A) Cell lysate from control (C, lane 1) and patient (P, lane 2) fibroblasts were subjected to SDS-PAGE and analysed by immunoblotting. **(B)** Lysate from skeletal muscle from patient (P, lane 2) and two controls (C1 and C2, lanes 1 and 3) were subjected to SDS-PAGE and western blotting. α-COXI, α-porin, α-COXII, α-Tom20 and α-β-actin antibodies were used for immunodetection.

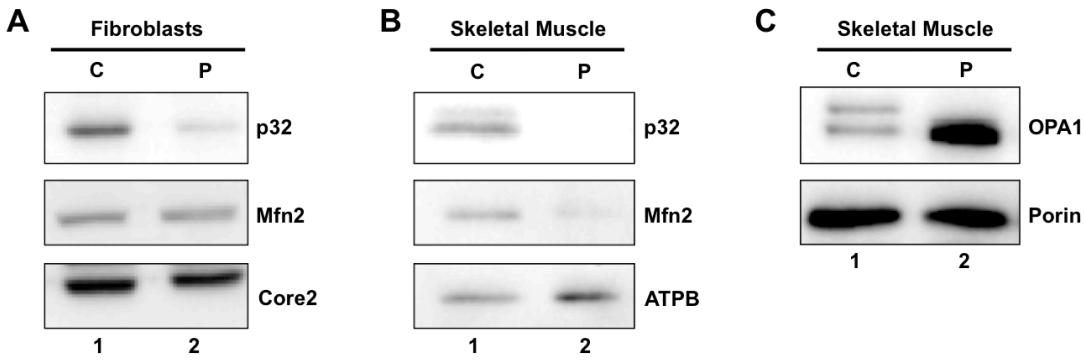

Figure S.4: Effects of p32 Mutation on Mitochondrial Fusion Proteins. (A) Cell lysate from control (C, lane 1) and patient (P, lane 2) fibroblasts were subjected to SDS-PAGE and analysed by immunoblotting. **(B** and **C)** Lysate from control (C, lane 1) and patient (P, lane 2) skeletal muscle were subjected to SDS-PAGE and western blotting. α-p32, α-porin, α-Mfn2, α-Core2, α-OPA1 and α-ATPB antibodies were used for immunodetection.